A Study of Renewable Energy in a Port Facility by Using Solar Organic Rankine Cycle Systems

Yalcın Durmusoglu[1], Selim Aksoy[1], Cengiz Deniz[1]

Abstract

Organic Rankine Cycle (ORC) system can generate electric energy by running at low temperatures. It is an alternative way of environmentally friendly, safe and cheap electric energy production. As a heat source which can be inducted to the system by a waste heat of any kind of industrial processes, solar energy etc. Therefore, recently range of application has been increasing widely speed in waste heat recovery facilities, or geothermal facilities and for electric energy production in residence. On the other hand, global climate change is one of the vital problems for a healthy world future. As it affects all sectors, maritime transportation is affected by means of precautions to prevent causes of climate change as well. Correspondingly energy efficiency in ship operations has developed as an innovative solution in recent years. Because, ships consume plenty amount of energy while both navigating and berthing in port. In order to minimize environmental pollution caused by ships, usage of renewable energy sources is important. Supporting ships from a port facility energy source is called Onshore Power Supply (OPS). For this purpose, usage of ORC systems that can run with solar energy in ports as OPS is proposed in this paper.

Keywords: *Efficiency, Energy, Maritime, OPS, Ports.*

1. INTRODUCTION

70% of emissions from ships in the worldwide to occur within 400 km from the coast, ship and port sourced emissions to affect health of people negatively especially live in coast towns have been scientifically proven [1]. 19.000 people to be caught lung cancer only because of emissions from ports or ships, and 60.000 people to die because of different diseases caused by yet these emissions have been confirmed according to the international research related diseases caused by air pollution sourced by ship and port operations [2].

Studies on reducing emissions to minimum in ships and ports have been enhanced in last 20 years. European Union member countries have started “Green Port” project in order to reduce emissions from ships in ports [3]. In addition, European Union has been adopting administrative and technical regulations after determining that air pollution from maritime operations is going to exceed air pollution from land operations. So that, air pollution caused by ships is reduced gradually. Due to sea water used for cooling the generators of ships in port service wouldn’t be needed when internal electricity system is not used, water policy; intended for reducing emission values from exhaust gases, air policy; when alternative renewable energy is used, energy policy subjects are corresponding to green port policy. In recent years, it is considered that presenting better service in this way for ports and obtaining electricity from port facility (OPS) for ships during in port would be more environmentally friendly [4]. In this sense, wind power, solar energy, hydraulic energy and geothermal energy are main alternative energies that ports will be able to use as renewable energy sources [5].

Possible energy saving potential is indicated as %10 - %15. Studies on energy savings in ports should be cared about seriously, because %10 energy saving is accepted as equal to reducing daily 310 tonnes of CO_2 emission.

For this purpose, International Maritime Organization (IMO), The Marine Environment Protection Committee (MEPC), has initiated a study on “Energy efficiency and emission control of ships in port vicinity” [6]. The aim of the study is explained as, “A Sustainable Maritime Transportation System needs efficient port facilities to keep the operational efficiency of ships at the highest level (e.g. hull cleaning and propeller polishing facilities, specialized fuel and power supply services). The logistics infrastructure should allow ships to sail at optimal speeds for their charted trajectories (e.g. cargo logistics and port planning, just-in-time berthing, weather routeing). All these elements would form part of a "holistic" energy efficiency concept for the whole system. Innovation and best practices for efficient ship operation and ship-to-shore interfacing should be rigorously pursued.” by IMO [6].

In this paper, Organic Rankine Cycle (ORC) facility, which is an alternative energy generating way for a port, is proposed as model. This facility is designed as supported by solar energy, which is a renewable energy source. Possible amount of energy saving for port is calculated by designed ORC facility. Beside this, effect of the system on amount of CO_2 emission is estimated.

[1] *Correspond author. ydurmusoglu@itu.edu.tr;*

1.1. Solar Energy Applications: An Organic Rankine Cycle (Orc) System

Renewable energy types are sustainable sources [4]. Their major advantage is environmental sensitivity by generating electrical energy with ensuring low carbon emissions. Only disadvantage is unit energy generating cost still to be expensive. But this would be eliminated by time.

With regard to energy efficiency of ports available renewable energy sources are such as;

- Solar energy,
- Fuel cell,
- Hydraulic power,
- Wind power,
- Tidal current force.

In 2000, the United Nations Development Programme, UN Department of Economic and Social Affairs, and World Energy Council published an estimate of the potential solar energy that could be used by humans each year that took into account factors such as insolation, cloud cover, and the land that is usable by humans. The estimate found that solar energy has a global potential of 1,575–49,837 EJ per year (Table 1) [7].

Table 1. Annual Solar Energy Potential by Region (Exajoules) [7].

Region	North America	Latin America and Caribbean	Western Europe	Central and Eastern Europe	Former Soviet Union	Middle East and North Africa	Sub-Saharan Africa	Pacific Asia	South Asia	Centrally planned Asia	Pacific OECD
Minimum	181.1	112.6	25.1	4.5	199.3	412.4	371.9	41.0	38.8	115.5	72.6
Maximum	7,410	3,385	914	154	8,655	11,060	9,528	994	1,339	4,135	2,263

Nowadays, solar energy is mostly used for the purpose of heating, cooling, cooking and electrical energy generation. There are photovoltaic systems for electrical energy generation. But efficiency of these systems is so low and they convert solar energy to electrical energy with efficiency of %5 - %20 depending on their own structures [8].

ORC systems are used for converting solar energy to electrical energy as well. ORC system can generate electrical energy by running at low temperatures. It is an alternative way of environmentally friendly, safe and cheap electrical energy production. As a heat source which can be inducted to the system by a waste heat of any kind of industrial processes, solar energy etc. Therefore, recently range of application has been increasing widely speed in waste heat recovery facilities, geothermal facilities and for electric energy production in residence. A simple ORC system which is running by solar energy and its components are presented in Figure 1.

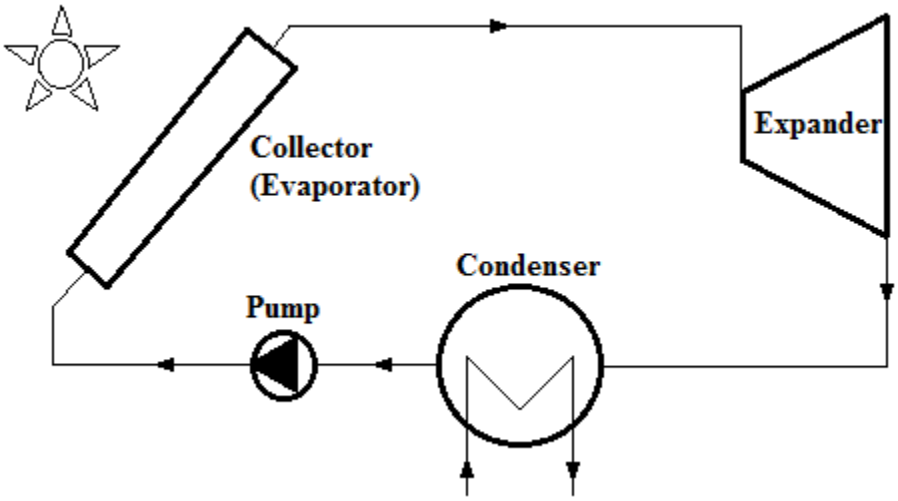

Figure 1. Simple solar based ORC system.

Work fluids used in cycle are organic fluids, which are able to become superheated steam phase at low temperatures. So they have high capability to do work. Work fluid becomes superheated steam state getting heated by solar energy with the help of collectors. Then, by means of expanding in the expander it does work and system generates electrical energy. Work fluid is transferred to collectors again by a pump after leaving expander and condensing in condenser. In this way cycle is completed.

In ports, heat input to ORC system is able to supply by solar energy and heat output from ORC system is able to carry through sea water. Therefore, port regions can be mentioned as potential application areas for ORC systems.

1.2. A Port Case Study: Evyapport/Kocaeli

In this study, application of ORC system is designed by considering an example port and energy generation potential is analysed for relevant port. In terms of environment CO_2 emission reducing is calculated by designed system as well. Port region used in this study is "Evyapport", which is located at Marmara Region in Kocaeli provincial border and at coordinates of 40°46'25" N - 29°42'40" E (Fig.2). Port serves for both container ships and tanker ships. Number of container ships served in port and number of handled containers according to years is presented in Table 2 [9].

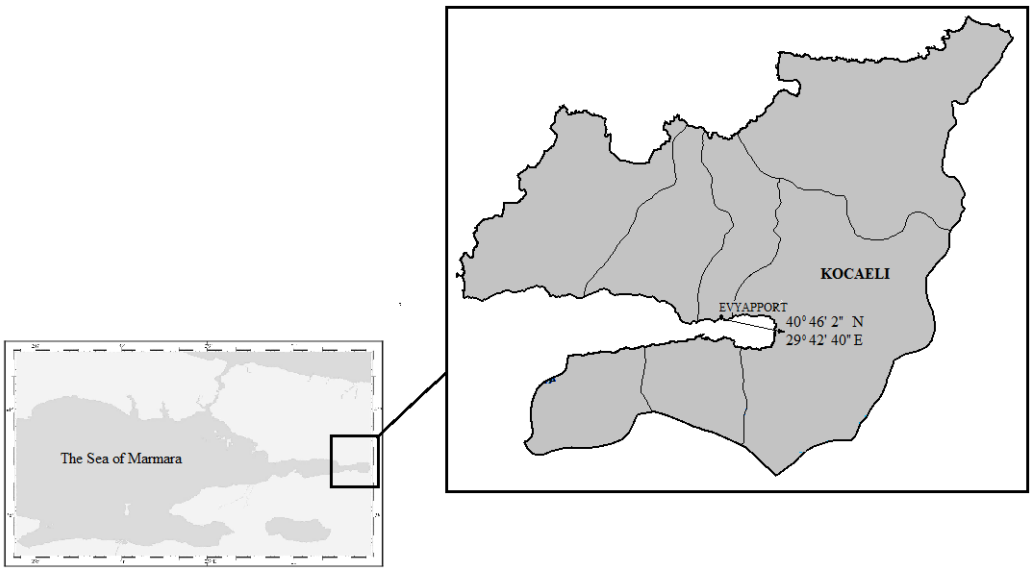

Figure 2. The case study port: Evyapport- Kocaeli.

Table 2. Annual container ship capacity and number of container ships in Evyapport

Years	Capacity of ships (TEU)	Number of Container ships	Average (TEU/ship)
2008	109000	205	532
2009	156000	431	362
2010	248000	558	444
2011	283000	614	461
2012	400169	797	502
2013	457537	874	523
2014	522970	995	526
2015	605385	1067	567

source: www.evyapport.com

Average hoteling time in berth of a container ship is accepted as 21 hours according to Table 3 [10].

Table 3. Average hoteling time in berth of a container ship.

Type of Ships	Fuel consumption rate (kg /1000.GT-hour)	Average hoteling time in berth(hours)
Container ships	5.0	21

source: Trozzi and Vaccaro, 1995.

Daily average sunshine duration of port region and daily average solar energy data [11] are presented in table 4. And sea water monthly data is presented in table 5 [12].

Table 4. Solar energy data of Evyapport and neighbour regions.

	Months:	JAN	FEB	MAR	APR	MAY	JUN	JUL	AGU	SEP	OCT	NOV	DEC
Kocaeli	A	1,42	2,27	3,2	4,38	5,59	5,98	5,8	5,23	4,14	2,82	1,68	1,21
	B	3,29	4,17	5,2	6,55	8,56	9,79	10,44	9,59	7,96	5,4	3,95	3,06
Derince	A	1,47	2,36	3,21	4,4	5,6	5,99	5,82	5,24	4,16	2,8	1,7	1,2
	B	3,3	4,19	5,21	6,58	8,58	9,78	10,44	9,59	7,96	5,4	3,97	3,09
Gebze	A	1,43	2,33	3,19	4,39	5,6	5,99	5,8	5,23	4,15	2,8	1,69	1,2
	B	3,3	4,2	5,28	6,67	8,64	9,88	10,52	9,63	7,94	5,36	3,95	3,08
Gölcük	A	1,42	2,18	3,23	4,43	5,63	6,05	5,85	5,27	4,17	2,89	1,7	1,22
	B	3,28	4,15	5,17	6,54	8,64	9,76	10,39	9,57	8	5,43	4	3,04
Kandıra	A	1,38	2,21	3,15	4,3	5,54	5,91	5,74	5,17	4,06	2,77	1,62	1,2
	B	3,3	4,15	5,2	6,51	8,48	9,81	10,49	9,61	7,89	5,36	3,87	3,05
Karamürsel	A	1,42	2,24	3,25	4,45	5,62	6,05	5,83	5,29	4,2	2,9	1,7	1,22
	B	3,29	4,18	5,22	6,64	8,52	9,8	10,3	9,5	8,03	5,41	4,05	3,09
Körfez	A	1,46	2,36	3,2	4,39	5,61	5,99	5,83	5,25	4,16	2,8	1,69	1,2
	B	3,3	4,18	5,23	6,6	8,59	9,8	10,4	9,59	7,93	5,37	3,95	3,07
Merkez	A	1,43	2,28	3,22	4,41	5,61	6,01	5,82	5,25	4,17	2,84	1,7	1,21
	B	3,28	4,17	5,15	6,46	8,56	9,74	10,4	9,57	8	5,45	3,99	3,06

A : Total solar radiation in (kWh/m2-day); B: Hours of Sunshine (hour/ day)

Table 5. Monthly sea water data of Evyapport.

Izmit/Kocaeli	JAN	FEB	MAR	APR	MAY	JUN	JUL	AGU	SEP	OCT	NOV	DEC
Average temperature (oC)	6.2	6.7	8.7	13.1	17.6	21.8	23.8	23.7	20.4	16	11.9	8.4
Average maximum temperature (oC)	9.7	10.7	13.2	18.5	23.2	27.5	29.5	29.6	26.2	20.8	16.3	11.9
Average minimum temperature (oC)	3.3	3.6	5	8.8	13	16.9	19.1	19.3	16.2	12.5	8.6	5.5
Average solar radition time (hour)	2.3	3	4.6	5.3	7.2	8.5	9.3	9.6	7.1	4.5	3.4	2.3

source: www.mgm.gov.tr

Assumptions for some parameters in ORC system (Fig. 2) calculations by considering above data for Evyapport are presented in Table 6 and results are shown in Table 7.

Table 6. Assumptions of some parameters of ORC systems.

Assumptions of parameters:	**Symbol**	**Value**	**Unit**
Amount of Solar radiation	I_{rad}	44	kWh/m^2.day
Average day of sunshine	t_{sd}	6.5	h/day
Total area of solar collectors	A_c	3	m^2
Efficiency of solar collectors	η_C	0.55	-
Average sea water temperature input value of condenser	$T_{sw,in}$	16	^{o}C
Difference between input and output sea water temperature value of condenser	ΔT_{SW}	7	^{o}C

2. RESULTS AND DISCUSSION

A Solar based Organic Rankine Cycle (ORC) system is considered (Fig.3a and Fig.3b) to supply alternative electricity energy to a container terminal where is in Kocaeli, Izmit. The ORC system consists of five main parts which are a parabolic collector, an evaporator, an expander, a condenser and a circulation pump. The system utilizes the solar energy and generates electricity for the terminal. The calculation methods based on theoretically that is proposed in literature. For this approach it can be concluded that there is electiricity potential up to 2 MWh/year on the region. The ORC system can work between 25.59 bar and 9 bar pressures. The working fluid is R134a and mass flow rate is 0.06 in kg/s. Also it is assumed that 1 kWh electrical

power is equal to 0.75 kg CO_2 emission [13], due to this approach it can be estimated that CO_2 emission up to 1.5 tonnes/ year is saved from the atmosphere.

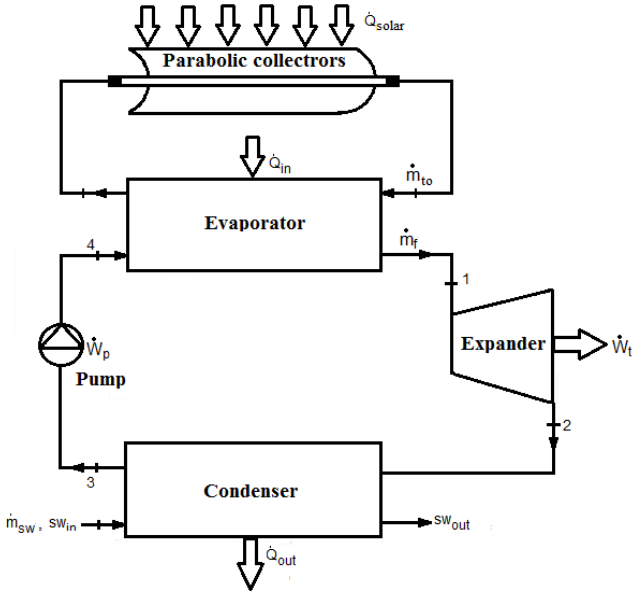

Figure 3a. A considered solar based ORC system for a container ship port.

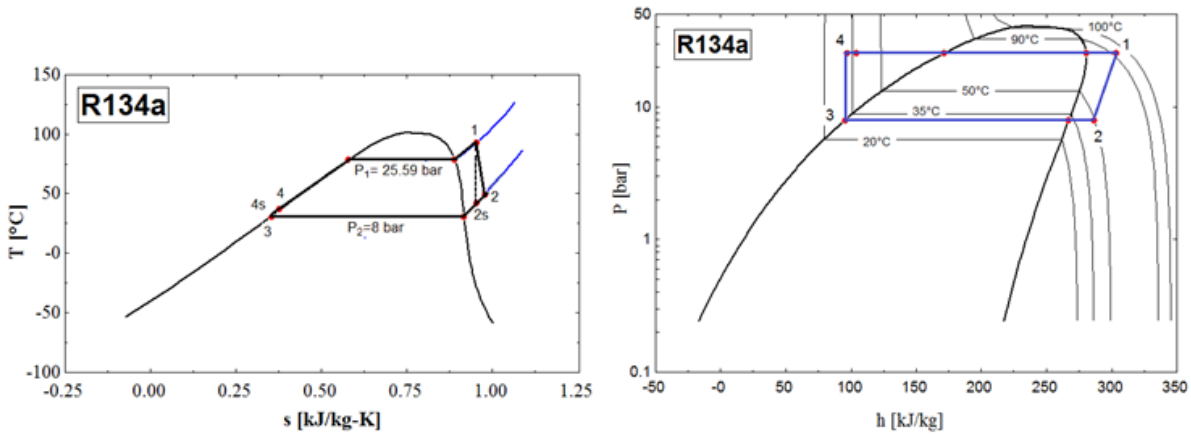

Figure 4. T-s and P-h diagrams of ORC system used of working fluids R134a

3. CONCLUSION

The ORC systems are one of the best alternative electricity power production facilities which are using waste heat recovery. Therefore it can be proposed to ports for fulfilling their electricity demands due to the On Shore Power (OSP) programs that highlights by IMO and EU commissions. However the potential of ORC systems, it cannot be satisfactory to generate electricity. But they have a great potential for improving. Such as a cascade ORC system, a recuperated ORC system, a LNG fuelled ORC system etc. Also solar based ORC system can be considered with cascade systems, thus it can produce a high amount of power. Also by considering these systems save environment, they are good solutions for alternative electricity energy generating for ports.

REFERENCES

[1] Azzellino A., Kofoed J.P., Landfred C., Margheritini L., Pedersen M.L. (2013). A Marine Spatial Planning framework for the Optimal Siting of Marine Renewable Energy Installations:Two Danish Case Studies. Journal of Coastal Research, Special Issue No.65:1623-1628

[2] NABU LIFE, 2014, Working Paper: Clean Air in Ports

[3] Murat Yapıcı, Birsen Koldemir, Limanlarda Alternatif Yenilenebilir Enerji Kulanımının İncelenmesi,II. Ulusal Liman Kongresi, 5-6 Kasım 2015. Izmir.

[4] Worley Parsons, Seminar Notes, Energy Efficiency in Sustainable Port Development and Operations, AAPA 2013 Marine Terminal Management Training Program, September 12, 2013.

[5] Boyle, G. (2004). Renewable Energy Power for a Sustainable Future. Oxford University Press. London.
[6] IMO MEPC 68/INF.16, March 4, 2015.
[7] United Nations Development Programmeand World Energy Council. "Energy and the challenge of sustainability". September 2000. Retrieved August 2015.
[8] http://www.eie.gov.tr
[9] http:// www.evyapport.com
[10] Trozzi C., Vaccaro R., Nicolo L., Air pollutants emissions estimate from maritime traffic in the Italian harbours of Vinice and Piombino, The Science of the Total Environment, 169, 257-263, 1995.
[11] http://www.marka.org.tr/Uploads/Files/DoguMarmaraBolgesi_YenilenebilirEnerji Raporu.pdf
[12] http://www.mgm.gov.tr
[13] S&P Industry Survey, Electric Utilities, Justin McCann, August 9, 2007.

A Novel Broadband Single-Layer Reflectarray Antenna Design for X-Band Applications

Hande Bodur[1], Sibel Cimen[1], Gonca Cakir[1], Sibel Unaldi[2]

Abstract

In this work, X-Band single layer broadband reflectarray antenna is presented. The designed reflectarray antenna with variable size resonant elements are operating at 10 GHz. The phase characteristic of unit cell structure is obtained with the CST Microwave Solver. The absolute value of the reflection phase range is 350 degree is achieved by different dimensions of patches. The unit cell consists of three main sections which are patch, substrate and ground plane. A 12x12 unit cells reflectarray are designed on a 120x120 mm^2 square plane. Also pyramidal horn antenna is used for centre-feed configuration. The gain bandwidth of the proposed reflectarray is improved by adjusting the design parameters. According to the simulation results, the max gain of reflectarray antenna is 20 dB and it has %17 1-dB gain bandwidth.

Keywords: *Broadband, reflectarray antenna, unit cell.*

1. INTRODUCTION

High gain antennas are used in communication systems and radar applications. Conventional parabolic reflector has high-gain performance but it has many disadvantages which are difficult manufacturing and the main beam directing process. In recent years microstrip reflectarray antenna is used according to parabolic reflectors. Low cost, low profile, small antenna mass, easy manufacturing, no feeding networks and electronically-beam direction ability are advantages of microstrip reflectarray antennas. In the reflectarray antenna designs, the unitcells have important roles. The unitcells must be designed to produce a phase shift when illuminated by the center feed for produce a collimated beam in a specified direction as shown in Figure 1 [1]-[3].

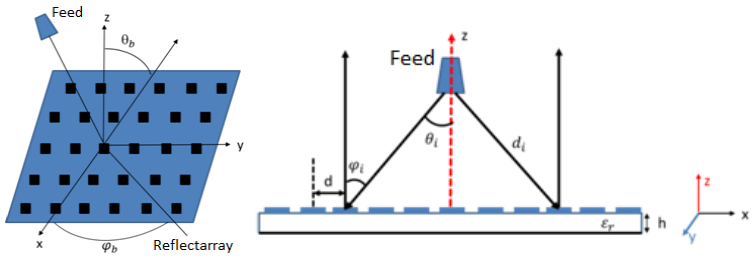

Figure 5. Mechanism of reflectarray antenna

The restrictive problem of reflectarray antennas is narrow bandwidth. Differential spatial phase delays of radiating elements leads to narrow bandwidth performance. Multilayer or thick substrate can be overcome this problem with extended phase range [4], [5]. However, it brings some disadvantages such as difficult manufacturing, high cost and large mass. In recent times, narrow bandwidth problem is solved by printing multi-resonance elements on single layer substrate. This feature brings wide linear reflection phase range as multilayer structure [6], [7].

In this work, X-Band (8-12 GHz) single layer broadband reflectarray antenna for enhancing bandwidth performance operating at 10 GHz is presented. The unitcell of reflectarray antenna consist of cross and square aperture loop.The absolute value of the reflection phase range is 350 degree is achieved by different dimensions of patches. This smooth and linear reflection phase range is improved gain bandwidth performance. A 12x12 unitcells, 144 elements reflectarray are designed on a 120x120 mm^2 square plane. The technique of variable size patches around their resonance size is used with the inhomogeneous edge to edge spacing. On reflecting surface there is on array of passive designed patches illuminated by pyramidal horn antenna.

2. DESIGN OF UNITCELL

The unitcell of reflectarray antenna consist of cross and square aperture loop. The dimension of designed unitcell is l_1=10 mm X 10 mm which is 0.33λ at 10 GHz. The substrate of thickness h=1.524 mm and relative permittivity is ε_r=3 (Figure 2). The other parameters which are used in the design process is shown in Table 1.

[1] *Hande Bodur: Kocaeli University, Department of Electronics and Communication Engineering, 41380, İzmit/Kocaeli, Turkey.* hande.bodur@kocaeli.edu.tr

[2] *Sibel Ünaldı : Bilecik Şeyh Edabali University, Department of Electrical and Electronics Engineering, 11230, Gülümbe/Bilecik, Turkey.* sibel.unaldi@bilecik.edu.tr

Table 7. The parameters of unitcell

parameter	(mm)
l_2	variable (4 mm - 9.5 mm)
l_1	10
d_1	0.08
d_2	0.9

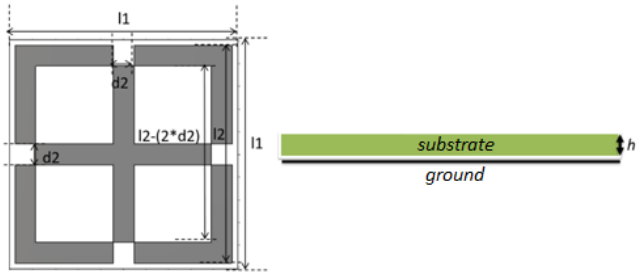

Figure 2. Unitcell

In the simulation, the wave guide model is choosen to produce phase characteristics of the unit cell [8]. The two walls of the wave guide which include tangential component of the electric field are perfectly magnetic conductor (PMC), the another two walls which include vertical component of the electric field are perfectly electric conductor (PEC) as shown in Figure 3. Thus, behavior of electric field is infinite at the PEC border and behavior of magnetic field is infinite at the PMC border. The wave guide is terminated with designed unit cell to obtain reflection characteristics relates to structure. The phase characteristics and operational bandwidth of unitcell is evaluated by variable parameter l_2 (Figure 4).

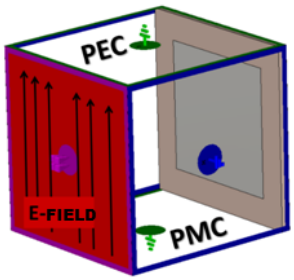

Figure 3. The waveguide model

The phase characteristics of unitcell at different frequencies must be obtained in reflectarray antenna design. To improve operational bandwidth performance, the phase graphs should be nearly parallel to each other at different frequencies [9]. For this purpose, the unitcell have been analyzed at 9-12 GHz frequency range. As seen from the Figure 4, the curves are nearly parallel to each other.

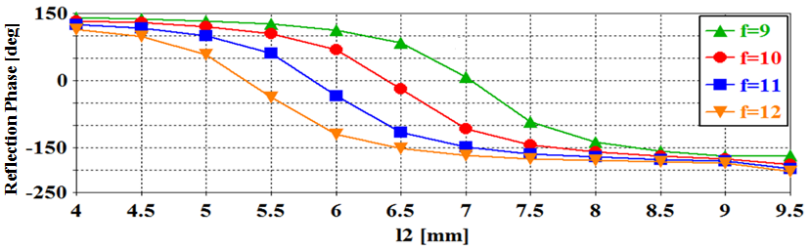

Figure 4. Reflection phase at different frequency

3. DESIGN OF REFLECTARRAY ANTENNA

Spherical waves from the source in the focal point comes to each unit on reflectarray by way of different lengths. In order to direct this reflected wave towards a certain direction, this phase delay should be compensated with unit cell elements. The required operation is done with equation (1).

$$\varphi(x_i, y_i) = -k_0 sin\theta_b cos\varphi_b x_i - k_0 sin\theta_b sin\varphi_b y_i \quad (1)$$

Where k_0 is the free space propagation constant, $x_i and y_i$ give the coordinates of the i*th* element of the reflectarray antenna. On the other hand, the phase of reflected wave from each element on reflectarray is equal to the total propagation from the source with phase shift of each element (2).

$$\varphi(x_i, y_i) = k_0 d_i + \varphi_R(x_i, y_i) \quad (2)$$

$\varphi_R(x_i, y_i)$is the phase shift of i*th* element, d_i is the distance source and $(x_i, y_i)_{th}$ element [10]. Using equation (1) and (2), necessary equations derived for desired phase shift value calculation for each element.

$$\varphi_R(x_i, y_i) = k_0 d_i - k_0 sin\theta_b cos\varphi_b x_i - k_0 sin\theta_b sin\varphi_b y_i \quad (3)$$
$$\varphi_R(x_i, y_i) = k_0 (d_i - sin\theta_b cos\varphi_b x_i - sin\theta_b sin\varphi_b y_i) \quad (4)$$
$$\varphi_R(x_i, y_i) = k_0 (d_i - (cos\varphi_b x_i + sin\varphi_b y_i) sin\theta_b) \quad (5)$$
$$d_i = \sqrt{(x_i - x_f)^2 + (y_i - y_f)^2 + (z_i - z_f)^2} \quad (6)$$

As a result of the equation obtained by (5) and (6) a phase shift value of each element can be calculated. x_f, y_f and z_f indicate coordinate of source antenna. The phase change in equal (5) can be obtained by the variance of any geometric parameters in the structure of the unit cell.

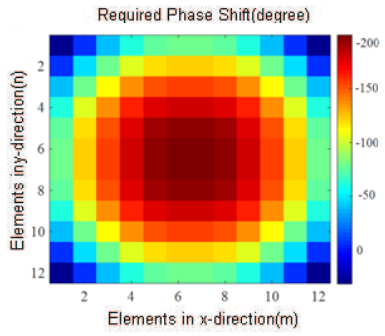

Figure 5. The phase value of each element at the reflecrarray

Sizes of elements on reflectarray is obtained by using the relation between phase value in Figure 5 and element size-phase value in Figure 4. A 12x12 unit cells, 144 elements reflectarray is designed on a 120x120 mm^2 square plane for X band applications at 10 GHz operating frequency. Figure 6 is presenting the designed reflectarray antenna. The focal length (F) is distance between array surface and horn antenna aperture 115 mm, F/D ratio is 0.95. Pyramidal horn antenna is used for centre-feed configuration and it is placed centre of the reflectarray at the focal distante (F).

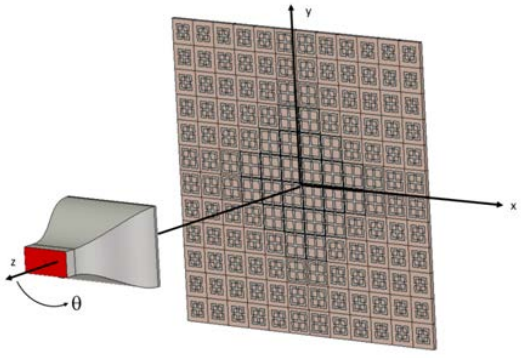

Figure 6. 12x12 reflectarray antenna

Radiation patterns of reflectarray antenna in E-plane (ϕ=90^o) and H-plane (ϕ=0^o) at f=11 GHz is shown in Figure 7. The max gain of reflectarray antenna is 20 dB and it has %17 1-dB gain bandwidth as shown in Figure 8.

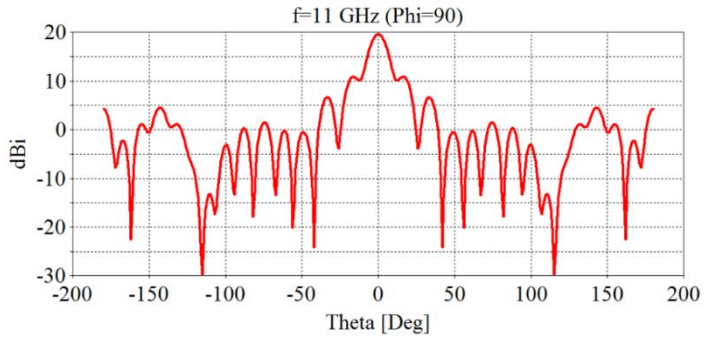

Figure 7. Radiation patterns of reflectarray antenna (E-plane (ϕ=90°) and H-plane (ϕ=0°)) at f=11 GHz

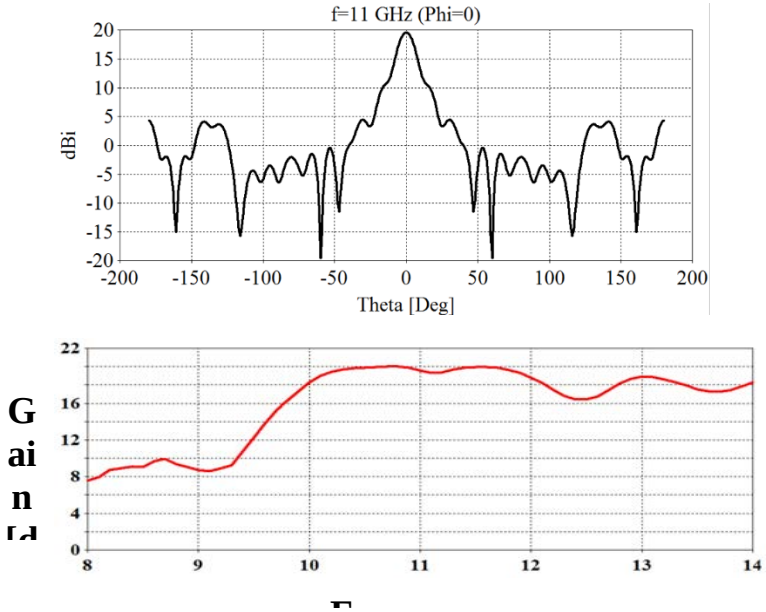

Figure 8. The gain graph according to frequency

4. CONCLUSION

A 12x12 unit cells, 144 elements, X band (8-12 GHz) single layer microstrip reflectarray antenna at the 10 GHz operation frequency is designed and presented in this work. The designed reflectarray consist of cross and square aperture loop, dielectric substrate and ground plane. The unit cell has 350 degree absolute phase range with variable patch size. The gain bandwidth of the proposed reflectarray is improved by adjusting the design parameters. Additionally, reflectarray antenna is fed by pyramidal horn antenna and simulated. The result of simulations show that the max gain of reflectarray antenna is 20 dB and it has %17 1-dB gain bandwidth.

ACKNOWLEDGMENT

The authors wish to acknowledge the assistance and support of The Scientific and Technological Research Council of Turkey (TUBITAK) for supporting this work (Project No: 114E500).

REFERENCES

[1]. J Huang and J Encinar, *Reflectarray Antennas*, JohnWiley and Sons,Inc., 2008.
[2]. J. Huang, "Microstrip reflectarray," in *Antennas and Propagation Society* International Symposium, 1991. AP-S. Digest, 1991, pp. 612–615 vol.2.
[3]. S.D. Targonski, D.M. Pozar, and H. D. Syrigos, "Analysis and design of millimeter wave microstrip reflectarrays," in *Antennas and Propagation* Society International Symposium, 1995. AP-S. Digest, 1995, vol. 1, pp. 578–581 vol.1.
[4]. J.A. Encinar, "Design of two-layer printed reflectarrays for bandwidth enhancement," in Antennas and Propagation Society International *Symposium, 1999. IEEE*, 1999, vol. 2, pp. 1164–1167 vol.2.
[5]. J.A. Encinar and J.A. Zornoza, "Broadband design of three-layer printed reflectarrays," Antennas and Propagation, IEEE Transactions on, vol. 51, no. 7, pp. 1662–1664, 2003.
[6]. Yuezhou Li, M.E. Bialkowski, K.H. Sayidmarie, and N.V. Shuley, "Microstrip reflectarray formed by double elliptical ring elements," in Antennas and Propagation (EuCAP), 2010 Proceedings of the Fourth European Conference on, 2010, pp. 1–5.

[7]. Qin-Yi Li, Yong-Chang Jiao, and Gang Zhao, "A novel microstrip rectangular-patch/ring- combination reflectarray element and its application," Antennas and Wireless Propagation Letters, IEEE, vol. 8, pp. 1119–1122, 2009.
[8]. F.-C.E. Tsai and M.E. Bialkowski, "Designing a 161-element kuband microstrip reflectarray of variable size patches using an equivalent unit cell waveguide approach," Antennas and Propagation, IEEE*Transactions on*, vol. 51, no. 10, pp. 2953–2962, 2003.
[9]. Yuezhou Li, M.E. Bialkowski, and A.M. Abbosh, "Single layer reflectarray with circular rings and open-circuited stubs for wideband operation," Antennas and Propagation, IEEE Transactions on, vol. 60, no. 9, pp. 4183–4189, 2012.
[10]. D. M. Pozar and T. A. Metzler , " Analysis of a refl ectarray antenna using microstrip patches of variable size , " Electronics Letters , April 1993 , pp. 657 – 658.

Hande Bodur was born in 1993. She graduated from the B.S degree in June 2015 and started M.S. degree in September 2015 in electronics and communication engineering at Kocaeli University (KOU), Kocaeli, Turkey. From February 2016 to still now on, she is a Research Assistant with the Microwave & Antennas Laboratory.

Sibel Çimen was born in Çanakkale, in 1980. She received the B.S, M.S and PhD degrees in electronics and communication engineering from Kocaeli University (KOU), Kocaeli, Turkey, in 2002, 2005 and 2009 respectively. From 2005 to 2009, she was a Research Assistant with the Microwave & Antennas Laboratory. Since 2010, she has been an Assistant Professor with the Electronic and Communication Engineering Department, Kocaeli University, KOU. Her research interests include numerical methods for planar structures, metamaterials and design of UWB antennas and microstrip filters.

Gonca Çakır received the BSEE, MSEE, and PhD degrees in electronics and communication engineering from Kocaeli University (KOU), Kocaeli, Turkey, in 1996, 1999, and 2004, respectively. Currently, she is an associate Professor with the Engineering Faculty, KOU. Her research interests include analytical and numerical methods for planar structures (transmission lines, circuits, and antennas), radars, RCS prediction techniques, and metamaterials.

Sibel Ünaldı received the B.S. degree in electrical and electronics engineering from the Zonguldak Karaelmas University and M.S. degree inelectronics and communication engineering the from the Yıldız Technical University in 2011 and 2015 respectively. From February 2013 to still now on, she is a Research Assistant at Bilecik Şeyh Edebali University. Her research focused on Frequency Selective Surfaces and microstrip antennas.

The Monitoring Sediment Concentration with Turbidity and ADV Backscatter Strength for Different Sediment Sizes

***Ramazan Meral*[1]**

Abstract

Measurements of suspended sediments in rivers are important for understanding soil losses, controlling water pollution, planning and management of water storage structures. Due to temporal and spatial variation, measurement of suspended sediments is very difficult. The traditional technique for measuring concentration is direct water sampling method which has many sampling and laboratory difficulties. However, this technique is restrictive in its ability to provide continuous monitoring of suspended sediment concentration. Acoustic measurement is alternative indirect methods to determined sediment concentration. Acoustic Doppler velocimeter (ADV) can be used be used to estimate suspended sediment concentration (SSC) with the signal to noise ratio (SNR)in the water. In this study particles size affecting and SNR values was investigated with using four different sediment sizes groups (0-50, 50-100, 100-200 and 200-250 micron). SNR values had good relationships with SSC values for all sediment size groups, higher R^2 values were obtained than turbidity measurements. (R^2=0.9737-0.9977). These relations were observed for lower than 40 dB and 1 $g.l^{-1}$ sediment concentrations. The other point was SNR values are strongly affected from small chancing in sediment concentration. This property can be accepted as advantages for sensitive measurement for mentioned concentration intervals. As a result of this study it could be concluded that SNR values can be used as alternative method for continuous sediment monitoring.

Keywords: *Sediment, Turbidity, Signal to noise ratio Water pollution*

1. INTRODUCTION

Continuous sediment monitoring in river has many difficulties due to temporal and spatial changes depending on many factors such as flow, basinandclimatic characteristics. The sampling and filtering method is generally used for direct measurement. This gravimetric measurement represents the standard methodology to obtain quantify suspended sediment and consists of physically separating of sediment materials from water sample. This method has not capability to provide spatial and temporal changing of sediment concentration, and it required more labour and time consuming [1,2].

This requirement has led to new devices and method, especially the using of backscattered signal by particles in water has gained important with technological advances in recent years. The acoustic backscattering systems (ABS) has capability of simultaneously measuring with high spatial-temporal resolution of suspended sediment concentration, provide information on flow profiles and bedforms [3]. Acoustic Doppler velocimeter (ADV) operates an acoustic frequency and measures the phase change caused by the Doppler shift in acoustic frequency that occurs when a transmitted acoustic signal reflects off particles in the water. This property can provide information about the (SSC) in the water; although, they are designed for flow velocity measurements with using ABS [4,5].

Several studies have conducted with acoustic doppler velocimeter to estimate suspended sediment concentration (SSC) with using relationship between SNR (Signal to noise ratio) and measured SSC values. Hosseini et al. [6] observed strong relation between the concentration of the sediment and signal to noise ratio of the instrument. The sediment concentration measured conventionally from the siphon sampling to calibrate ADV devices and for producing a calibration curve relating backscattering intensity and sediment concentration. They found linear relationship with 0.02-0.1mm coefficients.

Salehi and Strom [7] examined the relationship between suspended sediment concentration (SSC) and the signal to noise ratio (SNR) with 6 MHz velocimeter in laboratory water. They used four different synthetic and natural mud mixtures and different combinations. For all sediment types and less than 1500 mg/l concentration, calibration equations were obtained of the obtained $\mathrm{Log}(SSC) = C_1 . SNR + C_2$; and R^2 values for all calibrated equations were greater than 0.98.

Ha et al. [8] conducted a laboratory experiment to reveal the relationship between acoustic backscatter strength and the SSC. They used three different Acoustic Doppler velocimeter (ADV) and with different frequencies (5, 10 and 16 MHz). Results showed that all devices had not a good linear relationship; however backscatter strength can be well correlated with the SSC. They suggested that an ADV could be a useful instrument to estimate suspended cohesive sediment concentration.

The known of the relationship between sediment particle size and Turbidity or SNR can be used continues monitoring of sediment transport at river for different sediment properties conditions. This study conducted at laboratory condition for similar river sediment conditions: different particle size and concentrations. The interaction of SSC with Turbidity and SNR were investigated and calibration equations were obtained to estimate SSC.

2. MATERIAL AND METHODS

The sediment tower (50 liters) was used to prepare suspended sediment which was mixed with a propeller operated by electric motor to supply homogeneity in tower. Natural sediment material was used as 0-50µm, 50-100µm, 100-200µm, and 200-250µm size groups. The first experiments result indicated that ADV was not capable measuring for high sediment concentration (SSC>1.5 mg.L^{-1}). That why, nearly 25 different concentration were used between 0.0 and 1.5 g L^{-1} for all

The signal was obtained by ADV devices, Sontek Flowtracker Handheld 10 Mhz ADV (Figure 1). FlowTracker uses acoustic Doppler technology to measure 2D in a small sampling volume located a fixed distance (10cm) from the probe. Sound generated by the transmitter bounces of suspended particles in the water. This reflected sound returns to the receivers, is averaged together by processor, and results in water velocity measurements that are recorded at a rate of once per second. The signal is a function of the amount and type of suspended sediments present in the sampling volume, as a result this ADV could be used to measure SSC if the acoustic response to sediment is known(Ha et al 2009). The calibration equation were were derived with relation of Signal to noise ratio (SNR) measured by an acoustic doppler velocimeter and known SSC of the water.

Corresponding author: Bingol University, Department of Biosystem Engineering, 12000, Bingol, Turkey. rmeral@bingol.edu.tr

sediment size groups. ADV read 60 values for per minute and total 120 SNR values were taken during 2 minutes for each concentration.

Figure 1. Acoustic Doppler Velocimeter (ADV), Sontek Flowtracker

The regression models were carried out to determine relationship between known sediment concentrations with measured SNR values. These relationships were evaluated by using determination coefficient (R^2) and root mean squared error (RMSE)

3. RESULTS AND DISCUSSION

Results of measurements showed that SNR values were increased depend on increasing of SSC (Fig 2). The really good relationships were obtained between SNR and SSC values for all sediment size groups. (R^2=0.9737-0.9977). These relations were observed for lower than 40 dB and 1 g.L^{-1} sediment concentrations. But for small size sediment group (<50µm) was obtained good results up to 2 g.L^{-1} concentration. The other point is SNR values are strongly affected from small chancing in sediment concentration. This property can be accepted as advantages for sensitive measurement for mentioned concentration intervals. Aydın [3] took into account this point and reported that SNR values can be used up to 0.4 g.L^{-1} concentration for flooding conditions at rivers. Similarly Ha et al.[8] obtained good linear relationship between SNR and SSC for 0.9 -1.5 g.L^{-1} concentration intervals, and the importance of devices frequency was emphasized their study. Salehi and Strom[7] used experimental data within these similar concentration range, to develop calibrated equations of the logarithmic linear form with R^2 values for all calibrated equations were greater than 0.98. In addition they indicated that the predicted SSC values are sensitive to changes in the coefficient constants.

The effect of particle size on calibration equation was observed especially for less than 50µm sediment size group in this study concentration. But the clear effect was not observed between the other size groups. It showed that a single calibration equation can be produced for higher than 50µm sediment size groups. Rouhnia et al.[9] concluded that the growth of mud flocs did influence the SNR recorded by the ADV, and that the sensitivity of the signal to changes in floc size was higher for flocs with diameters less than 80µm.

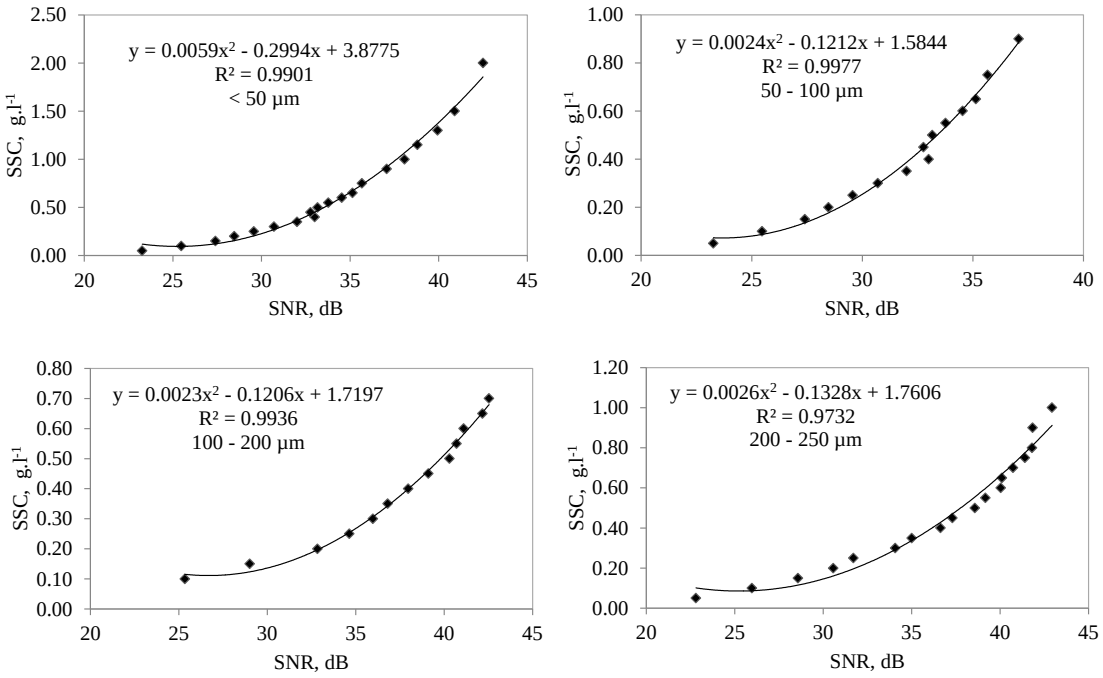

Figure 2. The relationship between sediment concentration and SNR

4. CONCLUSION

Acoustic method is promising alternative for continuous sediment monitoring but sediment size properties should be considered for each method. Acoustic Doppler velocimeter can be used to estimate suspended sediment concentration in the water; although, they are designed for flow velocity measurements. This study results showed that measured SNR values are strongly related with sediment concentration in water and it can be used sensitive estimation with calibration equation. This method has limitation for high concentration, but it can be advice to estimate concentration for except of flood river condition with to determine total sediment transportation with flow discharge.

REFERENCES

[1] P. D. Thorne and D. H. Hanes, A review of acoustic measurement of small-scale sediment processes. Cont. Shelf Res. 22, pp. 603-632, 2002.
[2] D.H. Schoellhamer and S.A. Wright, Continuous monitoring of suspended sediment discharge in rivers by use of optical backscatterance sensors. In: Bogen, J., Fergus, T., and Walling, D.E., Eds., Erosion and Sediment Transport Measurement: Technological and Methodological Advances, International Association for Hydrological Science Publication 283, p. 28-36, 2003.
[3] R. Aydın, Estimation of suspendent sediment concentration using acoustic methods. A Thesis Submitted to the Graduate School of Engineering an Sciences of Izmir Institute of Technology, 2009.
[4] F. Pedocchi, M.H. Garcia Acoustic measurement of suspended sediment concentration profiles in an oscillatory boundary layer, Cont. Shelf Res., 46 , pp. 87–95, 2012
[5] M. Guerrero, R.N. Szupiany, M. Amsler, Comparison of acoustic backscattering techniques for suspended sediments investigation, Flow Measurement and Instrumentation, 22(5), pp. 392–401, 2011
[6] S.A. Hosseini, A. Shamsai, B. Ataie-Ashtiani, Synchronous measurements of the velocity and concentration in low density turbidity currents using an Acoustic Doppler Velocimeter, Flow Measurement and Instrumentation, 17, pp. 59-68, 2006.
[7] M. Salehi and K. Strom, Using velocimeter signal to noise ratio as a surrogate measure of suspended mud concentration, Continental Shelf Research, 31, pp. 1020–1032, 2011
[8] H.K. Ha, W.Y. Hsu, J.P.Y. Maa, Y.Y. Shao, C.W. Holland, Using ADV backscatter strength for measuring suspended cohesive sediment concentration, Continental Shelf Research, 29, pp. 1310-1316, 2009
[9] M. Rouhnia, A. Keyvani, Strom, Do changes in the size of mud flocs affect the acoustic backscatter values recorded by a Vector ADV?. Continental Shelf Research, 84, pp. 84-92, 2014.

ICENS
INTERNATIONAL CONFERENCE ON ENGINEERING AND NATURAL SCIENCES
24-28 May 2016 /Sarajevo

An Integer Programming Based Heuristic for 3D-Packing Problem

Ahmet Reha Botsali[1]

Abstract

Placing rectangular boxes in a container is a well-known problem and it is referred as 3D-packing problem in the literature. The objective is to minimize the height of the used container space during packing. Since the problem is NP-Hard it is not possible to find optimal solutions for large sized problems. For this reason, there are several heuristic methods proposed for this problem in the literature. In this study, we compare two different models which are based on integer programming and constraint programming techniques. Initial results show that integer programming model performs better than constraint programming model. Yet, the effectiveness of the integer programming model decreases as the problem size gets larger. In order to find a trade-off between solution quality and the computation time, we propose a heuristic which is based on the integer programming model. The heuristic finds good quality solutions in reasonable time.

Keywords: *3D-Packing, Integer Programming, Optimization*

1. INTRODUCTION

Placing rectangular boxes into a container with respect to minimum space requirement is a well-known problem that gathers interest of both academicians and practitioners. The objective is to minimize the height of the used container space during packing. Since the problem is NP-Hard it is not possible to find optimal solutions for large sized problems. For this reason, there are several heuristic methods proposed for this problem in the literature. As an example [1] considers different box placement strategies and uses a Tabu search algorithm to minimize the height of the placed box in the container. He and Huang [2] propose an algorithm that is called Fit-Degree-Algorithm. Basically, this algorithm evaluates the degree of convenience of a box being placed with respected to the previously placed box. They compare their algorithm with several algorithms from the literature. Another approach in the literature is placing the box in the container creating layers or walls between different sets of placed boxes [3], [4]. In this study, we give two different models (integer programming and constraint programming) for finding the optimal solution for 3D rectangular packing problem and propose a heuristic based on the integer programming model.

Corresponding author: Necmettin Erbakan University, Department of Industrial Engineering, 42300, Meram/Konya, Turkey.
rbotsali@konya.edu.tr

2. OPTIMIZATION MODELS

It is possible to represent 3D packing problem as a mathematical programming or constraint programming model. In this section, both models are investigated. Below, first the constraint programming model is given.

2.1 Model Parameters

N: Number of boxes

XX: X dimension length of the container

YY: Y dimension length of the container

$dimx_{ij}$: X dimension length of box i for orientation j, $i \in \{1 \ldots N\}$, $j \in \{1 \ldots 6\}$

$dimy_{ij}$: Y dimension length of box i for orientation j, $i \in \{1 \ldots N\}$, $j \in \{1 \ldots 6\}$

$dimz_{ij}$: Z dimension length of box i for orientation j, $i \in \{1 \ldots N\}$, $j \in \{1 \ldots 6\}$

2.2 Model Variables

ZZ: Minimum required height of the container

x_i: X coordinate of the center of the box i, $i \in \{1 \ldots N\}$

y_i: Y coordinate of the center of the box i, $i \in \{1 \ldots N\}$

z_i: Z coordinate of the center of the box i, $i \in \{1 \ldots N\}$

t_i: Orientation of the box i, $i \in \{1 \ldots N\}$, $t_i \in \{1 \ldots 6\}$

nx_{ij}: Binary variable takes value 1 if box i's and j's projections intersects on the x coordinate, $i\epsilon \{1\ldots N\}$, $j\epsilon \{1\ldots N\}$

ny_{ij}: Binary variable takes value 1 if box i's and j's projections intersects on the y coordinate, $i\epsilon \{1\ldots N\}$, $j\epsilon \{1\ldots N\}$

nz_{ij}: Binary variable takes value 1 if box i's and j's projections intersects on the z coordinate, $i\epsilon \{1\ldots N\}$, $j\epsilon \{1\ldots N\}$

2.3 Objective Function and the Constraints

Minimize ZZ (1)

Subject to:

$$ZZ \geq z_i + dimz_{it_i}/2 \qquad \forall i \in \{1..N\} \qquad (2)$$

$$x_i \geq dimx_{it_i}/2 \qquad \forall i \in \{1..N\} \qquad (3)$$

$$y_i \geq dimy_{it_i}/2 \qquad \forall i \in \{1..N\} \qquad (4)$$

$$z_i \geq dimz_{it_i}/2 \qquad \forall i \in \{1..N\} \qquad (5)$$

$$x_i \leq XX - dimx_{it_i}/2 \qquad \forall i \in \{1..N\} \qquad (6)$$

$$y_i \leq YY - dimy_{it_i}/2 \qquad \forall i \in \{1..N\} \qquad (7)$$

$$nx_{ij} + ny_{ij} + nz_{ij} \geq 1 \qquad i < j,\ \forall i,j \in \{1..N\} \qquad (8)$$

$$\left|x_i - x_j\right| \geq nx_{ij}.(dimx_{it_i} + dimx_{jt_j})/2 \qquad i < j,\ \forall i,j \in \{1..N\} \qquad (9)$$

$$\left|y_i - y_j\right| \geq ny_{ij}.(dimy_{it_i} + dimy_{jt_j})/2 \qquad i < j,\ \forall i,j \in \{1..N\} \qquad (10)$$

$$\left|z_i - z_j\right| \geq nz_{ij}.(dimz_{it_i} + dimz_{jt_j})/2 \qquad i < j,\ \forall i,j \in \{1..N\} \qquad (11)$$

In the above model, the first constraint set ensures that minimum used height of the container (ZZ) should be larger than the top faces of all boxes. Constraint sets (3)-(7) state that the boxes should be placed within the container boundaries. Constraint set (8) states that at least one of the projections of two different boxes on X, Y or Z axis should not intersect with each other. If this constraint does not hold for a particular pair of boxes, this means the volume of these boxes intersect with each other and this is not feasible. Constraint sets (9)-(11) guarantee that if projections of a pair of boxes do not intersect on a particular axis, then on this axis, the projections of these boxes should not touch to each other.

The above optimization model can be solved for different sized problem using IBM ILOG's CP Solver. However, as the size of the problem gets larger, finding the optimal solution becomes more difficult. Another alternative can be using IBM ILOG's Cplex Solver which is highly effective for solving integer linear programming problems. However, using variables as parameter indices as seen in above constraints does not conform to integer linear programming standards. In order to model this problem as an integer linear programming model, the following additional variables are introduced.

2.4 Additional Variables

mx_{ij}: Binary variable takes value 1 if the projections of boxes *i* and *j* on the X axis do not intersect and box *i* is on the left of box *j* with respect to X axis. $i,j\epsilon \{1\ldots N\}$, $i\neq j$

my_{ij}: Binary variable takes value 1 if the projections of boxes *i* and *j* on the Y axis do not intersect and box *i* is on the left of box *j* with respect to Y axis. $i,j\epsilon \{1\ldots N\}$, $i\neq j$

mz_{ij}: Binary variable takes value 1 if the projections of boxes *i* and *j* on the Z axis do not intersect and box *i* is on the left of box *j* with respect to Z axis. $i,j\epsilon \{1\ldots N\}$, $i\neq j$

o_{ij}: Binary variable takes value 1 if box *i* is placed in the *j*th orientation, $i\epsilon \{1\ldots N\}$, $j\epsilon \{1\ldots 6\}$

dx_i: X dimension length of the box $i,i\epsilon \{1\ldots N\}$

dy_i: Y dimension length of the box $i,i\epsilon \{1\ldots N\}$

dz_i: Z dimension length of the box $i,i\epsilon \{1\ldots N\}$,

With the addition of these new variables, the following integer linear programming model is constructed. In the model, *M* stands for a very large number.

2.5 Integer Linear Programming Model

Minimize ZZ (12)

Subject to:

$ZZ \geq z_i + dz_i/2 \quad \forall i \in \{1..N\}$ (13)

$x_i \geq dx_i/2 \quad \forall i \in \{1..N\}$ (14)

$y_i \geq dy_i/2 \quad \forall i \in \{1..N\}$ (15)

$z_i \geq dz_i/2 \quad \forall i \in \{1..N\}$ (16)

$x_i \leq XX - dx_i/2 \quad \forall i \in \{1..N\}$ (17)

$y_i \leq YY - dy_i/2 \quad \forall i \in \{1..N\}$ (18)

$mx_{ij} + my_{ij} + mz_{ij} + mx_{ji} + my_{ji} + mz_{ji} \geq 1 \quad i < j,\ \forall i,j \in \{1..N\}$ (19)

$x_i - x_j \geq (dx_i + dx_j)/2 - (1 - mx_{ji}).M \quad i < j,\ \forall i,j \in \{1..N\}$ (20)

$x_j - x_i \geq (dx_i + dx_j)/2 - (1 - mx_{ij}).M \quad i < j,\ \forall i,j \in \{1..N\}$ (21)

$y_i - y_j \geq (dy_i + dy_j)/2 - (1 - my_{ji}).M \quad i < j,\ \forall i,j \in \{1..N\}$ (22)

$y_j - y_i \geq (dy_i + dy_j)/2 - (1 - my_{ij}).M \quad i < j,\ \forall i,j \in \{1..N\}$ (23)

$z_i - z_j \geq (dz_i + dz_j)/2 - (1 - mz_{ji}).M \quad i < j,\ \forall i,j \in \{1..N\}$ (24)

$z_j - z_i \geq (dz_i + dz_j)/2 - (1 - mz_{ij}).M \quad i < j,\ \forall i,j \in \{1..N\}$ (25)

$\sum_{j=1}^{6} dimx_{ij} \,.\, o_{ij} = dx_i \quad \forall i \in \{1..N\}$ (26)

$\sum_{j=1}^{6} dimy_{ij} \,.\, o_{ij} = dy_i \quad \forall i \in \{1..N\}$ (27)

$\sum_{j=1}^{6} dimz_{ij} \,.\, o_{ij} = dz_i \quad \forall i \in \{1..N\}$ (28)

$\sum_{j=1}^{6} o_{ij} = 1 \quad \forall i \in \{1..N\}$ (29)

In the integer linear programming model, the objective function remains same. Constraint sets (13)-(18) defines the boundary of the container. The conditions stated by constraint sets (9)-(11) in constraint programming model are ensured by constraint sets (19)-(25). The length of x, y and z axis dimensions of a box is determined by one of its six possible orientations as shown by constraint sets (26)-(28). Finally, constraint set (28) ensures that each box has a particular orientation.

Table 1 compares the performance of these two models on sample data. The x and y dimensions of the container is 20x20 units. The dimensions of the boxes are randomly generated between 1 and 20 units. Although, the performance of integer linear programming model is better than constraint programming model, as the problem size gets larger, finding the optimal solution gets more difficult even by integer linear programming model. For this reason we propose a heuristic based on integer linear programming model. The details of the heuristic is given in the next section.

Table 8. Solution time comparison of integer linear and constraint programming models

Problem Size as Number of Boxes	5	8	10	12	15
Time Required by Integer Linear Programming Model	0,06 secs	0,73 secs	3,94 secs	9,5 secs	2567 secs
Time Required by Constraint Programming Model	0,19 secs	1,17 secs	561,14 secs	>30000 secs	>30000 secs

3. PROPOSED HEURISTIC

As given in the previous section, for small sized problems, the linear integer programming model finds the optimal solution. Taking this fact into account, the original set of boxes is divided into groups and starting from the bottom of the container each group of boxes is placed on the previously placed groups of boxes optimally. This heuristic is tested on sample data

where the x and y dimensions of the container is 20x20 units. The dimensions of the boxes are randomly generated between 1 and 20 units and the problem size is a hundred boxes.

Table 2. Heuristic performance for a problem size of 100 boxes

Number of Boxes per Group	1	2	3	4	5	6	7	8	9	10
Best Solution Found for Container Height (cm)	402	393	395	377	379	374	375	366	363	364
Time Required by the Heuristic (secs)	36,82	19,61	18,01	30,32	43,54	82,66	130,56	256,22	245,88	421,99

The results given in Table 2 show that even for a 100 boxes sized problem, this method generates solutions in reasonable time. On the other hand, the quality of the solutions found by the heuristic depends on the order of boxes and the box groups in addition to the size of the box groups. As the test data show, increasing the number of boxes per group generally increases the solution quality. In the most extreme case when there is only one group of boxes, the heuristic becomes as solving the original integer linear programming model.

4. CONCLUSIONS

In this study, we analyze 3D-packing problem and provide two different optimization models. Initial computations show that the performance of the integer linear programming model is better than the performance of the constraint programming model. Yet as the problem size gets larger, optimization models cannot find the optimal solution in reasonable time. For this reason, a heuristic based on solving a sequence of integer linear programming model for a group of boxes is proposed. The performance of this heuristic depends on the size and the order of how groups chosen. it is possible to extend and embed this heuristic in popular meta-heuristic techniques like simulated annealing, Tabu search, etc. and currently, the author is working on this issue.

REFERENCES

[1] Allen, S. D., Burke, E. K., & Kendall, G. (2011). A hybrid placement strategy for the three-dimensional strip packing problem. European Journal of Operational Research, 209(3), 219–227. http://doi.org/10.1016/j.ejor.2010.09.023

[2] He, K., & Huang, W. (2011). An efficient placement heuristic for three-dimensional rectangular packing. Computers and Operations Research, 38(1), 227–233. http://doi.org/10.1016/j.cor.2010.04.015

[3] Bischoff, E. E., & Ratcliff, M. S. W. (1995). Issues in the development of approaches to container loading. Omega, 23(4), 377–390. http://doi.org/10.1016/0305-0483(95)00015-G

[4] George, J. A., & Robinson, D. F. (1980). A heuristic for packing boxes into a container. Computers and Operations Research, 7(3), 147–156. http://doi.org/10.1016/0305-0548(80)90001-5

ICENS
INTERNATIONAL CONFERENCE ON ENGINEERING AND NATURAL SCIENCES
24-28 May 2016 /Sarajevo

Minimization of Network Construction Cost for a Given Failure Probability

***Ahmet Reha Botsali*[1] , *Mehmet Aktan*[2]**

Abstract

Reliability of networks is an important issue that arises in different problem settings. In this study we focus on the initial construction of a network. Each edge in the network has a specific cost and this cost incurs if the related edge is included in the network construction. In addition to the cost factor, each edge has a specific reliability level which shows the probability that the connection represented by that edge will be working at a particular time. Our objective is to minimize the total cost of the edges included in the network construction. On the other hand, the constructed network should satisfy a minimum probability level such that all the nodes of the network are connected to each other at any given instance. We present a simulated annealing algorithm for this problem and share our preliminary results.

Keywords: *Network Construction, Reliability, Optimization, Simulation*

1. INTRODUCTION

Network design is one of popular problems that attracts attention of researchers from different disciplines. This problem may arise in many different settings such as the design of power networks, design of circuit boards, construction of highways in a country, etc. The common point in these problems is the network structure that is going to be constructed. Basically, a network is composed of a set of nodes and a set of edges. The edges between network nodes show the relationship between nodes. Depending on the direction of the edges, networks can be directed or undirected. In Figure 1, two sample networks are displayed.

Reliability is another issue related to the functioning of networks. In this study, we define reliability as the probability level that the network system functions properly. The reliability level of the network is important with respect to the outcomes of the network failure. For instance, building a supply chain with unreliable partners may result in considerable profit loss or constructing a power transmission system with materials having high failure rates may result in frequent power cuts.

There are various studies in the literature on the network design and reliability Simulation has been used in literature to estimate network reliability. Wagner et al. [1] used simulation as a complementary method for analyzing the reliability of water distribution networks. For this simulation, the distribution system is modeled as a network whose pipes and pumps fail randomly, according to probability distributions with user-specified parameters. Similarly, Najm et al. [2] used simulation to estimate the expected current waveform required for the analysis of electromigration failures in power supply and ground buses of CMOS VLSI circuits.

Heuristic search algorithms have been used on network reliability optimization problems. Atiqullah and Rao [3] presented an algorithm which selects the optimal set of links that maximizes the overall reliability of a network subject to a cost restriction, given the allowable node-link incidences, the link costs and the link reliabilities. The algorithm employed a variation of the simulated annealing (SA) approach coupled with a hierarchical strategy to achieve the global optimum. Pierre et al. [4] presented an application of SA to the problem of designing computer communication networks to find the least-cost network topologies that satisfies a given set of performance and reliability constraints. Ravi et al. [5] applied a non-equilibrium SA technique to find the global optimum of system cost of two kinds of complex systems subject to constraints on system reliability and the optimum number of redundancies which maximize the system reliability, subject to constraints on system cost, weight, and volume in a multistage mixed system. Cunha and Sousa [6] applied SA to search for the least-cost design of a looped water distribution network. Deeter and Smith [7] used genetic algorithms (GA) to design networks when considering all-terminal reliability byminimizing cost given a reliability constraint. They allowed links to be chosen from different components with different costs and reliabilities. Dengiz et al. [8,9] presented GA with specialized encoding, initialization, and local search operators to optimize the design of communication network topologies.

[1]*Corresponding author: Necmettin Erbakan University, Department of Industrial Engineering, 42300, Meram/Konya, Turkey.*
rbotsali@konya.edu.tr

[2]*Necmettin Erbakan University, Department of Industrial Engineering, 42300, Meram/Konya, Turkey.*
maktan@konya.edu.tr

Srivaree-ratana et al. [10] considered to use artificial neural networks (ANN) as an alternative to Monte Carlo (MC) simulation for the estimation of all-terminal network reliability. They used the reliability estimates of the ANN on SA to search for the optimal network design. Papadrakakis and Lagaros [11] examined the application of ANN to reliability-based structural optimization of large-scale structural systems with evolution strategies, while the reliability analysis is carried out with the MC simulation. Altıparmak et al. [12] et al. compared the performances of hill climbing, SA and GA on maximizing reliability of computer communication networks with a fixed topology, subject to cost. Ramirez-Marquez and Coit [13] presented and compared a MC simulation approach that obtains accurate approximations to multi-state two-terminal network reliability. Ramirez-Marquez and Rocco [14] combined probabilistic solution discovery and MC simulation to minimize the cost of all-terminal networks subject to a reliability requirement. Altıparmak et al. [15] suggested a new encoding method for using ANN models to estimate the reliability of telecommunications networks with identical link reliabilities, using a compact, general set of inputs that describe the likely network reliability. Yeh et al. [16] proposed a particle swarm optimization algorithm based on MC simulation to minimize cost under reliability constraints for complex network reliability optimization problems. Gupta et al. [17] presented a GA based method to improve the reliability and power quality of distribution systems using network reconfiguration by defining two new objective functions to address power quality and reliability issues (such as feeder power loss, system's node voltage deviation, system's average interruption frequency index, system's average interruption unavailability index and energy not supplied) for the reconfiguration problem.

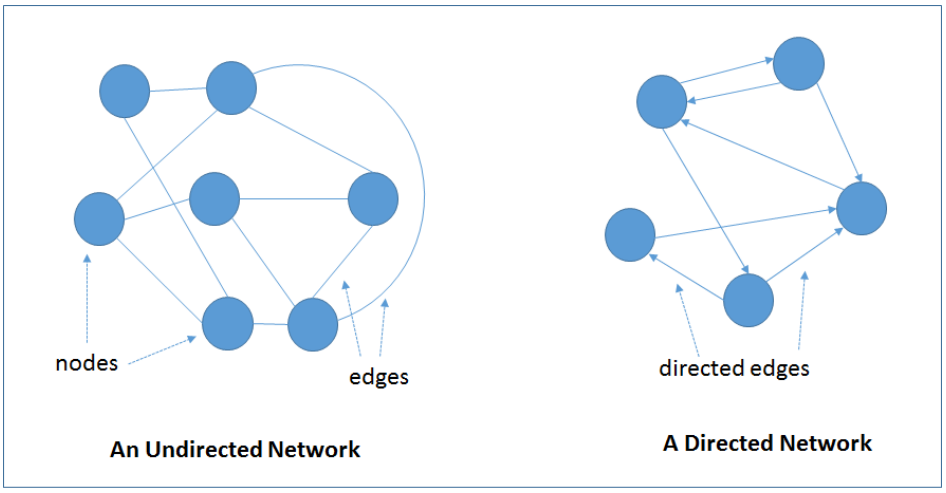

Figure 6. Network Examples

Mainly, the literature analyze network reliability problem when there is a disruption probability for the facilities on the network. In fact, network reliability can be analyzed from two perspectives which are the reliability of the connections and the reliability of facilities. In this study, we focus on the connections and assume that network reliability depends on the failure rate of the connections.

2. NETWORK DESIGN AND SEARCH ALGORITHM

Similar to our previous study [18], the network design problem analyzed in this study assumes that the nodes and the potential edges between these nodes are known in advance. Each potential edge can be included in the network design with some cost. Furthermore, each edge has a failure probability in case it is included in network design. A network fails whenever there exist a node pair between which it is not possible to travel due to failure of one or more edges. The objective is to find the minimum cost network design such that the probability of network failure is above a certain level. As given in [18], this problem can be modeled as a mathematical programming model using the below parameters and variables.

***N*:** The set of nodes in the network

***E*:** The set of available edges that can be included in network design

c_{ij}**:** Cost of including the edge between nodes i and j in network design, $(i,j) \in E$

p_{ij}**:** Reliability probability showing that the edge between nodes i and j in network design does not fail, $(i,j) \in E$

***T*:**Minimum required reliability level of the network

x_{ij}**:** Binary decision variable that gets value one if the edge between nodes i and j is included in network design $(i,j) \in E$

S: Set of selected edges $(i,j) \in E$ where $x_{ij}=1$,

f(S): Reliability function showing the failure probability of the network with respect to the existing edges (S) (f*()* depends on x_{ij} and p_{ij} values where $(i,j) \in S$)

$$\min \sum_{(i,j)\in E} c_{ij} x_{ij} \quad (1)$$

$$f(S) \geq T \quad (2)$$

$$x_{ij} \in (0,1) \quad (3)$$

Although the above model seems simple, the difficulty of calculating the value of reliability function ***f0*** for a given set of existing edges makes it impractical. However, it is still possible to estimate the value of function ***f0*** using Monte Carlo simulation (Kroese et al. 2014). The pseudo-code of the simulation is given in Figure 2.

As it is seen, the failure probability of a given network design can be estimated computationally. This enables us to use different meta-heuristic techniques (such as genetic algorithms, simulated annealing, Tabu search etc.) to search over

different network design alternatives in order to find the minimum cost network design attaining the required reliability level A simulated-annealing for this problem is given in Figure 3.

1. Set *Reliability* to 0
2. For 1 to *Number_of_Simulation_Runs*
   - 2.1. Set *Temporary_Network* with no edges
   - 2.2. For each edge *(i,j)* in *Selected_Edges_Set_S*
     - 2.2.1. Create a random number *r* between [0,1]
     - 2.2.2. If $r \leq p_{ij}$ then add edge *(i,j)* to *Temporary_Network*
   - 2.3. If *Temporary_Network* is reliable then increase *Reliability* by 1
3. *Reliability = Reliability/Number_of_Simulation_Runs*
4. If *Reliability* ≥ *Target_Reliability_Level_T* then Network with *Selected_Edges_Set_S* is reliable.

Figure 2. Simulation algorithm to test reliability of a network with selected edge set s

The simulated algorithm shown in Figure 3 is similar to the one suggested by Botsalı and Aktan, [18] with a change. In this study, we start the simulated annealing algorithm with a network with all possible edges instead of a reliable network design that is found during random network design generations. By this way, we guarantee the feasibility of the solution at the beginning. At each iteration of the algorithm, current network design is modified either adding or canceling an edge randomly. When the modified solution satisfies reliability level requirement and has a better cost value than the current solution's cost value, then this modified solution is accepted as the current network design. If the modified solution has a worse cost value, then it is accepted with some probability as shown in Step 8.1.3.2.2. of Figure 3. The acceptance probability of worse solutions decreases as the temperature parameter of the algorithm decreases during the iterations. The reason for accepting a worse solution during search iterations is to encourage the algorithm to explore a higher portion of the search space. Throughout the iterations, the best solution found so far is stored and the temperature parameter is decreased gradually using a cooling rate parameter. When the temperature parameter of the algorithm drops below a specified limit, the algorithm terminates and the best solution found by the algorithm is displayed.

1. Set *Selected_Edge_Set_S* to all possible edges
2. Set *Best_Network = Current_Network;*
3. Set *Best_Network_Cost = Current_Network_Cost;*
4. Set *Current_Temperature*
5. Set *Finish_Temperature*
6. Set *Cooling_Rate* between [0,1]
7. Set *Number_of_Iterations*
8. While *Current_Temperature* ≥ *Finish_Temperature*
   - 8.1. For 1 to *Number_of_Iterations*
     - 8.1.1. Create *New_Network* and a *New_Selected_Edge_Set_S* _from *Current_Network* by adding or deleting an edge randomly to/from *Selected_Edge_Set_S*
     - 8.1.2. Check *Reliability* of *New_Network* using Monte Carlo simulation

8.1.3. If *Reliability* of *New_Network* ≥ *Target_Reliability_Level_T*

8.1.3.1. If *New_Network_Cost* ≤ *Current_Network_Cost;*

8.1.3.1.1. Set *Current_Network* = *New_Network*

8.1.3.1.2. Set *Selected_Edge_Set_S*= *New_Selected_Edge_Set_S*

8.1.3.1.3. If *New_Network_Cost* ≤ *Current_Network_Cost*

8.1.3.1.3.1. Set *Best_Network* = *Current_Network*

8.1.3.1.3.2. Set *Best_Network_Cost* = *Current_Network_Cost*

8.1.3.1.3.3. Set *Best_Selected_Edge_Set_S*= *New_Selected_Edge_Set_S*

8.1.3.2. If *New_Network_Cost*>*Current_Network_Cost;*

8.1.3.2.1. Create a random number *r* between [0,1]

8.1.3.2.2. If $r \leq e^{(Current\_Network\_Cost - New\_Network\_Cost)/Current\_Temperature}$

8.1.3.2.2.1. Set *Current_Network* = *New_Network*

8.1.3.2.2.2. Set *Selected_Edge_Set_S*= *New_Selected_Edge_Set_S*

8.2. Set *Current_Temperature* = *Cooling_Rate* x *Current_Temperature*

9. Display *Best_Network*, *Best_Network_Cost* and *Best_Selected_Edge_Set_S*

Figure 3. Simulated annealing algorithm to find minimum cost network with accepted reliability level

3. COMPUTATIONAL RESULTS

The algorithm is tested on several sized networks. The beginning and ending temperatures of the simulated annealing algorithm is set to 300 and 0.01, respectively. At each temperature, 15 neighborhood solutions are visited which are found either adding an edge or deleting and existing edge on the current solution. The cooling rate is set to 0.9. The reliability level is 0.8 It is set that 80% of the modifications on the current network solution is done by deleting a random existing edge and the remaining 20% of the modifications is done by adding a potential edge to the current network design. The edge cost and reliability parameters are generated randomly on intervals [0.8,1] and [0,10] respectively. A reliability of a network design is computed via 2000 iterations of Monte Carlo simulation. A typical convergence process of the algorithm is shown on Figure 4 for a problem instance.

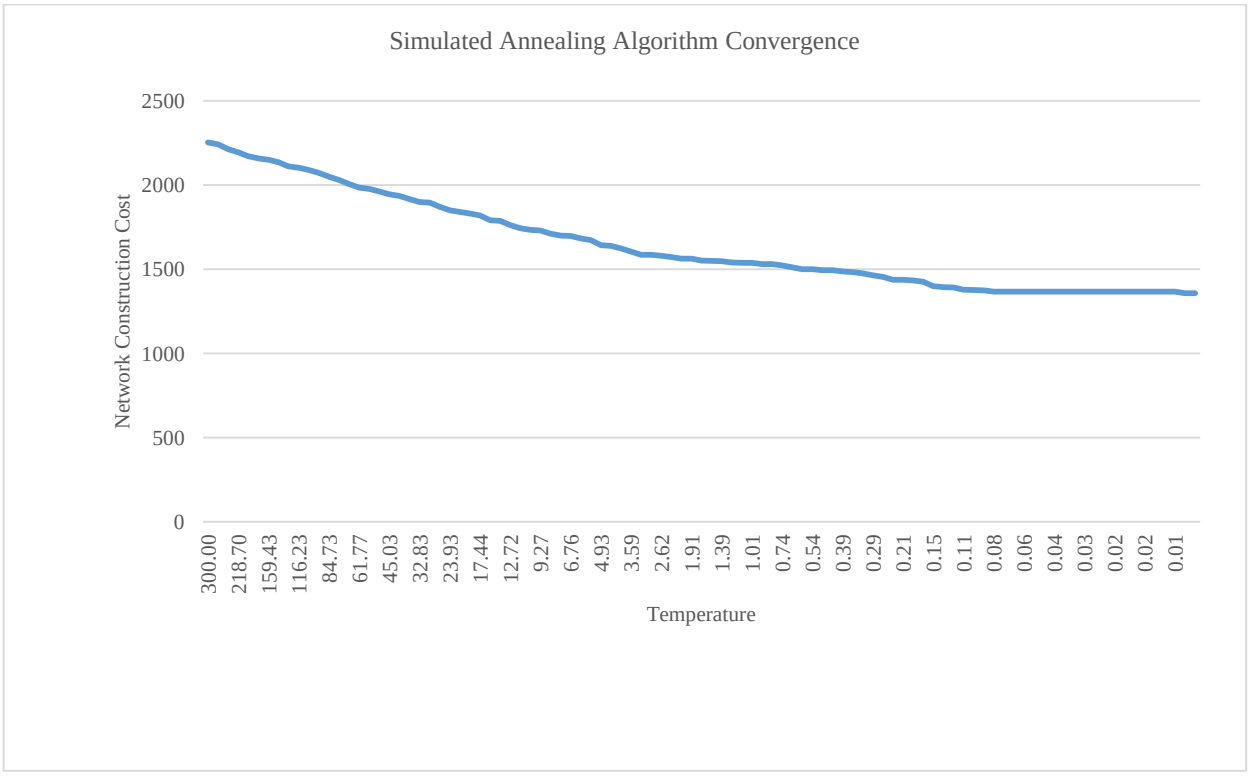

Figure 4. Simulated annealing algorithm convergence for a network with 30 nodes

Table 1 shows the result of the algorithm for five different instances. The solutions found by the algorithm generally decreases the total cost of including all potential edges in the network design by a percentage amount changing between 17.44% and 39.73%. In addition the computation time increases as the size of the network increases. This is due to the fact that the number of edges on a network with n nodes increases by $o(n^2)$.

Table 9. Computational results

Number of Nodes	All Edge Cost	Final Solution Cost	% Improvement to All Edge Cost	Time Required
10	218,2	164,9	24,41%	364,8
20	965,5	640,4	33,67%	885,2
30	2252,8	1357,8	39,73%	1479,9
40	3903,3	2687,1	31,16%	2382,6
50	6169,4	5093,26	17,44%	4003,1

4. CONCLUSIONS

Network reliability is an important issue that arises in different application areas. We focus on the reliability of connections in a network and propose Monte Carlo simulation to estimate the failure probability of a given network. We use simulated annealing algorithm and Monte Carlo simulation to find minimum cost network designs whose reliability is above a target level. Our preliminary computational results show that the algorithm has a performance of reducing the cost of including all potential edges in the network design by 17% to 40% by eliminating some of the edges. This computational approach can be used in many different ways in designing networks with reliability constraints. Currently, authors are working on the performance of different search algorithms on network design problem.

There are possible extensions. For example, failure probability can be assigned to nodes as well as edges or networks with directed edges can be designed instead of undirected networks. Regardless of the additional problem characteristics, the same simulation based search procedures can be applied to the new problems.

REFERENCES

[1] J. M. Wagner, U. Shamir, and D. H. Marks, "Water distribution reliability: simulation methods," J. Water Resour. Plann. Manage., 1988, Vol. 114, pp. 276-294.
[2] F. N. Najm, R. Burch, P. Yang, and I. N. Hajj, "Probabilistic simulation for reliability analysis of CMOS VLSI circuits," IEEE Transactions On Computer-Aided Design, 1990, Vol. 9, No. 4, pp. 439-450.
[3]. M. M. Atiqullah and S. S. Rag, "Reliability optimization of communication networks using simulated annealing," Microelectron. Reliab., 1993, Vol. 33, No. 9, pp. 1303-1319.
[4] S. Pierre, M-A. Hyppolite, J-M. Bourjolly, and O. Dioume, "Topological design of computer communication networks using simulated annealing," Engng. Applic. Artif. Intell., 1995, Vol. 8, No. 1, pp. 61-69.
[5] V. Ravi, B. S. N. Murty, and P. J. Reddy, "Nonequilibrium simulated annealing-algorithm applied to reliability optimization of complex systems," IEEE Transactions on Reliability, 1997, Vol. 46, No. 2, pp. 233-239.
[6] M. C. Cunha and J. Sousa, "Water distribution network design optimization: simulated annealing approach," J. of Water Resources Planning and Management, 1999, Vol. 125, pp. 215-221.
[7]. D. L. Deeter and A. E. Smith, "Heuristic optimization of network design considering all-terminal reliability," in Proc. Annual Reliability and Maintainability Symp. 1997, p. 194.
[8] B. Dengiz, F. Altıparmak, and A. E. Smith, "Local search genetic algorithm for optimal design of reliable networks," IEEE Transactions on Evolutionary Computation, 1997, Vol. 1, No. 3, pp. 179-188.
[9] B. Dengiz, F. Altıparmak, and A. E. Smith, "Efficient optimization of all-terminal reliable networks, using an evolutionary approach," IEEE Transactions on Reliability, 1997, Vol. 46, No. 1, pp. 18-26.
[10] C. Srivaree-ratana, A. Konak, and A. E. Smith, "Estimation of all-terminal network reliability using an artificial neural network," Computers & Operations Research, 2002, Vol. 29, pp. 849-868.
[11] M. Papadrakakis and N. D. Lagaros, "Reliability-based structural optimization using neural networks and Monte Carlo simulation," Comput. Methods Appl. Mech. Engrg., 2002, Vol. 191, pp. 3491–3507.
[12] F. Altıparmak, B. Dengiz, and A. E. Smith, "Optimal design of reliable computer networks: a comparison of metaheuristics," J. of Heuristics, 2003, Vol. 9, pp. 471–487.
[13] J. E. Ramirez-Marquez and D. W. Coit, "A Monte-Carlo simulation approach for approximating multi-state two-terminal reliability," Reliability Engineering and System Safety, 2005, Vol. 87, pp. 253–264.
[14] J. E. Ramirez-Marquez and C. M. Rocco, "All-terminal network reliability optimization via probabilistic solution discovery," Reliability Engineering and System Safety, 2008, Vol. 93, pp. 1689–1697.
[15] F. Altıparmak, B. Dengiz, and A. E. Smith, "A general neural network model for estimating telecommunications network reliability," IEEE Transactions on Reliability, 2009, Vol. 58, No. 1, pp. 2-9.
[16] W. Yeh, Y. Lin, Y. Y. Chung, and M. Chih, "A particle swarm optimization approach based on Monte Carlo simulation for solving the complex network reliability problem," IEEETransactions on Reliability, 2010, Vol. 59, No. 1, pp. 212-221.
[17] N. Gupta, A. Swarnkar, K. R. Niazi, "Distribution network reconfiguration for power quality and reliability improvement using genetic algorithms," Electrical Power and Energy Systems, 2014, Vol. 54, pp. 664–671.
[18] A.R. Botsalı and M. Aktan, "Network Construction with respect to Cost and Reliability Factors", Proceedings of 3rd International Conference on Modern Research's in Management, Economics & Accounting, 2016, İstanbyul, Turkey.

The Effect of Fin Spacing on Forced Convection Heat Transfer over Horizontal Tube with Conical Fins

***Gulay Yakar*[1]**

Abstract

In this study, the effect of fin spacing on forced convection heat transfer over a horizontal tube with conical fins was investigated experimentally. The experiments were carried out at three different fin spacings (10, 12 and 15 mm) in order to determine the best fin spacing. Working fluids used in the experiments were water as hot fluid and air as cold fluid. The temperature of hot fluid was 65 °C. The cold fluid was entered to the test section at eight different air flow velocities (2 – 20 m/s). Moreover, inclination angle of conical fins placed on a horizontal tube was 45º. Experimental results showed that heat transfer rates for 15 mm fin spacing were higher than those for 12 mm fin spacing at high Reynolds numbers while these rates were approximately equal at low Reynolds numbers. In addition, the heat transfer rates for 10 mm were lower than those for 12 mm and 15 mm for all Reynolds numbers.

Key words:*Conical fin, fin spacing, heat transfer, forced convection.*

1. INTRODUCTION

Many enhancement techniques divided as active and passive are used in order to increasing the thermal performance of heat exchangers. These techniques have been studied by many researchers. Mikielewicz et al. [1] made a three fold approach in order to investigate the air flow in the wind tunnel featuring transverse and inclined vortex generators. Fan et al. [2] studied characteristics of heat transfer, flow resistance and overall thermo hydraulic performance of turbulent airflow in a circular tube fitted with louvered strip inserts through numerical simulation. Their all data showed that the louvered strip is a promising tube insert which would be widely used in heat transfer enhancement of turbulent flow. Tan et al. [3] empirically investigated the heat transfer enhancement in a tube fitted with a square cut circular ring insert in the transitional and the fully turbulent flow regimes. Yakar and Karabacak [4] experimentally examined the thermal performance of perforated finned heat exchangers with angle of rotation θ. Their results showed an increase in effectiveness with an increasing number of transfer units. Thianpong et al. [5] experimentally investigated heat transfer, friction factor and thermal performance characteristics in a tube equipped withtwisted - rings. Şahin et al. [6] studied experimentally and numerically the heat performance and friction characteristics of a novel concentric tube heat exchanger with different pitches of helical turbulators for a Reynolds number range from 3000 to 14000. Their results showed that the heat transfer enhancements using turbulators were 2.91, 2.41, 2.18 and 1.99 times better than smooth tube for pitch distances of 20, 40, 60 and 80 mm, respectively. Aydin et al. [7] experimentally carried out decaying turbulent swirl flow in a circular tube. Muthusamy et al. [8] investigated heat transfer, friction factor and thermal performance factor in a cylindrical tube with conical cut out turbulator integrated with internal fins. Jasinski [9] presented results of the computer simulations of the flow in a circular pipe with a ball insertsturbulising the flow. The results of this syudy showed a googd correlation between the experiment and computer modelling.

Cafiero et al. [10] tested a new passive method for the heat transfer enhancement of “circular impinging jets. Their results indicated that the fractal turbulence promoter can provide a significant heat transfer enhancement for relatively small nozzle to plate separation. Zohir et al. [11] studied the effect of pulsation with different amplitudes on the heat transfer rates in a double tube heat exchanger with around the outer surface of the inner tube. Rivier et al. [12] examined the performances of a turbulator in respect to heat transfer and fluid friction characteristics in a heat exchanger tube. Sheikholeslami et al. [13] experimentally investigated turbulent flow and heat transfer in an coiled wire insertsair to water double tube heat exchanger. Chumpia and Hooman [14] tested five specimens of aluminium foam wrapped tubular heat exchanger for heat transfer performance and pressure drop characteristics. They presented the correlations to estimate the overall thermal resistance and pressure drop.

The goal of this study is to examine the effect of different conical fin spacings on heat transfer enhancement. In the experiments, conical fins for cross flow are used instead of traditional circular fins.

[1] *Corresponding author: Pamukkale University, Departmentof Mechanical Engineering, 20070, Kınıklı/Denizli, Turkey.*
gyakar@pau.edu.tr.

2. EXPERIMENTAL SET UP

The schematic diagram of the experimental set – up is shown in Figure 1.

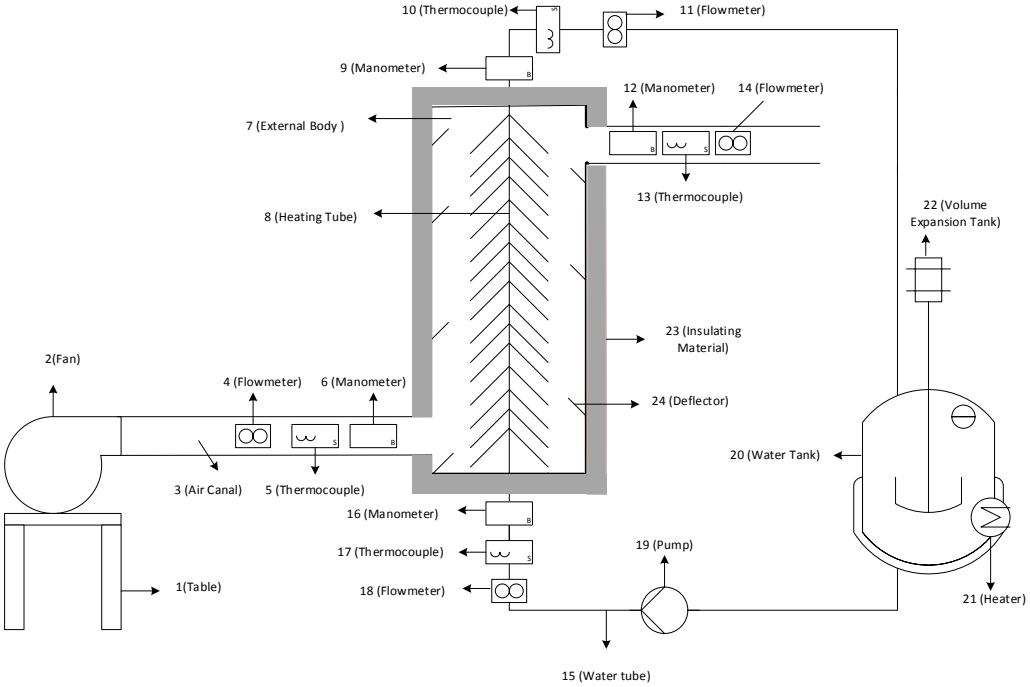

Figure 1.Scheme of experimental set up

In the set up seen in Figure 1, the air from a variable speed fan (number 2) which was placed on a table(number 1) is directed into the external body (number 7). The channel (number 3) length before the test section is long to obtain a fully developed flow at the entrance to the test section. The mass air flow rate at the entrance and at the exit of the test section was measured by a propeller type flow meter (number 4 and number 14). The inlet air velocity was adjusted by the fan. Inlet and exit air temperatures were measured by T type copper constant thermocouples (number 5 and number 13). The temperatures at the fin base (T_s) and between the conical fins (T_∞) were measured by termocouples of the same type at distances of 15, 45 and 75 cm along the test section. The input and output pressure difference of the air across the test section was measured by a manometer (number 6 and number 12). The tube side material in which water flows is galvanized steel (number 8). The conical fin material was also galvanized steel. Besides, the pressures (number 9 and number 16), temperatures (number 10 and number 17), and volumetric flow rate (number 11 and number 18) of the heating water were measured at the inlet and the exit of the heating tube. Theheating water was carried to the test section by a tube (number 15).The heating water, on the other hand, was heated by electrical heaters (number 21) that are located inside the 250 L water tank (number 20). The hot water was carried from the water tank to the test section by a pump (number 19). The body into which the test tube with conical fins was located was well insulated to minimize convective heat loss to surroundings. Moreover, the route of the air around the test tube with conical fins was lengthened by means of deflectors (number 24) located in the inner surface of the external body. All measurements were recorded by using software, PLC.

Uncertainties of the measured values in experiments; temperature on the air side ± 0.5 °C, tube diameter on the air inlet side is ±2mm, pressure difference on the air side is ± 0.16 mbar, velocity on the air side is ±0.2 m/s, pressure on the water side is ± 0.2 mbar, temperature on the water side is ± 0.1 °C and flow on the water side is ± 0.4 L/h.

In the present study, the external diameter of the body into which the heating tube is placed is 154 mm. The external diameter of the tube with conical fins is 27 mm. The inclination angle of the conical fins with respect to the tube axis is 45º. The values of pitch between conical finsare 10, 12, 15 mm. The thickness of the conical fin is 0.6 mm. On the other hand, the height of the conical fins is 35 mm for α = 45º. Figure 2 shows the tube with conical fins.

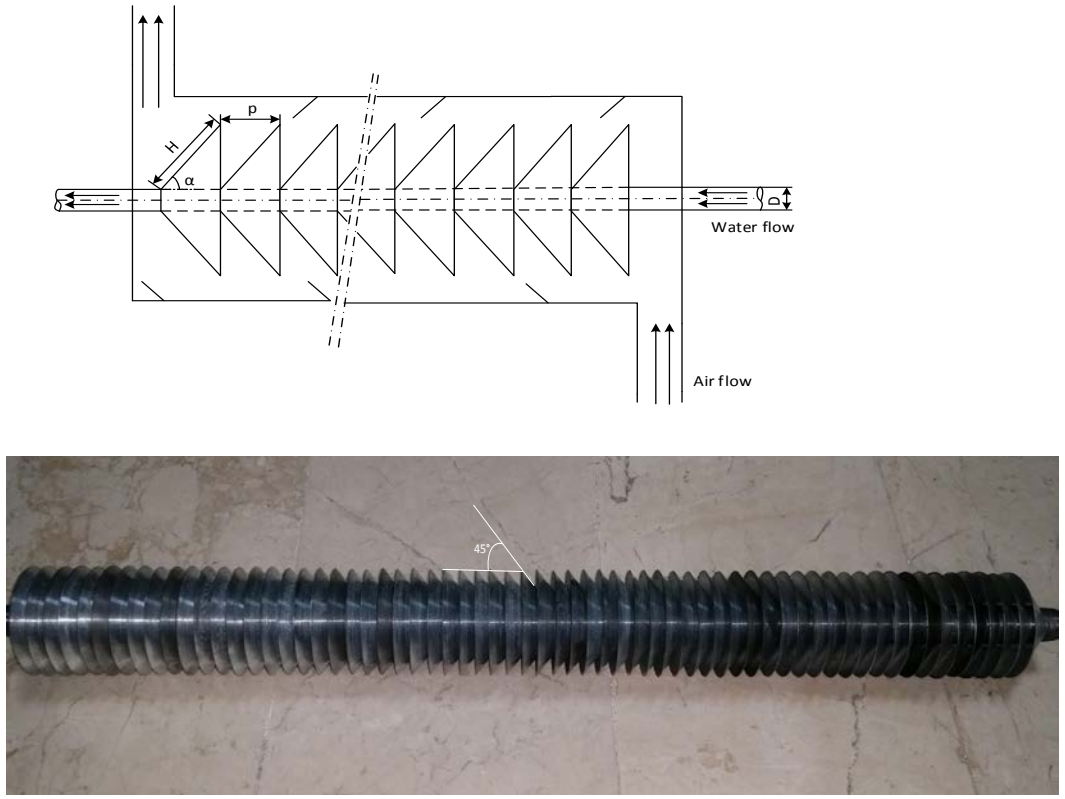

Figure 2.Tube with conical fins

3. IMPORTANT PARAMETERS

The heat loss to surroundings was found very small as the external body was well insulated. Therefore, the heat transfer happening inside the test section was taken into account. That is,

$$\dot{Q}_{water} = \dot{Q}_{air} = \dot{Q}_{conv} \quad (1)$$

in which

$$\dot{Q}_{air} = \dot{m}_{air} c_{p,air} \left(T_{o,air} - T_{i,air}\right) \quad (2)$$

and

$$\dot{Q}_{water} = \dot{m}_{water} c_{water} \left(T_{i,water} - T_{o,water}\right) \quad (3)$$

The convection heat transfer from the heating tube can be written by

$$\dot{Q}_{conv} = h A_{total} (T_s - T_\infty) \quad (4)$$

where A_{total} is the total heat transfer surface area on the circular tube with conical fins.

$$A_{total} = n\left(A_s + x_{fin} A_{fin}\right) \quad (5)$$

in which A_s is the heating tube surface area except total conical fin surface area and x_{fin} represents the conical fin efficiency. Moreover, n is number of conical fins.

The average heat transfer coefficient (h) and the average Nusselt number (Nu) are expressed as follows:

$$h = \frac{\dot{Q}_{conv}}{A_{total}(T_s - T_\infty)} \quad (6)$$

$$Nu = \frac{hD}{k} \quad (7)$$

The Reynolds number based on tube diameter is written as

$$Re = \frac{V_{max} D}{x} \quad (8)$$

and

$$V_{max} = \frac{\dot{m}_{air}}{\rho_{air} A_p} \quad (9)$$

in which V_{max} is the maximum velocity (velocity between two conical fins) and A_p is the area of reference section perpendicular to the flow direction between to conical fins.

4. RESULTS AND DISCUSSION

In order to testify the validity of the experimental set – up, the Nusselt number obtained from a smooth tube is compared with that from correlation of Churchill and Bernstein found in the literature [15] for cross flow over a cylinder.

Correlation proposed by Churchill and Bernstein:

$$Nu = \frac{hD}{k} = 0.3 + \frac{0.62 Re^{1/2} Pr^{1/3}}{[1+(0.4/Pr)^{2/3}]^{1/4}} \left[1 + \left(\frac{Re}{282{,}000}\right)^{5/8}\right]^{4/5} \quad (10)$$

Figure 3 shows the comparison of Nusselt number from Churchill and Bernstein correlation and obtained Nusselt number from the experimental results for air.

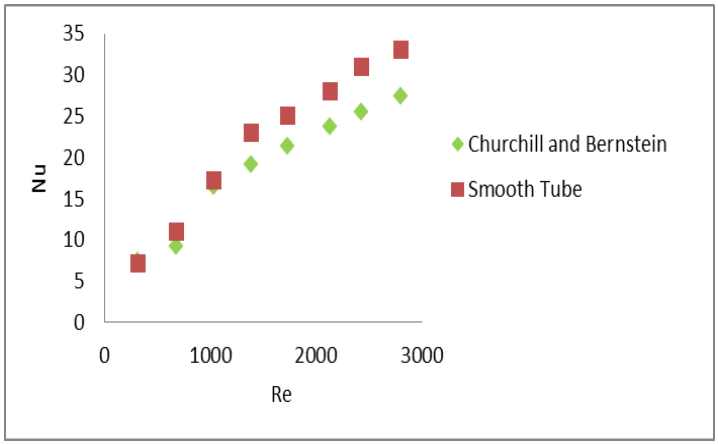

Figure 3.Verification of Nusselt numbers of smooth tube

The experiments were carried out at three different fin spacings (10, 12 and 15 mm) at inclination angle of 45º. The heat transfer values were determined fort the cross flow arrangement and eight different air flow velocities (2 – 20 m/s). The temperature of hot water that the air was heated was 65 °C.

Figure 4 shows the effect of different fin spacings on Nusselt number.

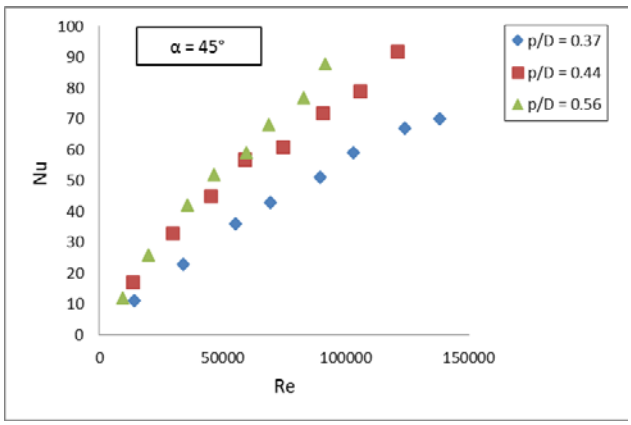

Figure 4. Effect of Reynolds number and fin spacing on Nusselt number

Figure 4 illustrates dependency of Nusselt number on Reynolds number. Increase in the ratio of spacing between the fins to diameter of them, p/D, manages heat transfer dominantly. Figure 4 points out that decrease in p/D leads to a drop in Nusselt number. Heat transfer due to use of fins with p/D = 0.37 is the least one compared to those of others. The difference among them is obvious with the increase of Re number. It can also be concluded that beyond a certain limit, $Re = 6x10^4$, there is an increasing difference between the Nusselt numbers of p/D = 0.56 and p/D = 0.44 (such ratios correspond to 15 and 12 mm respectively), although such difference vanishes as Re number becomes smaller than this limit. In fact increase of heat transfer, Nusselt number, with the spacing between the fins contradicts with those of increase in surface area. A reason coming into mind is the formation of big vortices for large spacings, such as 15 mm, between the fins. For larger values of $Re =$

$6x10^4$, the ratio p/D = 0.56 gives the best heat transfer coefficient. The same is not true for smaller values of Re number so we cannot refer any preferred fin spacing. Due to change in character of heat and mass flow around the conical fins we specify$Re = 6x10^4$ as a critical Reynold number.

Figure 5shows change of the fin efficiency with Reynolds number for three different fin spacings.

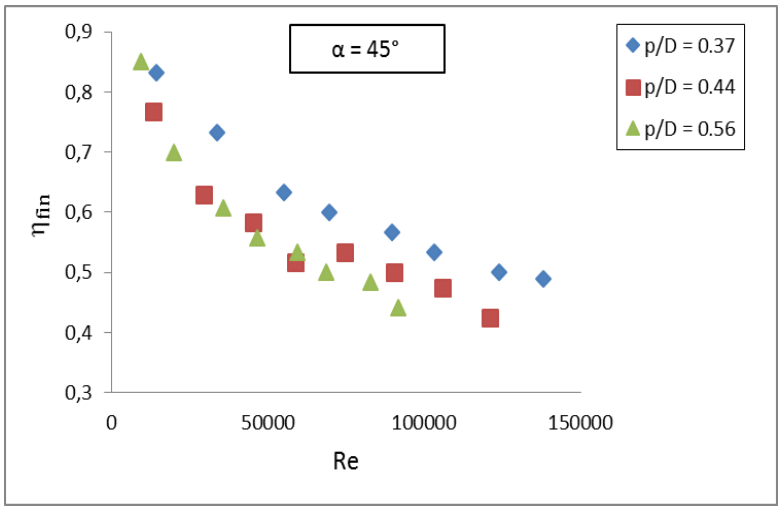

Figure 5.Change of fin efficiency with Reynolds number

Fin efficiency mainly depends on surface area, heat transfer coefficient and surface temperature of fins. From the figure (Figure 5) one can conclude that the efficiency diminishes with Reynolds number. Such a decrease of efficiency is a result of increased air flow velocity around fins. The increase of flow velocity leads to moderately low surface temperature along the fin, from the base to tip, and also lower fin efficiency. Although heat transfer coefficient increases with Reynolds number for all p/D's, a competing effects of heat transfer between the actual case which lessens due to reduced surface temperature, and ideal case (maximum heat transfer) lead to such decrease of fin efficiency. In other words, the more air velocity causes the lower surface temperature due to enhanced heat transfer coefficient and the lower fin efficiency. The main finding of this study, local minima of fin efficiency of the fin with p/D = 0.44. The efficiency reaches its minimum value at around$Re = 6x10^4$. The same situation is not valid for the other p/D's. For all Re numbers, the efficiency of fins with p/D = 0.37 is always highest. Up to $Re = 6x10^4$, the efficiency of the fins with p/D = 0.44 and 0.56 is almost the same. The discrepancy between them is explicit beyond this limit.

Figure 6 illustrates change in pressure drop with fin spacing. For all spacing, there is almost a significant pressure drop with increasing Reynolds number. The fins with p/D = 0.56 show greater pressure drop compared to the others. For $Re < 6x10^4$, no significant difference between the other fin spacings is observed. Greater values of Re number results in distinct pressure drops for each fin spacing. A tremendous increase of pressure drop for fins with p/D = 0.56 is clear enough. Such a high pressure drop for big spacing between fins originates from the flow structure among them and vortex flow around the fins.

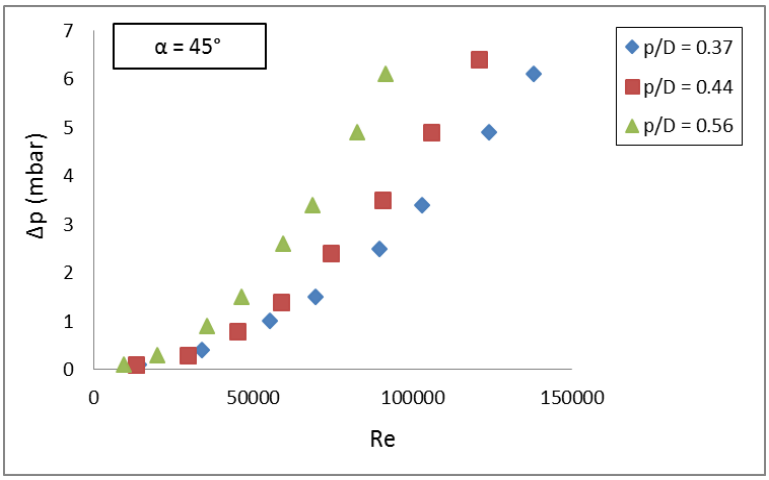

Figure 6. Change of pressure drop according to Reynolds number

5. CONCLUSIONS

The main conclusions of this study is summarized below.

1. For $Re < 6x10^4$, increase in spacing between fins leads to almost the same Nusselt numbers for 12 and 15 mm of spacings.
2. For $Re > 6x10^4$, the best heat transfer coefficient is for the the greater fin spacings, p/D = 0.56.
3. $Re = 6x10^4$ is assumed to be a critical Reynolds number which manages the character of the heat transfer over finned surface.
4. For all Re numbers, an increase of pressure drop is observed for all p/D's. However, the increase is more obvious for $Re > 6x10^4$. Below this limit, no significant difference is observed for p/D = 0.37 and 0.44 contrary to greater the spacing, 0.56.

To sum up, there is an optimal and cost saving fin spacing that gives comparably good heat transfer coefficient beyond a certain Reynolds number. For this study, p/D = 0.56 seems to be optimal fin configuration which gives almost the same heat transfer compared to narrower fin configurations. Moreover, one can define a critical Reynolds number for such fin structure, which equals to $6x10^4$.

ACKNOWLEDGMENTS

The author would like to express her appreciation to the Pamukkale University Scientific Research Projects Council, Turkey for providing financial support for ICENS 2016 symposium.

NOMENCLATURE

A_{total}	total heat transfer surface area (m^2)
A_s	heating tube surface area except total conical fin surface area (m^2)
A_{fin}	area of the conical fin on the tube (m^2)
A_p	area of reference section perpendicular to the flow direction between two conical fins (m^2)
$c_{p,air}$	specific heat capacity of air (kJ/kg°C)
c_{water}	specific heat capacity of water (kJ/kg°C)
D	outer diameter of heating tube (m)
H	height of conical fin (m)
h	heat transfer coefficient (W/m^2K)
k	thermal conductivity (W/m°C)
L	length of heating tube (m)
$\dot{m}_{air}$	mass flow rate of air (kg/s)
$\dot{m}_{water}$	mass flow rate of water (kg/s)
n	number of conical fins
Nu	Nusselt number
Pr	Prandtl number
p	distance between conical fins (m)
$\dot{Q}_{air}$	heat transfer rate of air (W)
$\dot{Q}_{water}$	heat transfer rate of water (W)
$\dot{Q}_{conv}$	convective heat transfer rate (W)
Re	Reynolds number
$T_{i,air}$	input temperature of air into test section (°C)
$T_{o,air}$	output temperature of air from test section (°C)
$T_{i,water}$	input temperature of water into test section (°C)
$T_{o,water}$	output temperature of water from test section (°C)
T_s	temperature of heating tube surface (°C)
T_∞	temperature of heated air (°C)
t	conical fin thickness (m)
V_{max}	maximum velocity (velocity between two conical fins) (m/s)

$V_{i,air}$	input velocity of air into test section (m/s)

Greek Symbols

ν	kinematic viscosity (m^2/s)
μ	dynamic viscosity (kg/ms)
α	conical fin inclination angle (°)
x_{fin}	conical fin efficiency
Δp	pressure drop (mbar)

Subscripts

air	air side
fin	fin
conv	convection
i	input
o	output
s	tube wall
water	Water side

REFERENCES

[1] D. Mikielewicz, A. Stasiek, M. Jewartowski, and J. Stasiek, "Measurements of heat transfer enhanced by the use of tranverse vortex generators," *Applied Thermal Engineering*, vol. 49, pp. 61 – 72, Nov. 2012.
[2] A. W. Fan, J. J. Deng, A. Nakayama, and W. Liu, "Parametric study on turbulent heat transfer and flow characteristics in a circular tube fitted with louvered strip inserts," *International Journal of Heat and Mass Transfer*, vol. 55, pp. 5205 – 5213, Jun. 2012.
[3] C. X. Tan, W. L. Mah, Y. M. Hung, and B. T. Tan, "On the role of inserts in forced convection heat transfer augmentation," *International Communications in Heat and Mass Transfer*, vol. 39, pp. 1138 – 1145, Jul. 2012.
[4] G. Yakar, and R. Karabacak, "Investigation of thermal performance of perforated finned heat exchangers," *Experimental Heat Transfer*, vol. 28, pp. 354 – 365, Jul. 2015.
[5] C. Thianpong, K. Yongsiri, K. Nanan, and S. Eiamsa – ard, "Thermal performance evaluation of heat exchangers fitted with twisted – ring turbulators," *International Communications in Heat and Mass Transfer*, vol. 39, pp. 861 – 868, Apr. 2012.
[6] H. M. Şahin, E. Baysal, and A. R. Dal, "Experimental and numerical investigation of thermal characteristics of a novel concentric type tube heat exchanger with turbulators," *International Journal of Energy Research*, vol. 37, pp. 1088 – 1102, May. 2012.
[7] O. Aydin, M. Avci, B. Markal, and M. Y. Yazici, "An experimental study on the decaying swirl flow in a tube," *International Communications in Heat and Mass Transfer*, vol. 55, pp. 22 – 28, May. 2014.
[8] C. Muthusamy, M. Vivar, I. Skryabin, and K. Srithar, "Effect of conical cut – out turbulators with internal fins in a circular tube on heat transfer and friction factor," *International Communications in Heat and Mass Transfer*, vol. 44, pp. 64 – 68, Apr. 2013.
[9] P. B. Jasinski, "Numerical study of the thermos – hydraulic characteristics in a circular tube with ball turbulators. Part 1: PIV experiments and a pressure drop," *International Journal of Heat and Mass Transfer*, vol. 74, pp. 48 – 59, Mar. 2014.
[10] G. Cafiero, S. Discetti, and T. Astarita, "Heat transfer enhancement of impinging jets with fractal – generated turbulence," *International Journal of Heat and Mass Transfer*, vol. 75, pp. 173 – 183, Apr. 2014.
[11] A. E. Zohir, A. A. AbdelAziz, and M. A. Habib, "Heat transfer characteristics and pressure drop of the concentric tube equipped with coiled wires for pulsating turbulent flow," *Experimental Thermal and Fluid Science*, vol. 65, pp. 41 – 51, Mar. 2015.
[12] M. Rivier, P. Sebastian, T. Goli, G. Raffray, and A. Collignan, "Heat transfer enhancement of a circular tube heat exchanger fitted with an elliptic shaped turbulator designed in the context of developing countries," *Applied Thermal Engineering*, vol. 81, pp. 92 – 101, Feb. 2015.
[13] M. Sheikholeslami, H. Hatami, M. Jafaryar, F. Farkhadnia, D. D. Ganji, and M. Gorji – Bandpy, "Thermal management of double – pipe air to water heat exchanger, *Energy and Buildings*," vol. 88, pp. 361 – 366, Dec. 2014.
[14] A. Chumpia, and K. Hooman, "Performance evaluation of single tubular aluminium foam heat exchangers," *Applied Thermal Engineering*, vol. 66, pp. 266 – 273, Feb. 2014.
[15] Y. A. Çengel, *Heat and Mass Transfer: A Practical Approach*, 3rd ed., McGraw – Hill, 2006.

Gülay YAKAR received her Ph.D. from Pamukkale University at Denizli in 2007. Her research interests include heat exchanger, cooling systems with absorptions, and exergyanalysis. She currently continues her experimental studies on the methods to increase the amount of heat transfer in shell and tube type heat exchangers.

General Overview of Cogeneration Systems in Turkey

Tolga Tane[1], Mustafa Kilic[2]

Abstract

This study is to present a general overview of cogeneration systems in Turkey. Cogeneration is one of the more significant subject for Turkey industry. Heavy and food industries are living many problems for their production processes. Therefore, our study is included this solution of the cogeneration case in Turkey. The aim of this study is to pose these cogeneration problems with solution cases. Turkey location is in the Middle-East. There is so turmoil area around the country. There are several energy problems that are living, now. So, Turkey must take their care to all of these misfortunes. By this way, energy is the greatest problem in this location. When Turkey implement these energy case with cogeneration solutions, we can develop immediately in this location. Particularly, heavy and food industries use more than energy then the other industry sectors. Their processes need to have more energy than the other's one. In this study, it will be also compared from previous similar studies. This study indicates significant subject to the renewables energy and fossil resources.

Keywords: *Cogeneration, Energy, Cost, Industry*

1. INTRODUCTION

There are many energy problems in the world. These are an energy crises and an extinction of energy resources. These problems can be solved by many alternative energy systems that cogeneration is the one of the important energy system. Heavy and food industries are living many problems for their production processes. Therefore, our study is included this solution of the cogeneration case in Turkey. The aim of this study is to pose these cogeneration problems with solution cases. A declination of Cogeneration is a Combined Heat and Power. Electricity and heat can be produced at the same time. Cogeneration that is to produce energy in efficiently way from the heat demand of the application is benefit for the building and factory energy. The efficiency of a cogeneration plant can come up with nearly 90% or more. This work is to present a general overview of cogeneration systems in Turkey.

Turkey location is in the Middle-East. There is so turmoil area around the country. There are several energy problems that are living, now. So, Turkey must take their care to all of these misfortunes. By this way, energy is the greatest problem in this location. In literature, there are several studies that cogeneration is more important energy than the other alternative and resources energies. Literature review as follows; Karellas and Braimakis [1] posed on energy–exergy analysis and economic investigation of a cogeneration and trigeneration ORC–VCC hybrid system utilizing biomass fuel and solar power in their research. Eyidogan et al. [2] used Organic Rankine Cycle for the power generation in Turkey. Can et al. [3] presented the exergy and economical analysis of a cogeneration plant system in Turkey. Exergoeconomic analysis of a cogeneration plant in an iron and steel factory were investigated by Mert et al. [4]. Alcan et al. [5] identified and discussed some of the important and critical decision criteria to select the best cogeneration system in their study. Saglam et al. [6] studied a micro-cogeneration system of a new PI tuning method for an industrial process. Inan et al. [7] performed to modelling of the change in national exchange rate model depending on the economic parameters of a natural gas cogeneration system. Ust et al. [8] provided guidance for the design of Dual-Miller Cycle cogeneration system in this study. Şevik [9] reviewed the historical process of electric generation from natural gas by cogeneration in Turkey and the World with a forecast of future supply and demand projections in energy. He et al. [10] investigated a water–power cogeneration plant by humidification dehumidification method. Aras [11] worked about the condition and development of the cogeneration facilities in Turkey. Taillon and Blanchard [12] investigated exergy efficiency graphs for thermal power plants. Arsalis and Alexandrou [13] studied on thermoeconomic modeling and exergy analysis of a decentralized liquefied natural gas-fuelled combined-cooling-heating-and-power plant.

When Turkey implement these energy case with cogeneration solutions, we can develop immediately in this location. Particularly, heavy and food industries use more than energy then the other industry sectors. Their processes need to have more energy than the other's one. In this study, it will be also compared from previous similar studies. This study indicates significant subject to the renewables energy and fossil resources.

[1] Corresponding author: Aksaray University, Department of Motor Vehicles and Transportation Technology, 68100, City Centre/Aksaray, Turkey.
tolgataner@aksaray.edu.tr
[2] *Adana Science and Technology University, Department of Mechanical Engineering, 01180 Seyhan/Adana, Turkey.*
mkilic@adanabtu.edu.tr

2. TECHNICAL DETAIL OF COGENERATION SYSTEM WITH CURRENT LOCATION

As cogeneration systems have got many different type that these are can be used by status. These statuses can change according to the location, energy efficiency, resources quantity, energy demand and the other factors. Cogeneration inputs are fuel and air, and outputs are electrical energy and thermal energy. The other output is a waste of heat. It can be seen Figure 1.

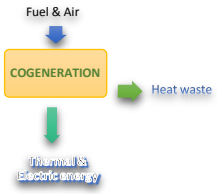

Figure 1. A general scheme of cogeneration process

Location is very significant factor for using cogeneration. Turkey location is in the Middle-East. There is so turmoil area around the country. There are several energy problems that are living, now. So, Turkey must take their care to all of these misfortunes. By this way, energy is the greatest problem in this location. When Turkey implement these energy case with cogeneration solutions, we can develop immediately in this location. Firstly, it can be showed a cogeneration map of Turkey.

2.1 A view of Middle East Energy Status and Future

Firstly, a view of the energy status was investigated Middle East energy for comparison to World energy. We can evaluate the comparison of Middle East and World for energy. In this study, these data were taken from International Energy Agency from World Energy Outlook Special Report [14]. In Figure 2, fossil-fuel savings from energy efficiency and fossil-fuel subsidy reform in the Bridge Scenario relative to the INDC Scenario can be seen in 2030.

Note: mb/d = million barrels per day; bcm = billion cubic metres; Mtce = million tonnes of coal equivalent.

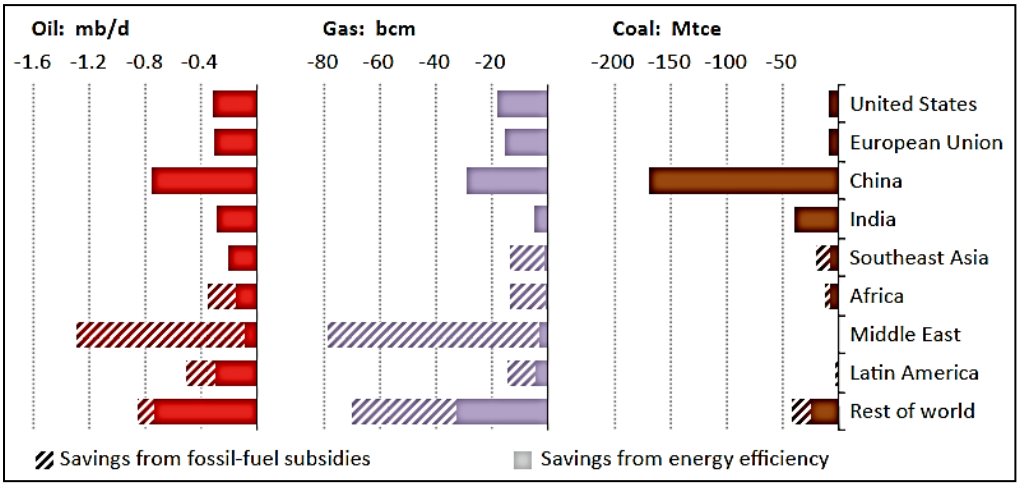

Figure 2. Fossil-fuel savings from energy efficiency and fossil-fuel subsidy reform in the Bridge Scenario relative to the INDC Scenario, 2030 [14]

In this scenario, we can't see any saving from energy efficiency of coal for Middle East. But for, saving from energy efficiency of oil and gas can be seen a little bit. This is the Middle East great problem. These countries can't use energy resources via efficiency of energy.

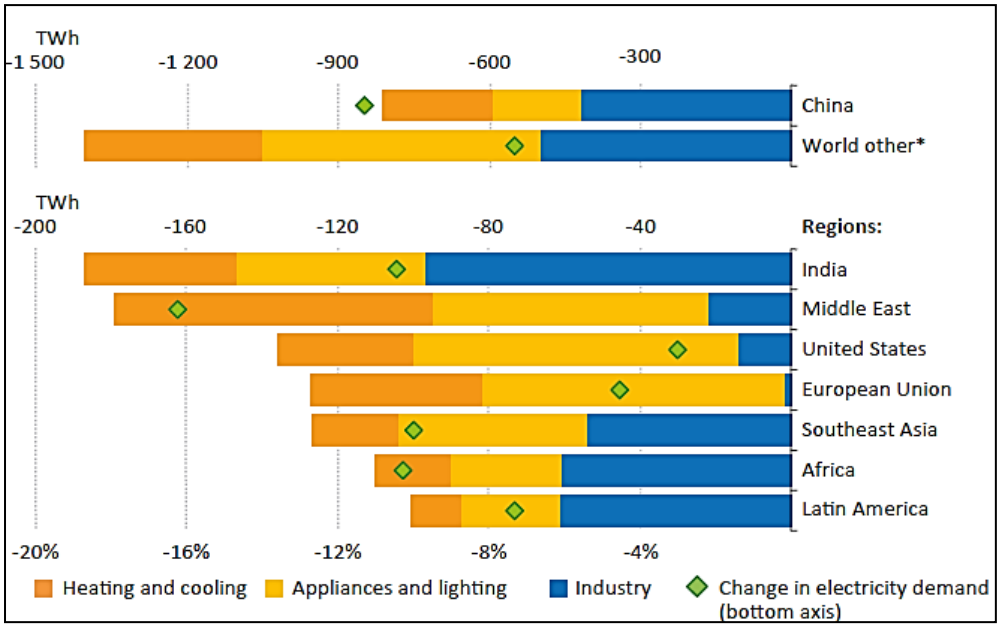

Note: World other represents all countries except for China. Note: TWh = terawatt-hour.

Figure 3. Electricity demand reduction by sector and region in the Bridge Scenario relative to the INDC Scenario, 2030 [14]

In Figure 3, it can be seen an electricity demand reduction by sector and region in the Bridge Scenario relative to the INDC Scenario, 2030. In Middle East, electricity demand is very high level. Electricity demands are industry to 20 TWh, appliances and lighting to 95 TWh and heating and cooling to 180 TWh, approximatively.

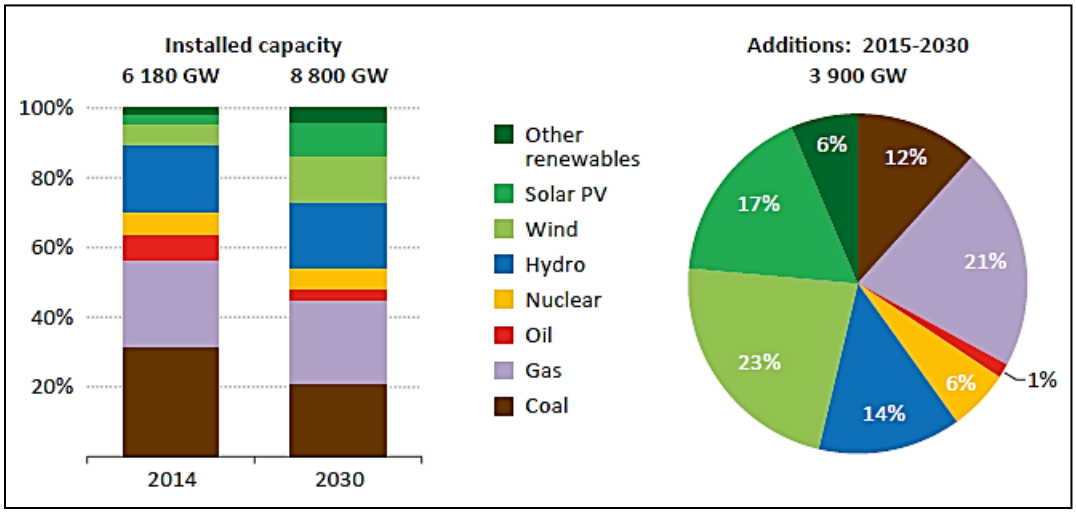

Figure 4. World power generation capacity mix and capacity additions in the Bridge Scenario [14]

In Figure 4, World power generation capacity mix and capacity additions in the Bridge Scenario can be foreseen. In the future, wind and gas energy will be become significant level.

Table 1. Middle East Power Generation (Mtoe) [14]

	Energy demand (Mtoe)					Shares (%)	
	1990	**2013**	**2020**	**2025**	**2030**	**2013**	**2030**
Power generation	**62**	**235**	**247**	**255**	**269**	**100**	**100**
Coal	0	0	1	1	1	0	0
Oil	27	100	79	64	50	42	19
Gas	34	132	157	168	180	56	67
Nuclear	-	1	5	13	18	0	7
Hydro	1	2	2	3	3	1	1
Bioenergy	-	0	1	2	4	0	1
Other renewables	0	0	1	4	12	0	4

Table 2. Middle East Electricity Generation (TWh) [14]

	Electricity generation (TWh)					Shares (%)	
	1990	**2013**	**2020**	**2025**	**2030**	**2013**	**2030**
Total generation	**224**	**930**	**1129**	**1241**	**1374**	**100**	**100**
Coal	0	0	3	4	5	0	0
Oil	98	340	277	233	187	37	14
Gas	114	565	786	881	963	61	70
Nuclear	-	4	20	48	71	0	5
Hydro	12	20	28	35	40	2	3
Bioenergy	-	0	3	6	14	0	1
Wind	0	0	3	9	23	0	2
Geothermal	-	0	0	0	0	0	0
Solar PV	-	0	5	14	42	0	3
CSP	-	0	3	10	28	0	2
Marine	-	-	-	-	-	0	0

In Table 1 and Table 2, it can be seen Middle East power generation quantity by the years. Most of the energy have been produced by the power generation from gas. The other energy resources as hydro, bioenergy, solar and wind energies have not been enough for the power generation. So, cogeneration has become very importance subject for Middle East.

By this way, Middle East countries should take a care about their energy demand so that this location is living very big turmoil for this energy crisis. Otherwise, they can't save their energy from these energy resources. This problem can be solved by planning of the cogeneration systems.

2.2. A view of Turkey Energy Status and Future

Secondly, a view of the energy status was researched Turkey energy status for comparison to Middle East energy status. We can determine the comparison of Turkey and Middle East for energy.

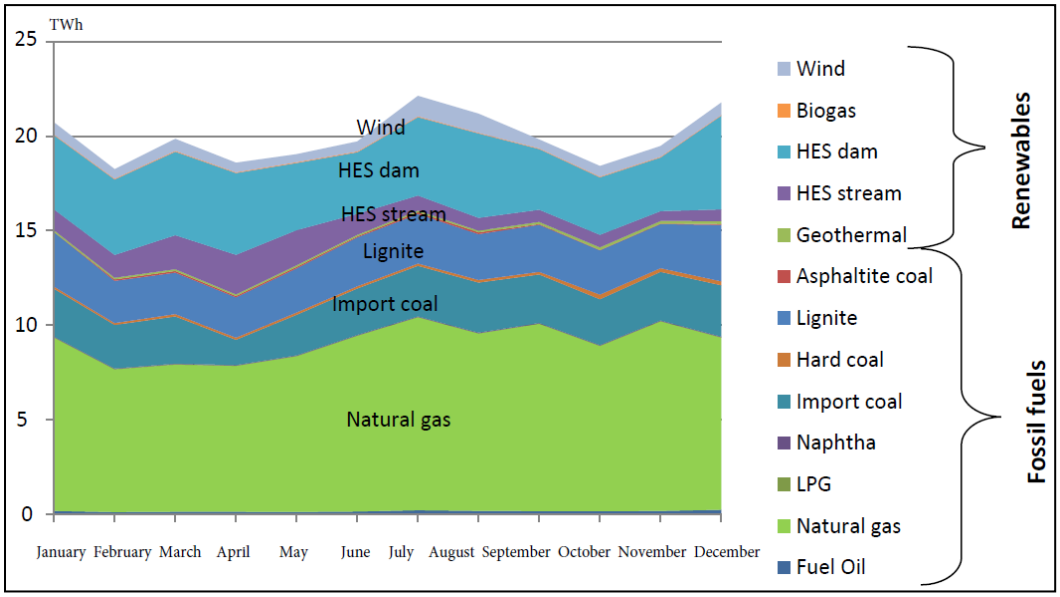

Note: This graph was taken from Republic of Turkey Ministry of Energy and Natural Resources for 2013.

Figure 5. Turkey's Energy Quantity (TWh) Production by Energy Resource Type [15]

In Figure 5, it can be seen Turkey's Energy Quantity Production by Energy Resource Type. Renewables energy production quantity are 68.5 [MWh]. Fossil fuels (Thermic energy) energy production quantity are 168.5 [TWh]

Table 3. Turkey Power Generation (Mtoe) [16]

	Energy production supply (Mtoe)					Shares (%)	
	1990	**2000**	**2005**	**2008**	**2020**	**2008**	**2020**
Power generation	**10.78**	**22.66**	**26.77**	**35.63**	**84.79**	**100**	**100**
Coal	3.78	6.93	7.15	10.37	28.15	29.1	33.2
Oil	0.74	1.70	0.91	1.35	1.10	3.8	1.3
Gas	1.90	8.38	12.13	17.70	29.25	49.7	34.5
Nuclear	-	-	-	-	5.51	-	6.5
Hydro	4.33	5.60	6.53	17.71	19.25	16.8	22.7
Wind	-	-	-	0.14	1.44	0.4	1.7
Geothermal	0.11	0.02	0.03	0.04	0.08	0.1	0.1
Combine Renewables & Waste	-	0.04	0.03	0.04	-	0.1	-
Solar	-	-	-	-	-	-	-

In Table 3, it can be seen Turkey power generation quantity by the years. Most of the energy have been produced by the power generation from gas and hydro. The other energy resources as geothermal, nuclear, solar and wind energies have not been enough for the power generation. Thus, cogeneration becomes an effective energy for Turkey's future.

3 RESULTS AND DISCUSSION

This study posed the comparison of previous study for cogeneration systems and efficiency. Thus, Turkey can choose her cogeneration systems for the energy problem. In Table 4, cogeneration system and efficiency can be seen clearly according to previous studies. When it can be researched detailed, cogeneration system has got energy and exergy efficiencies.

Table 4. Comparison of previous study for cogeneration systems and efficiency

Description of cogeneration system	Power Generation (P_{el})	Thermal efficiency (η_{th}) [%]	Exergy efficiency (η_{ex}) [%]	Payback period of the plant (years)	Author
Cogeneration and trigeneration ORC–VCC hybrid system utilizing biomass fuel and solar power	1.419 [kW]	5.54	71.03	7.0	Karellas and Braimakis [1]
Investigation of Organic Rankine Cycle (ORC) technologies	1 [MW]	85.00	-	2.7	Eyidogan et al. [2]
Cogeneration thermic power plant	180 [MW]	31.40	89.50	3.5	Can et al. [3]
Cogeneration plant in an iron and steel factory	39.5 [MW]	96.54	93.66	-	Mert et al. [4]
IGCC 5 BP Design IGCC (Integrated Gasification Combined Cycle) Steam Bagasse pellets	51.6 [MW]	86.10	39.00	-	Taillon and Blanchard [12]
LNG (Liquefied Natural Gas)-fuelled CCHP (combined-cooling-heating-and-power) system	12.82 [MW]	91.00	41.00	4.0	Arsalis and Alexandrou [13]

In Table 4, a cogeneration and trigeneration ORC–VCC hybrid system utilizing biomass fuel and solar power has got 1.419 [kW], thermal efficiency 5.54%, exergy efficiency 71.03% and payback period 7 years [1]. Eyidogan et al. [2] investigated an Organic Rankine Cycle (ORC) technologies that has got 1 [MW] power, thermal efficiency 85.00%, and payback period 2.7 years. A cogeneration thermic power plant was posed by Can et al. [3] that indicated 180 [MW] power, thermal efficiency 31.40%, exergy efficiency 89.50% and payback period 3.5 years [3]. A cogeneration plant in an iron and steel factory was investigated by Mert et al. [4] that posed 39.5 [MW] power, thermal efficiency 96.54%, exergy efficiency 93.66% [4]. Taillon and Blanchard [12] performed a IGCC 5 BP Design IGCC (Integrated Gasification Combined Cycle) that has got 51.6 [MW] power, thermal efficiency 86.10%, exergy efficiency 39.00% [12]. A LNG (Liquefied Natural Gas)-fuelled CCHP (combined-cooling-heating-and-power) system was showed by Arsalis and Alexandrou [13] that determined 12.82 [MW] power, thermal efficiency 91.00%, exergy efficiency 41.00% and payback period 4.0 years [13].

4 CONCLUSIONS

This work was to pose a general overview of cogeneration systems in Turkey. The aim of this study is to indicate that cogeneration can solve energy problem.

As Turkey implement these energy case with cogeneration solutions, we can develop immediately in this location. Particularly, heavy and food industries use more than energy then the other industry sectors. Their processes need to have more energy than the other's one. In this study, it will be also compared from previous similar studies. This study indicates significant subject to the renewables energy and fossil resources.

REFERENCES

[1] S. Karellas and K. Braimakis, *Energy–exergy analysis and economic investigation of a cogeneration and trigeneration ORC–VCC hybrid system utilizing biomass fuel and solar power*, Energy Conversion and Management 107, 103–113, 2016.
[2] M. Eyidogan, F. C. Kilic, D. Kaya, V. Coban, S. Cagman, *Investigation of Organic Rankine Cycle (ORC) technologies in Turkey from the technical and economic point of view*,Renewable and Sustainable Energy Reviews 58, 885–895, 2016.
[3] Ö. F. Can, N. Celik, I. Dagtekin, *Energetic–exergetic-economic analyses of a cogeneration thermic power plant in Turkey*, International Communications in Heat and Mass Transfer 36, 1044–1049, 2009.
[3] M. S. Mert, Ö. F. Dilmaç, S. Özkan, F. Karaca, E. Bolat, *Exergoeconomic analysis of a cogeneration plant in an iron and steel factory*, Energy 46, 78-84, 2012.
[4] P. Alcan, A. Balin, H. Baslıgil, *Fuzzy multicriteria selection among cogeneration systems: A real case application*, Energy and Buildings 67, 624–634, 2013.
[5] G. Saglam, C. C. Tutum, S. Kurtulan, *A new PI tuning method for an industrial process: A case study from a micro-cogeneration system*, Energy Conversion and Management 67, 226–239, 2013.
[6] A. Inan, E. Izgi, S. Ay, *Modelling of the change in national exchange rate model depending on the economic parameters of a natural gas cogeneration system: Turkey case*, Energy Conversion and Management 50, 1049–1055, 2009.
[7] Y. Ust, F. Arslan, I. Ozsari, M. Cakir, *Thermodynamic performance analysis and optimization of DMC (Dual Miller Cycle) cogeneration system by considering exergetic performance coefficient and total exergy output criteria*, Energy 90, 552-559, 2015.
[8] S. Şevik, *An analysis of the current and future use of natural gas-fired power plants in meeting electricity energy needs: The case of Turkey*, Renewable and Sustainable Energy Reviews 52, 572–586, 2015.
[9] W.F. He, D. Han, L.N. Xu, C. Yue, W.H. Pu, *Performance investigation of a novel water–power cogeneration plant (WPCP) based on humidification dehumidification (HDH) method*, Energy Conversion and Management 110, 184–191, 2016.
[10] H. Aras, *Condition and development of the cogeneration facilities based on autoproduction investment model in Turkey*, Renewable and Sustainable Energy Reviews 7, 553–559, 2003.
[11] J. Taillon and R.E. Blanchard, *Exergy efficiency graphs for thermal power plants*, Energy 88, 57-66, 2015.
[12] A. Arsalis and A. Alexandrou, Thermoeconomic modeling and exergy analysis of a decentralized liquefied natural gas-fuelled combined-cooling-heating-and-power plant, Journal of Natural Gas Science and Engineering 21, 209-220, 2014.
(2015) Energy Climate and Change, World Energy Outlook Special Report, The IEA website. [Online]. Available: https://www.iea.org/
(2013) Republic of Turkey Ministry of Energy and Natural Resources website. [Online]. Available: http://www.enerji.gov.tr/
(2009) Energy Policies of IEA Countries, Turkey 2009 Review, The IEA website. [Online]. Available: https://www.iea.org/

Analysis of Criteria Influencing Weather Temperature with AHP and DEMATEL Methods

Cemil Celik[1], Kasim Baynal[2]

Abstract

The weather affects significantly a large part of our daily lives. Therefore, an accurate forecast has an important place in human life. Especially, temperature forecast has a particular importance both live and the impact on other atmospheric parameters. The selection of parameters for weather forecasting models is a critical process affecting the forecasting. The interactions on each other of criteria and the degree of dependence criteria are an important step in the decision-making process in the temperatures forecasting process. The scope of this study; the eight most important criteria (Air pressure, water vapor pressure, relative humidity, wind speed, height, flora, land and seas and exposure) was determined to influencing the air temperature as a result of the literature research. In the first stage of the study; a ranking is formed by a ranking of weights obtained by pairwise comparisons of the criteria according to expert opinion with Analytic Hierarchy Process (AHP) method of the multi-criteria decision-making methods. In the second stage of the study; the ranking dependent weight value between each of the criteria is made with The Decision Making Trial and Evaluation Laboratory (DEMATEL) according to expert opinion. In conclusion; the results obtained with the two methods evaluated and interpreted.The researchers in the selection of the parameters they use in temperature forecasting models aimed to contribute with this study. In this study; AHP and DEMATEL methods of the multi-criteria decision-making methods are used in order to reveal their relationship with each other criteria in the temperature forecasting models.

Keywords: *AHP, DEMATEL, Multi-Criteria Analysis and Weather Forecast.*

1. INTRODUCTION

Weather forecasting information with atmospheric observations using the computer model can be defined as the determination of the temperature. The first trial of numerical weather forecasting was by L. F.Richardson in 1922, but it has not made a positive result. In the 1940s the Institue at Princeton led by Richardson for Advanced Study Chamey, Fjortfort and Von Neumann, has managed to develop 500 hPa dynamical numerical forecast using the recently invented computers equality to Tagged Barotropic vortisity in a more simple models from Richardson's version [1].

Scientists have begun to measure factors affecting the temperature such as air pressure and temperature conditions in the 17th century. This case, it helped to better understand the atmosphere and its processes and weather observation data was collected systematically. Later meteorologists began to work to map the datas such as temperature and humidity. This maps have allowed scientists to study to determine wind patterns and storm systems [2]. Today the weather forecast is done through the use of highly complex equations and powerful computer hardware.

Abrajano and others (Singapore) in 2009 was worked on the weather forecast. Their study has examined the effects of parameters that forecasts the temperature [1]. Tektaş (Turkey) has studied on the weather forecast in 2010. In this study they used ANFIS and ARIMA models [3]. Kumar (India), has studied the weekly temperature forecast in 2012. In this study, the weekly average of 520 between 1997-2006, he used the minimum and maximum temperature data [4].

As a result of this study and the literature research has been identified the eight most important criterias influencing the temperature. According to expert opinion in the first phase of the study with AHP method has been created a ranking with the weights obtained from the comparison of the two criteria. In the second phase of the study; according to expert opinion dependent weight values between each of the criteria affecting the temperature has been determined importance ranking of the criteria with the DEMATEL method. At the end of the study; The results obtained by both methods were evaluated and interpreted. With this study; it was intended to contribute to the researchers in the selection of the criterias which will be used in temperature forecasting models.

2. CRITERIA USED IN TEMPERATURE FORECAST

Many different methods can be used together in the temperature forecasting. The most important phase in the temperature forecast is identifying the parameters to be used. As a result of the literature research, is determined eight criterias that affecting the temperature. Also in this section, from multi-criteria decision-making technique the Analytic Hierarchy Process and The Decision Making Trial and Evaluation Laboratory (DEMATEL) techniques are used to contribute to resolving and to facilitate the understanding of the structural relationship of parameters with each other. The heat source of Earth is sun. All the energy coming from the sun can't reach the earth. A portion is reserved in the atmosphere a portion is reflected back from the

[1]*Corresponding author: Kocaeli University, Department of Industrial Engineering, 41380, İzmit/Kocaeli, Turkey.* cemil.celik@kocaeli.edu.tr
[2]*Kocaeli University, Department of Industrial Engineering, 41380, İzmit/Kocaeli, Turkey,* kbaynal@kocaeli.edu.tr

surface of the atmosphere. If considered 100% energy coming from the atmosphere; 25% of the energy is reflected into space with the impact of cloud and the atmosphere. The 25% is dispersed in the atmosphere and provides clarification of the shade and helps the sky appear blue. The 15% is absorbed by the atmosphere and provides heating of the atmosphere. 35% reaches the earth. 27% of this energy heats the earth. 8% after striking the Earth is reflected back into space. As a result of the literature research, has determined the eight most important parameters affecting the temperature. These parameters; air pressure, water vapor pressure, relative humidity, wind speed, height, flora and the distribution of land and sea.

Air pressure; pressure, one of the research topics of physical science, as the air pressure is an important issue of meteorology which is a branch of geophysics. Atmospheric gases turn around the earth; They surrounded the earth and they has a weight because they are under the influence of gravity. This weight, shows itself under the pressure to the materials at the bottom and inside the atmosphere. This is called air pressure [5]. There is a weight of gases forming the atmosphere and makes itself felt under the pressure.

Water vapor pressure; transferred particles into the vapor phase before touching the liquid surface the pressure made on the particle in the liquid phase is called the vapor pressure. If the temperature doesn't change the vapor pressure is also not changing. If any liquid temperature is increased, the number of transferred molecules into the gas phase will increase and depending on temperature the vapor pressure also increases.

Relative humidity; the amount of moisture present in the air, the moisture content which it can carry is called relative humidity. Relative humidity is expressed as percentage (%).Relative humidity is under the influence of absolute humidity and the maximum humidity. Maximum humidity is associated with temperature that's why the relative humidity is significantly affected from temperature. There is an inverse association between relative humidity and temperature.

Wind speed; blowing winds In the northern hemisphere from south in the south hemisphere from north increases the temperature because they came from the direction of the equator. Landward winds blowing from the sea gives cooling effect in the summer and warming in the winter. The winds blowing from the land towards the sea makes effects in the summer enhancing in the winter lowering the temperature. The winds carries the temperature from where they came to the place where it reaches.

Height; the reflected beam from the atmosphere warms the ground, that's why the lower floors are worm and the upper floors are colder. With the rise of each 200m the temperature is reduced by 1 ° C. Also places are more warmer during the day compared to lower places. Height increases temperature decreases.

Flora; forests are cool in summer, warm in winter. In forested areas the daily temperature difference is less, in the desert the temperature difference is high. Flora absorbs some of the sun's rays to prevent overheating of the ground during the day. At the night it prevents cooling, by keeping a portion of the rays. As a result, reveals important differences in terms of distribution of temperature in the area sparse and areas with the bushy flora.

The influence of the Land and the sea; It affects the climate of a place to be close to or far from the sea. By taking the same amount of solar energy the lands and the seas are not equally overheated. Land heats up fast and faster cooling, seas are late warming and late cooling.

Exposure; Situations of objects according to the Sun is called exposure. The slopes which are facing the sun warms up more. The southern slopes of the northern hemisphere, northern slopes of the southern hemisphere are warms more. Places with the slope is steep of the sun's rays, while other places where the slope is less is more oblique rays of the sun. Thus, places with more slope is warmer, where places with the less slope is less warm.

3. USED MATERIALS AND METHODS

Two different methods are used to achieve results in this study. With AHP method was created a ranking with the weights obtained from the comparison of the two criteria. With DEMATEL method the factors that affect the temperature has been ranked with the importance of the criteria determined in accordance with expert opinion dependent of weight values between them. At the end of the study; the results obtained by both methods were evaluated and interpreted.

Analytical Hierarchy Process (AHP) Method

Analytic Hierarchy Process (AHP) developed by Thomas L. Saaty and is one of the best known and most widely used multi-criteria decision-making method. Method uses purpose, criteria, sub-criteria and the alternative that create multi-level hierarchical structure. In this structure due to binary comparisons importance weight of each criteria is achieved [6]. AHP is a very effective method guiding decision-makers to achieve the results of the decision-making through multi-criteria problems.

AHP method; separating the problem into smaller parts is a logical process that allows the pairwise comparison of criteria and options [7]. Implementation steps of AHP are as follows: In the first step; hierarchical structure is created.In the second step; matrix of pairwise comparisons are made the basis of analytical hierarchy process is based on a binary comparison. Criterion and criteria in terms of decision options, binary comparisons are made with each other by a person or persons who decides. Thomas L. Saaty, has developed a scale used in binary comparison of the decision criteria and decision options. Decision criterias on this scale with binary comparison and decision options according to each decision criteria with binary comparison, between 1 and 9 (1-Equal, 3-More Important, 5-Strongly Important 7-Very Strongly Important 9-Extremely Important, 2,4,6,8 intermediate values) are evaluated according to a scale [8]. In the third step; Eigenvector equation is determined according to

Equation (2). In the binary comparison matrix according to other elements of each item showing its importance to calculate the eigenvectors. Matrix size of nx1 eigenvector is determined as follows. I = 1,2,3, …, n and j = 1,2,3, …, n including;

$$\square_{\square\square} = \frac{\square_{\square\square}}{\sum_{\square=1}^{\square} \square_{\square\square}} \quad (1)$$

$$\square_{\square} = \frac{\sum_{\square=1}^{\square} \square_{\square\square}}{\square} \quad (2)$$

To determine the importance of distribution of criterias, must be calculated the column vectors. W column vector, (1) number specified Equation b_{ij} of values formed by the matrix is derived from the arithmetic mean of the row element. In the fourth step; eigenvectors consistency is calculated. Consistency rate for each binary comparison matrices is calculated and it is desirable that the upper limit for the ratio of 0,10. In the fifth step; The overall result of the hierarchical structure is obtained. The previous four stages, calculated for the entire hierarchical structure. At this stage, the extent of the hierarchical structure of n units of each occurrence in mx1 size superiority column vectors can be combined in size mxn Equation according to (3) DW a decision matrix is created. With obtained matrix between the extent of W superiority vector is achieved by multiplying Equation given in (4) gives a results of R vector. I = 1,2,3, …, m and j = 1,2,3, …, n including;

$$\square\square = \lfloor \square_{\square\square} \rfloor \quad (3)$$

$$\square = (\square\square)\square \quad (4)$$

Decision makers should behave consistent when making comparisons between the criteria. Inconsistencies, without contradiction between the criteria, it requires comparisons compatible with each other. Inconsistency rate (IR) is calculated to measure whether decision-makers act consistency or not. If the ratio is greater than 0,10 it indicates that there is an inconsistency in the judiciary of decision-makers. In case of inconsistency the max = n, to find the degree of deviation from the using Equation (5) the Inconsistency Index (II) is obtained.

$$\square\square = \frac{\square_{\square\square\square} - \square}{\square - 1} \quad (5)$$

From II, the A matrix of n values corresponding to the Randomness index (RI) the ratio obtained by dividing is called the IR. This ratio is expected to be less than 10%. RI is shown in Table 1.

$$\square\square = \frac{II}{\square\square} \quad (6)$$

Table 1. Randomness Index

n	1	2	3	4	5	6	7	8	9	10	11	12	13	14	15
RI	0	0	0,52	0,89	1,11	1,25	1,35	1,4	1,45	1,49	1,51	1,48	1,56	1,57	1,59

3.2. Dematel Method

DEMATEL method; It was used to determine the relationship and interaction between the criterias. Is an approach that allows patterns to determine the causal relationship between the criteria. DEMATEL method; Can determine the relationship between the structure and system components which is the subject of this study. DEMATEL makes it possible to understand the patterns of the complex or intertwined problems with its aspect. Because of this superiority of DEMATEL techniques it has been considerable approach for many studies in the literature [9]. Nowadays DEMATEL method is widely used in many issues in the study of complex problems, which is developed by the Geneva Battelle Memorial Institute [10]-[11].

The method is consist mainly of four steps [12]-[13]. In a first step; by the group of experts the binary comparison scale (0-Disable, 1-Low impact, 2-Medium impact, 3-High efficiency and 4-Very high impact) with the help of laid out Direct Relationship Matrix (A) is created. In the second step; the values of A by using the minimum value (z) of the rows and columns of this matrix by normalizing the generated Normalized Relations Direct Matrix (N) is obtained. In the third step; with N and the unit matrix (I) with insertion into the process $[T = Nx (1-N)^{-1}]$ Total Relationship Matrix (T) is created. In the fourth step; total rows of T (D) and the total columns ® which is calculated using D-R and D+R with the help of values determined the receiver groups to sender. At this point, having positive D-R values of criterias are considered to have a stronger effect on others and these criteria is referred to as sender. Negative value of D-R and criteria which is called a receiver is considered to be more affected than other criteria. On other hand D+R values, shows the relationship between each criteria with other criteria and high D+R values of the criteria is considered to have a greater association with other criteria.

4. APPLICATION

In the first step of implementation is to determine the criterias that affect the air temperature. In the result of literature research, eight most important criterias are determined which affects the temperature. These criteria of multi-criteria decision-making methods; to determine the degree of importance of criteria with AHP and help to determine the importance of the relationship of the criteria with each other using the DEMATEL method four criteria has been determined that have the most impact on the temperature.

4.1. The Weighting of the Criteria with AHP Method

The importance of the scores of criteria relative to one another by affecting the temperature was scored by six experts. After these scores this evaluations have been inserted to the consistency analysis. Results of consistency analysis the first decision-making consistency rate is; 0.0763 second; 0.0892 the third; 0.0971 the fourth; 0.0960 fifth; 0.0853 and sixth of the decision-makers; 0.0965 have been found. With consistency rate smaller than 0.1 AHP methods have been continued. In the first phase of the AHP method; by taking the geometric mean of all the decision-makers evaluation the Table 2 was formed

Table 2. The geometric mean of evaluators

Criteria	Air pressure	Water vapor pressure	Relative humidity	Wind speed	Height	Flora	Land and Seas	Exposure
K1-Air pressure	1	2,06	2,78	5	4,36	5,01	6,32	6,3
K2-Water vapor pressure	0,49	1	3,41	5,14	4,16	4,79	3,57	5,38
K3-Relative humidity	0,36	0,29	1	2,34	3,87	4,53	4,79	4,16
K4-Wind speed	0,2	0,19	0,43	1	2,06	2,94	2,06	2,06
K5-Height	0,23	0,24	0,26	0,49	1	2,59	2,45	2,34
K6-Flora	0,2	0,21	0,22	0,26	0,39	1	1,57	1,19
K7-Land and Seas	0,16	0,28	0,21	0,49	0,41	0,64	1	1,68
K8-Exposure	0,16	0,19	0,24	0,43	0,43	0,84	0,59	1
Column Total	2,79	4,46	8,55	15,14	16,67	22,34	22,35	24,12

In the second phase of the AHP method; formed Table 2 of the geometric mean were normalized and Table 3 was formed. This normalized value, is formed by each value dividing to the total value of column.

Table 3. Consisting values from normalization

Criteria	K1	K2	K3	K4	K5	K6	K7	K8
K1	0,36	0,46	0,33	0,33	0,26	0,22	0,28	0,26
K2	0,17	0,22	0,4	0,34	0,25	0,21	0,16	0,22
K3	0,13	0,07	0,12	0,15	0,23	0,2	0,21	0,17
K4	0,07	0,04	0,05	0,07	0,12	0,13	0,09	0,09
K5	0,08	0,05	0,03	0,03	0,06	0,12	0,11	0,1
K6	0,07	0,05	0,03	0,02	0,02	0,04	0,07	0,05
K7	0,06	0,06	0,02	0,03	0,02	0,03	0,04	0,07
K8	0,06	0,04	0,03	0,03	0,03	0,04	0,03	0,04

In the third phase of the AHP method; criterias weight was determined, and shown in Table 4. Criteria weight is obtained by dividing the total number of rows of normalized values to the total number of criteria.

Table 4. Determination of criteria weight

Criteria	K1	K2	K3	K4	K5	K6	K7	K8	Row Total	W
K1	0,36	0,46	0,33	0,33	0,26	0,22	0,28	0,26	2,51	0,31
K2	0,17	0,22	0,4	0,34	0,25	0,21	0,16	0,22	1,98	0,25
K3	0,13	0,07	0,12	0,15	0,23	0,2	0,21	0,17	1,29	0,16
K4	0,07	0,04	0,05	0,07	0,12	0,13	0,09	0,09	0,66	0,08
K5	0,08	0,05	0,03	0,03	0,06	0,12	0,11	0,1	0,58	0,07
K6	0,07	0,05	0,03	0,02	0,02	0,04	0,07	0,05	0,35	0,04
K7	0,06	0,06	0,02	0,03	0,02	0,03	0,04	0,07	0,34	0,04
K8	0,06	0,04	0,03	0,03	0,03	0,04	0,03	0,04	0,29	0,04

With AHP method, as a result of the determination of criteria weights the most important criterias was found to be; air pressure 0.31, water vapor pressure 0.25, relative humidity 0.16 and wind speed 0.08.

4.2. The Weighting Of The Criteria With Dematel Method

With the aim of determining the relationship between the criteria the most effective criterias are determined by using the DEMATEL method. The relationship between the criteria in the DEMATEL method, it is determined by a group of experts consisting of six persons by using a binary comparison scale. In the first phase of the DEMATEL method; the creation of a direct relationship matrix and for the group decision finding the average matrix. Direct relationship matrix; making binary comparisons between criteria is determined by the group of decision-makers / experts. Obtaining the average of the generated direct relationship matrix, the average direct relationship matrix has been created and shown in Table 5.

Table 5. Direct Relationships Matrix

Criteria	K1	K2	K3	K4	K5	K6	K7	K8	Row Total
K1	0	3	3,25	3	3,5	3,5	4	3,5	23,75
K2	3,25	0	3	3,5	3	3,25	3,25	3,5	22,75
K3	3	3,75	0	3,25	3,75	3,25	3,25	3	23,25
K4	3,25	3,25	3	0	3,25	4	3,25	2,5	22,5
K5	2,25	1,75	1	2	0	2,5	2	1	12,5
K6	1,25	1,75	1,75	1,75	1,5	0	1,5	1,25	10,75
K7	1,5	2	2	2	1,25	1,75	0	1,5	12
K8	1,25	1,5	1,75	1,5	0,75	1,5	1,25	0	9,5
Column Total	15,75	17	15,75	17	17	19,75	18,5	16,25	

In the second phase of DEMATEL method; direct relationships matrix (C) is being normalized. Instead of X_{ij} elements a_{ij} elements are written; The biggest of the total value of rows and columns of the matrix is determined and average direct relationship matrix by dividing to this value shown in Table 6 is generated a normalized direct relationship matrix.

Table 6. Normalized Direct Relationship Matrix

Criteria	K1	K2	K3	K4	K5	K6	K7	K8
K1	0,00	0,13	0,14	0,13	0,15	0,15	0,17	0,15
K2	0,14	0,00	0,13	0,15	0,13	0,14	0,14	0,15
K3	0,13	0,16	0,00	0,14	0,16	0,14	0,14	0,13
K4	0,14	0,14	0,13	0,00	0,14	0,17	0,14	0,11
K5	0,09	0,07	0,04	0,08	0,00	0,11	0,08	0,04
K6	0,05	0,07	0,07	0,07	0,06	0,00	0,06	0,05
K7	0,06	0,08	0,08	0,08	0,05	0,07	0,00	0,06
K8	0,05	0,06	0,07	0,06	0,03	0,06	0,05	0,00

In the third phase of DEMATEL method; Using the normalized matrix (M) formation of the total relationship matrix (T). Total relationship matrix (T) is created using the normalized direct relationship matrix (M). The normalized matrix subtracted from units the matrix. (I-M) matrix, Table 7 is generated.

Table 7. (I-M) Matrix

Criteria	K1	K2	K3	K4	K5	K6	K7	K8
K1	1,00	-0,13	-0,14	-0,13	-0,15	-0,15	-0,17	-0,15
K2	-0,14	1,00	-0,13	-0,15	-0,13	-0,14	-0,14	-0,15
K3	-0,13	-0,16	1,00	-0,14	-0,16	-0,14	-0,14	-0,13
K4	-0,14	-0,14	-0,13	1,00	-0,14	-0,17	-0,14	-0,11
K5	-0,09	-0,07	-0,04	-0,08	1,00	-0,11	-0,08	-0,04
K6	-0,05	-0,07	-0,07	-0,07	-0,06	1,00	-0,06	-0,05
K7	-0,06	-0,08	-0,08	-0,08	-0,05	-0,07	1,00	-0,06
K8	-0,05	-0,06	-0,07	-0,06	-0,03	-0,06	-0,05	1,00

The normalized matrix subtracted from units the matrix, (I-M) will be the inverse of the matrix and Table 8 is generated.

Table 8. $(I\text{-}M)^{-1}$ Matrix

Criteria	K1	K2	K3	K4	K5	K6	K7	K8
K1	1,28	0,42	0,41	0,42	0,44	0,49	0,48	0,43
K2	0,4	1,3	0,4	0,43	0,42	0,47	0,45	0,42
K3	0,4	0,44	1,29	0,43	0,45	0,48	0,46	0,41
K4	0,4	0,42	0,39	1,3	0,42	0,5	0,45	0,39
K5	0,24	0,23	0,2	0,24	1,17	0,29	0,25	0,2
K6	0,18	0,21	0,2	0,21	0,2	1,17	0,21	0,19
K7	0,21	0,24	0,23	0,24	0,21	0,25	1,18	0,21
K8	0,17	0,19	0,19	0,19	0,16	0,21	0,19	1,13

Finally (M) matrix $(I-M)^{-1}$ matrix multiplied in Table 9 Total Relationship Matrix (T) is located and stage three is complete.

Table 9. Total relation matrix

Criteria	K1	K2	K3	K4	K5	K6	K7	K8	Di
K1	0,28	0,42	0,41	0,42	0,44	0,49	0,48	0,43	3,3614
K2	0,40	0,30	0,40	0,43	0,42	0,47	0,45	0,42	3,291
K3	0,40	0,44	0,29	0,43	0,45	0,48	0,46	0,41	3,3606
K4	0,40	0,42	0,39	0,30	0,42	0,50	0,45	0,39	3,2615
K5	0,24	0,23	0,20	0,24	0,17	0,29	0,25	0,20	1,8092
K6	0,18	0,21	0,20	0,21	0,20	0,17	0,21	0,19	1,5768
K7	0,21	0,24	0,23	0,24	0,21	0,25	0,18	0,21	1,7604
K8	0,17	0,19	0,19	0,19	0,16	0,21	0,19	0,13	1,4133
Ri	2,287	2,445	2,294	2,448	2,467	2,863	2,662	2,369	

In the fourth phase of DEMATEL method; affected and affecting (sender and receiver) is to determine the criteria groups. Total Relationship Matrix with a values of the rows total of D,columns total of R are obtained and the following table has been created. Based on the matrix found in the third phase; total D_i of the i'th row of this matrix; by i criteria sent to other criteria shows the total of direct and indirect effects. The sum of column R_i; It shows the sum of the effects coming from the other criteria by the same criteria. The effect values of criteria shown in Table 10.

Table10. Impact value of criteria

Criteria	Di	Ri	Di+Ri	Di-Ri
K1	3,3614	2,2867	5,6481	1,0747
K2	3,291	2,4452	5,7362	0,8458
K3	3,3606	2,2941	5,6547	1,0665
K4	3,2615	2,448	5,7095	0,8135
K5	1,8092	2,4665	4,2757	-0,6573
K6	1,5768	2,8626	4,4394	-1,2858
K7	1,7604	2,6623	4,4227	-0,9019
K8	1,4133	2,3688	3,7821	-0,9555

In the fifth phase of DEMATEL method; determination of the threshold value and drawing of effect diagrams. In this study, because of the threshold values was not specified the weight of cretarias calculated in the sixth phase and shown in Table 11. In the sixth phase of the DEMATEL method; determination of the criterias weight. Ranking is done after determining the weights of the criteria.

Table 11. Criteria weight

Criteria	$(D_i+R_i)^2+(D_i-R_i)^2$	$\sqrt{(\square_{\square} + \square_{\square})^2 + (\square_{\square} - \square_{\square})^2}$	W_i
K1	33,06	5,75	0,142
K2	33,62	5,80	0,143
K3	33,11	5,75	0,142
K4	33,26	5,77	0,143
K5	18,71	4,33	0,107
K6	21,36	4,62	0,114
K7	20,37	4,51	0,112
K8	15,22	3,90	0,096

With DEMATEL method the criteria weights; air pressure of 0.142, 0.143 water vapor pressure, 0.142 relative humidity and 0.143 wind speed were found. According to this results the effectiveness ranking is in the following form; wind speed, relative humidity, air pressure and water vapor pressure**.**

5. CONCLUSIONS

Air temperature is one of the forecast decision support methods. Forecasting close to the right temperature, primary agriculture, including many other sectors it is extremely important to be able to see the front. This way, the sectors may determine their strategies according to these forecasts. Businesses determining the appropriate strategy can provide superior to other competitors in the market. The most important factor in determining the right strategy; by determining the most accurate way the forecast affecting criterias.

In the first part of the study; literature research was made and eight effective criteria was determined which affects the temperature and those criteria according to expert opinion by applying the AHP and DEMATEL methods reduced to the most efficient four criteria and shown in Table 12.

Table 12. Determination of the criteria with AHP and DEMATEL methods

AHP-W		**DEMATEL-W**	
1. Hava Basıncı	0,31	1. Su Buhar Basıncı	0,143
2. Su Buhar Basıncı	0,25	2. Rüzgâr Hızı	0,143
3. Bağıl Nem	0,16	3. Bağıl Nem	0,142
4. Rüzgâr Hızı	0,08	4. Hava Basıncı	0,142

When weights of four effective criteria was collected by the AHP method it was found to be a power of 80%. In the DEMATEL was found to be 57% of the power of this weight. These results demonstrate that it can be clarified with this criteria the forecasting values of 80% with AHP and 57% with DEMATEL.

In this study, it is intended to contribute to researchers who will use the criteria selection in the temperature forecasting model.

REFERENCES

[1]. G. Abrajano, (Philippines), Md. Ahiduzzaman (Bangladesh), R. Ching (Philippines), Krismianto (Indonesia), Z. Liuhang (Singapore), Weather/Climate Prediction", Institute for Mathematical Sciences National University of Singapore, (19 Apr – 2 May 2009).
[2]. S. Eminger (University of St Andrews), The History of Weather Forecasting, May 2011.
[3]. M. Tektaş, Weather forecasting using ANFIS and ARIMA models", A case study for İstanbul, Marmara University, Vocational School of Technical Sciences, Turkey (2010).
[4]. P. Kumar, Minimum Weekly Temperature Forecasting using ANFIS", *Computer Engineering and Intelligent Systems*, Online Vol 3, No.5, 2012.

[5]. O. Erol, Genel Klimatoloji. Gazi Büro Kitabevi. Ankara, 1993.
[6]. T.L. Saaty, "A Scaling Method for Priorities in Hierarchical Structures", *Journal of Mathematical Psychology*, 15, 57-68, 1977.
[7]. T.L. SAATY and L.G. VARGAS, Models, Methods, Concepts and Applications of the Analytic Hierarchy Process, Kluwer Academic Publishers, Boston, 2000.
[8]. T.L. SAATY, "Relative Measurement and Its Generalization in Decision Making Why Pairwise Comparisons are Central in Mathematics for the Measurement of Intangible Factors The Analytic Hierarchy/Network Process", *Review of the Royal Spanish Academy of Sciences Series a Mathematics (RACSAM)*, 102(2): 251-318,2008.
[9]. J-K. Chen and I-S Chen., "A Pro-performance appraisal system for the university", *Expert Systems with Applications*, Cilt 37, No 3, 2108-2116, 2010.
[10]. E. Fontela and A. Gabus, "DEMATEL, Innovative Methods, Report no. 2, Structural Analysis of the World Problematique", Battelle Geneva Research Institute,1974.
[11]. E. Fontela and A. Gabus, "The DEMATEL Observer: Battelle Institute", Geneva Research Center, 1976.
[12]. W-H Tsai and W-C Chou, "Selecting Management Systems for Sustainable Development in SMEs: A Novel Hybrid Model Based on DEMATEL, ANP and ZOGP", *Expert Systems with Applications*, 36: 1444-1458, 2009.
[13]. E. Aksakal and M. Dağdeviren, "ANP ve DEMATEL Yöntemleri ile Personel Seçimi Problemine Bütünleşik Bir Yaklaşım" *Gazi Üniversitesi Mühendislik Mimarlık Fakültesi Dergisi*, 25(4): 905-913, 2010.

Phononic Crystal with Absolute Acoustic Band Gap in the Audible Frequency Range: Finite Element Analysis

Zafer Ozer[1], Muharrem Karaaslan[2], Oguzhan Ozer[3]

Abstract

Metamaterials are described as futuristic design materials with new and unusual electromagnetic properties. Acoustic or seismic metamaterial provide to design materials for unusual acoustic and mechanical features such as trapping, reflection or total transparency to acoustic or mechanical waves.

In this study, the propagation of acoustic waves in a two-dimensional composite medium constituted of a square array of parallel steel triangular prisms in air is investigated theoretically. In the low frequency regime, the band structure calculations agree with the finite element results. These calculations show that this composite material have a large absolute forbidden band in the domain of the audible frequencies.

Numerical analysis show that the transmission through an array of steel triangular prisms drops to noise level throughout frequency interval in good agreement with the calculated forbidden band.

Keywords: *Metamaterials, acoustic metamaterials, finite element method*

1. INTRODUCTION

Phononic crystals (PnC's) are artificial periodic structures consist of two or more different materials which inclusion placed is matrix material. The PnC structures could be solid–solid, fluid–fluid and mixed solid–fluid composite systems [1]. Different compositing of PnC have been studied by materials differencing both the inclusions and the matrix. There are many studies on the band gap feature of PnCs which waves in this specific frequency range cannot propagate. The forbidden band feature of PnC has been used noise attenuating and acoustic filtering [2-7].

Recently researchers focus on PnC and their applications on controlling the propagating of acoustic and mechanical waves. These artificial periodic structures have unusually properties such as negative refraction [8-9], wave trapping [10, 13], and sound focusing [8, 9]. By understanding the features of the PnC many application could be made for example seismic metamaterials [14], hypersonic device [15,16], and thermal conductance control [17,18] in sonic frequency, ultrasonic frequency and MHz and GHz frequencies [10-12].

Structures with negative index of refraction, has led to the design of a planar lens structure [8-9]. One potential use is the acoustic and thermal diode applications [17]. Depending on to advances in this field will lead to the design of complex circuits, acoustic imaging and acoustic detection technology.

Beside waveguide and acoustic control features of PnC's they are promising for the development of one-way acoustic and thermal devices. Many structures have been identified in the literature on this subject [19-23] which one of them a PnC rectifier of elastic waves with triangular holes in isotropic matrix material as a scatterer [23].

Due to the asymmetric structure of triangular shape scatterer which cause nonresiprocal propagating feature useful from the geometric effect on scattering the waves. It has been present the detailed transmission spectra and efficiency of PnC with triangular holes [24]. It has been showed that complete band gap can be broaden via decreasing lattice symmetry [25-28].

In this study we investigate the complete band properties of square lattice with triangular shape scatterer in unit cell and lens effect of the common PnC for different frequency (sonic and ultrasonic frequencies) range with FEM analysis. Proposed PnC consist of steel scatterer arrays with triangular shape in square lattice geometry.

2. MATERIALS AND METHODS

Figure 1(a) shows the 2D PnC array structure. The equilateral triangular inclusion materials and matrix can be set to different materials. For numerical calculation we used the lattice size of a=30 mm and the side of edges we changed 20 mm to 28 mm for an array of 10x14 triangular shape prism placed in a background material for sonic frequency and a=3 mm b=2.6 mm for ultrasonic frequency.

[1]*Corresponding author: Mersin University, Mersin Vocational High School, Department of Electronic and Automation, Mersin, 33335, Turkey.* zaferozer@mersin.edu.tr

[2] *İskenderun Technical University, Department of Electrical-Electronical Engineering, İskenderun, 31200, Turkey*

[3]*Kahramanmaraş Sutcu Imam University, Elbistan Vocational High School, Department of Electronic and Automation, Kahramanmaraş,46340, Turkey*

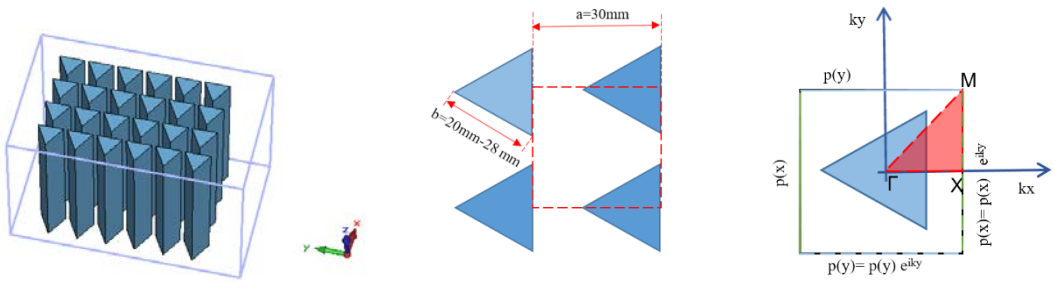

a) b) c)

Figure 1. Schematics of the structure composed of a periodic square array of equilateral triangles in air (a) unit cell of the structure (b), the Brillouin zone for a 2D square lattice (c).

The parameters of the materials we used in FEM analysis are shown in table 1. The absorber boundary condition is applied to the edge of the periodic structure and sound hard boundary conditions is applied to the edge of cylindrical composite for normal component of the air particles equal to zero. Left edge is defined as plane wave signal source with a pressure level of p0=1 [Pa].

Figure 1b shows the unit cell we used as a basis for the calculations. The structure is assumed to be infinite in *z* direction and periodic in the *x* and *y* directions. For the doubly periodic structure, $a_1$and a_2 are the basis vectors. The relation for the pressure distribution *p* for nodes lying on the boundary of the unit cell can be expressed via the Floquet-Bloch theorem as in eq. 1.

$$p(x + a_1 + a_2) = p(x)e^{i(k_x+k_y)} \quad (1)$$

The total pressure field (Pa) and the acoustic pressure level (dB) is observed over point A and point B placed front and back sides of PnC, respectively as seen in fig. 2 where the point B give us the transmission of the PnC. For FEM analyze the acoustic wave propagation in the PnC wherein we set the lattice parameter a=30 mm and the side edge of equilateral triangle cross section scatterers is increased from b=20 mm to b=28 mm by a step of 2 mm both forward and backward propagation.

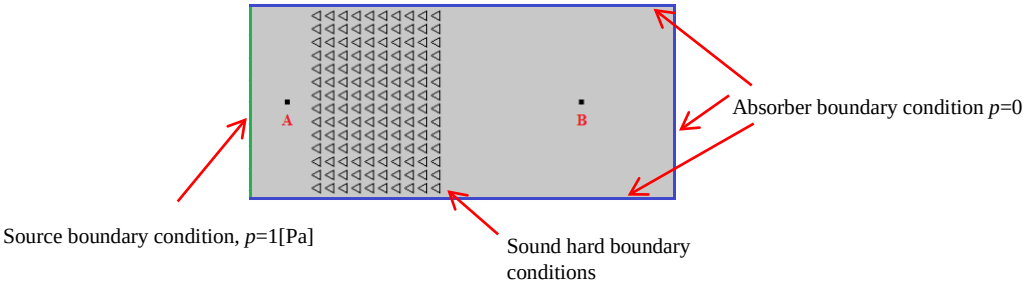

Figure 2. Conversional phononic crystal design

Table 1. Properties of the material used in the analysis

	Steel	**Air**
Speed of sound (m/s)	6100	343
Density (kg/m^3)	7850	1.25

3. RESULTS AND DISCUSSION

In this study, we investigated the propagating of the acoustic wave in PnC that periodically placed elastic steel triangular shape prism in the air by FEM analysis. For validating the results we compared the acoustic pressure level (dB) obtained via FEM analysis, the band gap by using the unit cell via FEM. As seen in fig. 3a and b the results are in good agreement with each other.

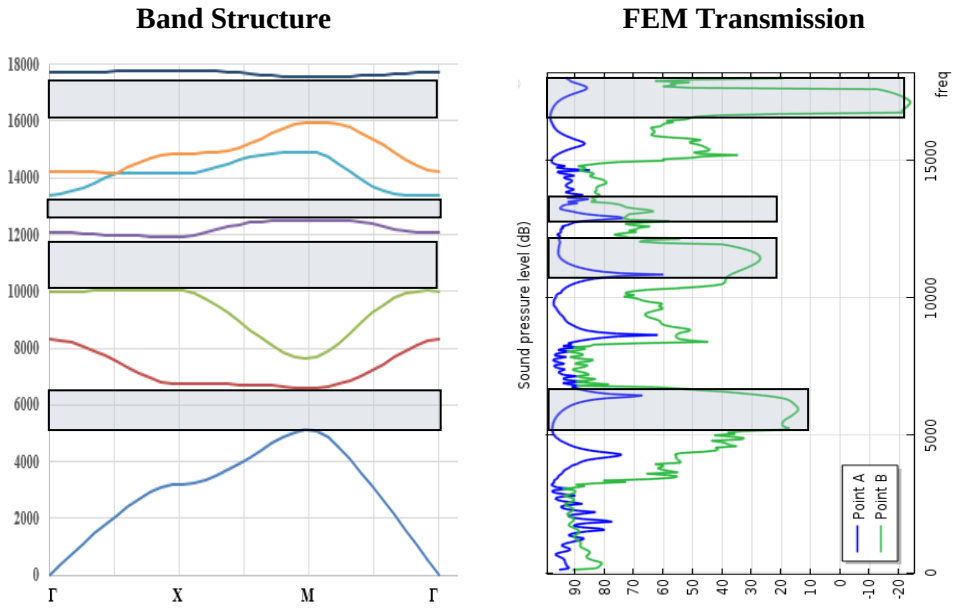

a) b)

Figure 3. a) A comparison of PWE computed band structure, b) FEA computed transmission measurements conventional phononic crystal system(a = 30 mm, b = 26 mm).

According to numerical analysis, the acoustic resonator has complete band gap at the center frequencycenter frequency is 5027 Hz between 4414 Hz and 5641 Hz which results in sound attenuation as seen in fig 3.

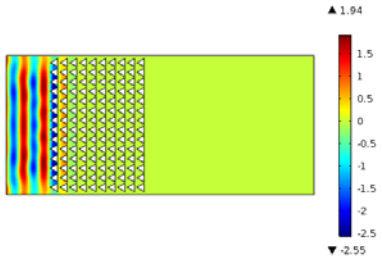

Figure 4. Acoustic wave has 3200 Hz frequency

Figure 4 show acoustic wave has 6200 Hz frequency in first band cannot propagate in PnC. The figure 5 shows parametric sound level investigation in terms of sound pressure (Pa) and sound pressure level (dB) at point B where lattice parameter a=30mm and edge of scatterer increased in the range of b=22 mm-28 mm, respectively.

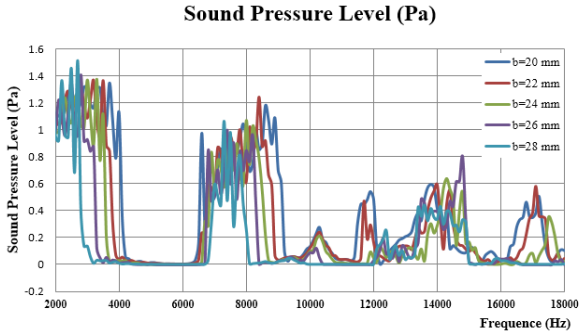

a)

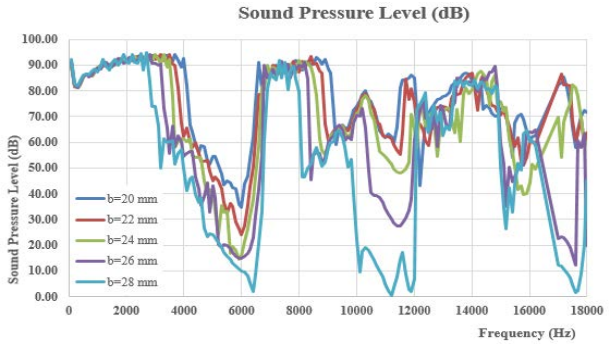

b)

Figure 5. Parametric sweep results at point B a) acoustic pressure (Pa) b) acoustic pressure level (dB)

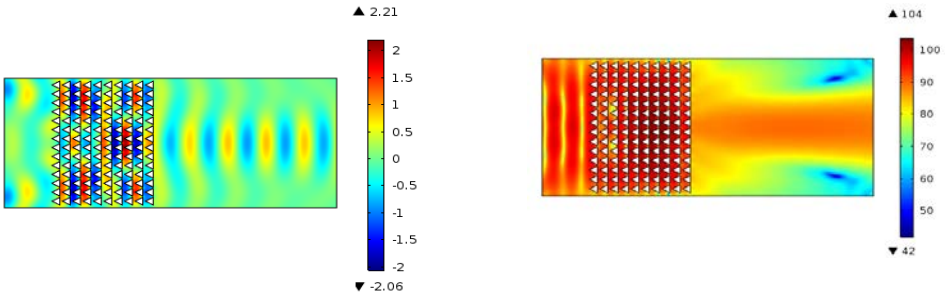

a) b)

Figure 6. Lens effect of acoustic wave a) Normalized total pressure field (Pa) b) Sound pressure level (dB)

The acoustic lens effect of the PnC analyzed with FEM. In proposed structure where edge of the triangular shape b=26 mm and lattice parameter a=30 mm in fig 2. at 3200 Hz PnC shows negative refraction and it has acoustic lens effect.

We also investigate band properties and lens effect of the proposed PnC by decreasing the sizes as mentioned. Proposed PnC also has the complete broad band gap and lens effect in ultrasonic frequency as seen in figure 7.

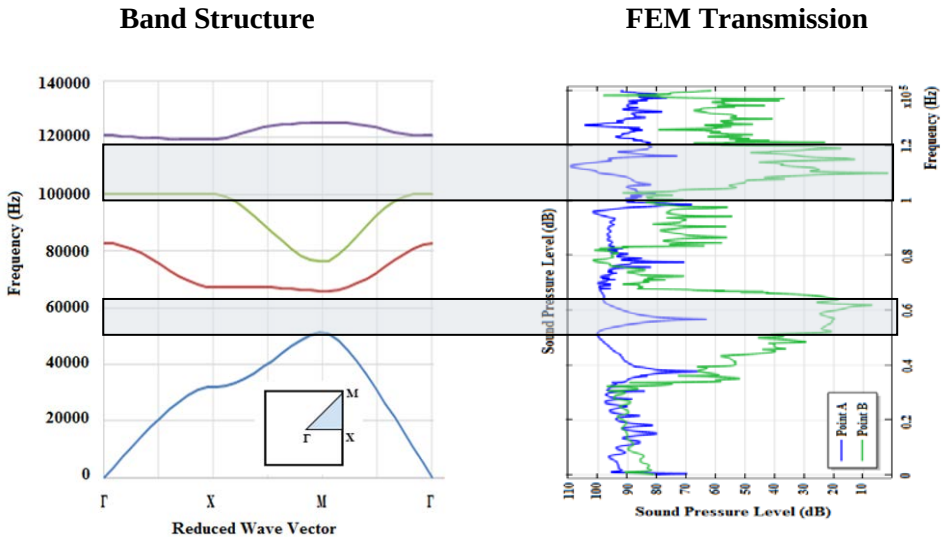

a) *b)*

Figure 7. a) Band structure of PnC b) normalized total pressure field (Pa) for ultrasonic PnC

4. CONCLUSIONS

The periodic structures have basic properties that waveguide, acoustic focusing, and negative refraction like as a band gap. These properties could lead to the designing of integrated phononic devices. In this study, band structure and propagation of longitudinal acoustic waves in 2D PnC were investigated with FEM.Simulated PnC has a wide band gap which provide acoustic attenuation level both sonic and ultrasonic frequencies. It could be lead to designing of devices where operate in different frequency ranges like acoustic cloaking, acoustic lenses, and acoustic sensors. Researchers will be focusing on analyzing and designing periodic, quasi periodic acoustic structures.

REFERENCES

[1] Y. Pennec, J. O. Vasseur, B. Djafari-Rouhani, L. Dobrzyńskia, P. A. Deymier, "Two-dimensional phononic crystals: Examples and applications", *Surface Science Reports*, vol. 65, pp 229–291, 2010.
[2] R. Martinez-Salaa , C. Rubioa , LM. Garcia-Raffib , JV. Sanchez-Pereza , EA. SanchezPereza , J. Llinaresa, "Control of noise by trees arranged like sonic crystals.", *J Sound Vib*, 291, 100–6, 2006.
LY. Wu , LW. Chen, "Acoustic band gaps of the woodpile sonic crystal with the simple cubic lattice.", *J Phys D: Appl Phys*, 44, 045402, 2011.
[3] Z. Fuster-Garcia, V. Romero-Garcia, JV. Sanchez-Perez, LM.Garcia-Raffi, "Targeted band gap creation using mixed sonic crystal arrays including resonators and rigid scatterers.", *Appl Phys Lett*, 90, 244104, 2007.
[4] V. Romero-Garcia , E. Fuster , LM. Garcia-Raffi, EA. Sanchez-Perez , M. Sopena, J. Llinares et al. "Band gap creation using quasiordered structures based on sonic crystals.", *Appl Phys Lett*, 88, 174104,2006.
[5] R. Pico, VJ. Sanchez-Morcillo, I. Perez-Arjona, K. Staliunas, "Spatial filtering of sound beams by sonic crystals." *Appl Acoust*, 73, 302–6, 2012.
[6] LS. Chen , CH. Kuo , Z. Ye, "Acoustic imaging and collimating by slabs of sonic crystals made from arrays of rigid cylinders in air.", *Appl Phys Lett*, 85, 1072, 2004.
[7] A. Sukhovich,L. Jing, J. H. Page,"Negative refraction and focusing of ultrasound in two-dimensional phononic crystals.", *Physical Review B*, Vol 77, 014301, 2008.
[8] N. Maetani, T. Kurose and K. Tsuruta, Numerical Simulation of Acoustic Waves in Two-Dimesional Phononic Crystal: Negative Refraction. Memoirs of Faculty of Engineering, -Okayama University, Vol. 44, pp. 7-12, 2010.
[9] D.P. Elford, "Band Gap Formation in Acoustically Resonant Phononic Crystals.", Doctoral Thesis, Loughborough University, 2010.
M.F. Su, R.H. Olsson, Z.C. Leseman and I. El-Kady, "Realization of a phononic crystal operating at gigahertz frequencies.", *Applied Physics Letters*, 96, 053111, 2010.
[10] F.L. Hsiao, A. Khelif, H. Moubchir, A. Choujaa, C. C. Chen, V. Laude, "Complete band gaps and deaf bands of triangular and honeycomb water-steel phononic crystals.", *Journal Of Applied Physics*, 101, 044903, 2007.
[11] R. Lucklum, M. Zubtsov, A. Oseev, M. P. Schmidt, S. Hirsch, F. Hagemann, "Phononic Crystals and Applications.", doi 10.5162/sensor2013/A3.1, 2013.
[12] S. Brûlé, E.H. Javelaudv, S. Enoch, S. Guenneau, "Seismic metamaterial: how to shake friends and influence waves?", http:// http://arxiv.org/abs/1301.7642 consulted 31.12.2015, 2013.
[13] B. Graczykowski, M. Sledzinska, F. Alzina, J. Gomis-Bresco, J.S. Reparaz, M.R. Wagner, C.M. Sotomayor, "Phonon dispersion in hypersonic two-dimensional phononic crystal membranes.", *Phys. Rev. B*, 91, 95414, 2015.
[14] E. Alonso-Redondo, M. Schmitt, Z. Urbach, C.M. Hui, R. Sainidou, P. Rembert, G. Fytas, "A new class of tunable hypersonic phononic crystals based on polymertethered colloids.", *Nature Communications*, 6, 1–8, 2015.
[15] BW. Li, L. Wang, G. Casati, "Thermal diode: rectification of heat flux.", *Phys Rev Lett*, 93:184301, 2004.
[16] N. Zen, T.A. Puurtinen, T.J.Isotalo, S. Chaudhuri, I.J. Maasilta, "Engineering thermal conductance using a two-dimensional phononic crystal.", *Nat. Commun.*, 5, 3435, 2014.
[17] HX. Sun , SY. Zhang , XJ. Shui, "A tunable acoustic diode made by a metal plate with periodical structure.", *Appl Phys Lett*, 100:103507, 2012.
[18] XF. Li , X. Ni, L. Feng, MH. Lu, C. He, YF. Chen, "Tunable unidirectional sound propagation through a sonic-crystal-based acoustic diode.", *Phys Rev Lett*, 106:084301, 2011.
[19] B. Liang, XY. Zou, B. Yuan, JC. Cheng, "Frequency-dependence of the acoustic rectifying efficiency of an acoustic diode model.", *Appl Phys Lett*, 96, 2010.
[20] N. Boechler, G. Theocharis, C. Daraio, "Bifurcation-based acoustic switching and rectification.", *Nat Mater Lett*, 10:665–8, 2011.
[21] Y. Tanaka, T. Murai, N. Nishiguchi, "Rectification of elastic waves in a thin plate.", *J Appl Phys*, 111:024507, 2012.
[22] S. Shirota, R. Krishnan, Y. Tanaka, N. Nishiguchi, "Rectifying acoustic phonons.", *J Phys*, Conf. Series, 92, 012115, 2007.
[23] R. Pico, VJ. Sanchez-Morcillo, I. Perez-Arjona, K. Staliunas, "Spatial filtering of"sound beams by sonic crystals.", *Appl Acoust*,73:302–6, 2012.
[24] R. Moussa, S. Foteinopoulou, L. Zhang, G. Tuttle, K. Guven, E. Ozbay et al, "Negative refraction and superlens behavior in a two-dimensional photonic crystal.", *Phys Rev B*, 71:085106, 2005.
[25] JF. Robillard, J. Bucay, PA. Deymier, A. Shelke, K. Muralidharan, B. Merheb et al, "Resolution limit of a phononic crystal superlens.", *Phys Rev B*, 83:224301, 2011.
[26] . Sukhovich, L. Jing, JH. Page, "Negative refraction and focusing of ultrasound in two-dimensional phononic crystals.", *Phys Rev B*, 77:014301, 2008.

Effect of Crown Margin Design on the Stress Distribution in Mandibular First Molar Restored by Means of IPS E-Max: A Finite Element Method

Zafer Ozer[1], Huseyin Yanik[2], Oguzhan Ozer[3]

Abstract

The purpose of this study was to evaluate the effect of the stress distribution of the crown margin design localization off critical sites in mandibular first molar under functional loading by using finite element analysis engineering tools. 2-dimensional teeth modeled by transferring the anatomical structure from the Wheeler.

Two dimensional finite element model of a mandibular first was presented. The bite force of 50N, 100N and 200N was applied vertically to the tooth longitudinal axis. Three models were considered to be restored with IPS E-max with a different margin design. Stress distribution was investigated using finite element analysis.

Keywords: *Mandibular first molar, all-ceramic restoration, IPS E-max, finite element method*

1. INTRODUCTION

Ceramics are the oldest structurally modified inorganic materials. The intended use of the ceramics on composite materials is their hard structure and resistant to abrasion and high temperatures. Due to the metal usage to increase strength of ceramics and the lack of sufficient transparency, aesthetic appearance and bio-compatibility in the ceramic restorations, researchers now interested in all ceramic systems [1].

Due to the fact that rigid structure, bio-compatibility and aesthetic appearance as natural tooth, Zirconia ZrO_2 and SiO_2 are commonly used ceramics in dentistry. While dental ceramics are not resistant to tensile stress, they have 100 times more resistance against compressive forces compare to tensile stress. So, tensile stress that causing failure need to be examined [2,14].

Recently, it has become important to improve mechanical durability of dental materials which used in dental restorations and perform the stress analyze of these materials in order to determine the stresses which occurs in dental structures [1-6]. Tensile strength of brittle materials such as ceramics corresponds to the tensile forces which these materials can resist per unit area. Therefore, tensile stresses in material need to be examined [15-17].

There are two types of stress analyze methods to examine stress of materials: theoretical and experimental [1].

Finite Elements Method (FEM) is an acceptable numerical solution method for a variety of mechanical problems [1-6,8,13,18]. It's appropriate that the stress analyze of living tissue has to be built on the model of this tissue because of the risk, high cost and the challenge of making stress analyze on the living tissue. Detecting areas with high fault risks because of high stress intensity under applied forces and obtaining suitable designs for increasing strength of the material can be achieved by applying force analysis [8].

By using FEM which has a lot of advantages in comparison with the other methods, realistic designs can be created with usage of realistic material models. Different materials can be used on this structures, so that displacement and stress distribution can be obtained accurately. Changing the geometry of the model, the properties of materials that used and the applied forces, more analysis can be done with much less time and cost [8].

For both the patient and the dentist, the fracture of teeth poses a significant problem. Mandibular first molars are most prone to fractures in posterior region[13].

The purpose of this study was to examine the effect of various margin designs on the stresses distribution in the mandibular first molar.

[1]*Corresponding author: Mersin University, Vocational High School, Mersin, 33335, Turkey. zaferozer@mersin.edu.tr*

[2] *Mersin University, Department of Electrical-Electronical Engineering, Mersin, 33343, Turkey*

[3]*Kahramanmaras Sutcu Imam University, Elbistan Vocational High School, Kahramanmaras,,46340,Turkey*

2. MATERIAL AND METHOD

In this study, it was used infrastructure ceramic *IPS e-max Press* and coating ceramic *IPS e-max Ceram* which are suitable alternative of all-ceramic systems in the lack of posterior tooth treatment and restoration. Mechanical properties of the infrastructure and coating ceramics that used in analyze were obtained from manufacturer firm and the mechanical properties of other materials were obtained from the literature as seen in Table 1 [1,6,13].

The analysis of stress distribution in mandibular first molars for different margin design was conducted by means of FEA. 2-dimensional model of the mandibular first molar was modelled basis on the anatomical form in Wheeler [7]. The opposing maxillary first molar crown was modelled for analysis.

The margin shape of cut tooth according to restoration species and the tooth to be restored is very important. For that purpose three different margin shapes created to examine stress distribution in different margins as seen in Figure 1.

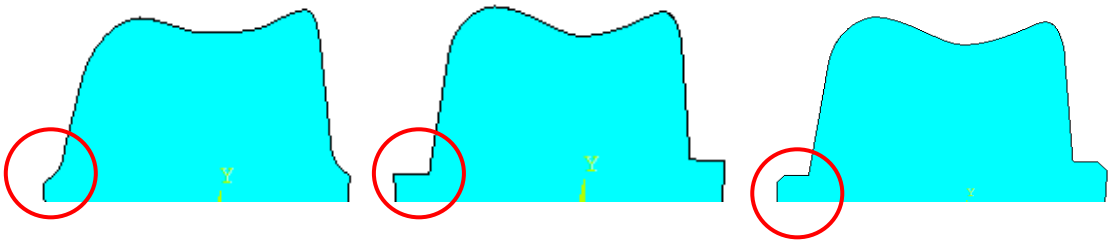

a) Chamfer *b) Shoulder* *c) Shoulder with Bevel*

Figure 1. Margin types of mandibular first molar

Table 1. Mechanical properties of materials used in models

Material	**Elastic Modulus E [MPa]**	**Poisson Ratio ϑ**	**Flexural Strength [MPa]**
IPS e-max Ceram	65000	0.24	90 ± 10
IPS e-max Press	91000	0.23	400 ± 40
Dentin	18600	0.31	
Alveoli Bone	14700	0.26	
Periodontium	68.9	0.45	

The tooth model was divided by triangular elements in order to perform calculations. The table shows number of nodes and elements used in models. The computerized model of the mandibular molar was fixed upper side the opposing maxillary first molar crown. The tooth models were divided by 8-node triangular elements where the element and node numbers are as seen in table 2 for performing the calculations.

Table 2. Number of elements and nodes used in models

Margin Type	**Element Numbers**	**Node Numbers**
Chamfer	1882	5787
Shoulder	1631	5052
Shoulder with Bevel	1891	5852

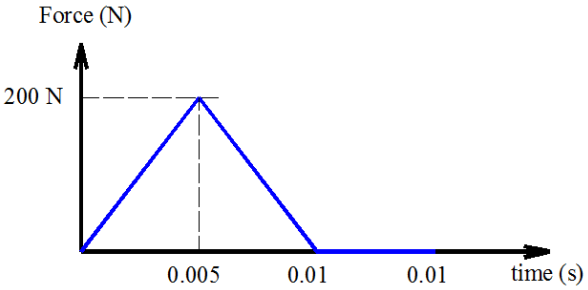

Figure 2. Time dependent loading of mandibular first molar

The time dependent occlusal force of 200 N were chosen in *y* direction for all model as show in Figure 2. It's reported that periodontal ligament significantly affects the distribution of stress. So we modelled the periodontal ligament of 0.1 mm width around the root [5].

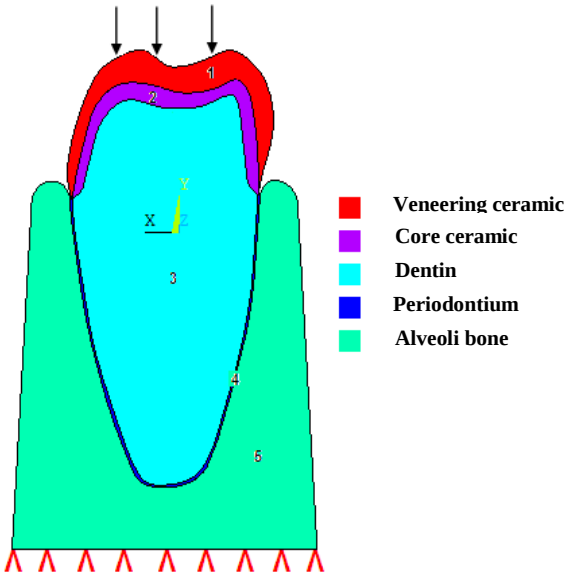

Figure 3. Boundary conditions and applied force

We assumed that the materials which used in models were homogenous, isotropic, and linear elastic. In order to compare the stress in the tooth subjected to the varying loads we were assumed that maximum 200 N time transient bit force applied to the tooth the expected occlusal contact areas. Table 3-5 shows compressive and tensile stresses of three different margin type under 50 N, 100 N and 200 N occlusal forces respectively. Table 6 shows maximum first principal stress distribution under 50 N, 100 N and 200 N occlusal forces.

Table 3. Stress distribution under 50 N occlusal loading

Margin Type	**Compressive Stress [MPa]**	**Tensile Stress [MPa]**
Chamfer	-24.20	12.49[1]
Shoulder	-22.04	9.44[1]
Shoulder with Bevel	-54.14	24.44[1]

Table 4. Stress distribution under 100 N occlusal loading

Margin Type	Compressive Stress [MPa]	Tensile Stress [MPa]
Chamfer	-48.40	24.98[1]
Shoulder	-44.08	18.88[1]
Shoulder with Bevel	-108.29	48.89[1]

Table 5. Stress distribution under 200 N occlusal loading

Margin Type	Compressive Stress [MPa]	Tensile Stress [MPa]
Chamfer	-96.80	49.96[1]
Shoulder	-88.16	37.76[1]
Shoulder with Bevel	-216.59	97.78[1]

1 Maximum normal stresses

Table 6. Maximum stress distribution occlusal loading

Margin Type	Ceramic Type	Applied Bit Force			Flexural Strength [MPa]	
		50 N	100 N	200 N	100%	EL
Chamfer Model	IPS emax Press[2]	9.23	18.47	36.94	400	160
	IPS emax Ceram[2]	34.33	***68.66***	***137.33***	90	36
Shoulder Model	IPS emax Press[2]	8.46	16.93	33.86	400	160
	IPS emax Ceram[2]	17.15	34.31	***68.63***	90	36
Shoulder with Bevel Model	IPS emax Press[2]	11.12	22.24	44.49	400	160
	IPS emax Ceram[2]	***58.41***	***116.82***	***233.65***	90	36

EL= Endurance limit

2 Maximum compressive stresses

3. RESULTS AND DISCUSSION

Tensile stress in the veneer ceramic is found to be higher at the points of the applied force. When we compared the stress distribution with respect to margin type, stress values on the veneer ceramic due to the applied force is higher than the value of safety limit which indicated by the firm and the stress values on the core ceramic is lower than the value of safety limit which indicated by the firm. Chamfer and Shoulder models can be used for the situations that does not exceed safety limits in accumulation of stress for restorations that used IPS emax Ceram and IPS emax Press ceramics. Shoulder with Bevel margin type is not recommended because of the stress accumulation above the safety limits in all loading forces. In regions where the intensity of accumulation is high, tensile stress exceeding the safety limit can be seen as a starting point of failure in long-term use. Higher bending resistance coating ceramics can be used to avoid breaking in this region. Using only infrastructure ceramic on the region which has the higher tensile force can improve the strength of the system.

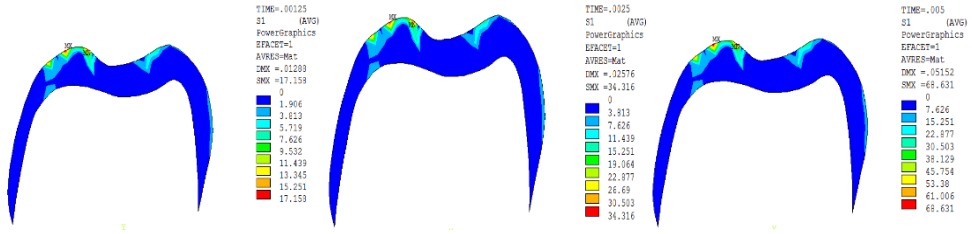

(a) *(b)* *(c)*

Figure 4. First principle distribution of stresses on veneer ceramic under a) 50 N, b) 100 N, c) 200 N forces on Shoulder margin

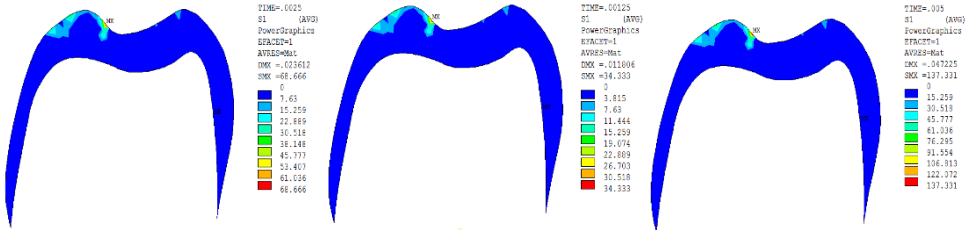

Figure 5. First principle distribution of stresses on veneer ceramic under a) 50 N, b) 100 N, c) 200 N forces on Chamfer margin

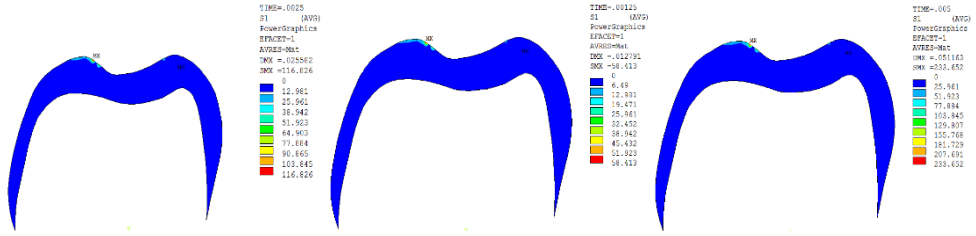

Figure 6. First principle distribution of stresses on veneer ceramic under a) 50 N, b) 100 N, c) 200 N forces on Shoulder with Bevel margin

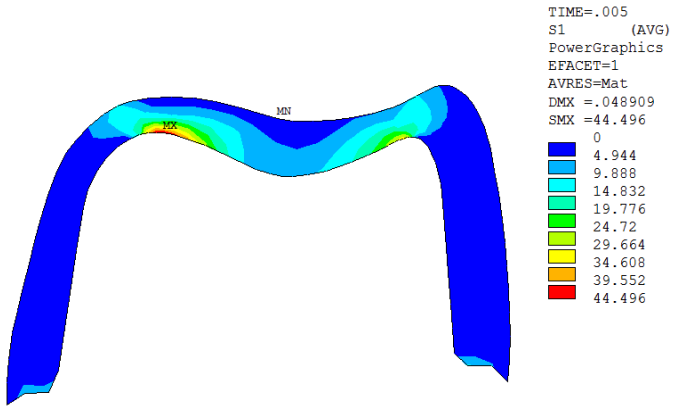

Figure 7. First principle stress distribution on core ceramic under 200 N force on Shoulder with Bevel Margin

When the stress distribution according to the margin type was observed, it was observed that the stress on the veneer ceramic in Shoulder type margin with 50 N and 100 N loadings are under the safety limit and safety limit exceeded at 200 N loading as we seen in figure 4. It was observed that the stress on the veneer ceramic in Chamfer type margin with 50 N loading is under the safety limit and 100 N and 200 N loadings are exceeded the safety limit as it seen in figure 5. Stress values on the veneer ceramic in Shoulder with Bevel type margin are exceeded the safety limit for all loading forces as it's seen in figure 6 and it was observed that it's not suitable to use in all-ceramic restorations. It was observed that the stress values on the core ceramic are under the safety limit for all margin models. It can be clearly seen in figure 7 in Shoulder with Bevel type margin which has the highest expectation as stress value but it's still under the safety limit. The region which has higher stress values on veneer ceramic are the points where the force is applied [3].

FEM is a convenient analysis method for simulating the behavior of structures under load. However, it is an approximating method, with a model consisting of a finite number of elements. Present study shows that the stress distribution under different forces in two different ceramic types as core and veneer and three different margin types as Shoulder, Chamfer and Shoulder with Bevel models. To confirm the results of the present study, clinical results should be available. But this is very tough task to do because of the structure of tooth and clinical requirements. To determine stress analysis and behavior of live tissues and organs under forces is very difficult, costly, risky and sometimes impossible. So FEM is an appropriate method to achieve and obtain the requirements thus it's allows us biomechanically functional design of a restored tooth and to have a better biometrics of the restoration materials in order to optimize the restorative criteria and material choice by simulation.

REFERENCES

[1] C. Kırcelli, İki Farklı Tam Seramik Sistemin Kullanıldığı Ü. Üyeli Sabit Protez Mukavemetinin Sonlu Elemanlar Stes Analizi ile İncelenmesi, Adana (2004).
[2] Yamamoto M. , Metal-Ceramics Principal and Methods of Makoto Yamamoto. Chicago: Quintessence Publishing Co. Inc. 1985.
[3]M. P. DITTMER, P. KOHORST, L. BORCHERS, R. SCHWESTKA-POLLY, & M. STIESCH, Stress analysis of an all-ceramic FDP loaded according to different occlusal concepts, Journal of Oral Rehabilitation, doi: 10.1111/j.1365-2842.2010.02147.x
[4] B. Dejak, A. Mlotkowski, C. Langot, Three-dimensional finite element analysis of molar with thin-walled prosthetic crowns made of various materials, Dental Materials, 28, 433-441, 2012.
[5] B. Dejak, A. Młotkowski, Finite element analysis of strength and adhesion of cast posts compared to glass fiber-reinforced composite resin posts in anterior teeth, THE JOURNAL OF PROSTHETIC DENTISTRY, DOI: 10.1016/S0022-3913(11)60011-5
[6] L. Z. Largura, MA Argenta, M T Sakima, ES Camargo, O Guariza-Filho and OM Tanaka, Bone stress and strain after use of a miniplate for molar protraction and uprighting: A 3-dimensional finite element analysis, American Journal of Orthodontics and Dentofacial Orthopedics, August 2014, Vol 146, Issue 2
[7] Wheeler RC, An atlas of tooth form. W. B. Saunders, Philadelphia, ABD, 1989.
[8] ADIGÜZEL, Ö. 2010 Sonlu Elemanlar Analizi, Dicle Dişhekimliği Dergisi, Cilt / Volume 11 · Sayı / Number 1 2010
[9] McDaniel RJ, Davis RD, Murchison DF, Cohen RB. Causes of failure among cuspal-coverage amalgam restorations: a clinical survey. J Am Dent Assoc 2000;131:173-7.
[10] Bader JD, Martin JA, Shugars DA. Incidence rates for complete cusp fracture. Community Dent Oral Epidemiol 2001;29:346-53.
Eakle WS, Maxwell EH, Braly BF. Fractures of posterior teeth in adults. J Am Dent Assoc 1986;112:215-8.
[11] Cavel WT, Kesley WP, Blankenau RJ. An in vivo study of cuspal fracture. J Prosthet Dent 1985;53:38-42.
[12] B. Dejak, A. Mlotkowski, M. Romanowiczi *Finite Element Analysis of Molar During Clenching and Mastication*, The Journal of Prosthetic Dentistry,Volume 90, Number 6, 591-597, 2003.
[13] S. Toksavul, M. Zor • M. Toman, M.A. Güngör, I. Nergiz, C. Artunç, Analysis of Dentinal Stress Distribution of Maxillary Central Incisors Subjected to Various Post-and-core Applications, Operative Dentistry, 2006, 31-1, 89-96.
[14] Fisher H., Weber M., Marx R., Life time prediction of all ceramic bridges by computational methods, J Dent Res, 2003, 82(3): 238-242
[15] Hojjaite B., Anusavice KJ., Three dimensional finite element analysis of glass ceramic dental crowns, J Biomechanics, 1990, 23(11):1157-1166.
[16] Pospiech P., Papavasiliou G., Goldhofer G., Gernet W., All ceramic resin bonded bridge. Eur J. Oral Sci, 1996, 104: 390-395
[17] B. Dejak, A. Mlotkowski, M. Romanowiczi *Finite Element Analysis of Mechanism of Cervical Lesion Formation in Simulated Molar During Mastication and Parafunction*, The Journal of Prosthetic Dentistry,Volume 94 Number 6, 520-529, 2005.

Process Design for the Recycling Of Tetra Pak Components

Mustafa Karaboyaci[1], Gozde Gizem Elbek[1], Mehmet Kilic[1], Aziz Sencan[1]*

Abstract

The Tetra Pak packaging which was originally designed and developed for milk is widely used in the packaging of many foods and beverages. It is important to recycle and recovery of Tetra Pak's due to the different types of recyclable materials included 75% paper, 20% polyethylene and 5% aluminum. There are serious problems in recycling of composite beverage cartons that completed their lifetime and became a waste. A larger part of this packaging waste is disposed in landfills. Therefore, our priority should be performing scientific studies for management of this waste and operating with appropriate management alternatives. In this study, assessment methods and processes of waste composite drinks cartons are researched, and an alternative way is shown which separately recovers cartons, paper, aluminum and polyethylene. Tetra Pak films were cut into over 40 mm pieces, and charged to the reactor with stirring with chloroform. Thus paper, aluminum and polyethylene dissolves in chloroform. The resulting polyethylene and solvent liquid was transferred to distillation unit. The mixture of aluminum and paper remaining in the reactor was boiled and stirred until it turns into a pulp. Filtration of water is ensured by waiting the pulp on the fine sieve and the percentage of remaining solid is determined by analysis at the end of this waiting period. Thus only aluminum is remaining in the reactor. With the designed system, the waste amount of countries going to the solid waste storage areas will decrease and the protection of our environment will be provided. Tetrapak recovery will be a long-term economic investment. Recycling sector will be a step more advanced. The study will also result in allowing new technologies and reducing raw material needs.

Keywords: *tetra pak, recycle, process design*

1. INTRODUCTION

One of the most significant components, that threatens the future of the world are solid wastes. Unfortunately growing population and technological developments has resulted in an increase in solid wastes. In addition, the changes in consumption habits affect the composition of the waste.

Composite cartons which containing layers of paper, plastic and aluminum, especially preferred for storage of beverage packaging type.

There are serious problems in recycling of composite beverage cartons that completed their lifetime and became a waste. A larger part of this packaging waste is disposed in landfills. Therefore, our priority should performing scientific studies for management of this waste and operating with appropriate management alternatives.

Materials that are made by the macro-level unification of two or more materials from the same or different groups in order to merge their best characteristics or to bring out a new characteristic are called “Composite Materials.” It can also be termed as the bonding of different materials or phases of materials with the objective of strengthening each other’s weaknesses and attaining a superior characteristic [2].

The purpose of using different materials together is to increase durability and flexibility and to combine the unique characteristics of each material. The predominantly paper-cardboard composite packages known as Tetrapak are especially preferred in the conservation of liquid food products and are commonly used throughout the world.

The composite drinking cartons used in the food sector especially for long-term conservation of liquid food products are made up of 75% paper, 20% polyethylene and 5% aluminum [3].

Its layers from the outside inwards is as follows;

1. Polyethylene: Protection against external effects and moisture

2. Printing Ink

3. Cardboard: Stability / Strength

4. Polyethylene: Adhesion layer

5. Aluminum Foil: Oxygen, flavor, light and ultraviolet radiation barrier

6. Polyethylene: Adhesion layer

7. Polyethylene: Liquid sealing layer

*[1] *Corresponding author: Süleyman Demirel University, Department of Chemical Engineering, 32260, Çünür/Isparta, Turkey. mustafakaraboyaci@sdu.edu.tr*

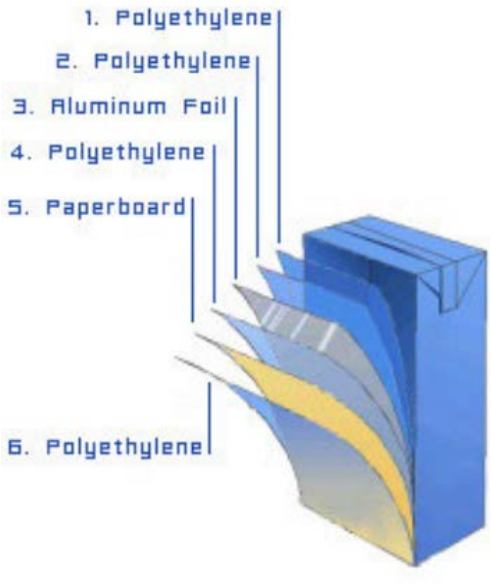

Figure 7. The six layers (Tetra Pak) [2]

Tetra Pak was founded by Ruben Rausing and Erik Wallenberg in 1951 in the Swedish city of Lund. As of January 2013, the company Tetra Pak has supplied approximately 173, 234 million packages so that 77,307 million liters of milk, juice, nectar and other products could be delivered to consumers around the world [5].

The efficient separation of the 3 components found in composite drinking cartons is done by a company named Alcoa Aluminio in Brazil using plasma technology. The facility was established in 2006 with a setup cost of 40 million dollars. After the separation of paper fibers using the hydropulping method, the aluminum and the plastic mixture is heated to 15.000°C and as a result of this process, pure grade aluminum and paraffin oil to be used in the petrochemical industry is produced. The amount of energy required in the facility to produce 1 ton of aluminum is 400-500 kWh. The plasma plant processes 8.000 tons of aluminum and plastic mixture in a year, which corresponds to 32.000 tons of aseptic material; but it is known that this method is very costly.

In Germany, the plastic and aluminum mixture is used as alternative fuel in cement kilns, functioning as a catalyst.

In the company called Corenso in Finland, the gasification method is applied. The aluminum and plastics separated from the paper fibers in the facility are sent to the Ecogas plant. At this stage, while aluminum is recovered in granular form, gas is obtained from polyethylene. The steam produced in the recycling process in gasification is used in paper production. The facility, which began operation in 2001, processes 85.000 tons of carton boxes a year; of which 50.000 tons comes from Germany, a couple of thousand tons comes from Holland, and the rest comes from Finland.

The first method used in the recycling of composite drinking cartons was the particle board method. The boards manufactured from processing the product without separating it into its components (thermal compression) were used in furniture, civil construction, and packaging industries. In later years, the recycling of paper (hydropulping) began, in which the paper fibers that constituted 75% of the composite drinking cartons were recovered. The remaining polyethylene and aluminum parts left after the composite drinking cartons undergo hydropulping is subjected to plastic product transformation, energy recovery, pyrolysis and plasma technologies; but the cost of these technologies are quite high, and the processes are complex.

Nowadays, the collected tetrapaks are accumulated in certified collection and separation facilities, in landfill areas, or burned in cement plants.

With this project, the paper, aluminum and polyethylene in waste tetrapaks shall be recycled, and the recovered materials shall be used to reduce the raw material needs of various facilities. Thus, the natural balance shall be protected against the increase in consumption that rises in parallel with the increase in human population.

At the same time, with the selling of the recovered materials as raw materials to related facilities, businesses be able to ensure high levels of energy saving. There are many establishments that can utilize paper, aluminum, and polyethylene as a source of raw material.

2. MATERIALS AND METHODS

Tetrapak films are cut in approximately 40mm sizes, and a 2 gr sample is mixed in a reaction flask with 40 ml (1 to 20) of chloroform in 65 ^{o}C for 2 hours. As a result of this process, paper, aluminum and polyethylene dissolved in the chloroform is produced in the flask. The dissolved polyethylene in the chloroform is transferred to the distillation unit, and solid polyethylene is obtained after the solvent is evaporated. As the solvent condensed in the distillation unit can be re-used in the

reaction flask, its continuous use makes it economical. Water is added (1 to 20) to the aluminum and paper left in the reaction flask to be boiled and mixed until it turns into paper-mache (pulp). The paper pulp is separated from the aluminum by watering and filtering it. The paper pulp is then placed on a fine sieve to allow the water to filter down; after the waiting period, the solid material content percentage is determined with analyses. Similar to the solvent, the re-use of the water is possible and is used when necessary. Thus, only the aluminum remains in the reaction flask.

3. RESULTS AND DISCUSSION

Experiments were performed in Suleyman Demirel University and it is altitude is over 1065 meter and so atmospheric pressure is over 674 mm Hg. So boiling point of the water is over 96,5 ºC. So dissolution of composite compounds takes more longer time than expected. Separation of all aluminum part from paper takes over 2 hours. After all aluminum separates from paper this means all polyethylene is dissolved. After this stage, the pulp is separated by filtration from polyethylene containing chloroform. After evaporation of chloroform 0,36 grams of polyethylene was obtained. In the literature it has been reported that tetra pak includes over 20 percent of LDPE. [1]. 0,36 gran is about %19 percent and it is consistent with the literature. After evaporation % 92 of solvent was recycled.

Filtered aluminum-paper mixture started to boil with 40 mL water. About 2 hour's paper start to divide to its fibers and being a pulp. Following this step, the paper is diluted by addition of water and a miscible fluid consistency. The liquid paper pulp filtered from aluminum with 10 mesh size filter. After filtering and drying 1,52 gram of paper pulp was obtained. In the literature it has been reported that tetra pak includes over 75 percent of paper [4]. 1,52 gran is about %76 percent and it is consistent with the literature. As in [6], they pyrolysis tetra pak composite for to obtain aluminum and they obtain about %7 of aluminum from waste tetra pak. In this study 0,12 gram aluminum obtained and it is %6 of the total weight and consistent with the literature.

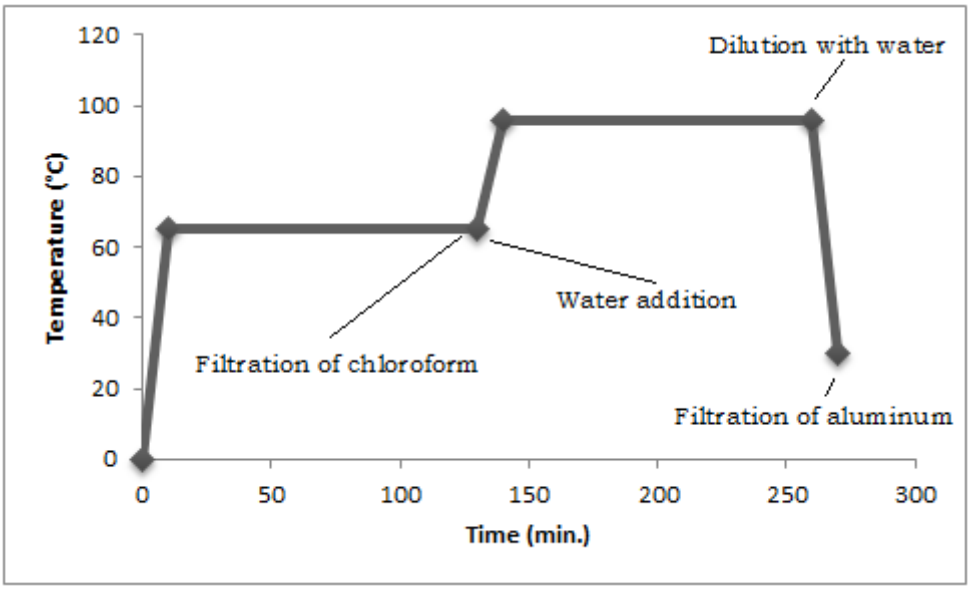

Figure 2. Process steps of tetra pak recycling

Figure 2 shows the details of Tetra Pak recycling process. As seen from the figure recycling process is easy to application. It takes about 4 hours to separate all compounds of the composite and all solvents are recyclable.

Figure 3 shows the disassembled components of the composites. First picture (a) is polyethylene, second picture (b) is dried paper pulp and third picture (c) is recycled aluminum.

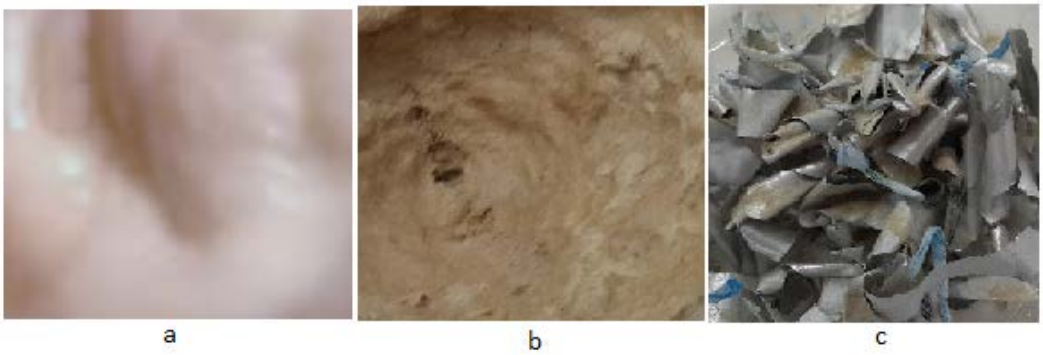

Figure 3. Separated components of Tetra Pak

4. CONCLUSIONS

Tetrapak films were put in reaction with chloroform under heat and pressure. The products of this reaction were paper, aluminum, and polyethylene dissolved in chloroform. Polyethylene was easily recovered in the distillation unit, and the chloroform from the distillation unit was re-used in the system. High-grade aluminum and paper were obtained by introducing water to the reaction flask. It was concluded that in terms of obtaining high-grade Tetrapak components, use of chloroform under heat and pressure was an interesting method as it resulted in requiring less duration and reaction times. Thus, the Tetrapak package that consisted of starting materials with different compounds was easily recycled. As a result of recycling, the damage to the environment and pollution due to increasing consumption habits will be prevented.

At the same time, with the selling of the recycled materials as raw materials to related facilities, businesses be able to ensure high levels of energy saving. There are many establishments that can utilize paper, aluminum, and polyethylene as a source of raw material.

The greatest reason why paper and carton (cardboard) manufacturers prefer recycled paper as raw materials is because they are able to obtain the cellulose necessary for paper for much cheaper. The paper that will be obtained in the envisaged project is in the form of paper-mache (pulp), which will be a reason for preference as it will not require any additional pulpification.

Aluminum, on the other hand, is used in many different industries in the manufacturing of millions of different products. Aluminum production from recycled aluminum, required 95% less energy in comparison to aluminum production from raw materials. When 1 kg of aluminum is recycled, 8 kg of bauxite mineral, 4 kg of chemicals, and 14kWh of energy is preserved. When all these are considered, the importance of aluminum recycling is evident.

ACKNOWLEDGEMENTS

This study is a part of the project supported by Suleyman Demirel University 4390-YL1-15 research project coordination unit.

REFERENCES

[1] Abreu M., Recycling Tha Fibres On Tetra Pak Cartons. Tetra Pak Canada Inc. 2000.
[2] Pietikäinen, V., Collection and recycling of beverage cartons at AIT. Project report. 2008.
[3] Ayrılmış, N., Candan, Z., Hızıroğlu, S. "Physical And Mechanical Properties Od Cardboard Panels Made From Used Beverage Carton With Veneer", Materials & Design, 29, 1897-1903. 2008
[4] Ayrılmış, N., Kaymakçı, A., Akbulut, T., Elmas, G. M. "Mechanical Performance Of Composites Based On Wastes Of Polyethylene Aluminum And Lignocellulosics" Composites: Part B, 47, 150-154.
[5] Tetra Pak Global Site. "Recycling And Recovery". [Online]. Available: http://www.tetrapak.com/environment/recycling-and-recovery/aluminium-and-polyethylene,
[6] Korkmaz, A., Yanık, J., Brebu, M., Vasile, C. "Pyrolysis Of The Tetra Pak", Waste Management, 29, 2836-2841. 2009.

Effect of High Dosage Air-Entraining Admixture Usage on Micro Concrete Properties

Ilker Bekir Topcu[1], Ozgun Atesin[2], Tayfun Uygunoglu[3]

Abstract

In concrete production, because of air entraining admixtures (AEA) are used for a small percentage by weight of cement (in the range from 0.06% to 0.2%), there is a possible risk adding more admixture in concrete than calculated from personnel or equipments sensitivity errors. In this situation concrete's strength and durability performances are diminishing. In this work, it was investigated the effect of high dosage air entraining admixture usage on mortar properties. It was carried out unit weight, flowability, setting time, air content, compressive strength, flexural strength, ultrasonic pulse velocity tests and microstructural inspections on specimens which were produced with 5 different dosages including control. As a result of experiments, in case of using admixtures with overdose, there would be loss of quality of physical and mechanical properties of concrete, for this reason it is concluded that, there must be some legal regulations using chemical admixtures sensitively.

Keywords: *Air-entraining; chemical admixture; micro-concrete; overdose.*

1. INTRODUCTION

Starting with the production, concrete has to endure various durability problems. One of these durability problems is freezing and thawing action whose catastrophic damage can be prevented (or diminished) with air entraining admixtures (AEA). Air entraining admixture allows a controlled quantity of small, uniformly distributed air bubbles to be incorporated during mixing which remain after hardening [1]. Air entrainers are used to develop a large number of small spherical air bubbles in the concrete (diameter in range from 50 to 300 micron [2,3]) which are homogeneous and stable after the mixing process. Compared to capillary pores and gel pores in concrete, entrained air voids are very much larger in size [4] but smaller than the entrapped voids. While water freezes inside the entrapped voids in concrete, it expands about 9% in volume. This volume change enforces internal pressure inside the concrete that exceeds its tensile strength, causing cracking, spalling and eventual disintegration. Providing space for ice in concrete in freezing conditions, entrained air voids help to diminish internal hydraulic pressure and thus protect the hardened concrete. Thus, the entrained air void in concrete is a desirable and intentionally produced void.

Because of air entraining admixtures are used for a small percentage by weight of cement (about 0.06% to 0.2%), there is a possible risk adding more admixture in concrete than calculated. Several researches [5–7] proved that air-entraining admixture dosage is the most significant parameter that affects concrete properties. Using AEAs with overdose may produce a reduction in strength [8], aggravate freeze-thaw damage [9], increase permeability and delay in setting [10].

The aim of this study is to determine the effect of overdose usage of air entraining admixture on concrete properties. For this purpose, it was produced mortars with the use of five different admixture dosages. All components (sand, water, cement) except admixture were treated equally. To determine the fresh state properties of mortar; unit weight, flowability, setting time and air content tests were conducted. To determine the properties of hardened state of mortars; compressive strength, flexural strength and ultrasonic sound velocity were observed. Finally micro structure analysis were conducted.

2. EXPERIMENTAL STUDY

2.1.Materials

Cement: Locally available CEM I 42.5 R ordinary Portland cement, which satisfies EN 197-1, was used. The chemical and physical properties of cement are given in Table 1.

Table 10*. Chemical and physical properties of cement.*

SiO_2	CaO	Al_2O_3	Fe_2O_3	MgO	Na_2O	K_2O	SO_3	LOI
19.42	63.80	4.47	2.70	1.21	0.28	0.59	2.89	4.18
Spec. Gravity		Blaine, cm^2/g		Compressive Strength, MPa				
3.06		3455		25.2 (2-day)		44.9 (7-day)		59.8 (28-day)

Mixing water: As mixing water, Eskişehir tap water was used. The chemical analysis of the drinkable water is given in Table 2.

Table 11. *Chemical analysis of mixing water.*

pH (20°C)	Cl- mg/l	SO_4 mg/l	Mg mg/l	Ca mg/l	Zn mg/l	Cu mg/l	Fe mg/l	NO_3 mg/l	ClO_2 mg/l
7.49	6.53	91.5	41.5	63.8	0.375	0.092	0.074	4.35	< 0.09

Sand: In order to produce mortar, CEN standard sand that satisfies EN 196-1 was used.

Admixture: In order to investigate the effects of air-entraining admixture, commercially available AEA, supplied from Grace Company, were used and its characteristics are given in Table 3.

Table 12. *Properties of AEA.*

Properties	AEA
Ingredient	Sodium salt mixture
Color	Brown
State	Liquid
Density g/ml (20°C)	1.009
pH (20°C)	6.6
Total Chloride %	< 0.10
Total Solid (%)	3.6

2.2.Method

In order to observe the differences in concrete by the dosage of admixture, cement and sand quantities were set to equal in each mixture. Mixing water was reduced as much as admixture amount. The water-cement ratio is selected as 0.50 for the mortar production. In principle, 5 different norm dosages including control were prepared for each admixture. But in order to reach definitive results for some tests, like compressive strength test, additional dosages in the range of 0% - 2% were applied. The designation and norm dosages of admixtures are given in Table 4.

Prepared mortar was cast into 4 x 4 x 16 cm dimensioned formworks made of steel directly after mixing. The samples were separated into groups, each cured at a constant temperature of 20 °C in the curing pool.

Table 13. The designation and norm dosages of admixture.

Admixture	Optimum Dosage[a]	Dosages and Designations				
		0%	0.1%	0.5%	1.0%	2.0%
AEA	0.06%- 0.2%	Control C-0	AEA-0.1	AEA-0.5	AEA-1	AEA-2

[a] Optimum dosage refers to dosage range that suggested by producer. It refers to a range, because optimum dosage must be assessed after preliminary trials depending upon the actual mix constituents and specifications required.

2.3.Tests

Fresh unit weight was obtained by following EN 12350-6. To evaluate the flowability of mixtures, the flow table tests were carried out following EN 1015-3 [11]. As a test procedure; after lifting the slump cone, two diameters perpendicular to each other are measured and their mean is noted as relative slump. To measure initial and final setting times, EN 480-2 code was followed. Using Vicat apparatus with the needle of (1.13±0.05) mm diameter, setting times were observed. Air content in fresh mortar specimens were measured with an apparatus that work with principle of pressure method which is based on Boyle's law [12]. Prepared mixture was poured into impermeable cast, then cast was pressurized to the certain pressure and then impermeability was removed in controlled manner. At this time air content was observed with the aid of manometer.

Ultrasonic wave transmission measurements were implemented using commercially available instrument that satisfies ASTM 597-02. Principally, a pulse is generated at one end of the specimen and the onset of the pulse is picked at the other side. The signal transition duration via specimen is observed. Distance that ultrasound applied to time ratio gives the ultrasonic pulse velocity value. Flexural and compressive strength were measured by means of a hydraulic press. Flexural strength tests were implemented on three 4x4x16 cm dimensioned specimens per mortar, satisfying the EN 1015-11 code. Specimens were placed to 3 point flexural strength apparatus (one-point loading) with the span of 10 mm. The loading rate in flexural tests was 0.05 MPa/sec. The six samples collected from the flexural rupture were used for the compressive analysis. The loading rate in compressive tests was 0.3 MPa/sec. Compressive strength values were collected at ages 7 and 28 days.

In this work, SEM analysis was carried out using Zeiss Supra 40VP. First, specimens were cut to small dimensions (1 cm x 1 cm) in order to fit into the sample holder. Samples were fixed to sample holder with carbon tape, then samples were covered with platinum using Quorum Q150R ES. Samples were placed to sample room of Supra 40VP and vacuumed environment was provided using inert nitrogen gas. Ensuring the observation conditions, specimens were analyzed and various photos were recorded.

3. RESULTS AND DISCUSSION

3.1. Fresh mortar properties

3.1.1. *Fresh unit weight*

Because of its nature, air entraining admixtures have an effect of diminishing unit weight of concrete. In this work, it was observed continuous reduction of unit weight with the increasing admixture ratio as seen in Fig. 1. The most important result of this test is that using AEA within the range of optimum dosage, namely 0.1%, has an effect of considerable drop of unit weight which corresponds to 16%, compared to control mixture. Another key point of the graph is that, speed of unit weight drop is diminishing after 0.5% of dosage.

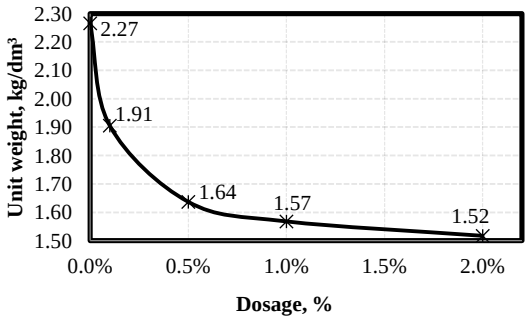

Fig. 1. *Fresh unit weight variation depending on admixture dosage.*

3.1.2. Flowability (Flow table).

As mentioned in literature, AEAs have an effect of imparting plasticity to the fresh concrete [4,13,14]. As can be seen in Fig. 2, using AEA with the dosage of 0.1%, increased flowability 34% compared to control mixture. But after optimum dosage there is no considerable flowability augmentation, even it can be said that there is no change after the dosage of 1%.

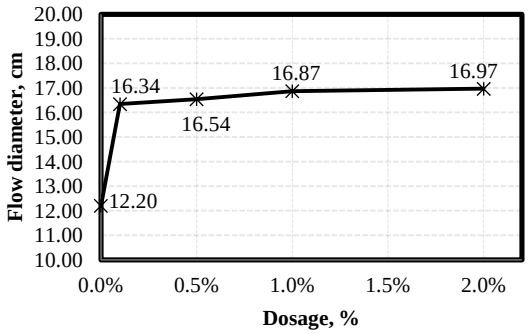

Fig. 2. Flow diameter values obtained from flow table.

3.1.3. *Setting times*.

Fig. 3 illustrates initial and final setting time results. Initial setting times are varying from 179 to 433 minutes, while final setting times vary from 239 to 588 minutes. After certain point for initial setting, namely 0.5%, there is no considerable change for initial setting time while dosage of the admixture is increasing. But, delay of the initial setting time of 2% AEA dosage corresponds to 254 minutes when compared to control mixture. Similar trends were observed for the final setting times. With the increment of dosage, final setting times were extended.

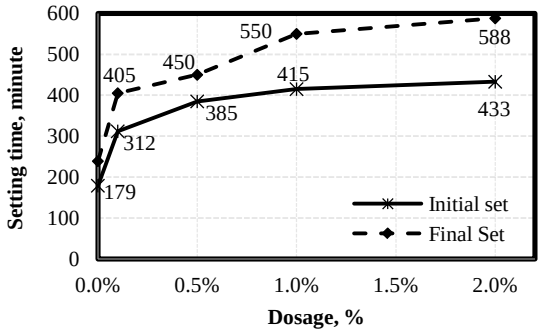

Fig. 3. Initial and final setting time variation depending on admixture dosage.

3.1.4. Air content

Probably the most important parameter for air entrained concrete is air content. As expected, with the increment of dosage, air content in mortar was augmented. As can be seen in Fig. 4, using AEA within the optimum dosage, namely 0.1%, has augmented air content more than twice compared to control mixture. Moreover, slightly exceeding the optimum dosage range, namely 0.5%, air content of mortar specimen escalated to 11.4%, nearly four times of control mixture. But, another significant point of this test is that there is no considerable air content augmentation beyond the dosage of 0.5%. Based on the test results, using AEA more than 0.5% dosage has no avail practically on the base of air content.

3.2. Hardened mortar properties

3.2.1 Ultrasonic pulse velocity

Ultrasonic pulse velocity test results at the age of 28-days are plotted in Fig. 5. Ultrasonic pulse velocity values are varying from 2.37 km/sec to 4.09 km/sec for AEA used mortars. AEA used mixtures' ultrasonic pulse velocity values were reduced 14.8%, 30.2%, 36.9, %39.6% and %42.7 compared to control mixture at 0.1%, 0.5%, 1%, 1.5% and 2% dosages respectively.

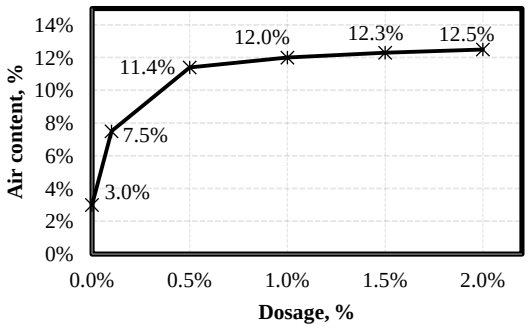

Fig. 4. Air content variation depending on admixture dosage

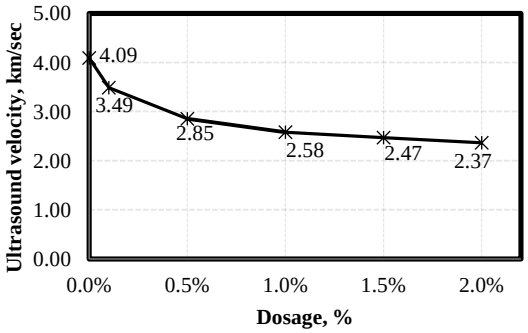

Fig. 5. Ultrasound velocity variation depending on admixture dosage

3.2.2. Flexural strength

AEA used mixtures' flexural strength values at the age of 28-days are presented in Fig. 6. With the augmentation of air content, flexural strength values were diminished because of reverse ratio of air content to strength. AEA used mixtures' flexural strength values were decreased 49.3%, 78.3%, 82.9%, 85.2% and 86.3% compared to control mixture at 0.1%, 0.5%, 1%, 1.5% and 2% dosages respectively. The key point of the graph is that there is a rapid drop of strength up dosage of 0.5%, but beyond this dosage there is no considerable strength drop.

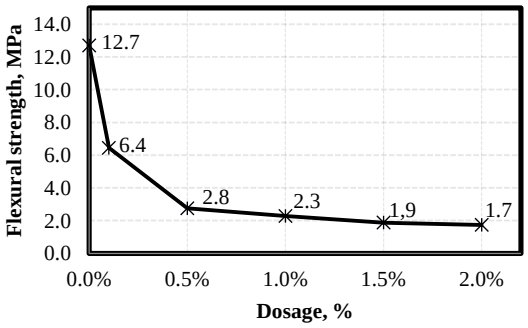

Fig. 6. *28-day aged mortar flexural strength variation depending on admixture dosage.*

3.2.3. Compressive strength

Compressive strength tests were conducted at the ages of 7 and 28 days old specimens. Fig. 7 illustrates the compressive strength variations depending on admixture dosage. Considering Fig. 7, there is a continuous compressive strength loss with the augmentation of dosage. But on the other hand, speed of compressive strength drop is diminishing after 0.5% of dosage. Although, there is a compressive strength reduction at the dosage of 0.1% compared to control mixture, strength gain depending on time is continuous and stable. But exceeding 0.1%, there is no strength gain depending on time; in other words, specimens reach their ultimate strength nearly at the age of 7 days.

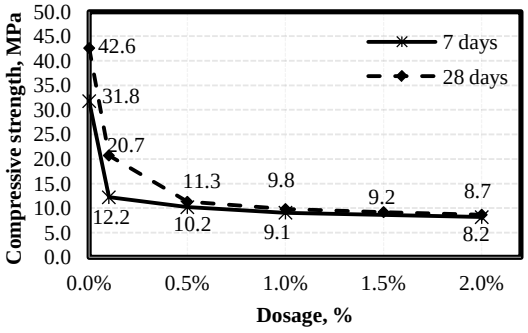

Fig. 7. *Mortars compressive strength variation depending on admixture dosage*

3.3. Microstructural analysis

Fig. 8 shows the result of SEM analysis of the 100 times magnified surface of the AEA included specimens at 90 days-age. Because there is no ingredient in mortar aside from main materials (such as sand, cement and water) that can be seen by SEM analysis, and the basis of the work is the entrained-air, air voids were investigated. Samples used for SEM analysis were taken from specimens with rupture technique, instead of cutting. Since the plane of examination does not usually cut through the center of the spheres [15], in order to observe true air void diameters, rupture technique was applied, because of specimens are tent to rupture the weakest section which is the centre of the void. Considering Fig. 8, samples have air voids in the range from 50µm to 500 µm in diameter. It can be easily seen in Fig. 8 that AEA changes concretes micro structure considerably.

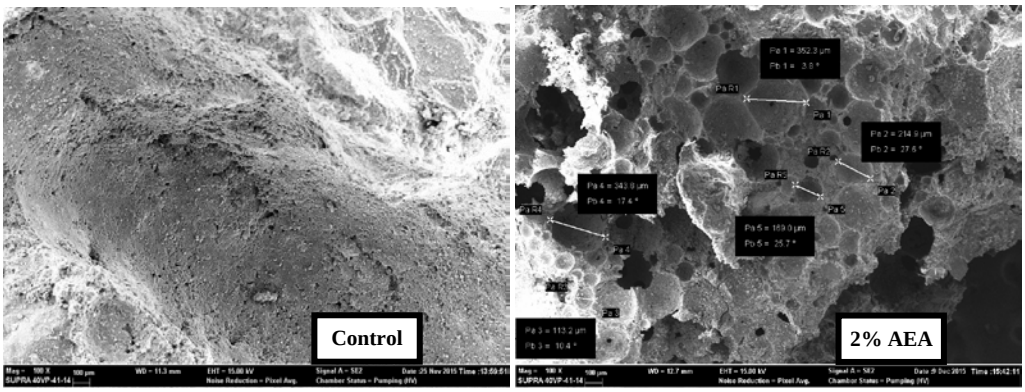

(a) (b)

Fig. 8. SEM image of specimens (magnification x100). (a) Without AEA, (b) 2% AEA

4. CONCLUSIONS

In this study it was investigated to determine the effect of overdose usage of air entraining admixture on concrete properties. To evaluate the possible effects, fresh state and hardened state tests were conducted. Also microstructural analysis was performed. Based on the experimental results, the following conclusions are drawn:

1. As expected, with the increment of dosage, AEA used mixtures' fresh unit weight values were decreased considerably. This drop corresponds to 33% at the dosage of 2% compared to control mixture.
2. It is known that spherical shape of AEA has an effect of enhancing workability. For this reason with the increment of dosage, specimens' flowability has augmented. But this augmentation trend tent to slow down after the dosage of 0.1%
3. It can be easily said that AEA usage extends setting times.
4. As expected, the more AEA usage, the more air content in concrete.
5. According to test results, it is obvious that AEA usage decreases the strength of concrete, both flexural and compressive. This result derives from the air void presence. For this reason, AEA must be used carefully on high strength concrete applications.
6. According to micro structural analysis, AEA has no effect on chemical composition and CSH formation of concrete. Differences of the physical properties of concrete with the dosage variation are due to air void presence in concrete.

With the sum of all tests and analyses, AEA must be used carefully and within the range of optimum dosages, otherwise there would be loss of physical and mechanical properties of concrete. For this reason, chemical admixtures in general, must be used in process of concrete production in plants and uncontrolled usage in the field must be prohibited.

ACKNOWLEDGMENT

This work was supported by Eskişehir Osmangazi University Scientific Research Fund (ESOGU BAP) under the project code 2014-359. The authors wish to express their gratitude to the ESOGU for its financial assistance.

REFERENCES

[1] TS EN 934-2+A1 Admixtures for concrete, mortar and grout - Part 2: Concrete admixtures - Definitions, requirements, conformity, marking and labelling, Turkish Standards Institution, 2013.
[2] J. Jasiczak, K. Zielinski, Effect of protein additive on properties of mortar, Cement and Concrete Composites. 28 (2006) 451–457.
[3] B. Łaźniewska-Piekarczyk, The frost resistance versus air voids parameters of high performance self compacting concrete modified by non-air-entrained admixtures, Construction and Building Materials. 48 (2013) 1209–1220.
[4] L. Du, K.J. Folliard, Mechanisms of air entrainment in concrete, Cement and Concrete Research. 35 (2005) 1463–1471.
[5] M. Pigeon, J. Marchand, R. Pleau, Frost resistant concrete, Construction and Building Materials. 10 (1996) 339–348.
[6] A.H. Akca, N.Ö. Zihnioğlu, High performance concrete under elevated temperatures, Construction and Building Materials. 44 (2013) 317–328.
[7] D.S. Zhang, Air entrainment in fresh concrete with PFA, Cement and Concrete Composites. 18 (1996) 409–416.
[8] M. Grantham, Advanced Concrete Technology, Elsevier, 2003.
[9] F. Rendell, R. Jauberthie, M. Grantham, Deteriorated Concrete: Inspection and Physicochemical Analysis, Thomas Telford Ltd, 2002.
[10] B. Łaźniewska-Piekarczyk, The methodology for assessing the impact of new generation superplasticizers on air content in self-compacting concrete, Construction and Building Materials. 53 (2014) 488–502.
[11] R. Yu, P. Spiesz, H.J.H. Brouwers, Development of an eco-friendly Ultra-High Performance Concrete (UHPC) with efficient cement and mineral admixtures uses, Cement and Concrete Composites. 55 (2015) 383–394.
[12] V.S. Ramachandran, Concrete Admixtures Handbook, Elsevier, 1996.
[13] M. Griffith, H.O. Sugo, A.W. Page, S.J. Lawrence, The Influence of Air Entraining Agent on Bond Strength and Mortar Microstructure., (2001) 357–366.
[14] B. Łaźniewska-Piekarczyk, Examining the possibility to estimate the influence of admixtures on pore structure of self-compacting concrete using the air void analyzer, Construction and Building Materials. 41 (2013) 374–387.
[15] S. Diamond, The microstructure of cement paste and concrete - A visual primer, Cement and Concrete Composites. 26 (2004) 919–933.

ICENS
INTERNATIONAL CONFERENCE ON ENGINEERING AND NATURAL SCIENCES
24-28 May 2016 /Sarajevo

Prioritization of Machine Failures with Pareto Analysis in Panel Radiator Manufacturing Process

Fatma Nur Arslan[1], Baha Guney[1], Cagatay Teke[1]*

Abstract

Competition, globalization and changing in customer demands affect companies directly nowadays. Companies aim to cope with competition, meet customer expectations and decrease costs for surviving. Achieving these objectives depends on higher availability of equipment comprise the system in a company. In addition, when a breakdown occurs, correct action should be conducted immediately. Therefore, failure types should be classified according to downtimes and frequencies of them. Maintenance department should prepare maintenance plans by taking the classification into consideration. In this study, downtimes and failure frequencies in panel radiator manufacturing process were investigated and Pareto analysis which is one of the approaches for statistical process control was carried out for classification the failure types in the manufacturing process. Thanks to Pareto analysis, failure types of machines were prioritized.

Keywords: *Pareto Analysis, maintenance planning, machine failure analysis*

1. INTRODUCTION

The increase of the business efficiency nowadays depends on the use of the resources in the most accurate and the best way. When analyzing business in terms of productivity, production resources provision, determination of tasks and goals, these require the effective interactions between all of the production resources as all management related functions regarding the use and interpretation of the results specified.

The efficiency of the machine is one of the most important factors affecting the profitability of businesses. The failure occurring during the operation due to production interruptions are one of the most important parameters affecting the efficiency of the machine. Car tire producing businesses especially rubber dough stage of obtaining the yield machine malfunctions resulting in the machine directly affect product quality and cost.

In this study, Panel Radiator Manufacturing factory, machine downtimes process of an important phase of the in the machine during acquisition failure caused by production losses during operation of the welded posture was observed, The reasons for this situation that causes with a maximum downtime have been investigated by using Pareto analysis in this work.

In this study, fault-induced shutdowns are listed based on importance through Pareto analysis. At the same time due to Pareto analysis the type of failures can be followed closely, in which the level is of significant importance and it specifies effectively which failure must be considered for attention.

2. LITERATURE REVIEW

Elevli S. and Yılmaz Y. H. Due to Pareto diagrams and logarithmic diagram a truck fleet operating in businesses for mineral spreaders were used in order to determine the priority fault types [2]Arvanitoyannis I. S. and Varzakas T. H. FMEA analysis has been done for the risk assessment of a factory engaged in the production of potato chips. Then, to optimize FMEA analysis Pareto analysis were utilized [1].Hall R. A. Knights P. F. and Daneshmend L. K. Engines analyzed in the mobile equipment fleet at a gold mine. In this study, Pareto analysis and condition-based maintenance planning were used [3]

3. METHOD

Many work of statistical process control are in Japan, Kaoru Ishikawa, with seven statistical process control techniques around 95% of problems can be solved in a businesses. In the process we encountered below one of the seven statistics used for the solution of problems.

- Pareto analysis
- Histogram
- Cause and Effect Diagram
- Control Table
- Control Chart

*[1] Corresponding author: Sakarya University, Department of Industrial Engineering, 54180,Serdivan /Sakarya, Turkey fatmanurarslan08@gmail.com

- Defect Concentration Distribution

- Distribution Diagram

Pareto analysis is commonly used by process development engineers.

Pareto analysis is a statistical technique that provides ease in decision classifying data obtained. Pareto chart is used for classification. Italian economist and sociologist Wilfredo Pareto has revealed the Pareto principle, which is bearing his name. Many researches and studies have been done and received for various businesses as the result of Pareto as stated as follows.

80% as the result in normal distribution, 20% from the most important reasons, 15% of the afterwards results, 30% from the leading cause, the remaining was found to be 5% while 50% was arise from the resources.

20% of the equipment is an example of the research that accounts for approximately 80% of the cost. Pareto principle was emerged in the literature because these rates of 70-30, 80-20 or 90-10 are used as guidelines. Pareto analysis are also referred to as the ABC analysis.

Pareto analysis is the most important reason for the different number, severity rating is a technique used to distinguish it from the less. In this technic incident it can be shown graphically and it can be addressed as the most important problem reason and indicating that weight that should be given and also assist in the identification of priorities [5]

Pareto diagram can be created in six steps:

1. Listing of all elements: First you need to determine the faults occurring in businesses. Then the collection of the number of all types of faults that cause a malfunction and It constitutes the first phase of the listing..

2. Measurement of element: In a certain time (several months, several weeks and several years) a recording set used in the collection of data to be analyzed is regularly generated. Failures are recorded in the control board after detecting, analyzing numerical data collected and passed to the control board about the failure to be held.

3. Classification of Elements: At this phase the downtime information collected for various failure are classified from the largest to the smallest

4. Calculation of Cumulative Distribution: Every type of failure occurring is collected after downtime classification percentage of the total value of each downtime is calculated. Then the total percentage cumulative found is calculated.

5. Drawing of Pareto Chart: faults occurring in the machines are placed in columns considering its severity in equal intervals to the horizontal axis. The dampest failure is placed in the left column of the graph. After passing right hand of the graph the failure is gradually decreasing. The total downtime occurring in failures that occur in a specified time period is shown on the vertical axis. The total value of the faultier the total frequency of downtime that constitutes the columns' length. At the same time there are curves as indicated by the line in the Pareto chart. The graph curve starts from the left bottom edge and the sum of the corresponding values in the vertical axis until the whole column is completed at a height curve when it reaches the top right corner Situated at 100% level. This curve is drawn with the help of Pareto chart drawn before, later the Pareto chart that will be drawn allows the comparison. Pareto chart is located further to the right of the vertical axis and this axis gives the percentage of flagged downtime from 0 to 100. The percentage of downtime is found using the following formula:

Percentage of Downtime = (Downtime in column)/(Total Downtime) X 100

6. Pareto Chart Review: Pareto Chart helps the withdrawal of the most important failures due to our attention and efforts. Working with the longest downtime causes malfunctions, generally we may get more benefits and gains from working with lower downtime. Pareto chart is the most commonly used process control techniques, it allows the most accurate decision to be taken, the ability of the individual analysis chart and even though it is limited by the ability. Sometimes it is necessary that people who make analysis use his knowledge in order to take a decision. [5]

4. RESULTS AND DISCUSSION

Panel factory shutdowns that occur because of the very large industrial radiator factory production is being lost. All of the more obvious failure source causing this situation.

It cannot be removed so you need to give priority to cause some malfunctions. Which fault to determine whether priority should be given to the causes Pareto analysis is utilized .It through analysis failures are classified as cost of work on high weight is given.

Table 1: Causes of machine downtime

Downtime Causes	**Machine Stoppages**	**%**
Mechanical Failure	6115 min.. (101,92 hour)	50,95
Electrical Failure	3995 min. (66,58 hour)	33,29
Scheduled Failure	1892 min. (31,54 hour)	15,76
Final Total	12002 min. (200,03 hour)	100

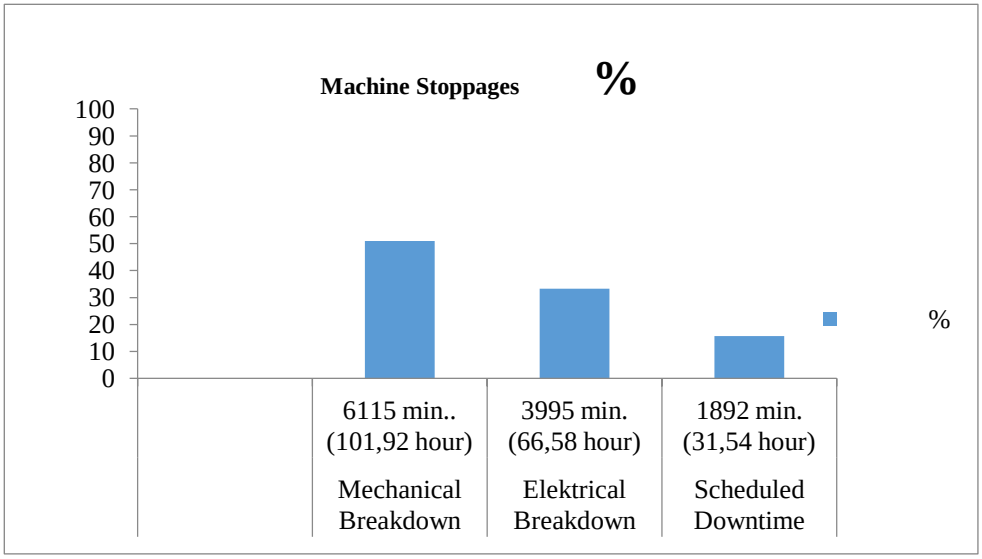

Figure 1: Pareto graphic of Machine downtime

This chart is based on interpretation; the most important of posture which causes the machine to stop mechanical failure. Factory if you want to be a minimum of downtime and accordingly if you invest, mechanical failure with 50, 95%, which is the most important cause of posture 1. It ranks. And we need to investigate the cause of the mechanical failure.

Table 2: Mechanical Failure Causes

Mechanical Failure Causes	**Machine Stoppages (Min.)**	**%**
Piston Failure	795	13
Water Connection Failure	580	9,48
Transformer Failure	545	8,91
Line Driver	510	8,34
Bus Duct Failure	510	7,36
Convector Failure	450	6,79
Sewing Machine Flow Failure	415	6,71
Gabarite Failure	410	4,5
Align Failure	275	4,33
Oil Hose Failure	265	3,76
Belt Breakage	230	3,27
Tape Fault	200	3,19
Hook Failure	195	3,03
Lower Head Crash	185	3,03
Gun Failure	185	2,94
Press Failure	180	2,69
Centre Electrode Disjuncture	165	2,62
Valve Failure	160	2,29
T- Jaw Failure	140	1,96
Motor Failure	110	1,8
Final Total	6115	

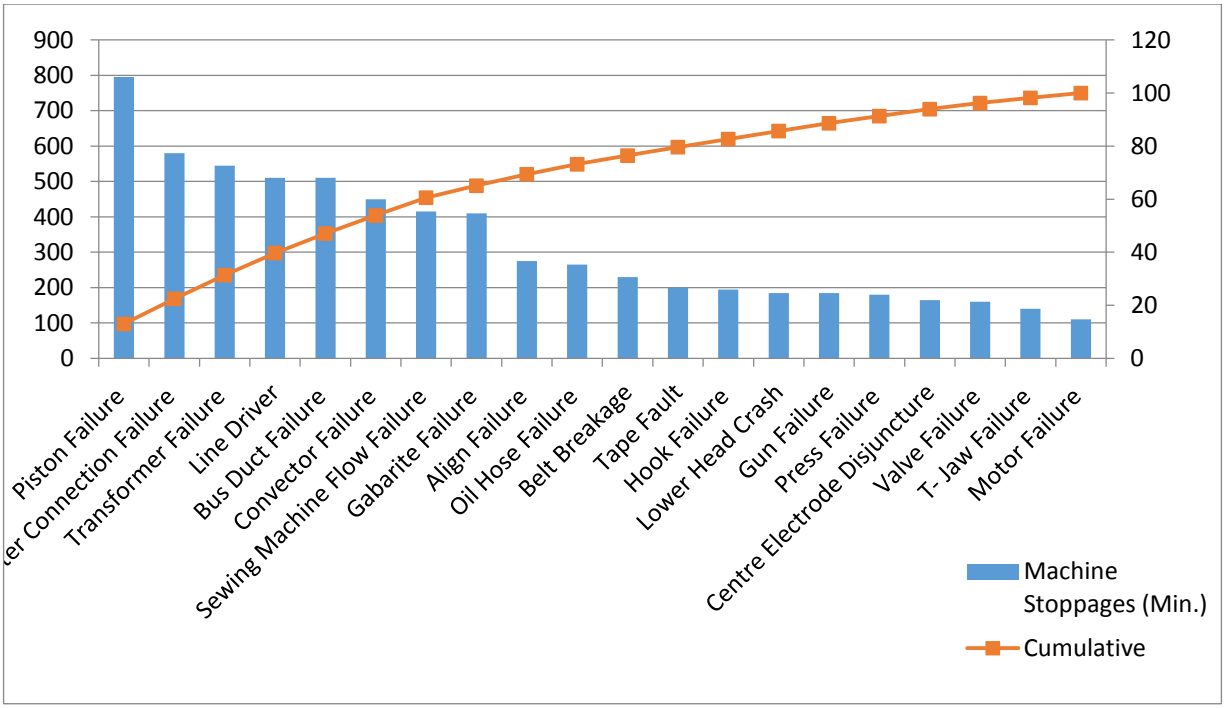

Figure2: Pareto Graphic of Mechanical Failure Causes

By looking at the results of this analysis; the percentage of errors is included in the A class 0 to 0.80. Error between 0.80 and 0.95 are included in the B class. C class of error between 0.95 and 1 it is included. It made a priority in practice the reasons for this stance in class for mechanical faults it should be given. However, by giving priority to these errors reduced machine downtime.

The machine has been found to be the very reason that stance 2. Event Electrical Failure. Electrical failures that caused the fault is identified. From the smallest and longest downtimes. It listed with up to downtime.

Table 3: Electrical Failure Causes

Electrical Failure Causes	**Machine Stoppages (Min.)**	**%**
Hoisting Engine Failure	590	14,77
Observation Failure	515	12,89
Centre Failure	505	12,64
Electric Arc Welding Failure	435	10,89
Drill Breakage	300	7,51
Encoder Failure	245	6,13
Hook Failure	225	5,63
Motor Failure	220	5,51
Bobbin Failure	215	5,38
Sheet Metal Fault	205	5,13
Cutting Angle Failure	180	4,51
Feed Bar Failure	145	3,63

Oil Pump Failure	135	3,38
Swich Failure	80	2
Final Total	3995 min.	

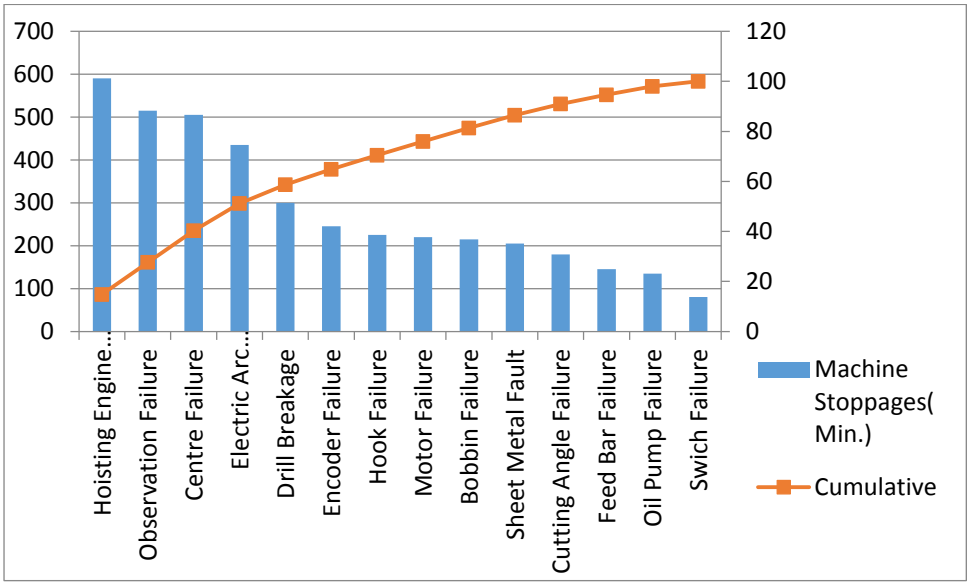

Figure 3: Pareto Graphic of Electrical Failure Causes

First, the need to pay attention to mistakes in A class. These hoisting engine failure, observation failure, Centre failure, electric arc welding failure, drill Breakage , encoder failure, Problem Punta failure, electrode welding failures, hook failure, motor failure, bobbin failure.

Examining the data received from the factory 556 one result of the many reasons to machine downtime 3 has been determined that the event is scheduled downtime.

Table 4: Scheduled Downtime Causes

Scheduled Downtime	**Machine Stoppages (min)**	**%**
Stocking Density	744	39,32
Sales Decrease	628	33,19
others (bank holiday, shift change)	520	27,49
Final Total	1892 min	

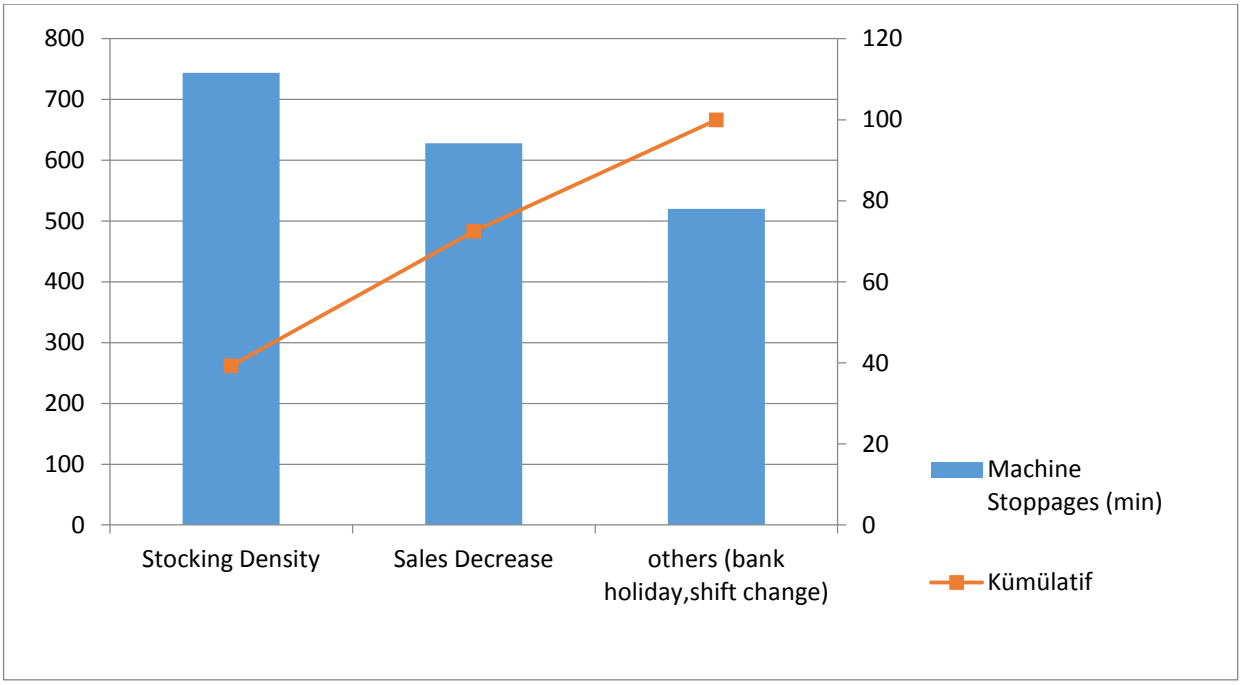

Figure 4:Pareto Graphic of Scheduled Downtime

By class A unplanned maintenance of 'the need to pay attention to the error priority to this error giving an envisaged that can reduce machine downtimes. İnventory and occupancy in this class if they pay attention to factors such as sales and take measures for their lack of machine downtime Prevent elongation.

5. CONCLUSIONS

In this study, an application was conducted in panel radiator manufacturing factory by using Pareto analysis which is one of the techniques for statistical process control.

The failures were divided three categorizes; A, B, C. According to order of precedence at results of analysis. The failures of category A were given prioritize, this failures occasioned stoppages must be minimize and must be taken category A. For this reason this failures minimize don't compose effective yield as the failure which are category A. B category failures should be taken into consideration after A category failures. The results of the classification outraised department must deal the failures according to order of presence and take precautions.

Panel factory shutdowns that occur because of the very large industrial radiator factory production is being lost. All of the more obvious failure source causing this situation.

It cannot be removed so you need to give priority to cause some malfunctions. Which fault to determine whether priority should be given to the causes Pareto analysis is utilized .It through analysis failures are classified as cost of work on high weight is given.

REFERENCES

[1] I, S. Arvanitoyannis and T.H. Varzakas " Application of Failure Mode And Effect With HACCP To Potato Chips Manufacturing" International journal of Food Science and Technology 42(12):1424-1442
[2] S. Elevli and Y.H. Yılmaz "Graphical Approach in Determining the Priority of seeing equipment failures" "Eskisehir Osmangazi University Journal of Engineering Faculty 22(1):31-48.
[3] R. Hall, P.F. Knights and L.K Daneshmend "Pareto Analysis and Condition-Based Maintenance of underground Mining Equipment" Institution of Mining and Metallurgy , Transactions Sections A14-A22
[4] B. Meriç and A. Özkal " Efficiency Analysis of a company producing upholstery factory" Uludağ University Journal of Engineering and Architecture7(1):131-140
[5] S. Özcan "Statistical Process Control from Technical Pareto Analysis and application of cement in Industry" Cumhuriyet University Journal of Economic and Administrative Sciences 2(2):151-174

ICENS
INTERNATIONAL CONFERENCE ON ENGINEERING AND NATURAL SCIENCES
24-28 May 2016 /Sarajevo

Mammogram Classification by Using Wave Atom Moments

Nebi GEDİK[1*]

Abstract

In the computer aided diagnosis system, feature extraction step is a very important to achieve a good classification performance. When considering the feature extraction, the most discriminative features are the key issue. According to the recent studies, multiscale transforms provide satisfactory results to obtain the effective features. This paper represents a method to classify mammograms by using wave atom moments. The method consists of application of wave atom to region of interests (ROIs) and computation of first-order moments from the coefficients of wave atom. Once, obtained the first-order moments for each ROI, feature matrix is constituted using them. Then, the features are ranked by using the statistical t-test technique and then a thresholding process is applied over the ranking values to determine the most effective features to classify the classes. The classification is repeated using support vector machine (SVM) till obtaining the optimal threshold point (point of effective feature set) that gives the best classification performance. Finally, the classification is performed last time via 5-fold cross validation using the feature set at the optimal point to validate the result. In the study, 228 mammograms from the Digital Database for Screening Mammography (DDSM) database are used and the mammograms are distinguished as normal or abnormal. Wave atom moments yield an accuracy of 94.74% with 18 features for abnormality detection. According to the result, wave atom moments are an effective way to obtain a reduced set of discriminative features for normal-abnormal classification of mammograms.

Keywords: *Wave atom moments, Mammography, Feature extraction, Feature reduction.*

1. INTRODUCTION

Breast cancer is a common disease among women and a major public health problem causing deaths [1,2]. The most effective way to fight the disease is early detection and treatment. For early and accurate detection of breast cancer, mammography is the most effective and common tool. However, interpretation of mammograms is hard to radiologists due to the large number of cases and subtle abnormalities. Therefore, computer-aided diagnosis (CAD) systems are developed to assist the radiologists. [3-7].

The CAD systems have been composed using different techniques [8,9]. Some of studies in the literature are focused on multi-resolution analysis methods to construct CAD system. Beura et al. [10] proposed an algorithm to classify mammograms as normal, benign or malignant. The proposed method consisted of two steps such as feature extraction and selection. Features were gray-level co-occurrence matrix (GLCM) of the coefficients that obtained from applying two dimensional discrete wavelet transform (2D-DWT) to ROIs. To select the effective features that give better classification accuracy among the large number of features, t-test and F-test method were employed, separately. Classification was performed using back propagation neural network (BPNN) classifier. The method was tested using the ROIs supplied from the mammographic image analysis society (MIAS) database and digital database for screening mammography (DDSM). According to the results, the features selected by *t*-test method outperformed to that of F-test with respect to accuracy. Dhahbi et al. [11] presented a feature extraction method to classify mammograms. The method based on curvelet transform and moment theory. Initially, applying discrete curvelet transform to ROIs, coefficients of the transform were obtained. Subsequently, four first-order moments of curvelet coefficients were computed in two ways: moments from coefficients of each band and moments from coefficients of each level. Then, the most effective features were selected using t-test ranking technique for each moment set. Finally, a k-nearest neighbor classifier (k-NN) was used to classify mammograms from MIAS and DDSM. Guo et al. [12] proposed a new hybrid method to improve the detection rate of micro-calcification in mammograms. Three main steps were used in the proposed method: (I) removing label and pectoral muscle by using the largest connected region marking and region growing method, and enhancing micro-calcification applying the combination of double top-hat transform and grayscale-adjustment function; (II) removing noise and other interference information, and obtaining the significant information by modifying the contourlet coefficients using nonlinear function; (III) classifying micro-calcifications using non-linking simplified pulse-coupled neural network classifier.

This paper represents a method to classify mammograms by using wave atom moments. The method consists of application of wave atom to ROIs and computation of first-order moments from the coefficients of wave atom. Once, obtained the first-order moments for each ROI, feature matrix is constituted using them. Then, the features are ranked by using the statistical *t*-test technique and then a thresholding process is applied over the ranking values to determine the most effective features to classify the classes. The classification is performed using support vector machine (SVM).

*[1] *Corresponding author: Department of Maritime Management, Faculty of Marine Sciences, Karadeniz Technical University, Surmene, 61530 Trabzon, Turkey.* ngedik@ktu.edu.tr

2. WAVE ATOM TRANSFORM

Wave atom transform is a novel version of the family of multiscale transforms introduced by Demanet and Ying [13]. Construction of wave atoms is carried out tensor products of adequately chosen 1-D wave packets. 2-D wave atoms $(\varphi_\mu(x))$ indexing by $\mu = (j, m, n) = (j, m_1, m_2, n_1, n_2)$ are formed by individually taking products of 1-D wave packets and using Hilbert transform (H) in the frequency plane [13]. Thus, 2-D dual wave atoms are defined as follows;

$$\varphi_\mu^+ (x_1, x_2) = \psi_{m_1}^j (x_1 - 2^{-j} n_1) \psi_{m_2}^j (x_2 - 2^{-j} n_2), \quad (1)$$

$$\varphi_\mu^- (x_1, x_2) = H\psi_{m_1}^j (x_1 - 2^{-j} n_1) H\psi_{m_2}^j (x_2 - 2^{-j} n_2), \quad (2)$$

Combination of equations (3) and (4) [13] is formed the tight frame for wave atoms as follows;

$$\varphi_\mu^{(1)} = \frac{\varphi_\mu^+ + \varphi_\mu^-}{2}, \qquad \varphi_\mu^{(2)} = \frac{\varphi_\mu^+ - \varphi_\mu^-}{2} \quad (3)$$

3. PROPOSED METHOD

The method starts by applying wave atom transform to ROIs. When coefficients of the transform are obtained, first-order moments are computed from the coefficients of wave atom sub-bands. Providing X_i, $(i = 1 \dots N)$ as coefficients of the transform, the first-order moments is defined as follows;

$$mean\ (\mu) = \frac{1}{N} \sum_{i=1}^{N} X_i \quad (4)$$

$$variance = \frac{1}{N} \sum_{i=1}^{N} (X_i - \mu)^2 \quad (5)$$

$$skewness = \frac{\frac{1}{N} \sum_{i=1}^{N} (X_i - \mu)^3}{s^3} \quad (6)$$

$$kurtosis = \frac{\frac{1}{N} \sum_{i=1}^{N} (X_i - \mu)^4}{s^4} \quad (7)$$

where μ is the mean, s is the standard deviation.

Calculation of moments is performed in two ways; calculation of moments from the coefficients of every band (packet of coefficients) and calculation of moments from the coefficients of every level (scale). In this study, the transform has four scale and two bands in every scale. So, 48 features are obtained via calculating the moments for each ROI, feature matrix is then constituted using them. Subsequently, the features are ranked based on the statistical *t*-test technique using equation (8) [14]. After that, a thresholding process is applied over the ranking values to determine the most effective features to classify the classes.

$$r_v = \frac{|\mu_1 - \mu_2|}{\sqrt{\frac{(s_1)^2}{N_1} + \frac{(s_2)^2}{N_2}}} \quad (8)$$

where $r_v$denotes ranking value and $\mu, s,$ and N are means and standard deviations of the class and numbers of ROIs in each class, respectively. The feature matrix is recreated using remained features after thresholding and classification performed using support vector machine (SVM). The classification is repeated till obtaining the optimal threshold point (point of effective feature set) that gives the best classification performance. Finally, the classification is performed last time via 5-fold cross validation using the feature set at the optimal point to validate the result. The flowchart of the present method is illustrated in Figure 1.

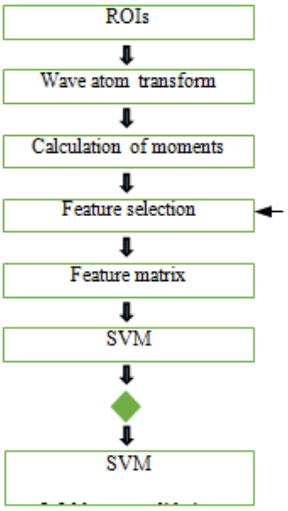

Figure 1. Flowchart of the proposed system.

4. EXPERIMENTAL WORK

To test the proposed system, ROIs obtained from DDSM [15] were used. DDSM database consists of 2548 mammograms (including 914 malignant, 870 benign and 764 normal), which were previously investigated and labeled by expert radiologists. The ROI set was created using manual cropping operation from original ones. ROIs were formed at 128 × 128 pixels size considering that the centers of ROIs corresponded with given centers of abnormalities. In case of normal mammograms, cropping was randomly performed and normal ROIs were created from all tissue types equally (fatty, fatty–glandular, and dense–glandular). Generated ROIs were composed 228 images (114 normal, 50 malignant, 64 benign).

After generating datasets, wave atom transform was applied to ROIs, and coefficients of the transform were then obtained. Subsequently, first-order moments were calculated for every band and scale (8 bands and 4 scales), feature matrix was built using them. To determine and select the most effective features, ranking criterion and dynamic thresholding were used. The thresholding was performed over values of r_v, and the feature matrix was rebuilt using the features remained after thresholding. Classification was repeated according to the changing value of threshold. In the classification process, the dataset was divided into two groups as a training group (70% of the dataset) and a testing group (30% of the dataset). In the present study, iteration was performed 48 times which correspond to 48 ranking values, and the threshold point that provide highest accuracy result with the minimum number of features was chosen the optimal feature (the most significant features) point. Finally, the classification is performed last time via 5-fold cross validation using the feature set at the optimal point to validate the result.

5. RESULTS AND DISCUSSIONS

The proposed system was evaluated using the ROIs to classify mammograms as normal and abnormal. The performance of the SVM is illustrated in Figure 2a corresponding to the number of extracted features with different threshold values. Maximum accuracy was obtained with 18 features as 96.05%. Although there are several points that have same accuracy, that point was chosen because of considering the highest accuracy with the minimum number of features.

The classification was carried out again applying the 5-fold cross validation (CV) method using the optimal threshold points which gave the highest accuracy with the minimum number of features to validate the results. The optimized classification result (5-fold CV) and maximum accuracy result (70-30% ratio) were illustrated in Fig. 2b. The result for 5-fold CV was represented with error-bars that present the standard deviation between different folds. According to the results, the number of features decreases from 48 to 18 with good classification performance, and the proposed method has a convincing capability to distinguish the mammograms into normal and abnormal.

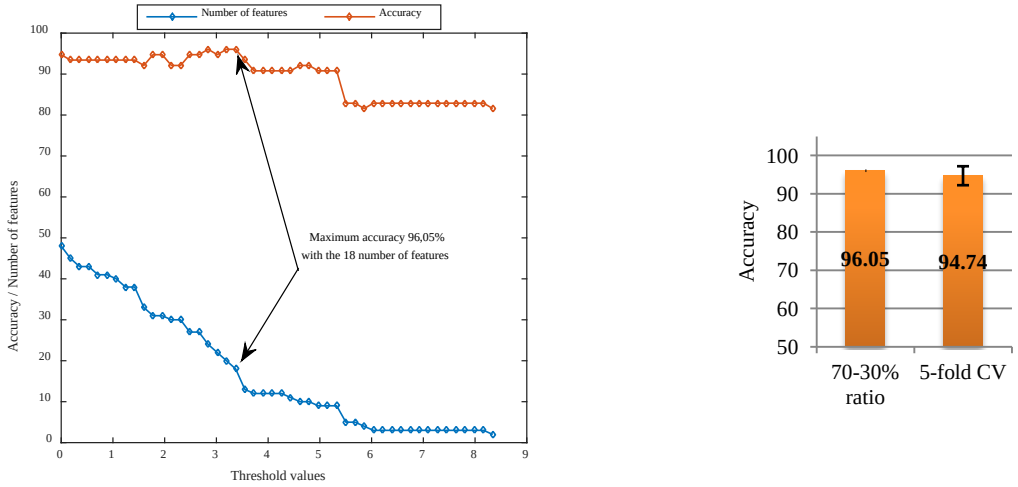

a b

Figure 2. Normal-abnormal classification results obtained from 70-30% ratio and 5-fold cross validation.

6. CONCLUSIONS

A feature set having well discriminative capability improve the accuracy and efficiency of classification processes, and also features with the small size are desirable. The proposed method allows a good classification result with the effective small-sized features using wave atom moments, *t*-test statistics, and dynamic thresholding. Hence, the system provides credible results for the classification of mammograms as normal and abnormal.

REFERENCES

[1]. S.K. Wajid and A. Hussain, "Local energy-based shape histogram feature extraction technique for breast cancer diagnosis," *Expert Systems with Applications*, vol. 42, no. 20, pp. 6990–6999, Nov.2015.
[2]. Y. C. Teh, G. H. Tan, N. A. Taib, et al., "Opportunistic mammography screening provides effective detection rates in a limited resource healthcare system," *BMC Cancer*, vol. 15, p. 6, May. 2015.
[3]. R. Nithya and B. Santhi, "Computer aided diagnosis system for mammogram analysis: A survey," *Journal of Medical Imaging and Health Informatics*, vol. 5, no. 4, pp. 653–674, Aug. 2015.
[4]. F.B. Garma and M.A. Hassan, "Classification of breast tissue as normal or abnormal based on texture analysis of digital mammogram,"*Journal of Medical Imaging and Health Informatics*, vol. 4, no. 5, pp. 647–653, Oct. 2014.
[5]. N. Gedik and A. Atasoy, "Performance evaluation of the wave atom algorithm to classify mammographic images," *Turk. J. Elec. Eng. & Comp. Sci.*, vol. 22, pp. 957–969, Jun. 2014.
[6]. A. Tahmasbi, F. Saki, and S.B. Shokouhi, "Classification of benign and malignant masses basedon Zernike moments,"*Computers in Biology and Medicine*, vol. 41, no. 8, pp. 726–735, Aug. 2011.
[7]. N. Gedik, "Breast cancer diagnosis system via contourlet transform with sharp frequency localization and LS-SVM," *Journal of Medical Imaging and Health Informatics*, vol. 5, pp. 1–9, Jun. 2015.
[8]. D. D. Costa, L. F. Campos and A. K. Barros, "Classification of breast tissue in mammograms using efficient coding," *Biomed Eng. Online*, vol. 10, no. 1, p. 55, Jun. 2011.
[9]. D. C. Pereira, R. P. Ramos, and M. Z. do Nascimento, "Segmentation and detection of breast cancer in mammograms combining wavelet analysis and genetic algorithm," *Comput Methods Programs Biomed*, vol. 114, no. 1, pp. 88–101, Apr. 2014.
[10]. S. Beura, B. Majhi, and R. Dash, "Mammogram classification using two dimensional discrete wavelet transform and gray-level co-occurrence matrix for detection of breast cancer,"*Neurocomputing*, vol. 154, pp. 1–14, Apr. 2015.
[11]. S. Dhahbi, W. Barhoumi, and E. Zagrouba, "Breast cancer diagnosis in digitized mammograms using curvelet moments," *Computers in Biology and Medicine*, vol. 64, pp. 79–90, Sep. 2015.
[12]. Y. N. Guo, M. Dong, Z. Yang, X. Gao, K. Wang, C. Luo, m. Yide, and J. Zhang, "A new method of detecting micro-calcification clusters in mammograms using contourlet transform and non-linking simplified PCNN," *Computer Methods and Programs in Biomedicine*, vol. 130, pp. 31–45, Jul. 2016.
[13]. L. Demanet, and L. Ying, "Wave atoms and sparsity of oscillatory patterns," *Appl. Comput. Harmon Anal.*, vol. 23, pp. 368–387, Nov. 2007.
[14]. H. Liu, J. Li, and L. Wong, "A comparative study on feature selection and classification methods using gene expression profiles and proteomic patterns," *Genome Inf.*, vol. 13, pp. 51–60, Jul. 2002.
[15]. DDSM database. [Online]. Available: http://marathon.csee.usf.edu/Mammography/Database.html

The Investigation of the Potential into Culture of Cocklebur (*Xanthium strumarium* L.)

Cuneyt Cesur, Belgin Cosge Senkal, Tansu Uskutoglu, Cennet Yaman

Abstract

Cocklebur (Xanthium strumarium L. - syn. X. sibiricum) belonging to the Asteraceae family is a very common weed in many parts of the world. It is an annual and has brown, hard, woody fruits, 1.0-3.5 cm long, with hooked spines. Each fruit of the plants contains two seeds. The plant has some medicinal properties and has been used in traditional medicine. Also, the researches were shown that X. strumarium has some biological properties such as anti-ulcerogenic, anti-inflammatory, diuretic, antifungal etc. Its seed has high oil content. According to results of studies on biodiesel properties of the oil; X. strumarium is a promising species as renewable resource for biodiesel production.

Keywords*: Xanthium L., weed, seed oil, biodiesel*

1. INTRODUCTION

Xanthium L. is represent in Turkey with 3 species (X. orientale / rough cocklebur, X. Spinosum / cocklebur , X. Strumarium / large cocklebur) and 3 subspecies (X. orientale subsp. italicum, X. strumarium subsp. Brasilicum, X. strumarium subsp. Strumarium) in total it have 6 taxon [1].

Xanthium L species are annual and still considered that haven't commercial properties. Because of that it is defined as weed. In cultivated area people are trying to remove for its harm effect to cultivated plant and same time they are spending both power and time[2]-[3]-[4]. As weed it can grow nearly all over the Turkey as it grows in Korea, Japan, America and Europe [5].

Almost the last two centuries fertile land for industry and urbanization are used irresponsibly. At the beginning of the 19th century the population of 1 billion, which is passed 7 billion at the beginning of the 21st century [6], such reasons like this day by day agriculture production and agriculture lands impose limitations. Feeding the growing population is a much more serious matter and each passing day increases the seriousness. Irresponsible use of existing water resources which is vital sources, makes it difficult to reach even for the needs of industry and cities. With global warming water resources are estimated drop more serious level in the future. When reaching of water impose limitations, also effect bio-diversity limitations and on the other hand its effect people life standard. Because of less water first its cause epidemic illness and effect public people health so cope with these problems we need to be studied better assess water and agricultural resources.

The vast majority of Turkish agriculture land doesn't have economical irrigation system. The biggest part of East Anatolia, Center Anatolia and Southeastern Anatolia regions and other land where there haven't got a river and dam which can use for irrigation and other highest area the only possibility is making dry farming. Therefore, in this wide area is a production system based on wheat and nearly 4 million hectare must be fallow. For many years, the plant production design which can't be rotated with other plants have some disadvantages. The first one is weakened the structure of the soil. The second is the lands are getting more infertile and the worst of all it has made the reduction of biodiversity. For that reasons in the dry land can better assess the plants should be brought into production system. Plants such as cocklebur can be considered for this purpose, while able to provide a variety of our country, unfortunately not sufficiently be utilized [7].

Cocklebur plant can be grown in almost every region of Turkey and all kind of soil conditions so it can be utilized dry land condition. Turkey have very rich plant diversity. More than about 12,000 species and taxa identified and more than %30 of them are unıque to Turkey [7]-[8].Our country still consider it as a weed but the features like, ıt can grow in dry land and its seed oil is reach up to %25.Cocklebur have a potential and can be used in rural area for obtain oil. In addition to being eligible for the study of human consumption that could be used for the needs of the oil industry in Turkey and ıt is essential to make the necessary research on this plant.

2. THE MORPHOLOGY OF COCKLEBUR

Cocklebur (X. strumarium veya X. sibiricum) can grow up to 1 m, it is an annual plant. It has developed a strong taproot, alternative leaves series 3-5 lobed, rough toothed leaves are connected with a long petiole. The plant's body is covered with small feathers and plant body is mottled purple. Flowers are white or pale green and it has monoecious flowers. Male flowers above female flowers located below and flowers settled in the form of clusters on the main and side branches [9] Flowers bloom on june-july and fruit ripening on August September [10].Fruits looks like egg shaped and length of fruit about 1-3.5 cm. There are two seeds in each fruit [11] (Fig. 1). Because of the noncultivation, cocklebur known as weed and plants show spread between the altitudes 0-1750. Cocklebur widely grown throughout Turkey (Fig. 2).


a-)Cocklebur plant appearance in the field


b-)Overview of the cocklebur fruit


c-) The view from interior of the cocklebur fruit

Figure 8. *Different pictures from cocklebur plant*

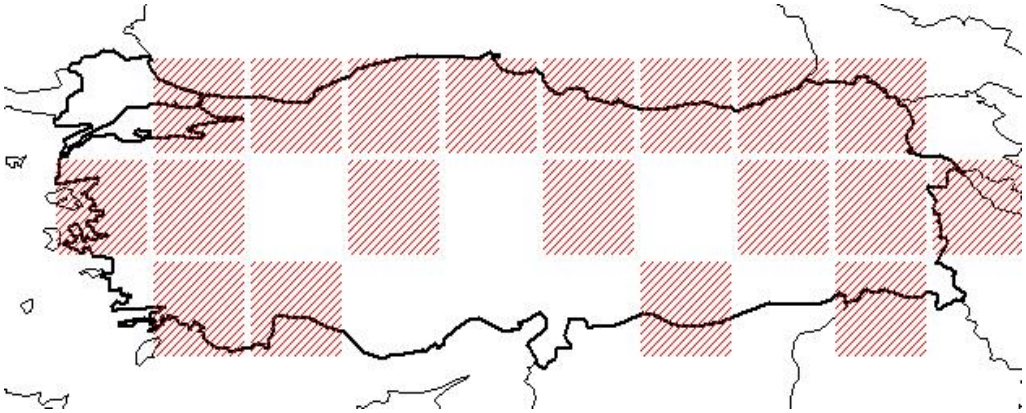

Figure 2. Cocklebur's (Xanthium L.) distribution in Turkey Geography

3. OPPORTUNITY TO BENEFIT FROM COCKLEBUR PLANT

Humankind has used multipurpose plant since dawn of the history. Until the beginning of the industrial revolution began hunting and gathering period, people have used plants as well as nutritional and therapeutic purpose. The period when people haven't knowledge of the production of synthetic drugs, people sought healing from plants. In modern times, although the weight given to synthetic drugs, people realized that side effects of drugs in recent years and given priority on treatment with plant-based medicines [12]-[13]-[14]-[15]-[16].

Studies conducted in our faculty 25% of cocklebur fruit oils were determined. When oil concentration analyzed, oleic (11.91%) - linoleic acid (76.97%) composition was determined as 88.88%. In addition, the plant is utilized as a tool different treatment and medication. In Chinese traditional medicine, it has been used for treatment of skin diseases and cancer [5]. The cocklebur plant from the resultant caffeic acid, antihyperglycemic (the amount of sugar in the blood) in studies which is examined on mice, the effect was found positive impact [17]. The plant has been found in many other studies on compounds showing bioactive properties such as antitumor, antibacterial, antifungal , antitussives (cough suppressants), anti-inflammatory (to reduce inflammation), antinociceptive (analgesic), hypoglycemic (blood sugar lowering), antimitotic (inhibitor of cell proliferation), antioxidants and insecticides (insecticide) [18]-[19].

Because of oil contain in seed and plant form like a woody biomass, cocklebur plant can be used as energy plant [20].Plants used for energy is much more environmentally friendly than other fossil fuels, the rate of emission of harmful gases which rate is very low on environment [21]-[22]. The world population is rapidly increasing with each passing day whereas fossil fuels for energy needs come the point of exhaustion every day. Scientist are turning to different energy sources in order to overcome the crisis and they are turning to renewable energy sources. Biodiesel which is obtained on plant oil, as a renewable energy source has reached a significant amount of use in the world. It is reported that about 15% of world energy derived from plant-based material [23]. Besides being environmentally friendly feature and also a source of energy is increasing interest in biodiesel. For this reasons oils derived from cocklebur possible to produce biodiesel. In the seed oil content up to 42.34% on cocklebur (Xanthium sibiricum Patr) was quite large potential for biodiesel production [24]-[22]. Dense and bushy structure Xanthium L. of producing biomass from wood, insulation material and erosion, flooding, flood, to prevent the negative effects of natural events such as landslides and it is possible to benefit from the breeding of the dam and basin [25]-[26].

4. CONCLUSION

Cocklebur (Xanthium strumarium) belong to Asteraceae family and genus Xanthium L., and it is a self-pollinating, annual plant. Nearly all regions of Turkey, this plant can grow even in the most adverse conditions, any economic importance in terms of agricultural production up to now has not been mentioned. Because there is no economic importance it is not intended as a cultural plants. However, when we look at the special composition of cocklebur and ability to grow in adverse conditions; cocklebur plant have economic potential and it can cultivation.

It is a fact that there is insufficient water resources throughout the world. Desertification due to lack of water resources and it is constantly increasing. Also in this case, not only bring routinized agricultural production, but also decrease the biodiversity and vitality. It seems to have become insufficient agricultural production necessary for the food industry with the contraction of the agricultural sector.

For that reasons, resources were obliged to take the necessary measures for the balanced use and arid areas better assess the identification of species and varieties can be gained even more importance. Cocklebur plant properties can serve this purpose. Understanding of the properties of the oil structure and it can be used at least in the industry, the plant can create a significant source.

As a result, the world is seen as weed plants but this plant can be grown in dry areas, thanks to features such as vegetable oil in the seed by about 25% it is a potential in terms of investigating the possibility of producing oil. In addition to the oil quality of the Cocklebur plant also investigated whether or not fit for human consumption, even oil needs which consumed in Turkey industry needs is essential to make the necessary research on this plant.

REFERENCES

[1] Güner A., Aslan S., Ekim T., Vural M., Babaç M.T. (edlr.) 2012. Türkiye Bitkileri Listesi (Damarlı Bitkiler). Nezahat Gökyiğit Botanik Bahçesi ve Flora Araştırmaları Derneği Yayını, İstanbul, 216s.
[2] Auld, B.A., McRae, C.F., Say, M.M. 1988. Possible Control of Xanthium spinosum by a Fungus. Agriculture, Ecosystem and Environment, 21: 219-223.
[3] Auld, B.A., Ridings, H.I., Say, M.M., Andrew, J. 1990. Field Applications of Colletotrichum orbiculare to control Xanthium spinosum. Agriculture, Ecosystem and Environment, 32: 315- 323.
[4] Bükün, B. 2011. Sesame (Sesamum indicum L.) Yield Loss Estimation With Common Cocklebur (Xanthium strumarium L.) Interference. Journal African Journal of Biotechnology, 10(71): 15953-15958.
[5] Kim, Y.S., Kim, J.S., Park, S.H., Choi, S.U., Lee, C.O., Kim, S.K., Kim, Y.K., Kim, S.H., Ryu, S.Y. 2003. Two Cytotoxic Sesquiterpene Lactones from the Leaves of Xanthium strumarium and Their In Vitro İnhibitory Activity on Farnesyltransferase, Planta Med., 69(4): 375-377.
[6] Gençtan, T. 2013. Ekoloji ve Tarım. Ekoloji 2013 Sempozyumu, 2-4 Mayıs, Tekirdağ.
[7] Deniz L., Serteserb, A., Kargıoğlu M. 2010. Uşak Üniversitesi ve Yakın Çevresindeki Bazı Bitkilerin Mahalli Adları ve Etnobotanik Özellikleri. AKÜ Fen ve Mühendislik Bilimleri Dergisi, 10(1): 57-72.
[8] Davis, P.H., Mill, R., Tan, K. 1988. Flora of Turkey and The East Aegean Islands (supplement), Edinburg University Pres, Vol.10.
[9] TUBİVES, 2015. http://www.tubives.com/index.php?sayfa=1&tax_id=4679, (Erişim tarihi: 24.11.2015).
[10] Agharkar, S.P. 1991. Medicinal Plants of Bombay Presidency. Scientific Publishers, Jodhpur, India, 230s.
[11]. Ronald, J. 1992. Xanthium strumarium. In: Fire Effects Information System.
[12]. Pandey, D.K., Tripathi, N.N., Tripathi, R.D., Dixit, N. 1982. Fungitoxic and Phytotoxic Properties of The Essential Oils of *Hyptis suaveolens.* Journal of Plant Disease and Protection, 89 (6): 344-349.
[13]. Dwivedi, S.K., Kıshore, N., Dwivedi, S.K. 1990. Fungitoxicity of Some Essential Oils Againts Macrophomina phaseoline. Indian Perfumer, 43(1): 20-21.
[14]. Duru, M.E., Çakır, A., Kordali, Ş., Zengin, H., Harmandar, M., Izumui, S., Hirata, T. 2003. Chemical Composition and Antifungal Properties of Essential Oils of Three Pistacia species. Fitoterapia, 74(1-2):170-176.
[15]. Melikoğlu, G., Kurtoğlu, S., Kültür, Ş. 2015. Türkiye'de Astım Tedavisinde Geleneksel Olarak Kullanılan Bitkiler. Marmara Pharmaceutical Journal, 19(1): 1-11.
[16]. Romeroa, M., Zanuyb, M., Rosellc, E., Cascanteb, M., Piulatsc, J., Font-Bardiad, M., Balzarinie, J., De Clerqe, E., Pujola, M.D. 2015. Optimization of Xanthatin extraction from Xanthium spinosum L. and Its Cytotoxic, Anti-Angiogenesis and Antiviral Properties. European Journal of Medicinal Chemistry, 90:491- 496.
[17]. Hsu, F.L., Chen, Y.C., Cheng, J. T. 2000. Caffeic Acid as Active Principle From The Fruit of Xanthium strumarium to Lower Plasma Glucose in Diabetic Rats. Planta Med., 66 (3): 228-230.
[18]. Alpaslan, P. 2013. Xanthium L. Bitkisinde Biyolojik Aktif Bileşiklerin İzolasyonu, Yapıların Aydınlatılması ve Asetilkolinesteraz ve Butirilkolinesteraz İnhibisyon Aktivitelerinin İncelenmesi. Trakya Üniversitesi Fen Bilimleri Enstitüsü, Kimya ABD, Yüksek Lisans Tezi, 129s.
[19]. Sarı, A. O., Oğuz, B., Bilgiç, A., Tort, N., Güvensen, A., Şenol, S.G. 2010. Ege ve Güney Marmara Bölgelerinde Halk İlacı Olarak Kullanılan Bitkiler. Anadolu, J. of AARI, 20(2): 1- 21.
[20]. WeiHe, X., Cheng Jiang, R. 2010. Oil Contents and Relative Components of Fatty Acid in The Seeds of Five Energy Plants. Renewable Energy Resources, 28(2): 62-66.
[21]. Bükün, B. 2012. Enerji Bitkilerinde Yabancı Ot Sorunları ve Neden Oldukları Kayıplar. Tarım Makinaları Bilimi Dergisi, 8(3): 279-285.
[22]. Fei, C., Hanna, M.A., Dejing, Z., Hu, L., Quan, Z., BaoAn, S., Song, Y. 201. Production of Biodiesel from Non-edible Herbaceous Vegetable Oil: *Xanthium sibiricum* Patr. Bioresource Technology, 140: 435-438.
[23]. Aktürk, Z. 2010. İnsan Sağlığı Açısından Biyokütle Enerjisi ve *Miscanthus x giganteus*. Konuralp Tıp Dergisi, 2(1): 41-45.
[24]. Cheng Jiang, R., WeiHe, X., Silva, J.A.T. 2012. Potential of Five Plants Growing on Unproductive Agricultural Lands as Biodiesel Resources. Renewable Energy, 41(1): 191-199.
[25]. Moore, J.E., Wolfe, J.D., Franklin, S.B. 2014. Growth Responses of Different Aged Individuals of *Xanthium strumarium* L. in Flooded Conditions. Journal of The Torrey Botanical Society, 141(1): 72-79.
[26]. Nagel, J. M., Wang, X. Z., Lewis, J. D., Fung, H. A., Tissue, D. T., Griffin, K. L. 2005. Atmospheric CO_2 Enrichment Alters Energy Assimilation, Investment and Allocation in *Xanthium strumarium*. Journal New Phytologist, 166(2): 513-523.

Determination of Reservoir Capacities Using Design Methods

Ulker Guner Bacanli[1]

Abstract

The storage reservoirs are designed to eliminate the surplus and deficit between input data, namely the flow, and requirements such as energy production, irrigation, river transportation water. The storage volume depends on three factors: magnitude and variability of the river flows, the size of the demand, and the degree of reliability.

In this study, the relationships between reservoir capacity, yield and reliability are investigated for a certain reservoir named as Adıgüzel Dam in the southwestern Turkey. For analyzing of the reservoir capacity, monthly and annual mean flow data on the years of 1963–1984 of Büyük Menderes stream has been used. The required reservoir capacity is tried to be estimated by using minimum flow, Alexander, Dincer, Gould's Gama, McMahon, Gould's synthetic data, behavior analysis and Moran and Gould probability matrix methods. Preliminary and final design methods have been compared. Based on the obtained results.

The "Minimum Flow Method" gives a very large storage volume while "Alexander Method" gives smaller storage volume. If compared with two methods above, "Dinçer Method" gives the largest storage volume. Gould's Gamma Distribution Method is more effective by the estimation of larger storage volumes if it is worked with annual data. At the stage of preliminary design, the most effective methods are Alexander, Dinçer and Gould's Gamma Method, respectively. "Monthly Water Budget Method" that is one of the critical period approach-methods, may be applicable under various operation-conditions as considered evaporation and all other losses and monthly and seasonal variation of the requirements Therefore, the method can be used safely in the design stage. Monthly Water Budget, Gould and Moran Probability Matrix Methods give relatively closer results to each other. Monthly Water Budget Methods gives longer unimpounding probability compared with Gould and Moran Probability Matrix Methods.

Keywords: *Low flow hydrology, Critical period, Probability matrix method, reservoir capacity-yield-reliability relationships*

1. INTRODUCTION

Reservoir storage is necessary to use the highly variable water resources of a river basin for beneficial purposes. Because water resources become limited. Reservoirs are designed for decreasing the instability between the flows brought by the river. The reservoir storage capacity methods which can be used for rapid assessment are designated as preliminary design techniques. After using preliminary design techniques to eliminate unsuitable reservoir sites from consideration, the remaining few should be evaluated using a final design technique. These techniques are often more complicated because they take into account most, or all, of the factors which influence storage (McMahon T.A. and Mein R.G.).

In the many studies had been represented in the development of models for determining reservoir storage for different conditions. Moran (1954) introduced a model that predicted the probability distribution of storage at the end of every successive year with an initial condition. Gould (1961) modified the derivation of the transition matrix in the Moran model to include seasonal flow variations and intra-year autocorrelation using monthly rather than annual flows. McMahon et al (2007) has examined which annual and monthly stream flows for 729 rivers from a global data set are used to assess the adequacy of five techniques to estimate the relationship between reservoir capacity, target draft (or yield) and reliability of supply. Bacanli and Baran (2006) investigated required reservoir capacity is tried to be estimated by using minimum flow, Alexander, Dincer, Gould's Gama, McMahon, Gould's synthetic data, behavior analysis and probability matrix methods. Bacanli and Koç (2006) investigated reservoir capacity-yield reliability relationships by using Moran probability matrix method. Bacanlı et al. (2003) investigated required reservoir capacity is tried to be estimated by using mass curve, residual mass curve, minimum flow, Alexander, Dincer, Gould's Gama and behavior analysis. Pilgir and Bacanli(2011) investigated required reservoir capacity is tried to estimate by using Moran and Gould probability matrix methods, behaviour analysis and the obtained results are evaluated.

[1] *Corresponding author: Pamukkale University, Department of Civil Engineering, 27000, Kınıklı/Denzili, Turkey.*

ugbacanli@pau.edu.tr

The purpose of this paper is investigated reservoir capacity by using as preliminary and final design techniques. Annual and mothly streamflows are used. The required reservoir capacity is tried to be estimated by using minimum flow approach, Alexander, Dincer, Gould's Gama, McMahon, Gould's synthetic data, behavior analysis, Gould's probability matrix and Moran's probability matrix methods. Each methods was evaluated by application for Adıgüzel Dam data. Before submitting your final paper, check that the format conforms to this template. Specifically, check the appearance of the title and author block, the appearance of section headings, document margins, column width and other features. Please make sure that the use of other languages in figures and tables is avoided. Papers should be checked by a native English speaker with expertise in the field prior to submission.

2. DATA

In this study, monthly and annual mean flow data, observed a period between 1963–1984, streamgauge stations for Adıgüzel Dam on Büyük Menderes Stream are used. (Büyük Menderes Cindere Projesi Planlama Raporu, 1986). The technical properties of Adıgüzel Dam are given in Table 1. A statistical property of flow data for Adıgüzel Dam is given in Table 2.

Table 1. The technical properties of Adıgüzel Dam

Statistical properties	Monthly Flow Volume (10^6 m^3)	Yearly Flow Volume (10^6 m^3)
Mean	67,53	810,33
Standard deviation	49,18	324,95
Variation coefficient	0,73	0,40
Skewness coefficient	1,84	0,50
Autocorrelation	0,79	0,61

Table 2. A statistical property of flow data for Adıgüzel Dam

Name	ADIGÜZEL
Location	Denizli
River	B.Menderes
Construction (starting and completio n) year	1976 - 1989
Dam volume	7125 dam^3
Height (from river bed)	144 m
Reservoir volume at normal water surface elevation	1076 hm^3
Reservoir area at normal water surface elevation	26 km^2
Irrigation Area	89600 ha
Capacity	62 MW
Annual Generation	280 GWh

3. METHODS

3.1. Preminary Design Methods

3.1.1. Minimum Flow Approach

Minimum Flow approach was proposed by Waitt in 1945. From the historical streamflow record, the lowest sub-sequences of flows of various durations (5, 10, 20, … monthly flow) are selected and plotted as mass flow against corresponding duration. Constant drafts are plotted as straight lines on this so-called drought curve graph. The critical storage is given by the ordinate at the origin when the draft line is tangential to the drought curve (Bayazıt, 1997 ; Mcmahon and Mein ,1986).

Total minimum monthly flows for Adıgüzel Dam flows were determined. Results are presented in Figure 1. According to Minimum flow approach, reservoir storage capacity for draft 90% and 75% were found 874.8 10^6 m^3 and 2013.1 10^6 m^3.

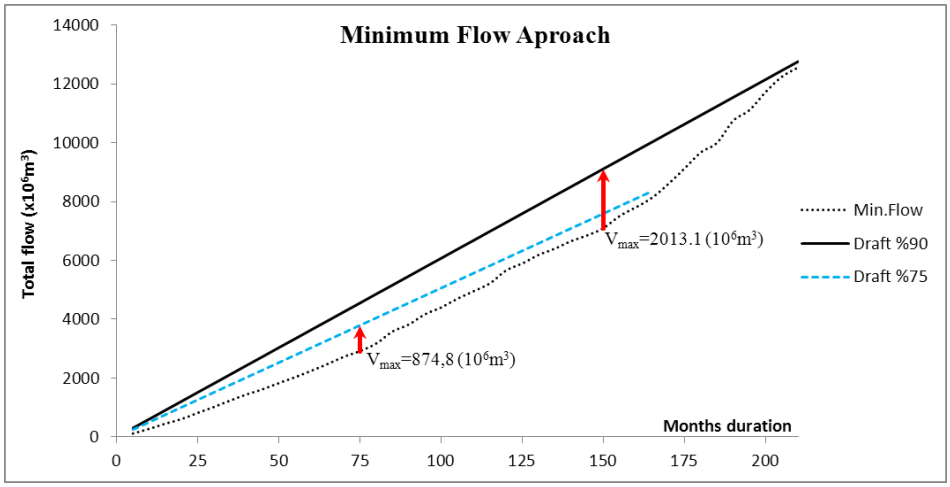

Figure 9. *Reservoir capacity-yield analysis by minimum flow approach*

3.1.2. Alexander's Method

Alexander (1962) extended these earlier approaches by developing a series of drought curves for different probabilities of occurrence and from these derived generalized storage-regulation-probability curves. In effect Alexander's approach may be considered as a development of Waitt's drought curve procedure. Alexander assumed that annual streamflow could be represented by a Gamma distribution from which he specified the mass inflows for various recurrence intervals. Draft lines were also superimposed on the drought curves as Waitt had done and storage capacity estimated as the difference between cumulative inflows and outflows (McMahon ve Mein, 1986).

According to Alexander method, The relationship between Storage-Draft-Risk is presented in Figure 2 for Adıgüzel Dam.

3.1.3. Dincer Method

Dinçer method was proposed by Dincer in 1966. Consider a sequence of annual flows, which are assumed independent, with a mean x and standard deviations.

In addition to the basic critical period assumptions (an initially full reservoir and only one failure during the critical period), the above derivation is based on a number of other assumptions, namely:

(i) that the critical period is large enough so that the n-year flows will tend towards a Normal distribution;

ii) that annual flows are independent; and

(iii) that the draft rate is uniform (McMahon ve Mein, 1986).

According to Dincer method, The relationship between Storage-Draft-Risk is presented in Figure 3 for Adıgüzel Dam.

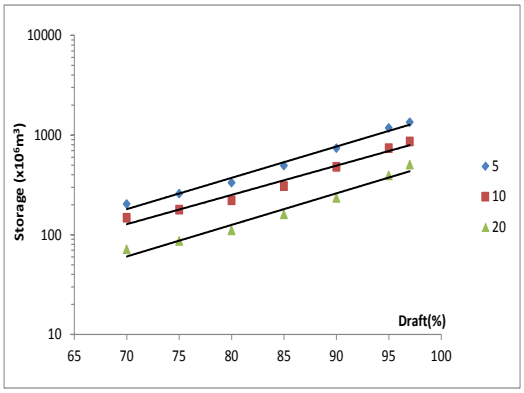

Figure 2. Reservoir capacity-draft-risk relationship Alexander's method

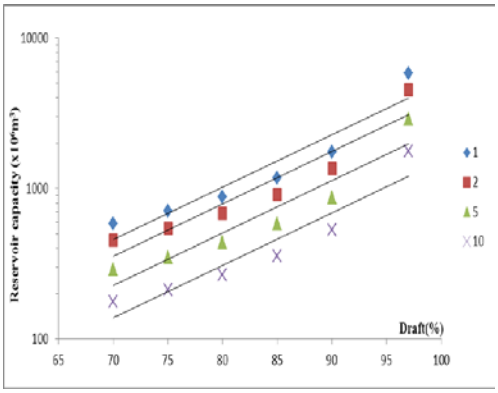

Figure 3. Reservoir capacity-draft-risk relationship Dincer's method

3.1.4. Gould's Gamma Method

Gould's Gamma method (Gould, 1964) can be thought of as a modification of Dincer's method. It uses the fact that, while parameters for the Normal distribution are easy to calculate and probability tables for it are readily available, the Gamma distribution usually is a better approximation to the distribution of annual flow data. The procedure is therefore to use the Normal distribution for the calculations, and then to apply a correction to approximate the Gamma distribution (McMahon ve Mein, 1986). According to Gould's Gamma method, the relationship between Storage-Draft-Risk is presented in Figure 4 for Adıgüzel Dam.

3.1.5. McMahon Method

For 156 Australian streams, McMahon (1976) used Gould's modified procedure to estimate the theoretical storage capacities for four draft conditions (90%, 70%, 50% and 30%) and three probability of failure values (2%, 5% and 10%) (McMahon ve Mein, 1986). According to McMahon method, The relationship between Storage-Draft-Risk is presented in Figure 5 for Adıgüzel Dam.

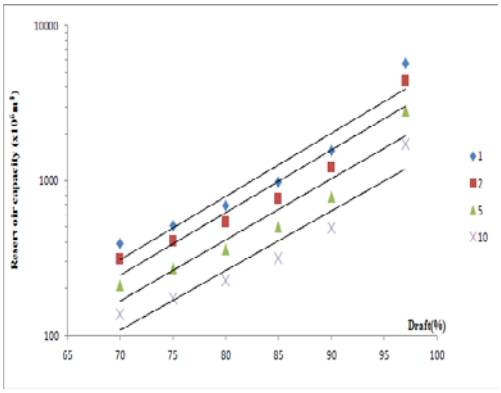

Figure 4. Reservoir capacity-draft-risk relationship with Gould's Gamma method

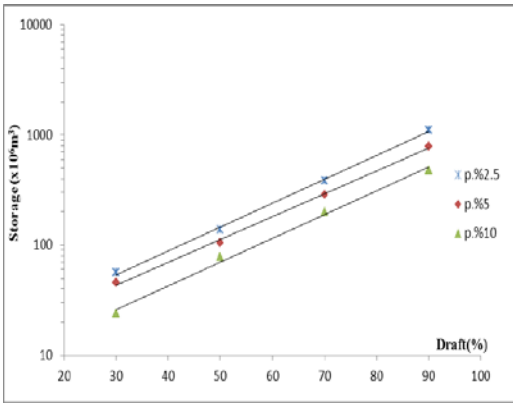

Figure 5. Reservoir capacity-draft-risk relationship with McMahon method

3.1.6. Gould's Synthetic Data Procedure

Using a three parameter log-normal model, Gould (1964) generated 240 sets of data, each equivalent to 10,000 years of independent flow events. The 240 sets were analysed for different combinations of eight draft rates, five storage sizes and six values of skewness. Gould also provides a correction factor for assuming annual serial correlation is zero (McMahon ve Mein, 1986). According to Gould's Synthetic Data Procedure, The relationship between Storage-Draft-Risk is presented in Figure 4 for Adıgüzel Dam.

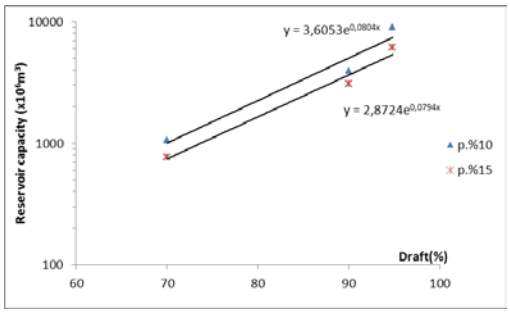

Figure 6. Reservoir capacity-draft-risk relationship with Gould's Synthetic Data Procedure

3.2. Final Design Procedures

3.2.1. Behaviour Analysis

In behaviour analysis, the changes in storage content of a finite reservoir are calculated using a mass storage equation thus:

$$Z_{t+1} = Z_t + Q_t - D_t - \Delta E_t - L_t \qquad 0 < Z_{t+1} < C \qquad (1)$$

Where, Z_{t+1} storage at end of the t^{th} time period; Z_t storage at beginning of the t^{th} time period; Q_t inflow during t^{th} time period; D_t release during t^{th} time period; ΔEt net evaporation loss from reservoir duringt^{th} time period; ; L_t other losses and C active storage capacity (McMahon ve Mein, 1986).

Monthly Water budget (continuity equation) method from critical period approaches, easily applied to which to the various operating conditions such as limited water, evaporation and other losses, monthly or seasonal variations of requirements. Therefore, the method is seen as an approach that can be used safely in final design stage (Özkul, 2010).

A result of the monthly water budget for Adiguzel Dam project data were obtained a 21% probability of failure of reservoir capacity. Therefore, reservoir capacity-draft-risk relationship using equation 1 for both different volumes and different drafts is shown in Figure 7.

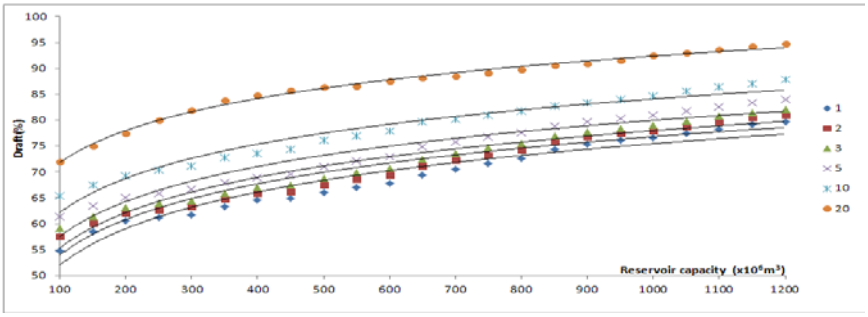

Figure 7. Reservoir capacity-draft-risk relationship with behaviour analysis

3.2.2. Gould's Probability Matrix Method

Gould (1961) modified the simultaneous Moran-type model to account for both the seasonality and serial correlation of inflows. He did this by using the transition matrix with a yearly time period, but accounting for within-year flows by using behavior analysis. Thus monthly flow variations, monthly serial correlation and draft variations can be included. In the approach storage capacity and draft are given, and probability of failure of the reservoir is determined. If draft or storage size is to be determined then a trial and error method needs to be utilized. (McMahon ve Mein, 1986). Results of Adıgüzel Dam with Gould's probability matrix

method are given Table 3, Table 4 and Table 6.

Table 3: Gould probability matrix for Adıgüzel Dam

Gould P.M		V_t Initial State						Steady State	
		i=0	i=1	…	…	i=20	i=m		
V_{t+1} Final State	j=0	0,409	0,409			0,000	0,000	Uniform(Steady) State Matrix	0,153
	j=1	0,045	0,045			0,000	0,000		0,027
	j=2	0,182	0,182			0,000	0,000		0,060
	…	0,000	0,000			0,000	0,000		0,022
	…	0,045	0,045			0,000	0,000		0,033
	…	0,000	0,000			0,000	0,000		0,020
	…	0,045	0,045			0,000	0,000		0,033
	…	0,000	0,000			0,000	0,000		0,024
	…	0,000	0,000			0,000	0,000		0,027
	…	0,000	0,000			0,000	0,000		0,035
	…	0,045	0,045			0,045	0,045		0,052
	…	0,045	0,045			0,091	0,000		0,041

	…	0,000	0,000	0,045	0,136		0,039
	…	0,045	0,045	0,091	0,000		0,037
	…	0,045	0,045	0,045	0,091		0,030
	…	0,045	0,045	0,000	0,045		0,029
	…	0,000	0,000	0,000	0,000		0,039
	…	0,045	0,045	0,136	0,136		0,047
	…	0,000	0,000	0,182	0,182		0,050
	j=19	0,000	0,000	0,364	0,364		0,203
	j=20	0,000	0,000	0,000	0,000		0,000
	j=m	0,000	0,000	0,000	0,000		0,000
	∑	1	1	1	1	∑	1

Table 4: Adıgüzel Dam example of combining steady state probability with the conditional failure probability in Gould's procedure.

Zone	Steady state	Probability of failure from any starting in zone	Product of probabilities
	(Pr)	(*F*)	(P)
j=0	0,153	0,477	0,073
j=1	0,027	0,458	0,012
j=2	0,060	0,341	0,020
…	0,022	0,265	0,006
…	0,033	0,193	0,006
…	0,050	0,000	0,000
j=19	0,203	0,000	0,000
j=20	0,000	0,000	0,000
j=m	0,000	0,000	0,000
∑	Probability of Failure		**%13.00**

3.2.3. Moran's Probability Matrix Method

In Moran's probability matrix method is appropriate to choose the inflows, draft, and storage capacity as integer multiples of some arbitrary volume unit. Reservoir capacity can't be determined directly by this method. However, probability of failure (risk) which thanks limit (stable) probability distributions of determined capacity can be found. Inflow's histograms is drawn in Moran' probability method with constant draft., Reservoir capacity at the end of the period by assuming constant draft is determined as follows.

$$V_{t+1}^{*} = V_t^{*} + X_t^{*} - D^{*} \qquad 0 \le V_{t+1}^{*} \le C^{*} \qquad (2)$$

Where, V_t^* state at begining of the t[th] period of reservoir, V^*_{t+1} state at end of the t[th] period of reservoir, C^* reservoir capacity, D^* constant draft. * are shown units have been expressed at selected terms in unit volume. The begin of the period with 2 equation begins with a certain volume. Flow to enter into the reservoir for the formation of any volume flow at the end of the period is determined. A value of the transition probability matrix with using flow histogram is found. Transition probability matrix depending on coefficient of variation of flows is chosen. If how big dimensions of this matrix is chosen, as much it is increased the sensitivity of the results. (McMahon ve Mein, 1986; Bacanlı ve Koç, 2006; Özkul, 2010).

In a calculations for Adıgüzel Dam, active storage capacity 811 (x10^6m^3) and draft %97 are calculated by taking into account. Moran's probability matrix for Adıgüzel Dam is given in the Table 5. Gould and Moran probability matrix method results for different draft 75%, 90% and 97% is given Table 6.

Table 5: Moran's probability matrix for Adıgüzel Dam

		Initial State V_t							
		i=0	i=1	i=2	…	i=19	i=m		i=0,..,20
Final State Vt+1	i=0	0,591	0,500	0,409		0,000	0,000	Uniform(Steady) State Matrix	i=0 **0,152**
	i=1	0,045	0,091	0,091		0,000	0,000		i=1 0,022
	i=2	0,045	0,045	0,091		0,000	0,000		i=2 0,026
	..	0,000	0,045	0,045		0,000	0,000		.. 0,018
	..	0,000	0,000	0,045		0,000	0,000		.. 0,025
	..	0,045	0,000	0,000		0,000	0,000		.. 0,025
	..	0,000	0,045	0,000		0,000	0,000		.. 0,026
	..	0,000	0,000	0,045		0,000	0,000		.. 0,022
	..	0,000	0,000	0,000		0,000	0,000		.. 0,022
	..	0,045	0,000	0,000		0,045	0,000		.. 0,032
	..	0,045	0,045	0,000		0,000	0,045		.. 0,042
	..	0,000	0,045	0,045		0,136	0,000		.. 0,028
	..	0,045	0,000	0,045		0,000	0,136		.. 0,065
	..	0,045	0,045	0,000		0,091	0,000		.. 0,030
	..	0,045	0,045	0,045		0,045	0,091		.. 0,053
	..	0,000	0,045	0,045		0,000	0,045		.. 0,030
	..	0,045	0,000	0,045		0,045	0,000		.. 0,025
	..	0,000	0,045	0,000		0,045	0,045		.. 0,031
	..	0,000	0,000	0,045		0,091	0,045		.. 0,029
	..	0,000	0,000	0,000		0,091	0,091		.. 0,040
	m=20	0,000	0,000	0,000		0,409	0,500		m=20 0,258
	∑	1	1	1	, , ,	1	1		∑ 1

4. RESULTS

With different preliminary and final design methods was determined reservoir capacity. As a result of using methods can be possible make the following comments. A relationship between storage capacity and risk is not be established in the critical period approaches as minimum flow method. Also, reservoir capacity is quite changes depending on the length of data series. The reservoir must be assumed to be initially full and no variation from this condition is possible. The method of analysis does not take into account net evaporation losses. Because of them, It is estimated by these methods is usually larger than necessary reservoir capacity.

Other critical period (Alexander, Dincer and Gould's Gamma) methods are used to make more reliable estimates. This method is possible to define relationship between reservoir capacity-draft-risk. But in the Dincer's method, for non-normally distributed annual flows the procedure will tend to overestimate storage need, In addition, the procedure is based on annual data and seasonal need is not taken into account. But in the Gould's Gamma method, by assuming flows to be Gamma distributed rather than normally distributed, Gould overcomes one of Dincer's major assumptions, but in doing so, introduces a small approximation relating to the difference between the Normal and Gamma distributions. Despite of good results of Gould's Gamma methods, this method which Australian streams were developed should be used with attention. Alexander, Dincer, or Gould's Gamma Method for long-term critical periods (the largest store) are shown the best methods used in the preliminary design stage.

Table 6: Gould and Moran probability matrix method results for Adıgüzel Dam

Draft	Gould P.M	Moran P.M
97	12,71	15,24
90	5,71	6,41
75	0,20	0,11

From these studies we conclude that the Gould's probability matrix technique is a suitable analytical storage-yield procedure for final design. In addition, it is noted that the behaviour analysis, which was used as a basis for comparison, gave results consistent with theoretically acceptable procedures so long as the effect of initial conditions is recognized. Computed storage estimates with Moran's probability matrix method are independent of the starting conditions. This is in contrast to critical period techniques and is one of the prime advantages of matrix methods.

The "Minimum Flow Method" gives a very large storage volume while "Alexander Method" gives smaller storage volume. If compared with two methods above, "Dinçer Method" gives the largest storage volume. Gould's Gamma Distribution Method is more effective by the estimation of larger storage volumes if it is worked with annual data. At the stage of preliminary design, the most effective methods are Alexander, Dinçer and Gould's Gamma Method, respectively. "Monthly Water Budget Method" that is one of the critical period approach-methods, may be applicable under various operation-conditions as considered evaporation and all other losses and monthly and seasonal variation of the requirements Therefore, the method can be used safely in the design stage. Monthly Water Budget, Gould and Moran Probability Matrix Methods give relatively closer results to each other. Monthly Water Budget Methods gives longer un-impounding probability compared with Gould and Moran Probability Matrix Methods.

ACKNOWLEDGEMENT

The author expresses her thanks to the Scientific Research Projects Fund of Pamukkale University for providing support in participation to the ICENS 2016.

REFERENCES

[1] Ü.G. Bacanlı, S. Özkul and T. Baran, "Dicle Havzası Botan Çayı Örneğinde Farklı Yöntemlerle Biriktirme Haznelerinin Tasarımı"*I. Ulusal Su Mühendisliği Sempozyumu*, İzmir, 389 – 401. 2003.
[2] Bacanlı, Ü.G ve Koç, A.C; "Moran Olasılık Matris Yöntemiyle Hazne Tasarımı", Yenidere Barajı Örneği", *S.D.Üniversitesi, Fen B. Enstitüsü Dergisi*, 256-257s, 2006.
[3] Bacanli, Ü.G. and Baran, T., "Çine çayı örneğinde biriktirme haznelerinin tasarımında farklı yöntemlerin değerlendirilmesi" *Pamukkale Üniversitesi, Mühendislik Fakültesi, Mühendislik Bilimleri Dergisi*, 12/1, 27-36, 2006.
[4] Bayazıt, M., *Biriktirme Haznelerinin Tasarımı ve İşletilmesi*, İ.T.Ü. 200 s., 1997.
[5] Devlet Su İşleri Genel Müdürlüğü, XXI. Bölge Müdürlüğü, "Büyük Menderes Cindere Project Tec. Rep.", 189 s, 1986.
[6] Gould, B. W., "Statistical methods for estimatingthe design capacity of dams" *J. Inst. Engrs*., 33, 405-416, 1961.
[7] McMahon, T. A.; Mein, R.G., *River and Reservoir Yield*, Elsevier, 367 pp., 1986.
[8] McMahon, T. A; Pegram, G.G.S.; Vogel, R. M.; Peel, M.C.; "Revisiting reservoir store-yield relationships using a global streamflow database" *Advances in Water Resources*, 30, 1858-1872, 2007.
[9] Moran, P. A. P., "A probability theory of dams and storage systems", *Aust. J. Appl. Sci*., 5, 116-124, 1954.
[10]Özkul,S; "Çağlayan Barajı Aktif Hazne Hacminin Olasılık Matris Yöntemleriyle İrdelenmesi", *DSİ Teknik Bülteni* Sayı:107, 27-37s, 2010.

[11] Pilgir M., Bacanlı U.G., "Moran ve Gould olasilik matris yöntemini kullarak cindere baraji hacminin değerlendirilmesi", *VI. Hidroloji Kongresi*, Denizli, 22-24. Eylül.2010.

BIOGRAPHY

Ülker GÜNER BACANLI is an Associate Professor at Pamukkale University, Faculty of Engineering, Civil Engineering Department, Denizli, Turkey. Her research interests include hydrology, drought, time series analysis and water resources.

ICENS
INTERNATIONAL CONFERENCE ON ENGINEERING AND NATURAL SCIENCES
24-28 May 2016 /Sarajevo

Grouting Applications in Hacininoglu Hydroelectric Powerplant Energy Tunnel, Kahramanmaras, Turkey

Ahmet Ozbek[1], Sinan Kara[2], Murat Gul[2], Yusuf Uras[1], Li Yanrong[3]

Abstract

A contact and consolidation injections are used for reinforcing the various engineering structures. The parent rock structure where the engineering constructions built is very important in determining the injection mixture type. Joints and fractures of host rock affect the amount of injection. The Hacınınoğlu Hydropower Plant Energy Tunnel (HHPT) was built to supply water from regulator to plant. The HHPT is 5586 m long (670 m part was taken into consideration in this study), 7.10 m wide, internal diameter of 6.0 m, and horseshoe-shaped concrete lined tunnel. The tunnel was excavated in the crystallized limestone of Taşdökümü Formation, calc schist and dolomites of the Dedeardıçgediği Formation. Horizontal and near horizontal discontinuities that evolved due to natural causes and excavation were identified at the crown of tunnel. Those discontinuities are most commonly seen in the calc schist unit, thus the maximum injection volume was observed in this unit. The lowest injection quantity was observed in massive limestones. If the rock mass classification and discontinuity characteristics of the host rocks of HHPT were well determined, and if injection mixture ratio was set according to those data; time wasting and cost increasing should be prevented. First stage injection planning without the consideration of discontinuities of host rock was unsuccessful. The complete injection was supplied, after the second stage application in HHPT. Cement/water ratio was increased; additional bentonite, freeze accelerator and sand were used during second stage.

Keywords / Contact grouting; *Consolidation Grouting, Hacınınoğlu Hydropower Plant Energy Tunnel, Tunnelling.*

1. INTRODUCTION

A dam construction works are accelerated in recent years to meet energy requirement for society development. Tunnel as an underground facility accompanying the dam must be sealed against water leakage, for example a water tight lining can be used, so that the hydraulic conductivity is reduced [1]. To prevent water leakage and to fulfil inflow requirements, cement based grouting has been used in both practical and economic reasons [2]-[1]. The contact and consolidation grouting injections are commonly used methods for this purpose. The grouting demonstrates full capacity for filling the fractures of host rock, gaps between the host rock and engineering structures, as well as the cracks within engineering structures [3]-[4]. Thus, the joint features (spacing, roughness, filling, and aperture) play an important role in determining quantity of grout injected. Normally, massive rocks should take less grout than denselyfractured and highly porous rocks. In addition, successful grouting application is required quick freeze in fractures. Mixing ratio (sand/cement/water) is determined depend on grouting absorption of ground. However, underground water cause to additional water to grouting injection mixing in well and in ground, which changes the original mixing ratio via increasing of water percentage. New watery slurry prevents complete freezing. Thus new mixing ratio must take into consideration.

This study aims to investigate geotechnical evaluation of the contact and consolidation grouting injection application in between km 0+358 and km 1+028 km of the Hacininoglu Hydropower Plant Energy Tunnel (HHPT). The HHPT was opened within the Dedeardıçgediği Formation (Upper Permian-Middle Triassic) and the Taşdökümü Formation (Permian) as shown in Figure 3. Limestone, marl and claystone of the Dedeardıçgediği Formation metamorphosed to crystallized limestone, dolomite and calcschist under the green schist metamorphism and the Taşdökümü Formation consists of blackish, dark grey, crystalline limestone, marble and partly dolomitize levels [5].

2. BACKGROUND

The studied tunnel is located between the Sarıgüzel Hydropower Plant (HP; This plant and HHPT built on the Ceyhan River in northwest of Kahramanmaras city centre(Figure 1, SE Turkey). The HHPT designed to deliver water from regulator to power plant, is a concrete plated horseshoe tunnel, 5586 m long and 7.10 m wide (internal diameter of 6.0 m). A pocket was opened at each 500 m along the tunnel alignment during the excavation for easily transportation of excavated materials to the outside. In order to increaseexcavation speed, bi-directional tunnel face excavations were employed where the topography permits. Concrete coating and grouting injection applicationsimmediately followed the tunnel excavation.

[1] Corresponding author/ Ahmet Ozbek, *Department of Geological Engineering, Kahramanmaraş Sutcu Imam University, Kahramanmaraş, Turkey.* E-mail/ ozbekaderen@gmail.com,ozbeka@ksu.edu.tr,

[2]Department of Geological Engineering, Mugla Sıtkı Kocman University, Mugla, Turkey
[3]The University of Hong Kong, Hong Kong, China

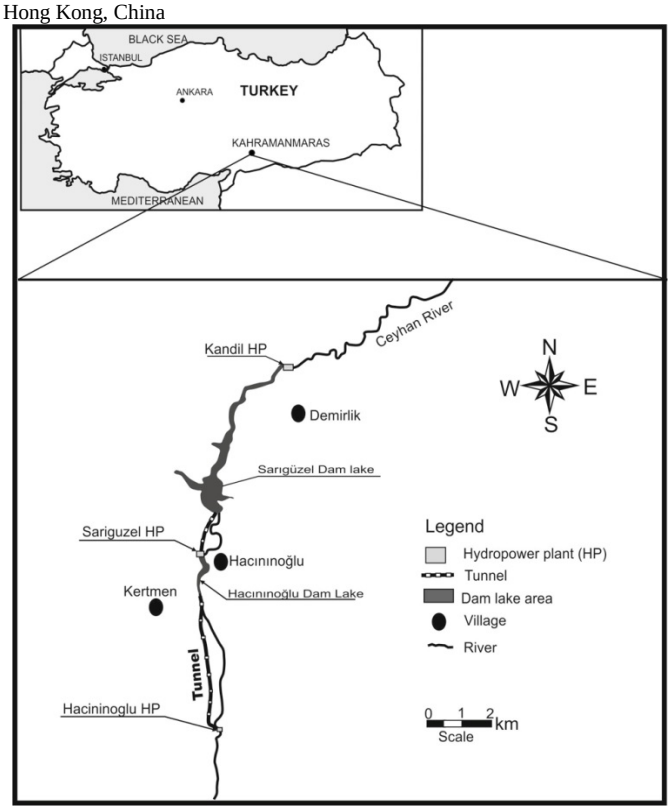

Figure 1. Location map of the study area.

The excavation sequence and support systems were selected in accordance with the Austrian Standard O-NORM B 2203 (1994) based on the concept of New Austrian Tunnelling Method (NATM) [6]. The HHPT was excavated within mainly crystallized limestone, calcschist and dolomite (Figure 2). The crystallized limestone between the km: 0+358-0+511, is massive, locally 5-50 cm thick bedded, slightly weathered, stable-moderate solid rock, closely spaced rough jointed and folded. Folding type is asymmetric recumbent folds inclined to south with low to moderate continuity (Figures 2). Foliated calcschist between km: 0+511-0+870 is highly weathered, thinly-bedded (<5 cm), moderately strong in the direction perpendicular to the foliation, weak-very weak in the direction parallel to the foliation. The foliation surfaces are closely spaced, slippery and have short to very short continuity (Figures 2). The dolomitic limestone in between km: 0+870-1+028 shows massive structure, durable in dry condition, easily distributed depend on water saturation (Figures 2).

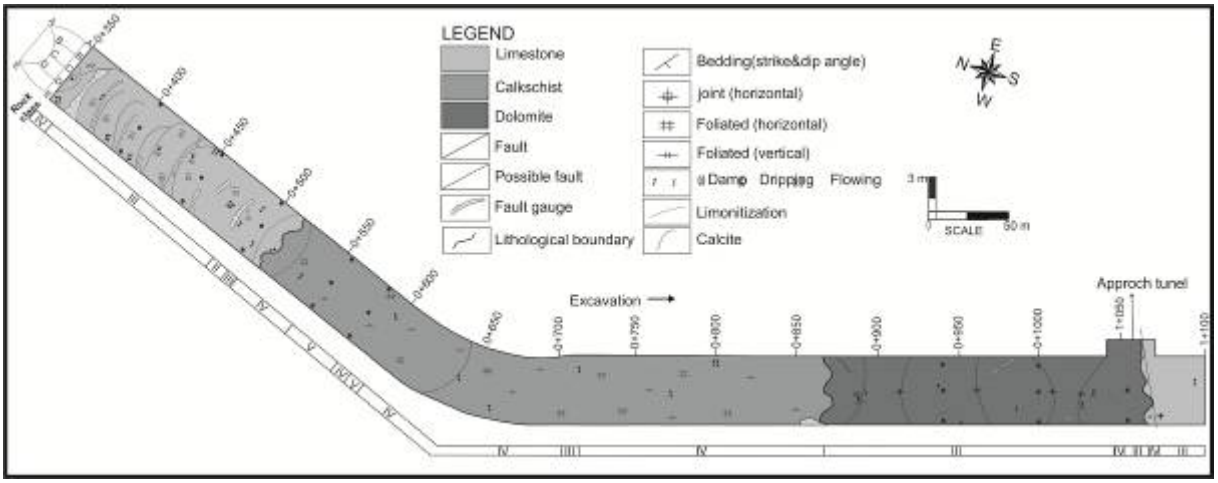

Figure 2. Geological propertiesalong longitudinal alignment ofthe Hacininoglu Hydropower Plant Energy Tunnel (HHPT).

3. GROUTING APPLICATIONS

Grouting for water control, could be described in general as a process of injecting fluids that set into cracks or voids of a rock mass. The most common fluid used for rock grouting is a mix of cement and water, which is injected at high pressure into the joint system by a pump [1]. The contact and consolidation grouting injection was applied to the HHPT between km: 0+358 - 1+028, at each 6 m between km 0+615 - 0+702 km, and at each 12.10 m in the rest of tunnel sections. The diameter of contact and consolidation grouting injection wells wereproposed by the consulting firm. The grouting projects were prepared by the tunnel engineer based on tunnel face maps, and RMR and Q classification system data obtained during the tunnel excavation. The contact grouting injection of the HHPT was applied as a staggered pattern according to shape of the energy tunnel as shown in Figure 3a. The consolidation injection was applied from eight different locations in accordance with shape of the tunnel (Figure 3b).

3.1. Contact Grouting

The contact grouting injection was applied immediately after the completion of invert concrete of HHPT. This injection is to fill the spaces between the concrete lining and host rocks so as to increase the stability and impermeability.

The contact grouting injection of the HHPT was applied as a staggered pattern according to shape of the energy tunnel as shown in Figure 3a. The 336 contact grouting wells (totally 252 m depth) were drilled. The wells extended 20 cm inside the host rock. Well 'A' was vertically inserted, while B and C were inclined at 45° at the crown. As shown in Figure 4 wells were located in staggered pattern at 3 m interval (A1, B1, C1, and A2, B2, C2).

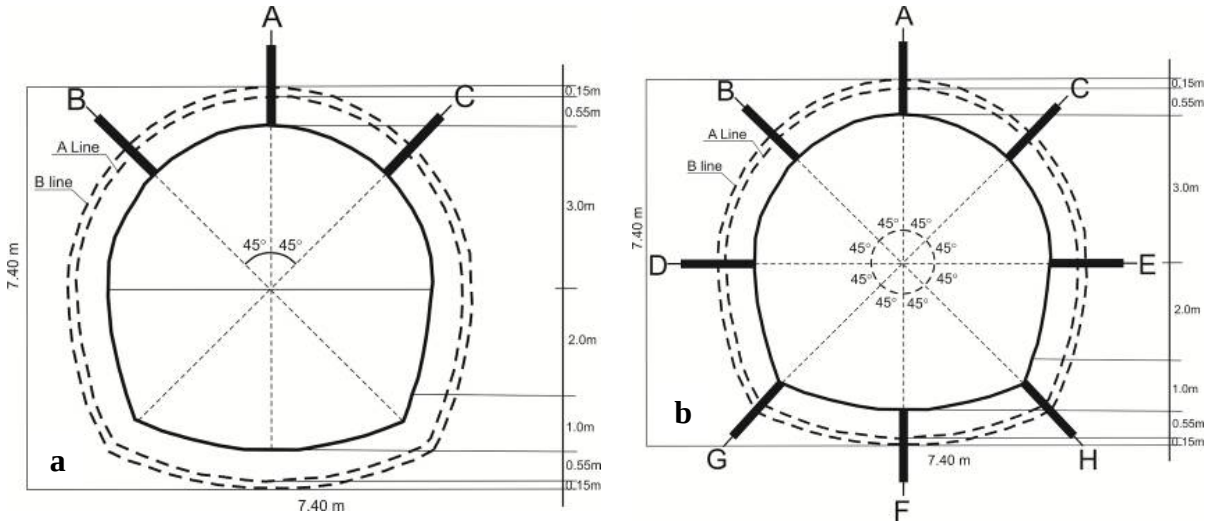

Figure 3. Pattern of contact (a) and consolidation (b) grouting in the Hacininoglu Hydropower Plant Energy Tunnel (HHPT).

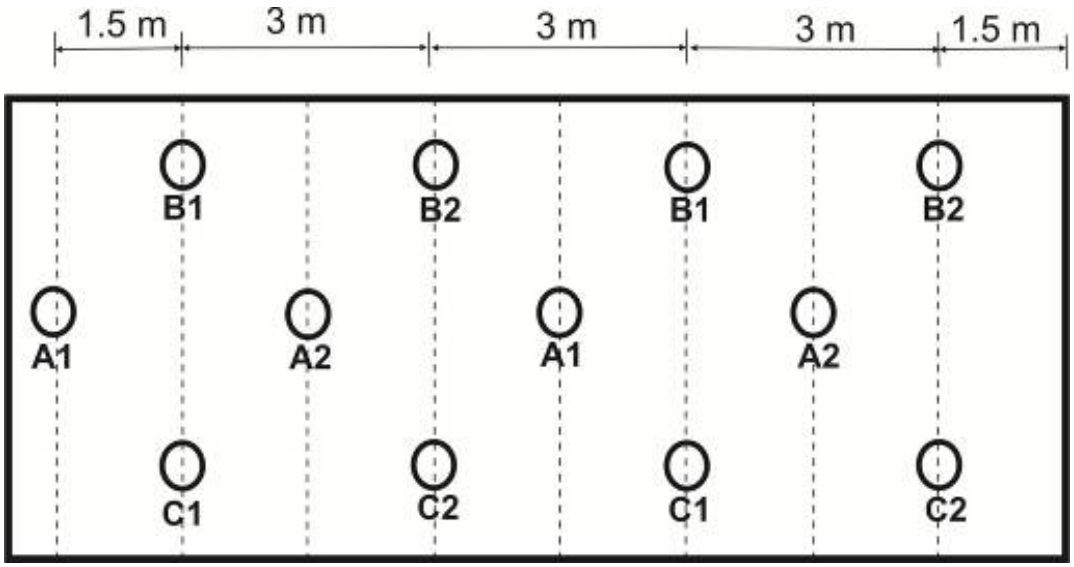

Figure 4. Drilling pattern of contact grouting wells in the Hacininoglu Hydropower Plant Energy Tunnel (HHPT).

The contact grouting injection started with unique mixture of cement-water-sand at the ratio of 1/1/1 [7]between km: 0+358 - 0+526. A mixer container (capacity of it 261 lt, with a 150 kg of cement, 145 kg of water, 150 kg of sand and 4.5 kg of bentonite) injected grout mixing to the hole with a pressure. The injection pressure was set as 3 kg/cm^2. The injection process continued until the well reach to REFU condition. When the desired pressure for REFU supplied in 10 minutes, stage grout was not injected, injection continued with the starting mixture. If the hole took a grout 0.3 l/min grouting or less during the 20 min, the well-considered to be reached to REFU state. The REFU term is a term express the grouting condition is supplied.

According to staggered pattern, the grouting wells of 'A, B and C' were drilled division by division. The injection valve stuck on hold as a close to hole cap. The grouting of side-wall wells (B and C rows) start at the beginning of the divisionto the end (Figure 4). The grouting injection applied to Well 'A' in the same way as Wells 'B and C'. After obtaining REFU in holes, valve at the end of the hose closed but not removed, injection devices left inside the hole. From time to time by opening the valve, grout coming was checked. If some grout is observed at the mouth of the well, grout injection kit hold on inside well until the freeze supplying.

Pressure tests were performed to evaluate the quality of contact grouting injection between km: 0+358 - 0+526 with the cement-water-sand mixture ratio of 1/1/1. In this section, six randomly selected wells were tested, grout injection quantity was found to be 0.3 Lugeon and it wasgreater than contact and consolidation injections instructions of the HHPT [8]. Subsequently, renewing of the contact injection on well with new mixing ratios was applied.

Initial cement-water-sand mixture (1/1/1 ratio respectively) filling gap between the tunnel and host rock had dense consistency. It was observed that this dense mixture caused plugging during the application that causes to increase the manometer level. Though grout injection was completed with required REFU, the high Lugeon values resulting from the following pressure tests indicated that this REFU was pseudo REFU.
The contact grouting injection ratio was initially planned as 1/1/1 mixture ratios. Consistency of mixture was dense due to high sand content. This consistent mixture caused an accretion at the mouth of well pipe. Thus, a manometer level of the injection pump was increasing. So, it is though that the REFU condition provided. However, it was determined that the accretion and plugging at the mouth of the well inhibited the grouting infilling the in between the tunnel and coating concrete (gap max. 5-7 cm).
The contact grouting injection was reapplied after observation of wells with the Lugeon values greater than 0.3 limit value during pressure test. Seventy eight (78) wells were opened and contact grouting injection was reapplied.

3.2. Consolidation Grouting

This type of grouting is applied for strengthen the basement where tunnel, galleries, shaft or any opened engineering structure; along the axis of tunnel; or used for filling the cracks and gaps to prevent hydrostatic pressure; and used to prevent differential settlements.

The consolidation grouting injections initiated at least 15 days after completion of the contact grouting applications in the HHPT. 896 well (3584 m) were drilled under comprise of the project. The consolidation injection was applied from eight different locations in length of 4.55 m including concrete in accordance with shape of the tunnel (Figure 3b). The holes are opened in staggered pattern, four injection sections with 3 m interval opened in 12.10 m long division. The sections were referred to "A1, D1, E1, F1", "B1, C1, G1, H1", and "A2, D2, E2, F2, B2, C2, G2, H2" respectively (Figure 5).

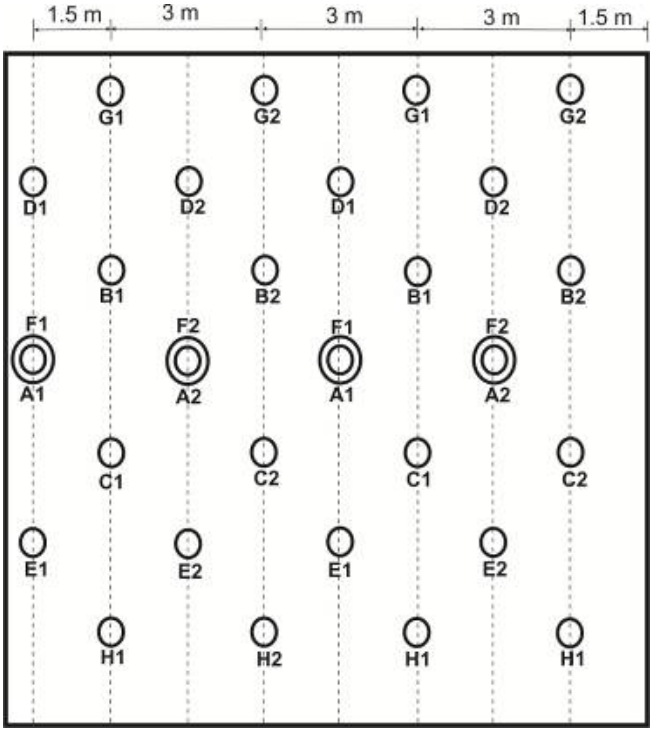

Figure 5. Drilling pattern for consolidation grouting in the Hacininoglu Hydropower Plant Energy Tunnel (HHPT).

The injection pressure was 3 kg /cm^2. The consolidation grouting injection was performed in single stage until the REFU condition supplied. It initiated with cement/water ration as 1/3 then increased 1/1 where it necessary in between km: 0+358 and 0+698, injection process was terminated after REFU requirements provided [7].

Pressure water test was performed to test whether or not success of the consolidation grouting injection in between km: 0+358 km and 0+698 km in randomly selected wells. The consolidation grouting application was evaluated as an unsuccessful according to consolidation injections instructions of the HHPT[8]. Thus, the consolidation grouting mixing ratio was revised.

The reason of failure of consolidation grouting was unfrozen grouting due to ratio of cement to water (initially 1/3, then 1/1). In addition, injection was conducted in winter season when the groundwater is in intense activity. It is thought that the application time also contributed to the failure.

The consolidation grouting applied to the new wells or reopened previous wells with new mixture ratios at the direction of administration in region where the wells with higher Lugeon value. The consolidation grouting injection started with 1000 lt injection with cement / water - 1/3 ratio by weight; then the grouting continued with an application of another 1000 lt with 2/3 ratio depend on regular injection absorption; after that the consolidation grouting injection followed with 1000 lt mixture with 1/1 ratio, 5000 lt with 7/5 mixture ratio, 5000 lt with 7/5 mixture ratio and 25 % sand, and 5000 lt with 7/5 mixture ratio and 50 % sand respectively. If the wells were refusing stage grouting and mixture in 10 minutes, whether the desired pressure was obtained, even in cement grout or mixtures (cement/water plus sand), the grouting application was found as unsuccessful. Thus the grouting started with the initial mixture ratio (1/3) that was applied twenty minutes. If the well absorbed a 0.4 lt / m / min or less grouting in twenty minutes, it was assumed that the well reached to REFU condition. The Calcium C($CaCl_2$), whose weight 3 % of cement, was used as additives in sandy mixtures. The consolidation grouting initiated with the cement / water ratio as 1/3, continued with 7/5 + freeze accelerator (sika ground) and sandy mixture (ratio presented in Table 7). As a result of this second stage of grouting application, the injection was successfully completed. This new mixing ratio was applied to the wells in between km 0+698 and 1+028. The value of pressure water test results in this area was under 0.5 Lugeon, so the injection process was considered as a successful, and consolidation injection terminated hloride.

4. CONCLUSIONS AND RECOMMENDATIONS

The consolidation and contact grouting injections between km: 0+358 - 1+028 of HHPT were evaluated in this study.

Injected contact and consolidation grouting quantity and tunnel host rock properties are presented in Figures 6 and 7. Accordingly, limestone of the Taşdökümü Formation was found in between the K-1 and K-3 (km: 0+358 - 0+514). The calcschist of Dedeardıçgediği Formation was in between the K-14 and K-51(km: 0+515 - 0+871); and dolomites of this formation in between the K-52 and K-64 (km: 0+872 - 1+028).

Maximum contact grouting injected to the calcschist of Dedeardıçgediği Formation (Figure 6). The main reason of it, undesired horizontal and subhorizontal discontinuities inclined through the HHPT observed in this formation. The least contact grouting injected to the limestone of Taşdökümü Formation, which is rigid and more durable during tunnel excavation (Figure 6).

The maximum consolidation grouting injection (applied to ensure the stability of concrete and surrounding rock; applied to regions with poor rock conditions and problems of seepage) was observed in limestone of the Taşdökümü Formation (Figure 7). The reason of it, this limestone densely fractured and cracked than other units. In addition, fractures are generally open; their continuities are short to medium. Fractures spacing's are narrow to very narrow than other units.

The calcschist of Dedeardıçgediği Formation are formed by weathered schist structure, fractures of it more closed and clay filled, the dolomite level of this formation is in massive structure and contains less cracks. So, consolidation injection was in less quantity (Figure 7).

The dense consistency of grouting caused an accretion and plugging at the mouth of injection well during the contact grouting. So that the grouting application was ended before the grouting reaching to spaces in between the tunnel host rock and coating concrete, which cause to the pseudo REFU condition. By this way, it was found that the injection was not successful as a result of the pressurized water injection tests. Then, the injection was completed with new mixing ratio.
The grouting application during winter season prevented to reach the REFU requirements in some consolidation well. The groundwater level had an intense activity during this season. Depend on this activity, the grouting injection was not supplied the freeze condition due to washing by groundwater and additional water content. It was observed that the cracks of grouted ground reopened, so the grouting injection was become unsuccessful. The second reason for the failure of REFU condition is sourced from the geological and structural properties of host rocks, such as the fracture, stratification, closed-filled fractures, and laminations. As a result of the water pressure tests, the wells have a higher Lugeon values were reopened or new wells were drilled, revised mixing grouting ratio was applied to those well based on the directions of administration.
According to the results of this work, it can be concluded that the amount of contact and consolidation grouting in tunnel and engineering structures are depending on geological and structural features of the host rock. Without taking into account the geological and structural characteristics, applications of the contact and consolidation grouting injection may fail. At that time, the injection with revised mixture ratio must be applied for successful grouting application. Take into consideration of the geological and structural features during the grouting injection will minimize the loss of cost and time.

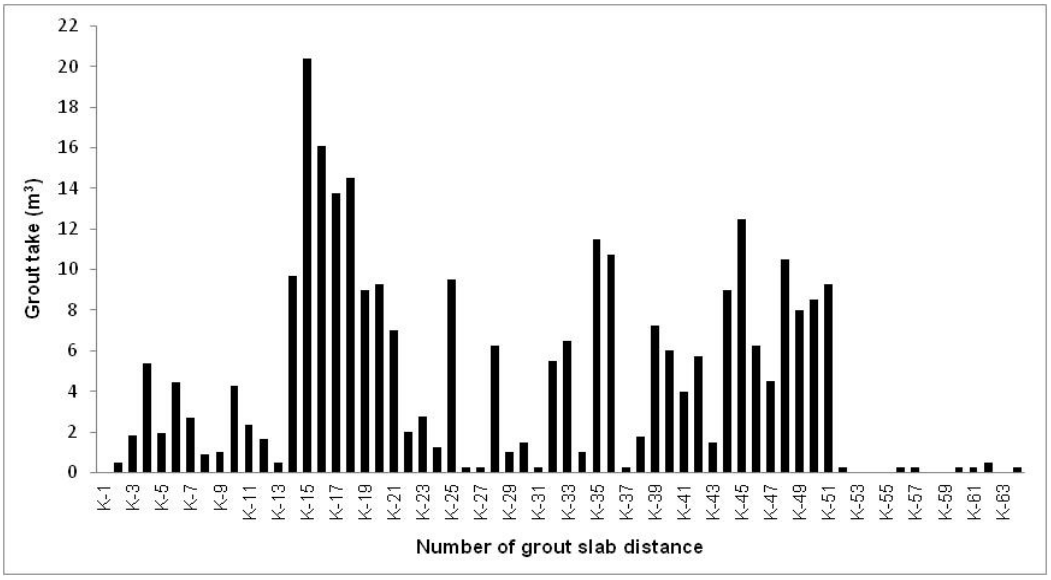

Figure 6. The quantity of contact grouting along the HHPT alignment.

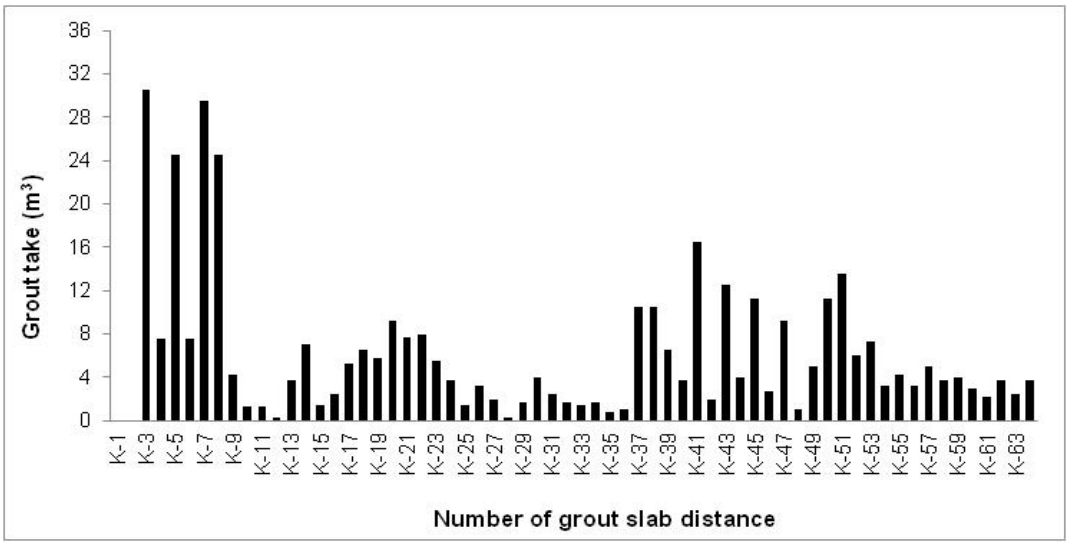

Figure 7. The quantity of consolidation grouting along the HHPT alignment

REFERENCES

[1] Dalmalm, T., (2004) Choice of Grouting Method for Jointed Hard Rock based on Sealing Time Predictions. Division of Soil and Rock Mechanics Department of Civil and Architectural Engineering Royal Institute of Technology, Stockholm, 250pp.

[2] Ewert, F.K., 1997. Permeability, Groutability and Grouting of rock related to Dam sites – Part 3 Hydrogeological Regime around Dams and Reservoirs, 8 (3). 215–248

[3] Fransson, A˚., 2001. Characterization of a fractured rock mass for agrouting field test. Tunnelling and Underground Space Technology. 16, 331–339.

[4] Yesilnacar, M.I., 2002. Grouting applications in the Sanliurfa tunnels of GAP, Turkey, Tunnelling and Underground Space Technology, 18 (4), 321-330.

[5] Baydar, O., Yergök, A.F., 1996. Geology of Southeastern Anatolia – Fold Thrust Belt – Amanos Mountains – Eastern Taurides. Department of Geological Survey of Mineral Research Institute of Turkey (MTA), Ankara, 90pp (in Turkish).

[6] Rabcewicz, L., 1964. The New Austrian Tunneling method. Water Power, 453–457.

[7] EN-SU Engineering Consulting Ltd. Co. 2009. Hacininoglu Regulator and HEPP Project (unpublished report, in Turkish).

[8] Hidrodizayn, 2009. Contact and Consolidation Grouting Application Instructions of the Hacininoglu Regulator and Hydroelectric Power Plant Tunnel (unpublished, in Turkish).

ICENS
INTERNATIONAL CONFERENCE ON ENGINEERING AND NATURAL SCIENCES
24-28 May 2016 /Sarajevo

PSIM Simulation of Flyback Converter for P&O and IC MPPT Algorithms

Harun Ozbay[1], Akif Karafil[1], Selim Oncu[2], Metin Kesler[3]*

Abstract

The output power of PV panels varies continuously depending on some environmental factors such as temperature, shading and solar radiation level and load conditions. PV panels have a nonlinear characteristic since they have different output power at different operating points. Therefore, dc-dc converters are required between PV panels and load to obtain the maximum power from the panels. In this study, the simulation of the flyback converter for two most commonly used MPPT algorithms specifically Perturb and Observe (P&O) method and Incremental Conductance (IC) method are achieved in PSIM and performance of the control techniques are compared. The simulation results of P&O and IC MPPT algorithms are compared for different solar radiation conditions.

Keywords: *Flyback, Maximum power point tracking (MPPT), Perturb and Observe (P&O), Incremental Conductance (IC), PSIM*

1. INTRODUCTION

Electric energy demand has been increasing recently due to the increasing population and industrialization. However, a great part of the electric energy has been met by fossil fuels such as oil and coal. Renewable energy sources have gained importance since the fossil fuels give harm to the environment and they will be exhausted in the near future. Among the renewable energy sources solar energy has been more attractive since it is clean, free and infinite [1, 2]. Among the renewable energy sources, the solar energy has gained popularity for energy demand recently and has been prompted. Therefore, the costs have reduced and studies in this field have increased. Although generating energy using PV panels has many advantageous, the efficiency of the panels is low depending on some environmental factors such as temperature, radiation level, shading, and dirt. Therefore, it becomes important to extract maximum power from PV panels by MPPT dc-dc converter [3].

In literature, many MPPT techniques are used to determine the maximum power point (MPP). Some of these MPPT techniques are fractional open circuit voltage, fractional short circuit current, perturb and observe, incremental conductance, lookup table method, neural network and fuzzy logic controller. Fractional open circuit voltage and short circuit current methods adopt approximation methods. However, these methods give low accuracy at MPP. On the other hand, a large database is needed for some MPPT techniques such as lookup table method, neural network and fuzzy logic. However, this increases the implementation complexity of the system. P&O and IC techniques are among the most used MPPT techniques. These methods are simple, high efficient, panel independent and provide high accuracy at MPP [4, 5].

In literature, some flyback converter applications with P&O MPPT method [6, 7], artificial neural network (ANN) P&O MPPT method [8] and IC MPPT method [9] have been studied. In the study, two most common used MPPT algorithms specifically P&O and IC methods are compared for flyback converter in PSIM.

2. FLYBACK CONVERTER

Figure 1 shows the PSIM simulation schematic of the flyback converter. The circuit consists of a power switch (S_1), transformer (1:n), magnetizing inductor of the transformer (L_m), rectifying circuit (D), output filter capacitor (C) and load resistance (R_o) [10]. PV panel (Perlight PLM-100P/12) with 100 W maximum power is modeled at PSIM for the simulated flyback converter. Six PV panels are connected in series and total 600 W power is obtained. The standard test conditions for the PV panel are as follows: 17.7 V maximum voltage and 5.65 A maximum current. The flyback converter parameters: L_m 0.3 mH, C 10 µF, R_o 400 Ω and transformer turns ratio 1:4. The switching frequency is determined as 50 kHz.

[1] *Bilecik Seyh Edebali University, Department of Electric, Vocational High School, 11210, Bilecik, Turkey.*

[*2] *Corresponding author: Karabuk University, Department of Electrical & Electronics Engineering, Engineering Faculty, 78050, Karabuk, Turkey, soncu@karabuk.edu.tr*

[3] *Bilecik Seyh Edebali University, Department of Computer Engineering, Engineering Faculty, 11210, Bilecik, Turkey.*

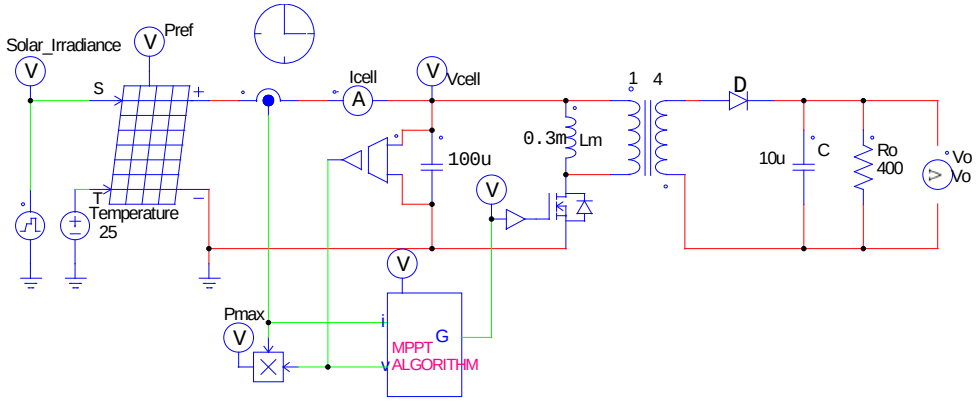

Figure 10. PSIM simulation schematic of the flyback converter

3. MPPT ALGORITHM METHODS

Load resistance must be equal to the optimal resistance in order to track the maximum power point. However, it is difficult to determine a fixed load corresponding this value. Therefore, a dc-dc converter is connected between PV panel and load to transfer maximum power from PV panel. The system is called as maximum power point tracking [11].

In literature, many MPPT techniques are used to determine maximum power point (MPP). P&O and IC methods are the most widely used MPPT techniques due to simplicity and low cost. However, in all MPPT techniques MPP is determined by changing the duty ratio (D) of the dc-dc converter [12].

3.1. P&O Method

P&O method is one of the most frequently used MPPT methods due to its simplicity, practicality and high efficiency. Moreover, the most important advantage of the method is that it is independent from some factors such as PV characteristic, temperature and radiation level in achieving MPP [13]. In P&O method, PV panel power is measured and compared with the previous one. If the power increases, perturbation direction is not changed. Otherwise, perturbation direction is reversed. Therefore, the operating point of the system moves towards MPP and oscillates around MPP under steady state conditions [14]. P&O simulation block diagram is shown in Figure 2.

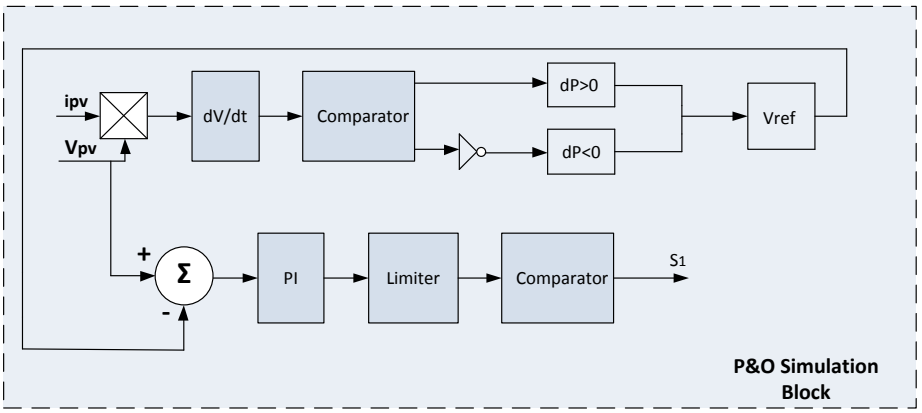

Figure 11. P&O simulation block

3.2. IC Method

Instantaneous voltage is adjusted according to MPP voltage in incremental conductance (IC) method. MPP voltage is dependent on incremental and instantaneous voltage of the PV panel. The principle of the method is that voltage-power characteristic curve of the PV panel is zero at MPP (dP/dV=0), greater than zero on the left of MPP (dP/dV>0), and smaller than zero on the right of MPP (dP/dV<0). Voltage-power characteristic showing the operating principle of IC method is given in Figure 3.

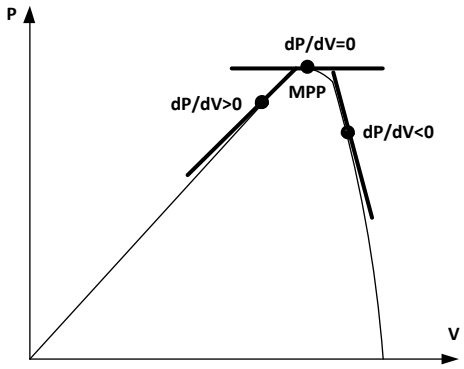

Figure 12. The operating curve of IC method

IC simulation block diagram is shown in Figure 4. The voltage and current values are used in IC block as input. The changes in voltage are converted into absolute value and the values are feedback to the positive input terminal of the comparator. If dV is not equal to zero, logic 1 will be the output. Otherwise, logic 0 will be the output. Therefore, it is determined whether dI is greater or lower than zero. In the third comparator it is determined whether dI/dV>-I/V or dI/dV<-I/V or not. Input logic combination activates Vn+K or Vn-K. So, the desired switching is provided by adding K to Vn or subtracting K from Vn [15, 16].

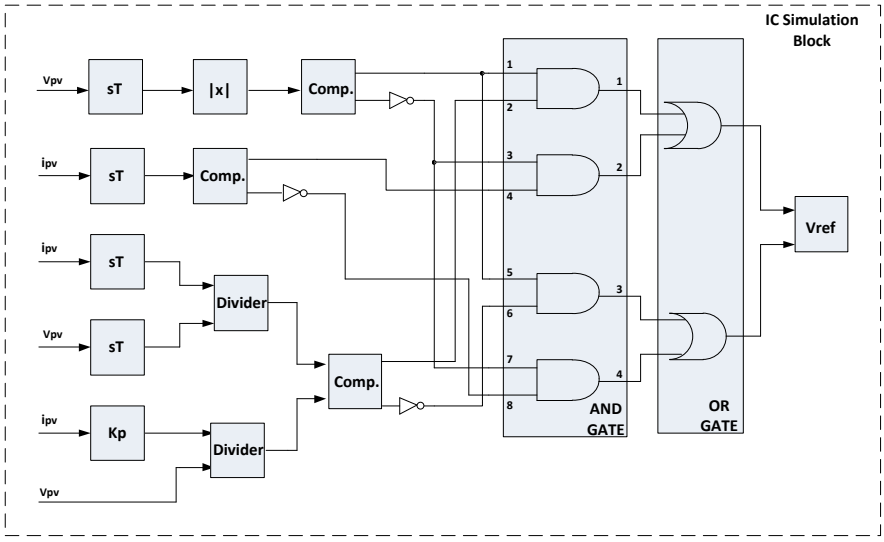

Figure 13. IC simulation block

4. SIMULATION RESULTS AND DISCUSSIONS

In the simulation, ramp and step inputs are applied to the input of solar radiation terminals to provide rapidly changing and slowly changing climate conditions. The simulation total time is 1 s. Solar radiation level is changed from 600 W/m^2 to 1000 W/m^2. The temperature terminal input remains constant at 25 °C in the simulation. Rapidly and slowly changing climate conditions are shown in Figure 5.

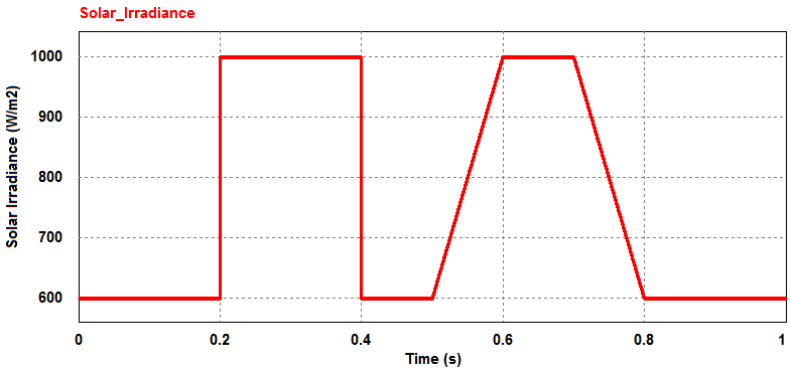

Figure 14. Rapidly and slowly changing radiation

The same standard environmental conditions are applied to compare the performance of P&O and IC MPPT algorithms. In Figure 6, P&O and IC MPPT algorithms tracking the maximum power point of PV panels are shown.

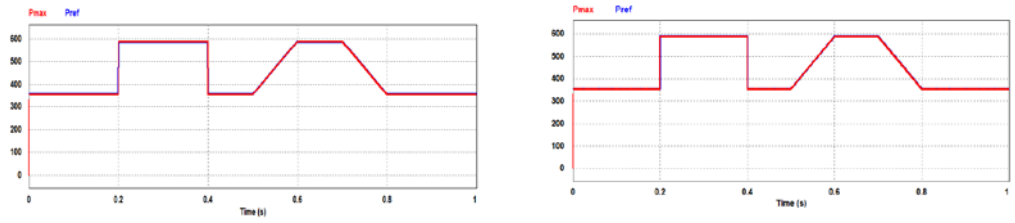

Figure 15. *(a) P&O MPPT algorithm* *(b) IC MPPT algorithm*

Figure 7 and 8 show the rapidly changing radiation effect on P&O and IC MPPT performance, respectively.

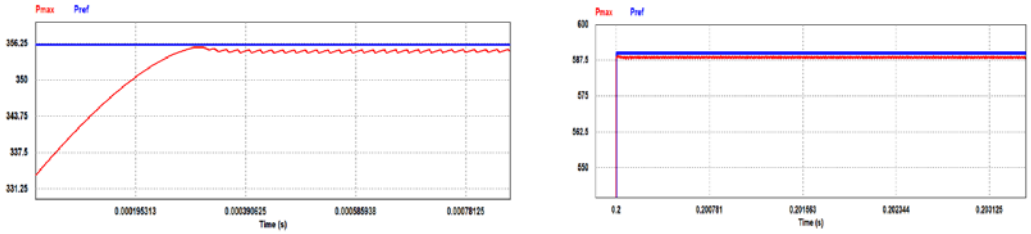

Figure 16. Zoomed window of P&O MPPT oscillations

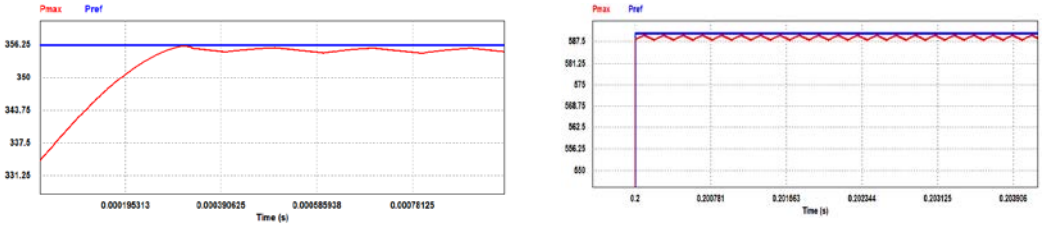

Figure 17. Zoomed window of IC MPPT oscillations

It can be concluded from the zoomed window Figure 7. showing the rapidly changing radiation that P&O oscillates around MPP resulting in some power losses. On the contrary, no such oscillations occur in IC algorithm. Moreover, P&O algorithm cannot find the new MPP quickly when radiation level changes rapidly. This is the main drawback of the P&O algorithm. IC algorithm finds the new MPP more accurately under rapidly changing radiation level. However, P&O MPPT is most commonly used due to its simplicity.

5. CONCLUSION

This paper presents the comparison of P&O and IC MPPT algorithms using PSIM simulation of the flyback converter under rapidly and slowly changing solar conditions by using PSIM. No significant differences are observed for P&O and IC MPPT algorithms when the climate changes slowly. However, IC algorithm finds the MPP quickly under rapidly changing climate conditions. Moreover, no additional oscillation occurs around MPP in IC algorithm. Therefore, it can be concluded that IC algorithm gives better results under rapidly changing climate conditions.

ACKNOWLEDGMENT

This research was supported by TUBITAK Research Fund (No: 115E104). The authors would like to thank for support.

REFERENCES

[1] M. Obi and R. Bass, "Trends and challenges of grid-connected photovoltaic systems–A review," *Renewable and Sustainable Energy Reviews*, vol. 58, pp. 1082-109, 2016.

[2]T. K. Soon and S. Mekhilef, "A fast-converging MPPT technique for photovoltaic system under fast-varying solar irradiation and load resistance," *Industrial Informatics, IEEE Transactions on*, vol. 11, no. 1, pp. 176-186, Feb. 2015.

[3] H. T. Duru, "A maximum power tracking algorithm based on I mpp= f (P max) function for matching passive and active loads to a photovoltaic generator." *Solar Energy*, vol. 80, no. 7, pp. 812-822, 2006.

[4] H. Bounechba, A. Bouzid, H. Snani, and A. Lashab, "Real time simulation of MPPT algorithms for PV energy system," *International Journal of Electrical Power & Energy Systems*, vol. 83, pp. 67-78, 2016.

[5] Q. Zhang, C. Hu, L. Chen, A. Amirahmadi, N. Kutkut, Z. J. Shen, and I. Batarseh, "A center point iteration MPPT method with application on the frequency-modulated LLC microinverter," *Power Electronics, IEEE Transactions on*, vol. 29, no. 3, pp. 1262-1274, 2014.

[6] Mohammad B. Shadmand, Robert S. Balog, and Haitham Abu Rub, "Maximum Power Point Tracking using Model Predictive Control of a flyback converter for photovoltaic applications." *Power and Energy Conference at Illinois (PECI)*, 2014. IEEE, 2014, pp. 1-5.

[7] Y. H. Kim, J. G. Kim, Y. H. Ji, C. Y. Won, and T. W. Lee, "Flyback inverter using voltage sensorless MPPT for AC module systems," *In Power Electronics Conference (IPEC), 2010 International IEEE*, 2010, pp. 948-953.

[8] P. Konghuayrob and S. Kaitwanidvilai, "Maximum Power Point tracking using neural network in flyback MPPT inverter for PV systems," *In Soft Computing and Intelligent Systems (SCIS) and 13th International Symposium on Advanced Intelligent Systems (ISIS), 2012 Joint 6th International Conference on IEEE*, 2012, pp. 1504-1507.

[9] J. Beopjun, N. Hyunjun, C. Yeonok, M. Euna, and C. GeumBae, "IncCond MPPT control using flyback converter," *In Electrical Machines and Systems (ICEMS), 2013 International Conference on* IEEE, 2013, pp. 357-361.

[10] Z. Housheng, "Research on MPPT for Solar Cells Based on Flyback Converter," *In Intelligent Computation Technology and Automation (ICICTA), 2010 International Conference onIEEE*, vol. 3, pp. 36-39, May. 2010.

[11] H. Rezk and A. M. Eltamaly, "A comprehensive comparison of different MPPT techniques for photovoltaic systems," *Solar Energy*, vol. 112, pp. 1-11, 2015.

[12] D. Ouoba, A. Fakkar, Y. El Kouari, F. Dkhichi, and B. Oukarfi, (2016). "An improved maximum power point tracking method for a photovoltaic system," Optical Materials, vol. 56, pp. 100-106, 2016.

[13] T. Esram and P. L. Chapman, "Comparison of photovoltaic array maximum power point tracking techniques," *IEEE Transactions on Energy Conversion EC*, vol. 22, no. 2, pp. 439, 2007.

[14] B. Subudhi and R. Pradhan, "A comparative study on maximum power point tracking techniques for photovoltaic power systems," *Sustainable Energy, IEEE transactions on*, vol. 4, no. 1, pp. 89-98, 2013.

[15] N. I. Natasha, W. T. Bhuiyan, and M. A. Razzak, "Implementation of Maximum Power Point Tracking in a photovoltaic inverter using Incremental Conductance technique," *In Electrical and Computer Engineering (ICECE), 2014 International Conference on IEEE*, pp. 329-332, Dec. 2014.

[16] H. Zheng, S. Li, K. Bao, and D. Zhang, (2012, May). "Comparative study of maximum power point tracking control strategies for solar PV systems," *In Transmission and Distribution Conference and Exposition (T&D), 2012 IEEE PES IEEE*,pp. 1-8, May. 2012.

Equilibrium and Kinetics Study of Bisphenol-A Adsorption by Bentonite Clay from Aqueous Solutions

Mehtap Tanyol[1]

Abstract

This work investigates the adsorption behavior of bisphenol-A from aqueous solution onto bentonite under various experimental conditions. The influence of the variables including pH, concentration of bisphenol-A and contact time was studied by batch method. The maximum sorption capacity was estimated as 0.94 mg/g at pH 9. The equilibrium data was evaluated using the Langmuir and Freundlich isotherm. The Langmuir model best describes the uptake of bisphenol-A, which implies that the adsorption of bisphenol-A on bentonite is homogeneous. The kinetic data were analyzed using Lagergren pseudo-first order and pseudo-second order equations. The pseudo-second order exhibited the best fit for kinetic studies, which indicates that adsorption of bisphenol-A was limited by chemisorption process.

Keywords: *Bisphenol-A, bentonite, isotherm, kinetic.*

1. INTRODUCTION

Bisphenol-A, polymer plastics, polycarbonates, which are classified as a type of endocrine disrupting chemicals (EDCs), are widely used as a monomer in the production of epoxy resins and other plastics [1]. As a result, bisphenol-A was determined in various environmental waters, with a level of 59.8 ng/L in drinking water, 17.2 mg/L in hazardous waste landfill, and up to 12 mg/L in rivers [2]. However, even at low concentrations (ng/L), bisphenol-A could cause endocrine disruption and due to its low biodegradability and high resistance to chemical degradation it could possess toxicological risks for animals and human [3]. In addition, bisphenol-A was reported to cause metabolic disorders such as diabetes and obesity in humans, to increase risk of miscarriage and cardiovascular diseases, and also as carcinogenic [4]. Hence, effective methods are required to be developed in order to remove bisphenol-A from the aquatic environment.

There are various methods to remove bisphenol-A from water and wastewater, such as adsorption, advanced oxidation processes, membrane processes and ozonization. On the other hand, some of these methods has been reported to produce harmful byproducts. Adsorption process is a quick and effective method for the removal of organic contaminants and this method is also noteworthy for not causing production of harmful by-products [5]. Various adsorbents such as agricultural waste [6], carbon nanotubes [7], zeolite [8], activated carbon [2], lignin [9], hydrogel beads[10], montmorillonite [11] and clay [12] were used to investigate the efficacy of adsorption process on removal of bisphenol-A. Among these, clay minerals exhibit a good potential in elimination of pollution from water and wastewater, due to its considerably high specific surface area, chemical and mechanical stability, high cation exchange capacity, and the negative characteristics of its surface [13].

The aim of this study is to evaluate the adsorption performance of natural bentonite clay used as adsorbent for the removal of bisphenol-A from the aqueous solutions.

2. MATERIALS AND METHODS

2.1. Bisphenol-A characteristics

The physicochemical characteristics of bisphenol-A are summarized in Table 1. Bisphenol-A is a hydrophobic compound with extremely low solubility in water and its high octanol-water partition coefficient allows bisphenol-A to be adsorbed easily in particles and adsorbents.

[1] *Corresponding author: Tunceli University, Department of Environmental Engineering, 62000, Tunceli, Turkey . mtanyol@tunceli.edu.tr*

Table 1. Physicochemical characteristics of bisphenol-A [14].

Paremeter	Value
Chemical name	2,2-(4,4-dihydroxydiphenyl) propane
Molecular formula (g/mol)	$C_{15}H_{16}O_2$
Molecular size (nm)	Molecular width *X*:0.383;
	Molecular width *Y*:0.587;
	Molecular width *Z*:1.068
Acid dissociation constant (pK_a)	9.6-10.2
Octanol/water partition coefficient (log*D*)	pH 1-8: 3.43; pH 10: 3.03
Dipole moment (Debye, D)	0.709
Henry's law coefficient (atm m^3/mol)	1.00E-11
Solubility in water (mg/L)	129

Bisphenol-A is uncharged within a wide pH range in most natural waters and wastewaters due to its extremely high pK_a value. This could be observed from the structure of bisphenol-A (Figure 1). In addition, physicochemical characteristics of bisphenol-A affect adsorption. Other parameters such as dipole moments and solubility might as well affect the adsorption [14].

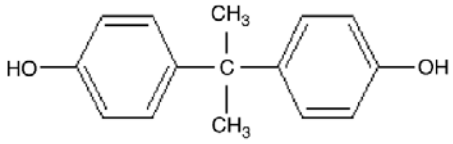

Figure 1. Chemical structure of bisphenol-A.

2.2. Adsorption experiments

In this study, bentonite samples used adsorbent as were supplied from Tokat (a province in Turkey) and were dried at 100 ° C to be used in adsorption experiments. 1 g/L stock solution of bisphenol-A was prepared in methanol by dissolving. Bisphenol-A solutions with certain concentrations (1-25 mg/L) used during the experiments were prepared by making necessary dilutions from the stock solution. The pH of the media was adjusted to the desired values through using diluted HCl and NaOH.

Batch order adsorption experiments were conducted in 250 mL erlenmayer flasks, by adding 1 g bentonite to 100 mL bisphenol-A solutions with different initial bisphenol-A concentrations, shaken at 250 rpm, at 25 °C. Samples of 5 mL were extracted from the solution at predetermined intervals during the mixing, in order to determine the concentration of bisphenol-A left in the media. Before the analysis, the samples were passed through a 0.45 µm filter membrane and the liquid part was analyzed for the remaining amount of bisphenol-A.

2.3. Analytical procedure

The resultant bisphenol-A solution was detected by using HPLC instrument (Shimadzu Prominence LC-20A) equipped with Kromasil C-18 (4.6 mm×150 mm, 5 µm) and a diode array detector (DAD). The selected detection wavelength was 226 nm. Mobile phase composition was acetonitrile/water (50:50, v:v) at a flow ratio of 1 mL/min. The column temperature was 35 ºC and the injection volume was 10 µL. The standard curve for bisphenol-A is linearly best fitted (R^2 = 0.99) with the concentration of bisphenol-A varied from 1.0 to 25 mg/L.

2.4. Adsorption isotherms

The amount of adsorbed substance in equilibrium or the adsorption capacity is generally expressed by adsorption isotherms. In this study, adsorption equilibrium was analyzed by using Langmuir and Freundlich isotherm models. Langmuir and Freundlich equations are as follows, respectively:

$$q_{eq} = \frac{q_m b C_{eq}}{1 + bC_{eq}} \quad (1)$$

$$q_{eq} = K_f C_{eq}^{\frac{1}{n}} \quad (2)$$

where q_{eq} is the adsorbed bisphenol-A amount at the time of equilibrium (mg/g), C_{eq} is the equilibrium concentration of the bisphenol-A in the solution (mg/L), q_m is the maximum adsorption capacity (mg/g) and b is the adsorption equilibrium constant related to the adsorption energy (L/g), K_f is the relative adsorption capacity and n is a constant dependent on the adsorption density.

2.5. Adsorption kinetics

Pseudo-first order and pseudo-second order kinetic models were used in order to understand the adsorption kinetics. The linear forms of pseudo-first order and pseudo-second order kinetic models could be expressed as follows, respectively:

$$log(q_{eq} - q_t) = logq_{eq} - \frac{k_1}{2.303}t \qquad (3)$$

$$\frac{t}{q_t} = \frac{1}{k_2 q_{eq}^2} + \frac{1}{q_{eq}}t \qquad (4)$$

Where q_t is the adsorbed bisphenol-A amount per gram adsorbent in any given time (mg/g), k_1 (1/min) and k_2 (g/mg/min) is the rate constant for pseudo-first order sorption and pseudo-second order sorption, respectively.

3. RESULTS AND DISCUSSION

Figure 2 presents the effect of contact time on the bisphenol-A adsorption on bentonite. In the beginning, the adsorption capacity increased rapidly due to increase of contact time, and then increased gradually until equilibrium. The time required to reach equilibrium is 20 minutes. Reaching equilibrium in a short period time in adsorption process is important in real-scale applications.

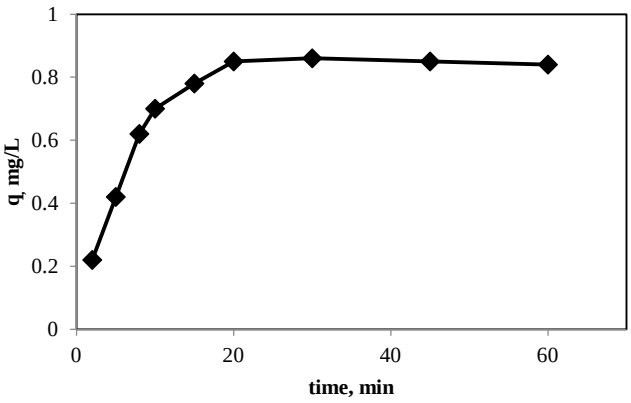

Figure 1. Time dependent change of adsorbed amount in bentonite bisphenol-A adsorption(Adsorption conditions: dosage = 1 g/100 mL, initial concentration =25 mg/L, temperature=25 ºC, pH=9, and agitation rate = 250 rpm).

The effect of initial pH on adsorption capacity of bisphenol-A could be seen in Figure 3. Adsorption capacity indicated an upward trend between pH 3 to 9, yet demonstrated a reduction trend in the range of pH 9 to 11. Once the pH of the solution is acidic, the surface of the adsorbate and adsorbent becomes positively charged and the adsorption capacity approximately remains constant. Similarly, solution has alkaline pH values, especially when the pH of the solution is higher than the pK_a value of the adsorbate (pK_a value of bisphenol-A 9.6-10.2), the charge of the adsorbate and the adsorbent surface becomes negative and adsorption capacity decreases [15]. These results are similar to Bautista-Toledo et al. [16] and to the results obtained in previous studies [17].

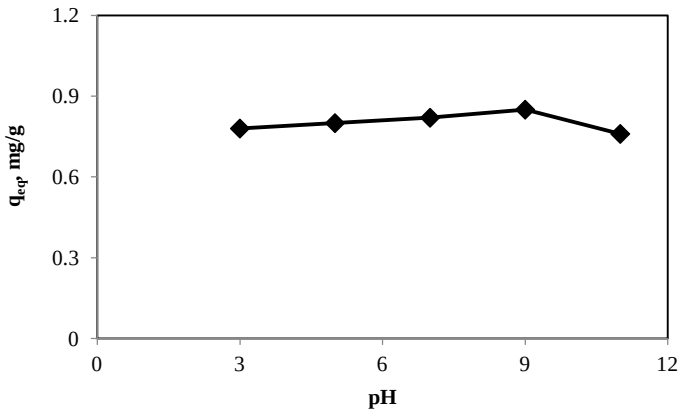

Figure 2. Effect of pH on bisphenol-A adsorption (Adsorption conditions: dosage = 1 g/100 mL, initial concentration =25 mg/L, temperature=25 ºC, and agitation rate = 250 rpm).

In modeling the adsorption data, surface characteristics of sorbents, adsorption mechanism and capacity or adsorption model constants values indicating anfinity were calculated using Langmuir and Freundlich isotherms (Table 2). Although, correlation coefficients of both isotherm models were high, adsorption data were found to provide a better fit with Langmuir model (R^2= 0,99). K_f value, which is the Freundlich isotherm constant and represents the adsorption capacity, was determined as 5.80 and n value, which represents the adsorption force, was found to be 4.13. Experimental value of n being greater than 1 indicates that bisphenol-A binds to bentonite by adsorption. q_m in the Langmuir equation is 0.94 mg/g and b is 0.28 L/mg. Greater value of the Langmuir isotherm constant q_m (0.94 mg/g) than the q_{eq} value (0.85 mg/g) demonstrates that bisphenol-A bind to the bentonite as a single layer.

Table 2. Isotherm coefficients for bispnenol-A adsorbed onto bentonite [a]

Langmuir model			Freundlich model		
q_m	b	R^2	K_f	n	R^2
0.94	0.28	0.997	5.80	4.13	0.956

[a] Adsorption conditions: initial concentration = 1-25 mg/L, adsorbent dosage = 1g/100 mL, agitation rate = 250 rpm, and pH 7.0.

Mathematical models that define the batch sorption process conducted under different experimental conditions are highly useful for process optimization or large-scale studies. In this study, pseudo-first order and pseudo-second order kinetic models were used in order to determine the mechanisms that control the process of adsorption. The k_1, k_2, q_{eq} values and correlation coefficients of these models are compared in Table 4. Although both models yielded high correlation coefficients, the correlation coefficients for the second order kinetic model were higher. Furthermore, theoretical q_{eq} values and experimental q_{eq} values provided a better fit with second order kinetics. Accordingly, sorption process could be defined by pseudo- second order kinetics. Pseudo-second order kinetic model is mainly based on the idea that process mechanism is controlled by chemical bonding or chemisorption in of adsorption processes. This means that adsorption of bisphenol-A on bentonite includes the valence force due to electron exchange or sharing between the adsorbate and absorbent [18].

Table 4. Pseudo-first and second order reaction rate constants for adsorption of bisphenol-A onto bentonite [a]

	Pseudo-first order kinetic model			Pseudo-second order kinetic model		
q_{eq}	k_1	$q_{eq,cal}$	R^2	k_2	$q_{eq,cal}$	R^2
mg/g	1/min	mg/g		g/mg/min	mg/g	
0.85	0.0053	0.78	0.975	0.0072	0.87	0.996

[a] Adsorption conditions: dosage = 1 g/100 mL, initial concentration =25 mg/L, temperature=25 ºC and agitation rate = 250 rpm.

4. CONCLUSION

The use of bentonite for adsorption of bisphenol-A from aqueous solution was investigated. The results of the adsorption characteristics of bisphenol-A indicate that it could be described well with the sorption kinetics rate constant (k_2) 0.0072

g/mg/min and pseudo-second order kinetics. Bisphenol-A sorption on bentonite provided better fit with the Langmuir model (R^2= 0.997) rather than the Freundlich isotherm. Furthermore, the adsorption capacity of bentonite increased with increasing the pH of the solution between the range of 3 to 9 and optimal adsorption pH was determined as pH 9.

REFERENCES

[1]. L.N. Vandenberg, I. Chahoud, V.Padmanabhan, F.J.R. Paumgartten, and G. Schoenfelder, "Biomonitoring studies should be used by regulatory agencies to assess human exposure levels and safety of Bisphenol A", Environ. Health Perspect., vol. 118, pp. 1051-1054, 2010.
[2]. G. Liu, J. Ma, X. Li, and Q. Qin, "Adsorption of bisphenol A from aqueous solution onto activated carbons with different modification treatments", J. Hazard. Mater., vol. 164, pp. 1275-1280, 2009.
[3]. H. Maruyama, H. Seki, Y. Matsukawa, A. Suzuki, and N. Inoue, "Adsorption behavior of bisphenol-A and diethyl phthalate onto bubble surface in nonfoaming adsorptive bubble separation", Chem. Eng. J., vol. 141, pp. 112-118, 2008.
[4]. N. Acevedo, B. Davis, C.M. Schaeberle, C. Sonnenschein, and A.M. Soto, "Perinatally administered bisphenol A as a potential mammary gland carcinogen in rats", Environ. Health Perspect. vol. 121, pp. 1040-1046, 2013.
[5]. Y.H. Kim, B. Lee, K.H. Choo, and S.J. Choi, "Selective adsorption of bisphenol A by organic–inorganic hybrid mesoporous silicas", Micropor. Mesopor. Mater., vol. 138, pp. 184–190, 2011.
[6]. Z.M. Lazim, T. Hadibarata, M.H. Puteh, and Z.Yusop, "Adsorption characteristics of bisphenol a onto low-cost modified phyto-waste material in aqueous solution", Water Air Soil Pollut., vol. 226: 34, pp. 2-11, 2015.
[7]. B. Pan, D. Lin, H. Mashayekhi, and B. Xing,"Adsorption and hysteresis of bisphenol a and 17α-ethinyl estradiol on carbon nanomaterials", Environ. Sci. Technol., vol. 42 (15), pp. 5480-5485, 2008.
[8]. W.T. Tsai, H.C. Hsu, T.Y. Su, K.Y. Lin, and C.M. Lin, "Adsorption characteristics of bisphenol-A in aqueous solutions onto hydrophobic zeolite", J. Colloid Interf. Sci., vol. 299, pp. 513-519, 2006.
[9]. W. Han, L. Luo, and S. Zhang, "Adsorption of bisphenol A on lignin: effects of solution chemistry", Int. J. Environ. Sci. Technol., vol. 9, pp. 543–548, 2012.
[10]. H. Kono, K. Onishi, and T. Nakamura, Characterization and bisphenol A adsorption capacity of cyclodextrin–carboxymethylcellulose-based hydrogels, Carbohyd. Polym., vol. 98, pp. 784-792, 2013.
[11]. Z.M. Wang, H. Ooga, T. Hirotsu, W.L. Wang, Q. Y. Wu, and H.Y. Hu, "Matrix-enhanced adsorption removal of trace bisphenol-a by controlling the interlayer hydrophobic environment of montmorillonite" Appl. Clay Sci., vol. 104, pp. 81-87, 2015.
[12]. K. Styszko, K. Nosek, M. Motak, K. Bester, and C.R. Chimie, "Preliminary selection of clay minerals for the removal of pharmaceuticals, bisphenol A and triclosan in acidic and neutral aqueous solutions", vol. 18, pp. 1134-1142, 2015.
[13]. P. Wu, Q. Zhang, Y. Dai, N. Zhu, Z. Dang, P. Li, J. Wu, and X. Wang, "Adsorption of Cu(II), Cd(II) and Cr(III) ions from aqueous solutions on humic acid modified Ca-montmorillonite", Geoderma, vol. 164, pp. 215-219, 2011.
[14]. W.S. Hue, D. Bing-zhi, and H.Yu, "Adsorption of bisphenol A by polysulphone membrane", Desalination, vol. 253, pp. 22–29, 2010.
[15]. L. Joseph, Q. Zaib, I.A. Khan, N.D. Berge, Y.-G. Park, N.B. Saleh, Y. Yoon, "Removal of bisphenol A and 17α-ethinyl estradiol from landfill leachate using single- walled carbon nanotubes", Water Res., vol. 45, pp. 4056-4068, 2011.
[16]. I. Bautista-Toledo, M.A. Ferro-Garcia, C. Moreno-Castilla, and F.J. Vegas Fernandez, "Bisphenol A removal from water by activated carbon. Effects of carbon characteristics and solution chemistry", Environ. Sci. Technol., vol. 39, pp. 6246-6250, 2005.
[17]. W.T. Tsai, C.W. Lai, and T.Y. Su, "Adsorption of bisphenol-A from aqueous solution onto minerals and carbon adsorbents", J. Hazard. Mater., vol. 134 (1-3), pp. 169-175, (2006).
[18]. B. Tugrul, S. Erentürk, S. Haciyakupoglu, N. Karatepe, N. Altinsoy, N. Baydogan, F. Baytas, B. Büyük, E. Demir and S. Gedik, "Kinetic and thermodynamic behavior of selenium on modified bentonite and activated carbon using radiotracer technique", Acta Phys. Pol. A, vol. 128, B-180, 2015.

Using Ant Colony Algorithm Method in the Disabled Service Vehicle Routing Problems

Yusuf Uzun[1], Yusuf Gurbuz[1], Gulay Tezel[2]

Abstract

Rehabilitation centers would wish it to be fast and the minimum cost of transportation problems in service for the disabled. Vehicle Routing Problem (VRP) aims to efficiently use by minimizing transportation costs of a vehicle fleet with a certain capacity efficiently. The aim of our problem is to minimize the total number of vehicles to be used and distance traveled. It has a certain capacity of each vehicle and a demand that must be met at a specific time period of each disabled. Each vehicle is obliged to make service for disabled people at a certain time period. In this study, ant colony algorithm metaheuristic method has been tried to reduce cost on vehicle routing problem.

Keywords: *disabled, ant colony algorithm, optimization*

1. INTRODUCTION

The meaning and approach undertaken for the disabled have showed changes in the historical process. In this approach, firstly the medical model has seen interest, later social model and the human rights-based model approach was accepted [1].

The medical is model predicting treating by repaired the defects in the human body and the disability is based on caused by people rather than a social phenomenon. The social model is indicated that prevent a problem with revealed socially rather than the person. The disability in this model is a product of the social structures and the environment that involved physical structure, social conditions and beliefs [2].

The remaining aspects in medical and social model have been filled by human rights model. In this model, the integration of the disabled with the society in which they live, emphasis has been on the fundamental rights and freedoms [3].

For to sustain the lives of persons with disabilities and can be a productive individuals in society must be made of a number of researches and regulations related to meeting educational, cultural, economic and social needs.

According to World Health Organization report, 10% of the population in developed countries and 12% of the population in developing countries is made up of disabled people [4]. The lived of approximately 600 million people with disabilities in the world and this numbers are expected to increase to time [5]. According to the Disability Survey 2002 conducted by the Turkey Statistical Institute and Department of Administration for Disabled People, 12.29% of the total population in Turkey will be disabled citizens. Approximately 8.5 million people with disabilities are consisting chronic illnesses 9.7%, 1.25% of orthopedic, mental 0.48%, speech and language 0.38%, hearing 0.37%, blind and visually impaired 0.6% [6].

For people with disabilities by the Ministry of Family and Social Policy is to provide opportunities care in the family. However, is offered alternative models different organizations for the disabled that are not able to care by their families.

Organizations providing rehabilitation service for people with disabilities desire quickly and the minimum cost of transport service problems. In this paper, has been studied minimal cost Vehicle Routing Problem with Time Windows (VRPTW) using Ant Colony Optimization (ACO) metaheuristic method. ACO, which studies artificial agent systems, takes inspiration from the foraging behavior of real world ants [7].

The work was arranged as follows: In Section 2, materials and methods was explained. In Section 3, evaluations of the study were described. In Section 4, conclusions were presented.

2. MATERIALS AND METHODS

2.1 Vehicle Routing Problem

Vehicle Routing Problem (VRP), by minimizing the costs of the vehicle fleet which has a certain capacity, is aims to be used effective stopping at various locations to provide services to people with disabilities. The aim of the problem is to minimize the number of vehicles to be used and the total travel distance. There is the capacity of each vehicle and a demand that must be met in a given time period of each disabled. Each vehicle is obliged to serve for disabled in a certain time window [8].

[1] *Corresponding author: Necmettin Erbakan University, Seydisehir Vocational High School, 42370, Seydisehir/Konya, Turkey.* yuzun@konya.edu.tr

[1]*Necmettin Erbakan University, Seydisehir Vocational High School, 42370, Seydisehir/Konya, Turkey.* ygurbuz@konya.edu.tr

[2] *Selcuk University, Department of Computer Engineering, 42000, Konya, Turkey.* gtezel@selcuk.edu.tr

The VRPTW can be defined as follows. Let $G = (V, E)$ be a graph connected between two disabled consist of a disabled set of $n + 1$ disabled which can be serviced within a specified time window, and a set E of arcs with non-negative weights d_{ij} and with related travel times, t_{ij}. The travel time t_{ij} includes a service time at disabled i, and a vehicle is permitted to arrive before the opening of the time window, and wait at no cost until service becomes possible, but it is not permitted to arrive after the latest time window. Node 0 represents the rehabilitation center. Each disabled i, apart from the rehabilitation center, imposes a service requirement q_i that can be a delivery from, or a pickup for the rehabilitation center. The objective is to find the minimum number of tours, K^*, for a set of identical vehicles such that each node is reached within its time window and the accumulated service up to any node does not exceed a positive number Q (vehicle capacity). Another objective is often either to minimize the total distance traveled or the duration of the routes. The tours are starting and ending at the rehabilitation center [9].

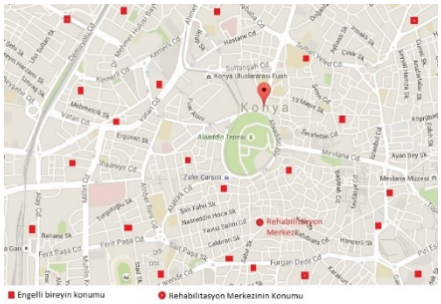

Figure 1. Representation of the disabled and rehabilitation center on the map

Polar coordinate system is used to calculate the distance from a two dimensional plane. In mathematics, the polar coordinate system is a two-dimensional coordinate system in which each point on a plane is determined by a distance from a reference point and an angle from a reference direction [10].

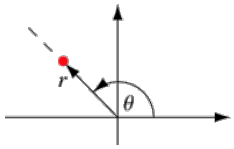

Figure 2. Representation of polar coordinate and angle

The following equations 1 and 2 are used for distance costs.

$$Cost(i) = -\alpha B(i) + \beta E + \gamma((\pi/360)\Theta) \quad (1)$$

$$B(i) = \sqrt{X(i)^2 + Y(i)^2} \quad (2)$$

where B is distance between the disabled and rehabilitation centers, E ending value of the service time, Θ polar coordinate value of the disabled in two-dimensional space, α, β and γ is respectively 0.7, 0.1 and 0.2 are weight values. In the calculation of the time window corresponding to the distance is used Euclidean equation.

Polar coordinates r and θ, Cartesian coordinates can be converted as follows [11].

$$x = r\cos\Theta \quad (3)$$

$$y = r\sin\Theta \quad (4)$$

The conversion formula obtained according to these two equations is as follows.

$$r = \sqrt{x^2 + y^2} \quad (5)$$

$$\Theta = arctan\frac{y}{x} \qquad x \neq 0 \quad (6)$$

If $x = 0$ and $y > 0$, $\theta = 90°$ ($\pi/2$ rad); $y < 0$, $\theta = 270°$ ($3\pi/2$ rad).

2.2 Ant Colony Optimization

Ant colony optimization has been formalized into a combinatorial optimization problem by Dorigo et al. [12]. ACO is using artificial ants to solutions the VRPTW problems. In Figure 3, the ACO algorithm behavior is described in pseudo-code. Algorithm consists of an initialization status and three components in the loop.

```
Set parameters, initialize pheromone trails
while termination conditions not met do
        Construct Ant Solutions
        Apply Local Search {optional}
        Update Pheromones
end while
```

Figure3. The ACO metaheuristic in pseudo-code

The main procedure of the ACO algorithm, via the loop construct, the loop of the three above discussed components of ACO algorithms: (i) construct ant solutions, (ii) apply local search, and (iii) update pheromones. The loop construct does not specify how these three activities are scheduled and synchronized. Otherwise, it does not say whether they should be executed in a completely parallel and independent way, or if some kind of synchronization among them is necessary. The designer is therefore free to specify the way these three procedures should interact [12].

Using ACO whose colony scale is *P*, an individual ant simulates a vehicle, and its route is constructed by incrementally selecting disabled until all disabled people have been visited. The disabled people, who were already visited by an ant or violated its capacity constraints, are stored in the impossible disabled people list (*tabu*). The decision making about combining disabled people is based on a probabilistic rule taking into account both the visibility and the pheromone information. Thus, to select the next disabled *j* for the *k*th ant at the *i*th node, the ant uses the following probabilistic formula [13].

The decision making about combining disabled people is based on a probabilistic rule taking into account both the visibility and the pheromone information. Thus, to select the next disabled *j* for the *k*th ant at the *i*th node, the ant uses the following probabilistic formula.

$$p_{ij}(k) = \begin{cases} \frac{\tau_{ij}^{\alpha} x\, \eta_{ij}^{\beta}}{\sum_{h \notin tabu_k} \tau_{ih}^{\alpha} x\, \eta_{ih}^{\beta}} \end{cases} \quad (7)$$

where $p_{ij}(k)$ is the probability of choosing to combine disabled *i* and *j* on the route, τ_{ij} the pheromone density of edge (*i*, *j*), η_{ij} the visibility of edge (*i*, *j*), α and β the relative influence of the pheromone trails and the visibility values, respectively and $tabu_k$ is the set of the infeasible nodes for the *k*th ant.

The 2-opt exchange method has been used for local search of the ACO algorithm. In the 2-opt exchange, all possible pairwise exchanges of disabled locations visited by individual vehicles are tested to see if an overall improvement in the objective function can be attained.

The updating of the pheromone trails is a key element to the adaptive learning technique of ACO and the improvement of future solutions. First, pheromone updating is conducted by reducing the amount of pheromone on all links in order to simulate the natural evaporation of the pheromone and to ensure that no one path becomes too dominant. This is done with the following pheromone updating equation;

$$\tau_{ij}^{new} = \rho\ \tau_{ij}^{old} + \sum_{k}^{K} \Delta\tau_{ij}^{k} \quad \rho \in (0,1) \quad (8)$$

Where τ_{ij}^{new} is the pheromone on the link (*i*, *j*) after updating, τ_{ij}^{old} the pheromone on the link (*i*, *j*) before updating, ρ the constant that controls the speed of evaporation, *k* the number of the route, *K* the number of the routes in the solution and *K*> 0 and $\Delta\tau_{ij}^{k}$ are the increased pheromone on link (*i*, *j*) of route *k* found by the ant. Specifically, the strategy is written as:

$$\Delta\tau_{ij}^{k} = \begin{cases} \frac{Q}{K\ x\ L} \frac{D^k - d_{ij}}{m^k x\, D^k} & if\ link\ (i,j)\ on\ the\ kth\ route \\ 0 & otherwise \end{cases} \quad (9)$$

Where *Q* is a constant, *L* the total length of all routes in the solution, i.e. $L=\sum_k D^k$, D^k the length of the *k*th route in the solution, $d_{ij}$the length of edge (*i*, *j*) and m^k the number of disabled in the *k*th routes and $m^k > 0$.

2.3 The Dataset

In this problem has been assumed that 100 are disabled. The datasets used in this study are shown in the following Table 1. In this study, is used C101 dataset from Solomon's benchmarking problem sets [14]. Total car capacity was considered to be 200. In this study, the main objective is tried to minimize total numbers of vehicles and the total distance.
The various factors are highlighted in the data set. These; geographical data (*X* and *Y* coordinate values), a number of disabled are served by vehicle, time constraint percentages of persons with disabilities and in the form of positioning and frequency of the time window. The x and y coordinated values of place that the disabled lived are determined randomly over two-dimensional planes. The coordinate that there is rehabilitation center has been adopted central point (0).

Table 14. Disabled location and service information

Attribute	Data Type
Disabled number	continuous
Coordinate X	continuous
Coordinate Y	continuous
Requested time	continuous
Service start time	continuous
Service end time	continuous
Service time	continuous

Table 2. Sample data of the data set

Disabled number	X	Y	Requested time	Service start time	Service end time	Service time
1	45	68	10	912	967	90
2	45	70	30	825	870	90
3	42	66	10	65	146	90
4	42	68	10	727	782	90

3 EVALUATION OF THE STUDY

In this study, ant colony optimization (ACO) algorithm approach in the disabled service vehicle routing problems was proposed. ACO algorithm is coded in Matlab programming. The flowchart of the approach used to obtain the optimum solution values is shown in Figure 4.

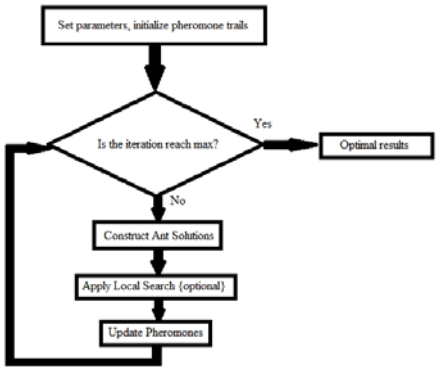

Figure 4. Flowchart for proposed the ACO method

The results obtained from experiments are given in Table 3.

Table 3. The results of application

Method	Distance	Number of vehicles	Total Travel Time
ACO	2872.7	19	2120.9

In the ACO metaheuristic method, has been setting maximum capacity of vehicles 200 and the number of ants 20. In the performed study, is calculated as the minimum total distance 2872.7, the number of vehicles 19 and total travel time 2120.9. Routes of the vehicles are shown in Table 4.

Table 4. Vehicle's routes obtained by the ACO method

Vehicles	Routes										
1	52	47	49	0	0	0	0	0	0	0	0
2	91	21	1	69	75	0	0	0	0	0	0
3	99	2	0	0	0	0	0	0	0	0	0
4	98	100	88	89	4	0	0	0	0	0	0
5	97	77	79	80	22	50	66	0	0	0	0
6	95	93	84	85	60	61	59	64	0	0	0
7	96	94	92	58	39	68	23	0	0	0	0
8	90	87	86	83	82	70	72	46	73	48	6
9	81	78	76	74	45	28	34	51	0	0	0
10	71	56	0	0	0	0	0	0	0	0	0
11	67	65	63	62	44	37	38	30	36	12	0
12	54	53	0	0	0	0	0	0	0	0	0
13	57	55	42	41	31	35	40	14	26	0	0
14	43	29	15	9	0	0	0	0	0	0	0
15	33	32	27	11	0	0	0	0	0	0	0
16	24	25	19	8	16	0	0	0	0	0	0
17	20	18	10	0	0	0	0	0	0	0	0
18	17	3	7	0	0	0	0	0	0	0	0
19	13	5	0	0	0	0	0	0	0	0	0

In Figure 5, is given the route information obtained by the ACO method. In this study, were obtained 19 routes for 100 disabled.

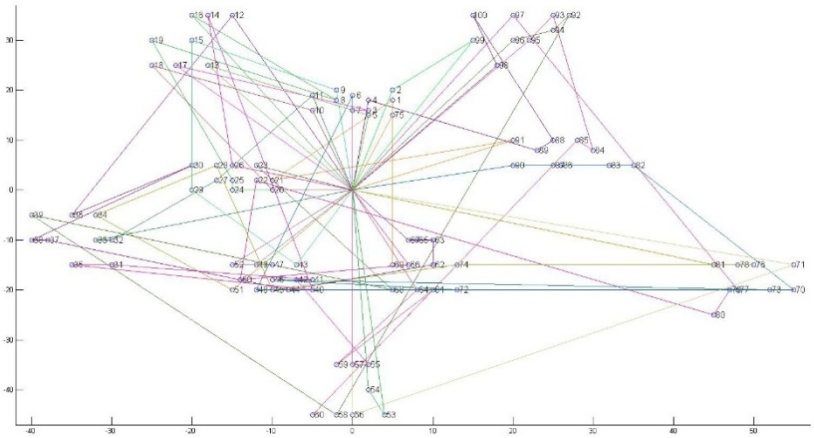

Figure 5. The routes obtained by the ACO method

4 CONCLUSIONS

Metaheuristic algorithms are currently one of the most effective methods of optimization applications in nowadays. In these methods, taking into account a starting solution is carried out a search strategy in the algorithm. Process be terminated with a specified stopping criterion and be presented to user obtained the solution.

Vehicle Routing Problem is a combinatorial optimization problem that is substantially determining logistics costs encountered with the development of the route plan for the business. In this paper, has been studied minimal cost VRPTW using ACO metaheuristic method.

In the study that conducted over the dataset is obtained minimum total distance, the number of vehicles was used and total travel time.

ACKNOWLEDGMENTS

This work was supported by Necmettin Erbakan University Scientific Research Projects (BAP) Coordinators hips.

REFERENCES

[1] "*Mevzuattan Uygulamaya Engelli Hakları İzleme Raporu 2013"*, Toplumsal Haklar ve Araştırmalar Derneği, İstanbul, 2014
[2] S. Moore, *Social Welfare Alive*, United Kingdom, Nelson Thornes Ltd., 2002, p.402
[3] F. Subaşıoğlu, *"Üniversitelerin Bilgi ve Belge Yönetimi Bölümleri'nin "Engellilik Farkındalığı" Üzerine Bir Araştırma"*, Bilgi Dünyası Dergisi, 2008, c. 9, vol. 2, p. 403
[4] A. Bilgin and Et. Al., *"1 Nolu Sağlık Ocağı Bölgesinde 18-58 Yaş Engellilik Sıklığı ve Engelliliği Belirleyen Etmenler"*, Sağlıkta Yaşam Kalitesi Sempozyumu Özet Kitabı, İzmir, 2004
[5] Öz-Veri, Başbakanlık Özürlüler İdaresi Başkanlığı Hakemli Süreli Yayını, 2006, 75
[6] Öz-Veri, Başbakanlık Özürlüler İdaresi Başkanlığı Hakemli Süreli Yayını, 2006, 28
[7] M. Dorigo, G. Di Caro and L.M. Gambardella, "Ant algorithms for discrete optimization", *Artificial Life*, 1999, vol. 5, no. 2, pp. 137–172
[8] J.-F. Cordeau, G. Desaulniers, J. Desrosiers, M.M. Solomon, and F. Soumis, "VRP with Time Windows", The Vehicle Routing Problem, *SIAM Monographs on Discrete Mathematics and Applications*, SIAM, Philadelphia, 2002a, pp. 157–193
[9] O. Braysy, *"Local search and variable neighborhood search algorithms for vehicle routing with time Windows"*, Acta Wasaensia 87, Universitas Wasaenis, Vaasa., 2001
[10] R.G. Brown and A. M. Gleason, *"Advanced Mathematics: Precalculus with Discrete Mathematics and Data Analysis"*, Evanston, Illinois: McDougal Littell. ISBN 0-395-77114-5, 1997
[11] (2016) Polar Coordinates website. [Online]. Available: http://mathworld.wolfram.com/PolarCoordinates.html
[12] M. Dorigo and G. Di Caro, "The ant colony optimization meta-heuristic", *In New Ideas in Optimization*, Corne, D., Dorigo, M., and Glover, F., Eds., McGraw-Hill, New York, 1999, p. 11
[13] M. Dorigo and K. Socha, *"An Introduction to Ant Colony Optimization"*, Technical Report TR/IRIDIA/2006-010, Université Libre de Bruxelles, 2006
[14] (2016) Dataset website. [Online]. Available: http://web.cba.neu.edu/~msolomon/c101.htm

The Effect of NANO-$Al_2O_3$and NANO-MoS_2 on Tribological Properties of Polyamide 46 (PA46) Nanocomposites

Oguz Unal, Salih Hakan Yetgin, Ferhat Yildirim, Mustafa Aydin

Abstract

In this experimental research, the tribological performance of pure Polyamide 46 (PA46), nano-Al_2O_3 filled Polyamide 46 (PA46-Al_2O_3) and nano-MoS_2 filled Polyamide 46 (PA46-MoS_2) were studied using a pin-on-disc tribometer against 1040 steel under dry sliding conditions. The influences of applied load and sliding speed on tribological properties were investigated. All the materials were dried at 100 ^oC for 4 hour before compounding. PA46 nanocomposites granules were fabricated on twin screw extruder. Thereafter, the specimens for tribological tests were produced using injection-molding machine. Tribological tests were carried out at sliding speeds of 0.5 and 1.0 m/s and applied load values of 20, 30 and 40N. The results show that the coefficient of friction for PA46 and nanocomposites were decreased while specific wear rate increased with increased applied load and sliding speed values. The coefficient of friction and specific wear rate of the PA46 polymer decreased with the addition of Al2O3 and MoS2. The specific wear rate for PA46 and nanocomposites are in the order of 10^{-13} and 10^{-14} m^2 / m.

Keywords: *PA46, MoS2, Al2O3, Friction, Wear*

1. INTRODUCTION

Polyamides (PAs) such as PA46, PA6 and PA66 widely used materials for tribological applications because of its perfect balance of various mechanical properties. Especially the chemical structure of PA46 offers an advantage compared to PA6 and PA66 [1]. PA 46 exhibits superior mechanical properties, such as high stiffness, high fatigue resistance, high thermal stability and good processability, owing to its high amide content per repeating unit and its symmetrical chain structure [2].

The tribological performance of PAs are closely related to the test conditions such as normal loads, sliding speed, sliding distance and transfer film characteristics [3-5]. The solid lubricants such as molybdenumdisulfide (MoS2) [6,7], polytetrafluroethylene (PTFE) [7, 8], ultra-high molecular weight polyethylene (UHMWPE) [8] and graphene [2] have been widely used for reduction the friction of PAs. The effect of test conditions and solid lubrications on friction and wear behavior properties of PAs have been reported in earlier papers [9-11]. Tang et al. [12] investigated the effect of nano-MoS2 on the tribological properties of aramid fiber reinforced PA6, they found that with the addition of nano-MoS2, worn debris multilayer laminar film was found on the wear scar, MoS2 transferred prior to PA6 and the friction coefficient and wear rate decreased. Wang et al. [13] reported a wear and friction reduction in carbon fiber reinforced PA1010 being filled with MoS2.They demonstrated that the improved properties were related to the increase in bond strength between the transfer film and counterface. Kishore et al. [14] analyzed the influence of sliding speed and load on the friction and wear behaviour of glass-reinforced polymer composites filled with either rubber or Al2O3 oxide particles; they reported that the wear loss increased with increasing load/speed. Scherge et al. [15] investigated aliphatic polyamide 46 (PA 46) polymers versus a lubricated steel disk with a pin-on-disk tribometer. They showed that under certain boundary conditions at transfer film forms and significantly reduces friction and wear.

In this study, the influence of sliding speed and load values on the friction and wear behavior of unfilled PA46 polymer, nano-Al_2O_3 filled PA46 and nano-MoS2 filled PA46 polymer nanocomposites were studied. Friction and wear tests were carried out on a pin-on-disc arrangement and at a dry condition. Tribological tests were performed at room temperature, under 20, 30, 40 N loads and at 0.5 and 1.0 m/s sliding speeds.

2. MATERIAL AND METHOD

In this study, the used materials polyamide 46 (Stanyl PA46) with 1.18 g/cm^3 density was obtained from Royal DSM (Holland). Nano-Al2O3 ve nano-MoS2 filled PA46 polymers were produced using a AYSA LAB30 co-rotating twin-screw extruder. The temperatures from the feed zone to the die of the extruder were 275, 280, 288, 295 and 300 ^oC, respectively. The diameter of the die is 4 mm. The screw speed was set at 70 rpm. All the materials were dried at 140 ^oC for 4 hour before compounding. The extruded polymer was obtained in the form of a cylindrical rod that was quenched in cold water and then pelletized. Then, the specimens for tribological tests were produced using the injection-molding machine Demag Stübbe S110, with an injection pressure of 500 bar and temperature profile of 275, 285, 295, 300 and 300 ^oC. The screw speed was fixed at 80 cm^3/s and the mould temperature was 30 ^oC.

Wear tests were carried out on a pin-on-disc wear test rig at room temperature under dry conditions. The cylindrical pin specimens had 5 mm diameter and 50 mm length. The rotating disc size was 100 mm in diameter and 5 mm in thickness. Figure 1 represents a schematic diagram of the pin-on-disc wear test configuration that was designed and used for this work.

Before testing, the pin surface was abraded against a 1000-grade paper to ensure good contact with the disc. Furthermore, all contact surfaces were cleaned with acetone and then dried. Each test was repeated three times and the average values were reported. After each test the mass loss in the pin was measured. Finally, the specific wear rate K_o (m^2/N) was calculated as;

$$K_o = \Delta m / L \,.\, F \,.\, \rho \quad (m^2 / N) \qquad (1)$$

Where Δm is average mass loss (g), L is sliding distance (m), F is applied load (N) and ρ is density of the materials (g/cm^3).

Figure 1. Wear test machine

3. RESULTS AND DISCUSSION

Table 2 shows the coefficient of friction values for PA46, PA46-Al_2O_3 and PA46-MoS_2 polymers tested at room temperature, at dry sliding conditions and under 20, 30 and 40N loads and at 0.5 and 1.0m/s sliding speed. The variation of the coefficient of friction with sliding time for PA46, PA46-Al_2O_3 and PA46-MoS_2 polymers tested under 30 N load value and 0.5 m/s sliding speed is presented in Figure 1. It is clearly seen from this figure that the coefficient of friction values for PA46 and its composites increases rapidly within the running in period and reaches a stable value within the steady state period. The initial coefficient of friction of PA46 was as low as 0.15. It increased to 0.43 when sliding about 50 min, and then remained the steady state period until the test was stopped. The tendency for the coefficient of friction of PA46-Al_2O_3 and PA46-MoS_2 polymers are about the same, but the coefficient of friction of PA46 is higher than that of PA46-Al_2O_3 and PA46-MoS_2 polymers in the steady state period. It was found that the coefficient of friction were obtained between 0.21-0.25 for PA46-Al_2O_3 and 0.14-0.19 for PA46-MoS_2 polymer nanocomposites.

Table 1. Tribological properties for unfilled PA46, PA46-Al_2O_3 and PA46-MoS_2 nanocomposites against steel disc tested at different sliding speed and load.

Materials	Load (N)	Sliding speed (m/s)			
		0.5	1.0	0.5	1.0
		Coefficient of friction (μ)		Specific wear rate (m^2/N)	
PA46	20N	0,4385	0,4255	6,8317E-14	8,9667E-14
	30N	0,4228	0,4206	7,4010E-14	1,0247E-13
	40N	0,4157	0,4121	7,6857E-14	1,1315E-13
PA46-Al_2O_3	20N	0,2546	0,2434	2,5359E-14	3,3812E-14
	30N	0,2232	0,2178	4,2265E-14	5,3536E-14
	40N	0,2115	0,2017	5,2831E-14	6,9738E-14
PA46-MoS_2	20N	0,1969	0,1915	2,1184E-14	2,9661E-14
	30N	0,1547	0,1423	3,9548E-14	4,5197E-14
	40N	0,1422	0,1382	4,6610E-14	5,2966E-14

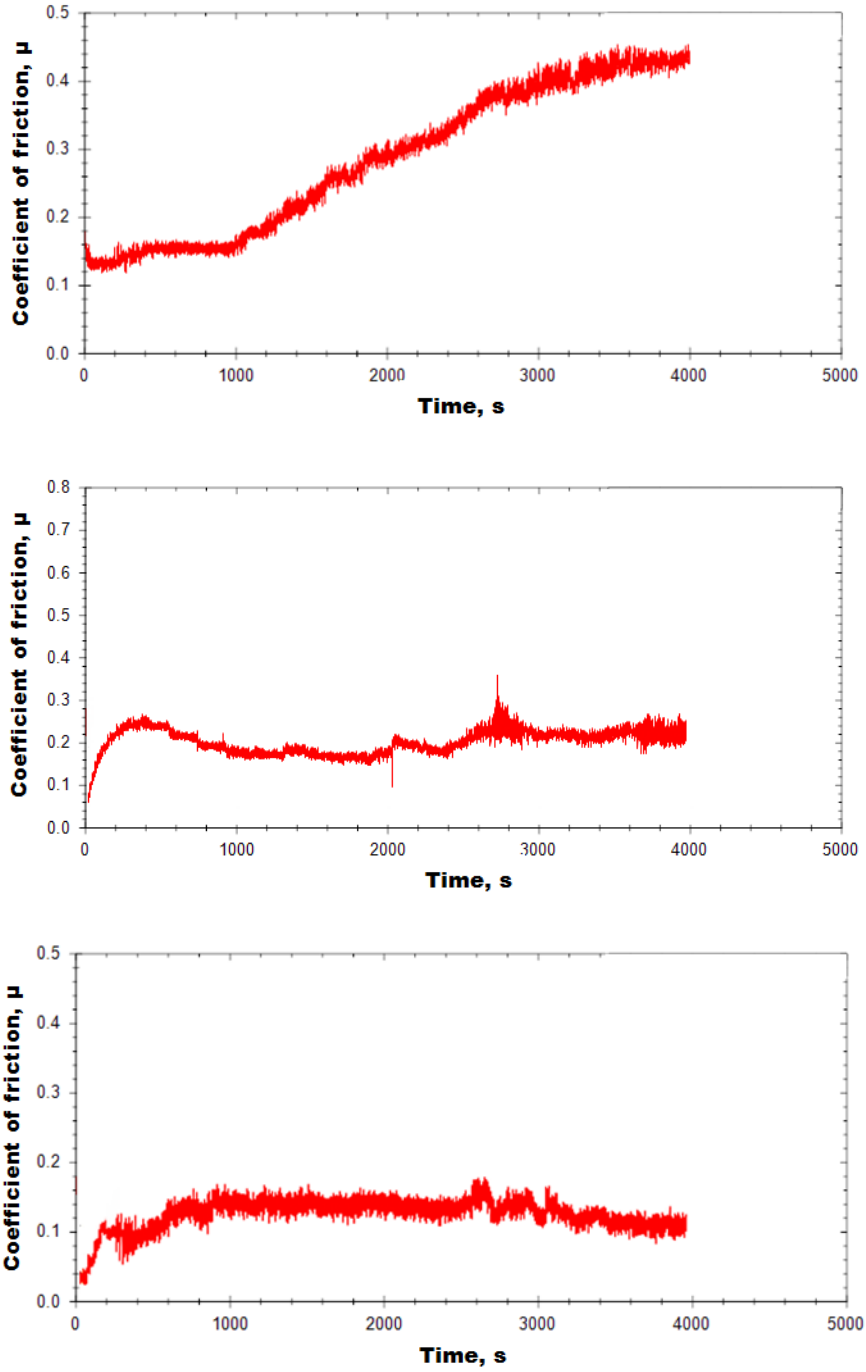

Figure 1. Variation of coefficient of friction with sliding time for unfilled PA46, PA46-Al_2O_3 and PA46-MoS_2 nanocomposites against steel disc (Applied load: 30N, sliding speed: 0.5m/s)

Figures 2 and 3 presents the variation of friction coefficients for unfilled PA46 polymer, PA46-Al_2O_3 and PA46-MoS_2 nanocomposites with applied load and sliding speeds, respectively. In Figure 2, for unfilled PA46 polymer, PA46-Al_2O_3 and PA46-MoS_2 nanocomposites at 0.5m/s sliding speeds, the coefficient of friction decreases with the increase in load. In the case of PA46, PA46-Al_2O_3 and PA46-MoS_2 nanocomposites, there is an average 5.4%, 20.3% and 38.4% decrease in the friction coefficient value for the increase in the applied load, respectively. In Figure 3, for unfilled PA46 polymer, PA46-Al_2O_3 and PA46-MoS_2 nanocomposites at 30 N applied load, the coefficient of friction decreases with the increase in the sliding speed. For unfilled PA46 polymer, PA46-Al_2O_3 and PA46-MoS_2 nanocomposites, there is an average decrease of 1.0%, 2.4% and 8.7% in the coefficient of friction value from 0.5 m/s to 1.0 m/s increase in the sliding speed. It is clear from these figures that the applied load influence is much higher than that of the sliding speed. Furthermore, the coefficient of

friction decreased significantly 89% for $Al2O_3$ addition to PA46 and 173% for MoS_2 addition to PA46 polymer nanocomposites. The similar results were obtained byAderikha [7].

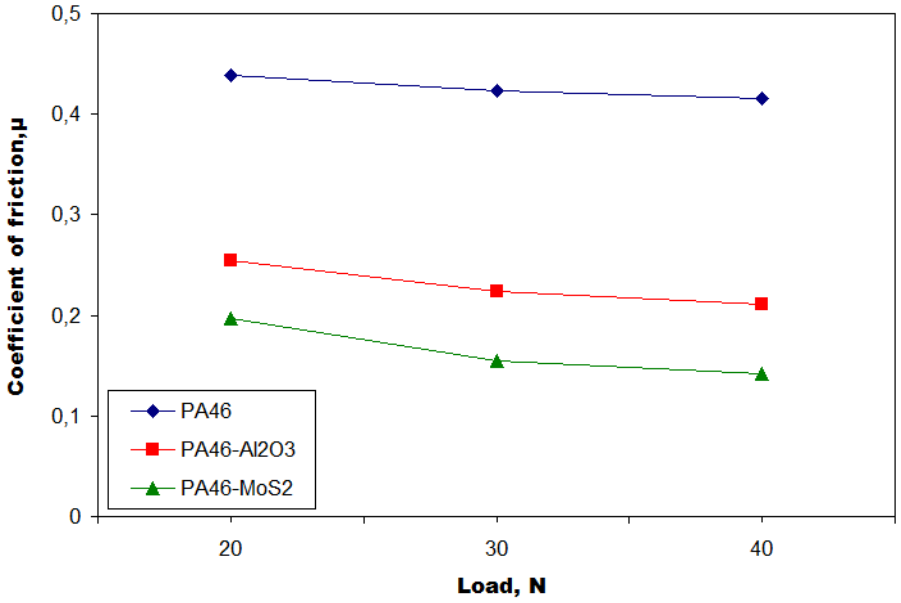

Figure 2. Variation of coefficient of friction with load for PA46 polymer, PA46-Al_2O_3 and PA46-MoS_2 nanocomposites tested against steel (Sliding speed; 0.5m/s).

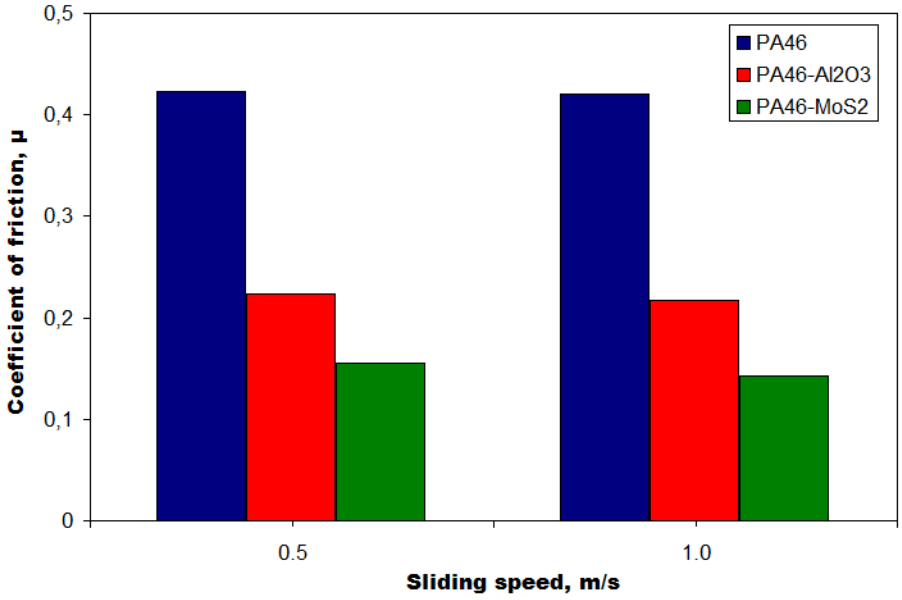

Figure 3. Variation of coefficient of friction with sliding speed for PA46 polymer, PA46-Al_2O_3 and PA46-MoS_2 nanocomposites tested against steel (Load; 30N).

Figure 4 and 5 illustrates the variation of specific wear rate with load and sliding speed, respectively. In general, the specific wear rate for PA46, PA46-Al_2O_3 and PA46-MoS_2 polymers were in the order of 10^{-14} m^2/N. The lowest wear rate is for PA46-Al_2O_3 with a value of $2.11x10^{-14}$ m^2/N while the highest wear rate is for PA46 with a value of $8.96x10^{-14}$ m^2/N. The wear rates of PA46-Al_2O_3 and PA46-MoS_2 are 165% and 202% lower than that of PA46 at 1.0 m/s sliding speed and 20 N applied load, respectively. For PA46 and its nanocomposites tested in this investigation within the applied load range of 20–40N, the specific wear rates are increased with the increase in the applied load. In Figure 5, the specific wear rate values for PA46, PA46-Al_2O_3 and PA46-MoS_2 polymers increase linearly with the increase in the sliding speed. In case of PA46, PA46-Al_2O_3 and PA46-MoS_2 polymers, there are about 38%, 26% and %14 increase in specific wear rate from 0.5 m/s to 1.0 m/s in the sliding speed at 30 N applied load, respectively. This is in a good agreement with the results obtained by Suresha [16].

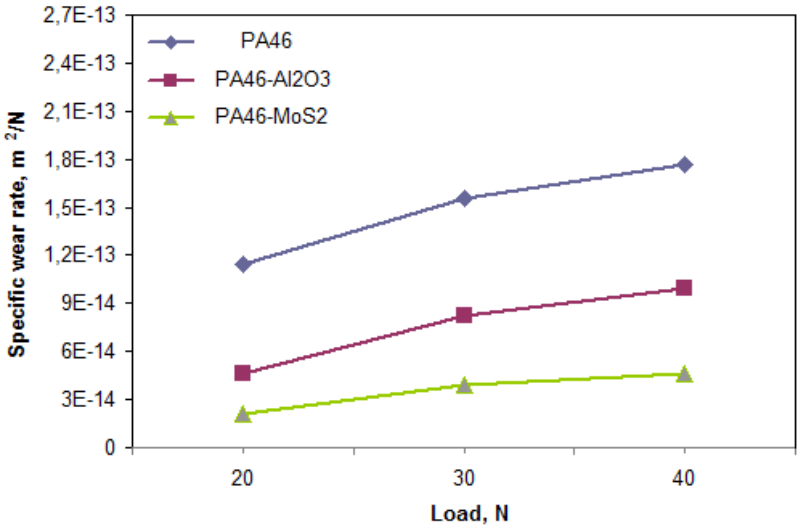

Figure 4. Variation of specific wear rate with load for PA46 polymer, PA46-Al_2O_3 and PA46-MoS_2 nanocomposites tested against steel (Sliding speed; 0.5m/s).

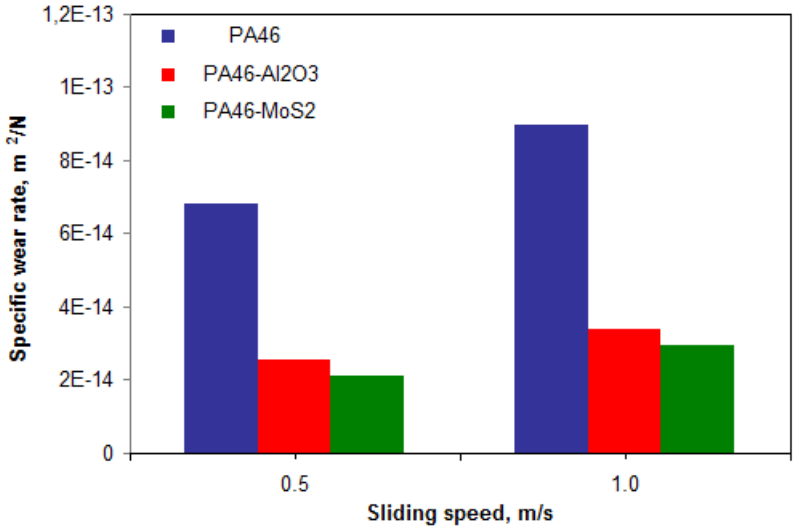

Figure 5. Variation of specific wear rate with sliding speed for PA46 polymer, PA46-Al_2O_3 and PA46-MoS_2 nanocomposites tested against steel (Load; 30N).

4. CONCLUSIONS

The tribological performance test of unfilled PA46, PA46-Al_2O_3 and PA46-MoS_2 at dry sliding conditions at different load and sliding speed reveals the following conclusions:

The wear rates of PA46, PA46-Al_2O_3 and PA46-MoS_2 were in the order of 10^{-14} m^2/N.
At the range of load and sliding speed studied in this work, the friction coefficient values decrease while specific wear rates of PA46, PA46-Al_2O_3 and PA46-MoS_2 increase with the applied load and sliding speed.
The lowest wear rate is for PA46-Al_2O_3 with a value of $2.11x10^{-14}$ m^2/N while the highest wear rate is for PA46 with a value of $8.96x10^{-14}$ m^2/N.
In general, the coefficient of friction and specific wear rate is much influenced by the change in the applied load.

REFERENCES

[1]. L.X. Zhao, L.Y. Zheng, S.G. Zhao, “Tribological performance of nano-Al2O3 reinforced polyamide 6 composites”, Mater. Lett., vol. 60, pp. 2590–2593, 2006.
[2]. F.C. Chiu, I-Neng Huang, “Phase morphology and enhanced thermal/mechanical properties of polyamide 46/graphene oxide nanocomposites”, Polymer Testing, vol. 31, pp. 953–962, 2012.
[3]. M. Watanabe, H. Yamaguchi, “The friction and wear properties of nylon”, Wear, vol. 110, pp. 379–388, 1986.
[4]. Q. Wang, X. Zhang, X. Pei, “Study on the synergistic effect of carbon fiber and graphite and nanoparticle on the friction and wear behavior of polyimide composites”, Mater Design, vol. 31, pp. 3761–3768, 2010.

[5]. W. Laigui, S. Yang, W. Liu, Q. Xue, "An investigation of the friction and wear behaviors of polyphenylene sulfide filled with solid lubricants", Polmy Eng Sci, vol. 40, pp. 1825-1832, 2000.
[6]. M.H. Cho, S. Bahadur, A.K. Pogosian, "Friction and wear studies using Taguchi method on polyphenylene sulfide filled with a complex mixture of MoS2, Al2O3, and other compounds", Wear, vol. 258, pp. 1825–1835, 2005.
[7]. V.N. Aderikha, A.P.Krasnov, V.A.Shapovalov, A.S.Golub, "Peculiarities of tribological behavior of low-filled composites based on polytetrafluoroethylene (PTFE) and molybdenum disulfide", Wear, vol. 320, pp. 135–142, 2014.
[8]. Y.L. You, D.X. Li, G.J. Si, X. Deng, Investigation of the influence of solid lubricants on the tribological properties of polyamide6 nanocomposite, Wear, vol. 311, pp. 57–64, 2014.
[9]. S. Zhou, Q. Zhang, C. Wu, J. Huang, "Effect of carbon fiber reinforcement on the mechanical and tribological properties of polyamide6/polyphenylene sulfide composites", Mater Design, vol. 44, pp. 493–499, 2013.
[10]. Z. Chen, T. Li, Y. Yang, X. Liu, R. Lv, "Mechanical and tribological properties of PA/PPS blends", Wear, vol. 257, pp. 696–707, 2004.
[11]. Q, Zhao, S, Bahadur, "The mechanism of filler action and the criterion of filler selection for reducing wear", Wear, pp. 225–229, 1999.
[12]. G. Tang, W.J. Huang, D.F. Chang, W.Z. Nie, W.J. Mi, W. Yan, "The Friction and wear of aramid fiber-reinforced polyamide 6 composites filled with nano-MoS2", Polym-Plast Technol Eng, vol. 50, pp. 1537–1540, 2011.
[13]. J.X. Wang, M.Y. Gu, B.S. Hao, S.R. Ge, "Investigation of the influence of MoS2 filler on the tribological properties of carbon fiber reinforced nylon 1010 composites", Wear, vol. 255, pp. 774–779, 2003.
[14]. S.P. Kishore, S. Seetharamu, S. Vynatheya, A. Murali, R.K. Kumar, "SEM observations of the effects of velocity and load on the sliding wear characteristics of glass fabric-epoxy composites with different fillers", Wear, , vol. 237, pp. 20–27, 2000.
[15]. M. Scherge, J. Kramlich, R. Böttcher, T. Hoppe, "Running-in due to material transfer of lubricated steel/PA46 (aliphatic polyamide) contacts", Wear, vol. 301, pp. 758–762, 2013.
[16]. B. Suresha, B.N. Ravi Kumar, M. Venkataramareddy, T. Jayaraju, "Role of micro/nano fillers on mechanical and tribological properties of polyamide66/polypropylene composites", Materials and Design, vol. 31, pp. 1993–2000, 2010.

Investigation of Crystallization BEhavior of Talc Filled PP Polymer and Foams

Salih Hakan Yetgin, Huseyin Unal

Abstract

In this study, PP polymer and 20%talc filled PP (PP-T) polymer composite materials were used. PP polymer and PP-T composite were foamed by using conventional injection molding method. The decomposition temperature of chemical endothermic foaming agent was 140°C and the total gas capacity was about 130 ml/g. Foaming agent added to polypropylene and talc filled PP composite between 1% and 2% by weight. Phasetransition temperature such as meltand crystallizationtemperatures,enthalpyand crystallizationratesof polymer and polymer foam samples were determined using differential scanningcalorimeter (DSC). The effect of chemical foaming agent content and talc filler addition on the thermal behaviors of PP polymer and PP-T composite were investigated.

Keywords: *PP, Injection molding, Foaming agent, Crystallization*

1. INTRODUCTION

Semi-crystalline polymers are used in many applications due to its high rigidity and high strength. Cellular plastics have been used wide range of application recently due to its lightness and moderate mechanical properties [1]. Crystallization behavior of semi-crystalline polymers is quite different compared to amorphous polymers due to the effect of the foaming behavior and foam structure. The effect of the crystal structure depends on the foaming process in semi-crystalline polymers. The crystal structure affects both of the nucleation and cell growth due to the heterogeneous nature of semi-crystalline polymer and non-uniform distribution of foaming agent in the polymer matrix in batch foam process. Doroudiani et all [2], uniform cells with small cell size have achieved in the low-crystalline polymers while non-uniform structure have achieved in high crystalline polymers. This is the reason for the authors attributed to the different solubility of the gas in different parts of the polymer. Baldwin et all [3] have achieved higher cell density in the semi-crystalline polymers according to amorphous polymers. The interface between crystalline and amorphous regions is act as cell nucleation sites during the foaming process.

In the present work, unfilled PP (PP) and 20% talc filled PP (PP-T) polymer composite materials were used. PP polymer and its composite were foamed with using convectional injection molding method. Melting of temperature, crystallization temperature, melt enthalpy and crystallinity values were determined by using differential scanning calorimetry. The effects of talc filler and chemical foaming agent content on thermal properties of PP polymer and PP-T polymer composite materials were investigated.

2. MATERIAL AND METHOD

2.1. Materials

In this study, unfilled polypropylene with a density of 0.90g/cm^3 and melt flow index of 25g/10min. (230^{o}C/2.16kg) (trade code: PP3374E3) supplied by Exxon Mobile, talc filled PP polymer composite with a density of 1.04g/cm^3 and melt flow index of 4g/10min. (230^{o}C/2.16kg) (trade name and code: Vapolen 220 TPP) supplied by Vatan Plastic, Istanbul/Turkey materials were used. Chemical blowing agent (Foaming MB-FA 2984 PE) was obtained by Tosaf Compound Inc., İstanbul, Turkey. Its decomposition temperature is about 140^{o}C and mass of decomposition is 130ml/g. Conventional type of injection molding machine was used to produce PP polymer foam and talc filled PP polymer composite foams. Materials used and its coding are given in Table 1.

Table 1. Materials used and its coding in the study.

No	Composition of materials used	Abbreviation
1	Polypropylene	PP
2	Polypropylene polymer foam with 1% chemical blowing agent	PP-1
3	Polypropylene polymer foam with 2% chemical blowing agent	PP-2
4	Talc filled polypropylene composite	PP-T
5	Talc filled polypropylene composite foam with 1wt.% chemical blowing agent	PP-T-1
6	Talc filled polypropylene composite foam with 2wt.% chemical blowing agent	PP-T-2

2.2. DSC (Differential Scanning Calorimetry) test

Thermal properties such as melting of temperatures, enthalpy values and crystallization temperature of unfilled PP, foamed PP and PP-T composites were studied by means of a Thermo Scientific EK90C/SII brand Exstar 6000 model differential scanning calorimeter, previously calibrated with indium. The weights of the un-foamed and foamed samples were approximately 10 mg. The experiments were carried out between 30 and 200°C under nitrogen gas, with a heating rate of 10°C/min.

Crystallization rates in percent ($X_{c\,\%}$), of unfilled PP and PP foam material can be calculated by using Equation 1. [5].

$$X_c\,(\%) = (\,\Delta H_m / \Delta H_m^{\,0}\,) \times 100 \qquad (1)$$

ΔH_m = enthalpy of melt,

$\Delta H_m^{\,0}$ = enthalpy of melt of 100% crystalline unfilled PP polymer ($\Delta H_m^{\,0}$ = 207.1 J/s).

Moreover, to calculate of crystallization rates in percent ($X_{c\,\%}$), of talc filled PP polymer and its foam polymer materials unfilled PP and PP foam material equation 2 was used [6, 7].

$$X_c\,(\%) = (\,\Delta H_m / \Delta H_m^{\,0} \;x\; W_{polymer}\,) \times 100 \qquad (2)$$

$W_{polymer}$ = weight rate of polymer matrix

3. RESULTS AND DISCUSSION

Figure 1 shows the optical microscope of PP polymer foam and PP-T polymer composite foam materials produced by using different injection parameters. Closed cell structure was obtained for the foam samples. The talc mineral added to PP polymer was affected the both the number of cells and cell diameter. Melting thermo-grams (endothermic) of chemical blowing agent is given in Figure 2. Chemical foaming agent showed two melting peaks. Smaller peak shows melting of temperature of polyethylene polymer that supports chemical foaming agent. Bigger peak illustrates melting of temperature of chemical foaming agent. Melting temperature of the carrier polymer (PE) is determined as 112.1°C. The degradation temperature of the foaming agent was 146.9°C and the maximum temperature at which degradation occurs has 169.2°C. Chemical foaming agent showed endothermic reaction and temperature has absorbed during decomposition reaction. Degradation reactions, which occur quite slowly compared to the exothermic chemical foaming agent and decomposition was completed in between 146.9-184.3°C. Slow decomposition of the foaming agent is more suitable for a successful foams process [8].

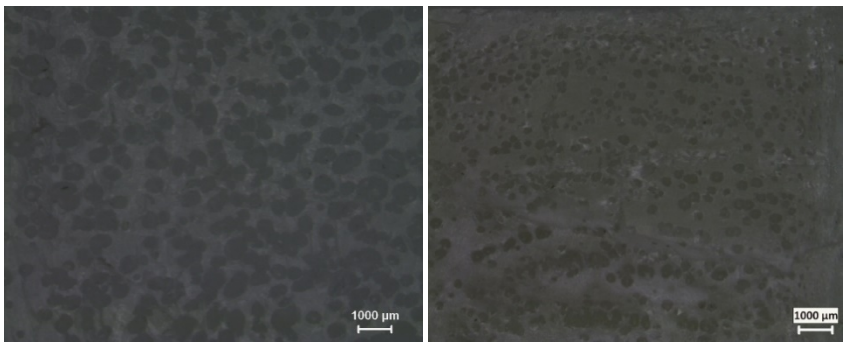

Figure 1. Optical micrographs of PP polymer foam and PP-T polymer composite foam materials

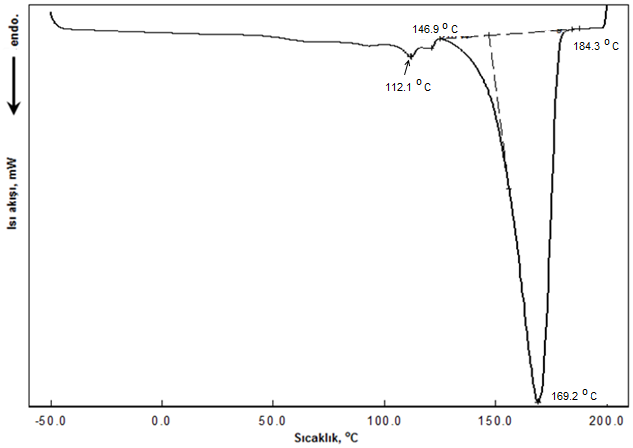

Figure 2. Melting thermo-grams (endothermic) of chemical blowing agent

Melting thermo-grams of PP polymer and PP polymer foam materials are given in Figure 3. Thermal properties of PP polymer, PP-T composite and theirs foams is given in Table 1.The melting enthalpy of 100% crystalline polypropylene phase are accepted as 207.1 J/s [5, 9] and crystallization rate are calculated using Equation 1 and 2. The melting temperature of the pure PP and PP foam wasn't observed a significant change. Melt temperature was obtained 167.8^{o}C for pure PP polymer while 1% and 2% filled foaming agent samples were obtained 164.6^{o}C. Melting enthalpy and % crystallinity was decreased with the amount of foaming agent increased. The crystallinity of the pure polypropylene polymer obtained 38.4% while with the addition of the foaming agent to PP polymer, the crystallinity was decreased to 37.3% and to 36.6'%. Depending on the amount of foaming agent, decrease in crystallinity was obtained 2.9% and 4.9%. Yuan et al. [10] investigated the effect of nitrogen gas on the crystallinity rate for polyamide polymer and concluded there is no effect on crystallinity of nitrogen gas. However, they stated that crystallinity of polymer increases with the addition of nano-clay filler for injection molding process.

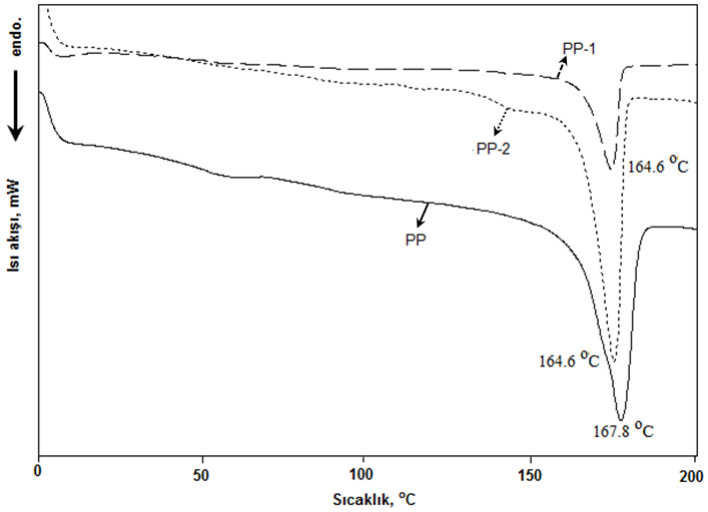

Figure 3.Melting thermo-grams of PP polymer and PP polymer foam materials

Table 1. Thermal properties of PP polymer, PP-T composite and theirs foams

Samples	Melting temperature (^{o}C) T_m	Melting Enthalpy, ΔH_m	Crystallinity X_c
PP	167.8	79.6	38.4
PP-1	164.6	77.4	37.3
PP-2	164.6	75.9	36.6
PP-T	166.0	87.4	52.7
PP-T-1	164.9	86.4	52.1

PP-T-2	164.9	85.9	51.8
Köpük Ajanı	169.0*	492.0	----

* Maximum temperature at decomposition

Melting thermo-grams of PP-T polymer composite and PP-T polymer composite foam materials are given in Figure 4, As shown in Fıgure 4, the melting temperature of PP-T and its foams were obtained between 165-166^{o}C. The talc mineral is added to PP polymer decreased melt temperature about 1.8^{o}C. This reduction in the melting temperature, it may decrease the size of the crystals due to presence of talc mineral [11]. Similar results were obtained by Brostow [12] when PP polymer, ceramic filled PP and ceramic filled PP/EPDM polymer composite was used. Lubomir et al [13], reported that the talc mineral is added in different amount reduced the melting temperature of PP/EPDM polymers and this reduction increases with increasing amount of talc. The melting temperature was reduced about 3^{o}C by the addition of additives. However, Yuan xin [14] reported that both talc and nano-clay particles added to PP polymers not influenced the glass transition and melting temperature.

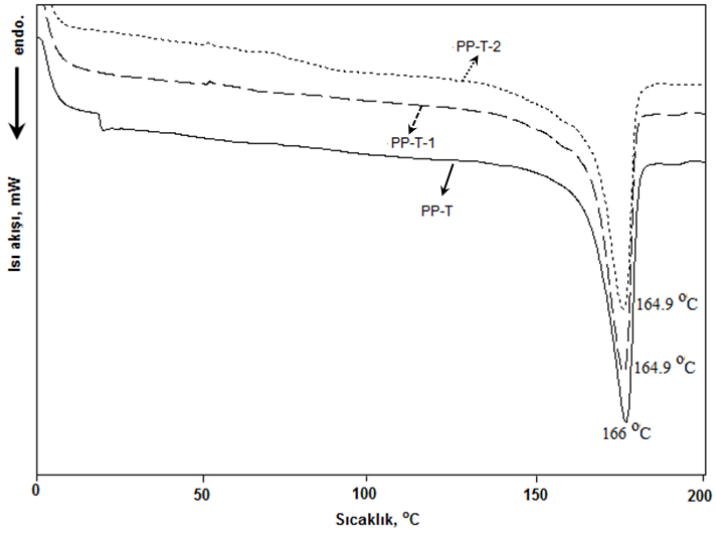

Figure 4. Melting thermo-grams of PP-T polymer composite and PP-T polymer composite foam materials

Foamed PP-T polymer composite sample has also reduced the melting temperature. Jiang et al. [1] concluded that blowing agent such as $scCO_2$ thathas smaller molecules decrease at melting temperature of semi-crystalline polymer. In another study, the CO_2 were determined to decrease the melting temperature of PP polymer [15]. When the crystallization rates are analyzed, crystallization rate of talc filled PP polymer is higher than the pure PP polymer. Crystallization rate of 38.4% for pure PP was obtained 52.7% with talc addition. Crystallization rate of the talc filled PP polymer has increased 37.2%. Similar results also obtained from Su et al. [16]. The minerals added into polymer matrix, reducing the size with increasing the number of spherulites and provide additional nucleation sites [17]. Number of nucleation sites is higher of talc filled PP composite polymer sample than the pure PP polymer. This situation leads to the development of a large number of smaller crystalline units [18]. Hornsby [19] carried out a study using PP polymer, ethylene/propylene rubber (EPR) elastomer and glass spheres. With the addition of EPR, crystallization temperature (Tc), crystallization starting temperature (Tc onset) and melting temperature (Tm) value decreased. They found that the crystallinity lower than that of pure PP polymers. When maleic anhydride-modified EPR used Tc_{onset} and T_c values unchanged, but temperatures T_1 and T_2 (T_1: $T_{c,\ onset}$ - Tc; T_2: T - T_c) was lower than the pure PP polymers. The reason for this is smaller spherules that develop which cause increase in crystalinity rate. Reduced heat capacity of the spherulites was changed by reducing the melt temperature. Premphet [20] investigated the crystallization behavior of 40% $CaCO_3$ filled PP composite and concluded crystallinity of PP increased with the increase $CaCO_3$ filler content that behaves nucleating agent.Similar results were obtained by Tara et al. [21] with talc addition to TPO polymer. They stated that talc minerals act such as nucleating agent effects crystallization and crystallization temperature of the PP spherulite. The crystallization rate of talc filled PP polymer foam was obtained 51.8% and 52.1% depend on the amount of foaming agent. the crystallization rate increases with the addition of talc filler in the PP polymer materials with 1% and 2% blowing agent while crystallization rate decreases with the increase in blowing agent content for PP polymer materials with 1% and 2% blowing agent. This increase, although it changes by the amount of foaming agent, was obtained 39.6% for 1% foaming agent, and 41.5% for 2% foaming agent. In previous studies, some researchers stated decreasing of crystalliniy is suitable for foaming of polymer material [22]. Filler added to the polymer, prevent deformation and movement of the matrix. This effect is talc mineral filler in PP polymer matrix which affect the nucleation process depends on the strong nucleating agent. Talc can cause the change the crystal structure from increases the weak β form to strong α form of PP matrix.The melting temperature is about 152 ° C for β form [13, 23]. Results of the experiments, a melting temperature were obtained about 165-167 °C. This indicates that the formation of α form. Sarrionandia et al. [24] reported that showed a single peak at

167 °C and all samples have α form in PP/EPDM/talc composite. Lubomir et al. [13] also reported that the melt temperature was obtained as 170°C and formation of the typical α form at this temperature.

According to the analysis results of exothermic DSC curve, crystallization temperature (T_c), the crystallization starting temperature ($T_{c,\ onset}$) and crystallization enthalpy (ΔH_c) values of the PP and PP foams are given in Table 2 and Figure 5. Crystallization temperature of pure PP polymer sample was 111°C while crystallization temperatures increased 1-1.5°C by the addition foaming agent and obtained 112 and 112.5°C. The crystallization enthalpy (ΔH_c) is proportional to the heat of crystallization of the sample and it is the degree of crystals. Changes in ΔH_c shows the change in crystallinity [26]. Crystallization rate and crystallization enthalpy decrease with foaming of PP polymer. The crystallization temperature of the PP polymer has increased significantly when 20% talc added to PP polymer. Crystallization temperature of pure PP polymer sample was 111°C while crystallization temperatures increased 13-14°C by the addition talc mineral and obtained between 124-126°C (Figure 6). The crystallization onset temperature (Tc onset) was obtained about 127°C. The increase in these two temperatures is linked to the formation of nuclei in the first stage. $T_{c,onset}$, is a temperature that is starting nucleating. Also, strong nucleating agents causes an increase in the $T_{c,onset}$ temperature [23]. In other words, the talc acted as nucleating agent and caused the increased both crystallization and crystallization onset temperature.

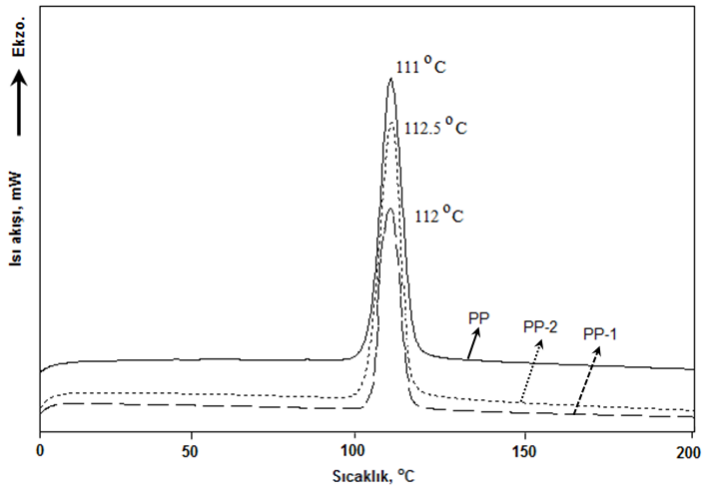

Figure 5. Crystallization thermo-grams of PP polymer and PP polymer foam materials

Crystallization enthalpy and crystallization temperature was increased by the addition of talc minerals to HDPE polymer [18]. In another study, when nano-CaCO3 added to PP polymer, the crystallization temperatures of the PP matrix increased. CaCO3 is stated that acts as nucleating agent in PP matrix [16]. Brostow et al. [12] reported that the crystallization temperature of PP polymers approximately 6°C increased and was obtained 89.3°C by adding ceramic powder into PP polymer. Crystallization temperature at which the cells and cell walls become stable is important temperature in the formation of polymer foam. A high crystallization temperature, which means the later solidification of the cells in the polymer foam structure.Therefore, high crystallization temperature is advantageous the growth of the cell during the foam formation.

Table 2. Crystallization values PP polymer, PP-T composite and theirs foam materials

Samples	Crystallization Temperature (°C)	Crystallization Starting Temperature	Crystallization Rate (°C)	Crystallization Enthalpy, (J/g)
	T_c	$T_{c\ onset}$	$T_{c\ onset}$- T_c	ΔH_c
PP	111.0	113.7	2.7	94.0
PP-1	112.0	115.2	3.2	93.2
PP-2	112.5	116.3	3.8	92.7
PP-T	124.6	127.3	2.7	96.8
PP-T-1	125.9	129.0	3.1	89.6
PP-T-2	125.9	129.1	3.2	79.4

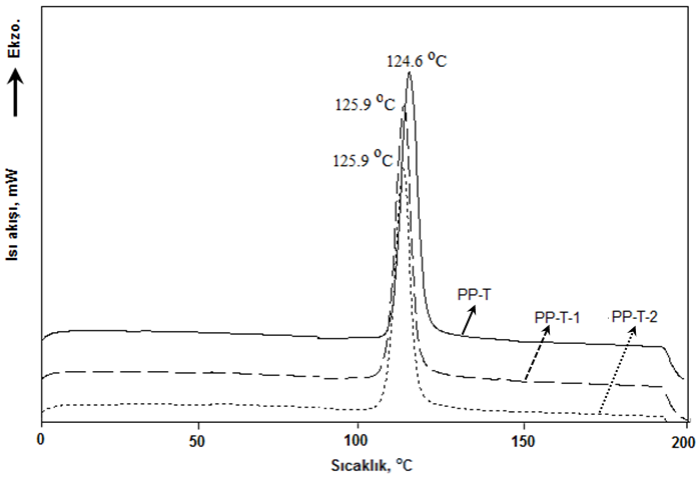

Figure 6. Crystallization thermo-grams of PP-T polymer composite foam materials

4. CONCLUSIONS

From this work, the following conclusions can be drawn:

Melting of temperature is obtained 164.6°C for PP polymer foam materials with 1% and 2% chemical foaming agent addition while melting of temperature is obtained 167.8°C for unfilled polypropylene. Crystallization amount decrease with the increase in chemical foaming agent content in the PP polymer material from %38.4 to %37.3 and %36.6. Decreasing in crystallization rate are %2.9 and %4.9 depending on foaming agent amount in PP polymer material. Melting of temperature is obtained between 165 and 166°C for PP-T polymer composite and PP-T polymer composite foam material. The crystallization rate is obtained about 52.7% for talc filled PP composite while crystallization rate is about 38.4% for unfilled PP polymer. Crystallization rate increased about 37.2% with the increase in talc filler content in PP polymer. Crystallization temperature is obtained 112 and 112.5°C for PP polymer foam materials with 1% and 2% chemical foaming agent addition while crystallization temperature is obtained 111°C for unfilled polypropylene. In addition, crystallization temperature is obtained between 124 and 126°C for talc filled PP polymer composite material.

ACKNOWLEDGEMENT

The authors would like to show their acknowledgment of the support of the University of Dumlupinar, scientific research project commission (BAPK) under the Project No: 2014-84

REFERENCES

[1]. X.L. Jiang, T. Liu, Z.M. Xu, L. Zhao, G.H. Hu,W.K. Yuan, “Effects of crystal structure on the foaming of isotactic polypropylene using supercritical carbon dioxide as a foaming agent”, J. of Supercritical Fluids, vol. 48, pp. 167–175, 2009.
[2] S. Doroudiani, C.B. Park, M.T. Kortschot, “Effect of the crystallinity and morphology on the microcellular foam structure of semicrystalline polymers”, Polym. Eng. Sci., vol. 36, pp. 2645–2662, 1996.
[3]. D.F. Baldwin, C.B. Park, N.P. Suh, “A microcellular processing study of poly(ethylene terephthalate) in the amorphous and semicrystalline states. Part I: microcellular nucleation”, Polym. Eng. Sci., vol. 36, pp. 1437–1445, 1996.
[4]. TS EN ISO 11357-1, May 2001, Plastics - differential scanning calorimeter (DSC) - Part 1: General principles.
[5]. J.I. Velasco, C. Morhain, A.B. Martinez, M.A. Rodrıguez-Perez, J.A. de Saja, “The effect of filler type, morphology and coating on the anisotropy and microstructure heterogeneity of injection-moulded discs of polypropylene filled with aluminium and magnesium hydroxides. Part 2. Thermal and dynamic mechanical properties”, Polymer, vol. 43, pp. 6813–6819, 2002.
[6]. P. Mareri, S. Bastide, N. Binda, A. Crespy, 1998, Mechanical behavior of polypropylene composıtes containing fine mineral fıller: effect of filler surface treatment, Composites Science and Technology, 58, 747-752.
[7]. S. S. Jikan, Z. M. Ariff, A. Ariffin, “Influence of filler content and processing parameter on the crystallization behaviour of PP/kaolin composites”, J Therm Anal Calorim, vol. 102, pp. 1011–1017, 2010.
[8]. Q. Zhou, C.B. Cong, “Exo-endothermic Blowing Agent and its Foaming Behavior”, Journal of Cellular Plastics, vol. 41, pp. 225-234, 2005.
[9] A.V.D. Wal, J.J.Mulder, R.J. Gaymans, “Fracture of polypropylene: 2. The effect of crystallinity”, Polymer, vol. 39/22, pp: 5477-5481, 1998.
[10]. Y Muan, T. Lih-Sheng, “Microstructure and mechanical properties of microcellular injection molded Polyamide-6 nanocomposites”, Polymer, vol. 46, pp. 7273–7292, 2005.
[11]. C. Bendjaouahdou, S. Bensaad, “Properties of polypropylene/(natural rubber)/organo-montmorillonite nano-composites prepared by melt blending”, Journal of Vınyl & Additive Technology, pp. 48-57, 2001.
[12]. W. Brostow, D. Tea, G. James, L. Jesse, “Thermal and mechanical properties of EPDM/PP+thermal shock-resistant ceramic composites”, J. Mater. Sci., vol. 46, pp: 2445–2455, 2011.
[13]. L.J. Lubomir, J. Pavlina, L. Barbora, T. Richard, G. Richard, R. Neil, “Effect of the talc filler content on the mechanical properties of polypropylene composites”, Journal of Applied Polymer Science, vol. 110, pp. 2742–2747 2008.

[14]. Z. Yuanxin, R. Vıjay, M. Hassan, J. Shaik, P.K. Mallick, "Experimental study on thermal and mechanical behavior of polypropylene, talc/polypropylene and polypropylene/clay nanocomposites", Materials Science and Engineering A, vol. 402, pp: 109–117, 2005.
[15]. Z-M. Xu, X-L. Jiang, T. Liu, G-H. Hu, L. Zhao, Z-N. Zhu, W-K. Yuan, "Foaming of polypropylene with supercritical carbon dioxide", J. of Supercritical Fluids, vol. 41, pp. 299–310, 2007.
[16]. X. Su, H. Youqing, Q. Jinliang, L. Yiqun, Z. Xiaohong, G. Jianming, S. Zhihai, H. Fan, Z. Manli, "The Relationship between microstructure and properties in PP/Rubber powder/nano-$CaCO_3$ ternary blends", Macromol. Mater. Eng., vol. 289, pp. 275–280, 2004.
[17]. P.S. Upinder, K.B. Bidyut, C.R. Bidhan, Evaluation of mechanical properties of polypropylene filled with wollastonite and silicon rubber", Materials Science and Engineering A, vol. 501, pp: 94–98, 2009.
[18]. S. Karrad, J.M.L. Cuesta, A. Crespy, "Influence of a fine talc on the properties of composites with high density polyethylene and polyethylene/polystyrene blends", Journal of Materials Science, vol. 33, pp. 453-461, 1198.
[19]. P.R. Hornsby, K. Premphet, "Influence of phase microstructure on the mechanical properties of ternary phase polypropylene composites", Journal of Applied Polymer Science, vol. 70, pp: 587–597, 1998.
[20]. K. Premphet, P. Horanont, "Phase structure and property relationships in ternary polypropylene/elastomer/filler composites: Effect of elastomer polarity", Journal of Applied Polymer Science, vol. 76, pp: 1929–1939, 2000.
[21]. J.M. Tara, "Properties and Foaming behavior of thermoplastic olefin blends based on linear and branched polypropylene", Degree of Master of Science (Engineering), Queen's University, Kingston, Ontario, Canada, 2007.
[22]. H-X. Huang, J.K. Wang, X.H. Sun, "Improving of cell structure of microcellular foams based on polypropylene/high-density polyethylene blends", Journal of Cellular Plastics, vol. 44, pp. 69-85, 2008.
[23]. Y.W. Leong, A.M.B. Bakar, Z.A.M. Ishak, A. Ariffin, B. Pukanszky, "Comparison of the mechanical properties and interfacial interactions between talc, kaolin, and calcium carbonate filled polypropylene composites", Journal of Applied Polymer Science, vol. 91, pp. 3315–3326, 2004.
[24]. M. Sarrionandia, A. Lopez-Arraıza, J. Aurrekoetxea, A. Arostegui, "Structure and mechanical properties of a talc-filled polypropylene/ethylene-propylene-diene composite after reprocessing in the melt state", Journal of Applied Polymer Science, vol. 114, pp. 1195–1201, 2009.
[25]. J.I. Velasco, M. Antunes, O. Ayyad, J.M. Lopez-Cuesta, P. Gaudon, C. Saiz-Arroyo, M.A. Rodriguez-Perez, J.A. De Saja, "Foaming behaviour and cellular structure of LDPE/hectorite nanocomposites", Polymer, vol. 48, pp: 2098-2108, 2007.
[26]. A. Ariffin, A.S. Mansor, S.S. Jikan, Z.A.I. Mohd, "Evaluation of hybridizing talc and surface-treated kaolin on the properties of PP hybrid composites", Journal of Reinforced Plastics and Composites, vol. 29, pp. 3429-3441, 2010.

Mapping with the Image Processing Method of Damage Regions with Respect Composite Laminates Subjected to Low Velocity Impact

Memduh Kara[1], Yusuf Uzun[1], Huseyin Arikan*[1]

Abstract

In this study , uni-directionaly reinforced laminates that arranged e-glass / epoxy composite samples in the form [+ 45 / -45 / 90/0]$_s$ and [+ 45 / -45 / 90/0]$_{2s}$ was applied low-velocity impact tests at impact energies of 10, 20 and 30 J has been obtained 8 and 16 laminated sample. Low-velocity impact tests were performed with the drop weight test device. Low-velocity impact damage was created on the samples depending on the different impact energies as a result of experiments conducted with hemispherical various impactor. The impactor mass was 6.350 kg. Digital imaging process method was applied images of the samples subjected to impact damage and damage maps for each damage zone were extracted. Also, change graph of damage area depending on the impact energies has been omitted. Changing damage zones were extracted. Also, change graph of damage area depending on the impact energies has been omitted.

Keywords: *image processing method, low-velocity impact, failure analysis*

1. INTRODUCTION

Composite materials have been used as a valid advantageous alternative for structural materials, replacing not only steel but even light alloys in the construction of some parts of vehicular body, spaceship, and aerodynamic structures and so forth. These materials are subjected to a wide spectrum of loadings during in-service use. Dynamic impact loadings, particularly in impact type events, represent a serious design condition for use of laminated composites for in-service applications, for example, dropping of tools during maintenance of the aforementioned industries. One of the properties of the laminated composite structures is that they are more susceptible to impact damage than similar metallic structures. If a composite laminate is subjected to normal low-velocity impact, invisible damage consisting of internal delamination might be induced [1]. Understanding the damage involved in the impact of composite targets is important in the effective design of a composite structure. For these reasons, numerous experimental and analytical techniques have been developed to study the dynamic response of composite structures subjected to transient dynamic loading. Some of the prominent work in this area is briefly mentioned in the following [2]. Damage mechanisms in composite materials are fairly complex, involving the interaction of matrix cracking, fiber matrix debonding, fiber pullout, delamination and fiber breakage. Generally, they occur simultaneously making the stress and failure analysis more difficult [3]. Impact failure in composites consists of various fracture modes which combine giving rise to a quite complex three-dimensional pattern [4–6]. Due to the complex features of damage mechanisms, more than one method is usually required for a complete non-destructive evaluation of impact induced damage. Advantages and disadvantages of different available techniques depend on the type of damage to be detected and on the test conditions in which sophisticated laboratory techniques can give highly accurate results, but may not be able to assess the state of the structure under in-service conditions [7]. There are various investigation techniques for determination of damages on composite materials. These are acoustic emission, thermography, dye penetrant, stereo X-ray radiography and ultrasonics. [8–10]. Unlike these methods, Image processing techniques are used in this study for determination of damages on composites. Delamination is observed to be the major failure mode. There for delamination areas are determined using image processing.

2. MATERIALS AND METHODS

2.1. Materials and specimens

In this study unidirectional E-glass/epoxy composite laminates were used. The laminates were cut into specimens of 140x140 mm in dimension with an average thickness of 1.6 and 3.2 mm. Stacking sequence of 8 laminated sample is [+45/-45/90/0]$_s$ and 16 laminated sample is [+45/-45/90/0]$_{2s}$.

[1] *Corresponding author: Necmettin Erbakan University, Seydisehir Department of A.C. Engineering, 42370, Konya, Turkey.* harikan@konya.edu.tr

The impact tests performed at impactor mass (6.35 kg) for three different impact energies (10, 20 and 30 Joule) were conducted with a drop weight testing machine (Figure 1). The radius of the impactors with a hemispherical nose was 6 and 12 mm. The composite specimen with dimensions of 140 mm by 140 mm was clamped on a fixture along a square circumference having a 100 mm side. The center of each plate was exposed to impact loading. The differences in the impact responses of specimens with varying width are characterized.

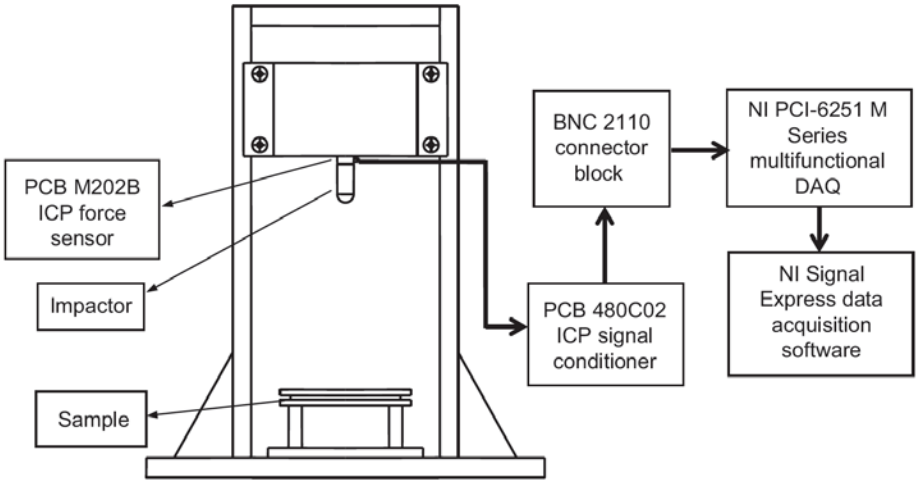

Figure 1. The Test rig [11]

2.2. Image Processing

Image processing involves processing or altering in an existing image. An image consists of a two-dimensional array of numbers. The color or gray shade displayed for a given picture element (pixel) depends on the number stored in the array for that pixel. The simplest type of image data is black and white. It is a binary image since each pixel is either 0 or 1. The next, more complex type of image data is gray scale, where each pixel takes on a value between zero and the number of gray scales or gray levels that the scanner can record. Most gray scale images have 256 shades of gray. The most complex type of image is color. Color images are similar to gray scale except that there are three bands, or channels, corresponding to the colors red, green, and blue. Thus, each pixel has three values associated with it [12].

Edge detection is one of the fundamental operations in image processing. The edges of items in an image hold much of the information in the image. The edges tell you where items are, their size, shape, and something about their texture.

Image segmentation is the process of dividing an image into multiple parts. This is typically used to identify objects or other relevant information in digital images. In segmentation, the computer attempts to find the major objects in the image and separate or segment them from the other objects [13].

Color mapping is a function that maps the colors of one (source) image to the colors of another (target) image [14]. A colormap is matrix of values between 0 and 1 that define the colors for graphics objects such as surface, image, and patch objects. MATLAB draws the objects by mapping data values to colors in the colormap.

3. EXPERIMENTAL STUDY

In this study, an image processing approach to detect damage regions with respect composite laminates subjected to low velocity impact was proposed. The process steps of the proposed approach are given bellow;

Colormaps can be any length, but must be three columns wide. Each row in the matrix defines one color using an RGB triplet. An RGB triplet is a three-element row vector whose elements specify the intensities of the red, green, and blue components of the color. The intensities must be in the range [0,1]. A value of 0 indicates no color and a value of 1 indicates full intensity. For example, this is a colormap with five colors: black, red, green, blue, and white [13].

Figure 2. Colormap(jet) function used in the study

To create a custom colormap, specify map as a three-column matrix of RGB triplets where each row defines one color. An RGB triplet is a three-element row vector whose elements specify the intensities of the red, green, and blue components of the color. The intensities must be in the range [0,1].

It basically represents a walk on the edges of the RGB color cube from blue to red (passing by cyan, green, yellow), and interpolating the values along this path [13].

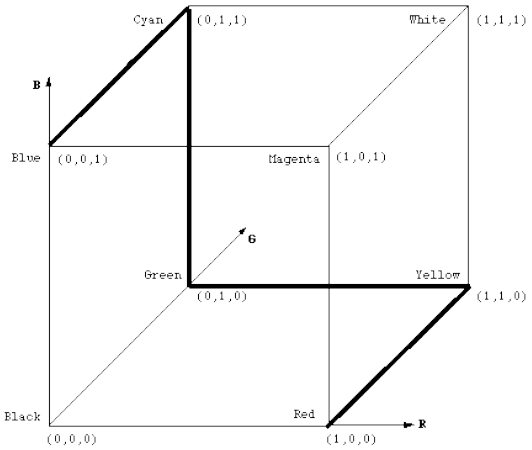

Figure 3. RGB color triplet cube

The RGB triplet values for common colors are shown in Table 1.

Table 15. The RGB triplet values for common colors

Color	RGB Triplet
Yellow	[1,1,0]
Magenta	[1,0,1]
Cyan	[0,1,1]
Red	[1,0,0]
Green	[0,1,0]
Blue	[0,0,1]
White	[1,1,1]
Black	[0,0,0]

4. EVALUATION OF THE STUDY

The damages on glass/epoxy and Kevlar composite samples can be observed by directing light beam from the back of the damaged areas. The size and nature of layer separation together with the existing matrix cracks can be determined with naked eyes [15]. After impact at various impact energy levels, high-resolution photographs of the damaged areas at the front of the test samples were taken using a simple backlighting method [1]. Image processing approach was applied these high-resolution photographs to detect damage regions with respect composite laminates. Figures 4–7 just show damaged areas of the specimens obtained using backlighting for specimens and photographs which were applied image processing, respectively.

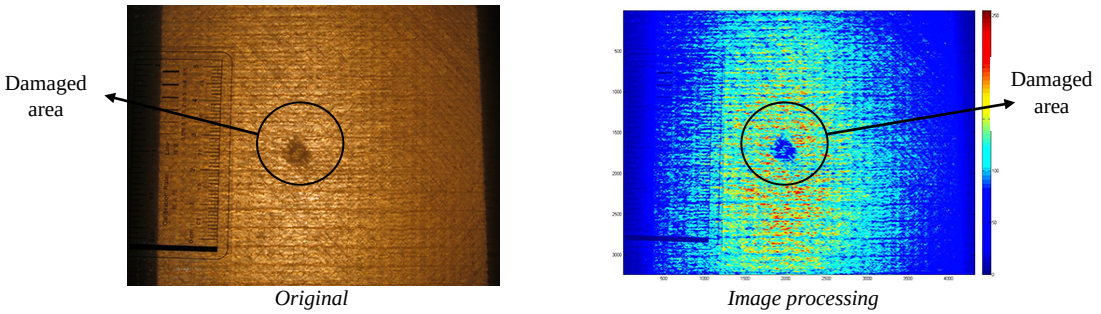

Original *Image processing*

(a)

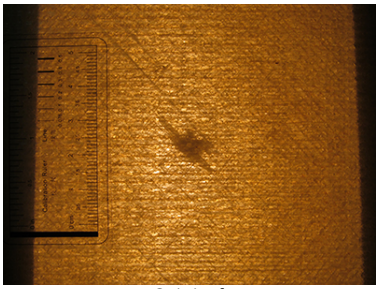
Original

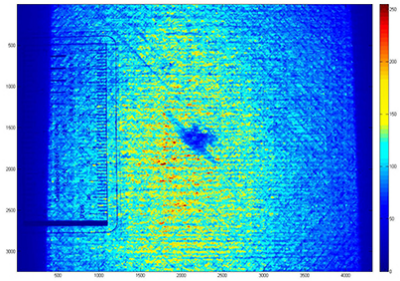
Image processing

(b)

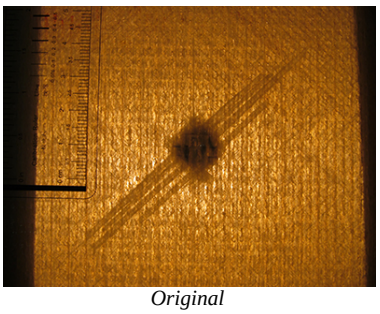
Original

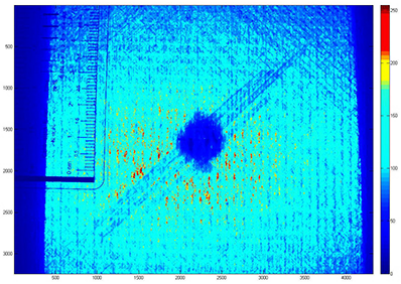
Image processing

(c)

Figure 4. Original and image processing view of 8 laminated sample subjected to (a) 10, (b) 20, and (c) 30 J impact energy levels. (12 mm in diameter hemispherical impactor)

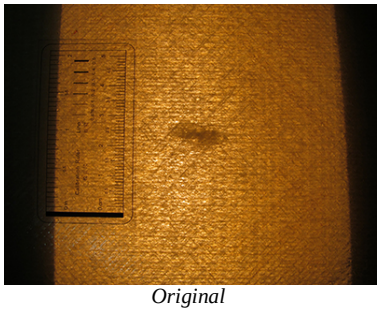
Original

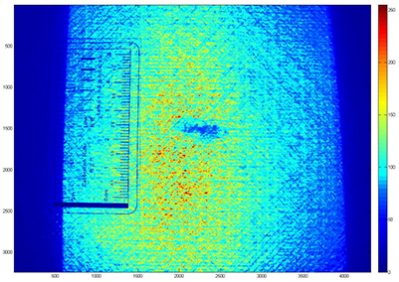
Image processing

(a)

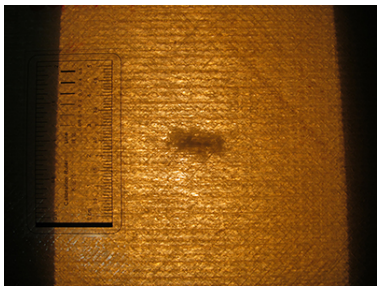
Original

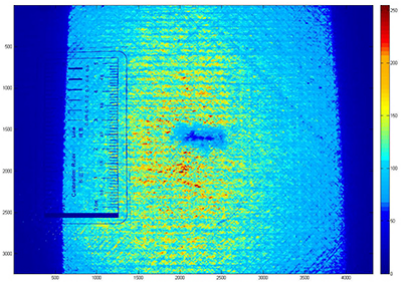
Image processing

(b)

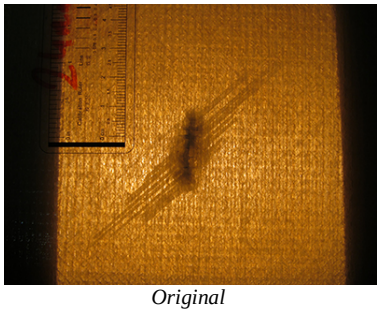
Original

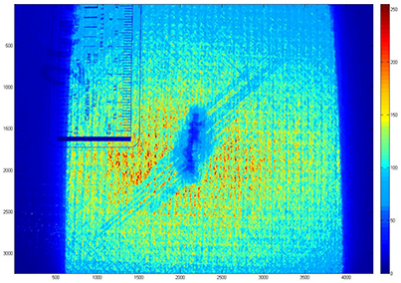
Image processing

(c)

Figure 5. Original and image processing view of 8 laminated sample subjected to (a) 10, (b) 20, and (c) 30 J impact energy levels. (24 mm in diameter hemispherical impactor)

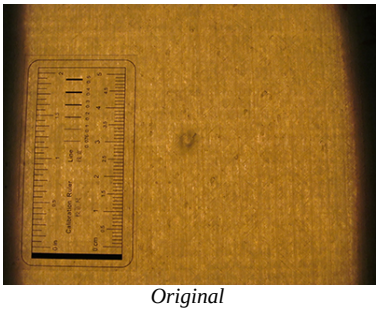

Original

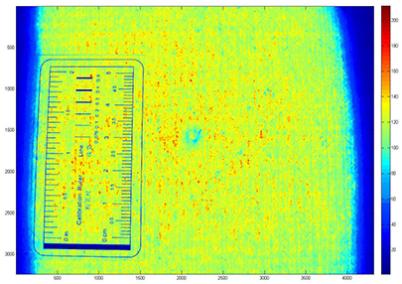

Image processing

(a)

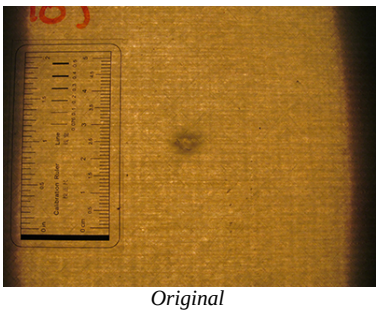

Original

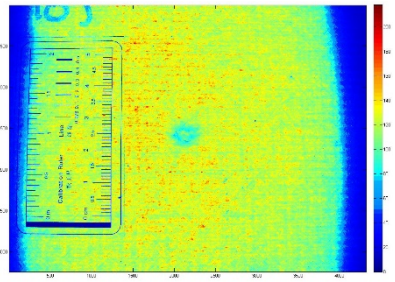

Image processing

(b)

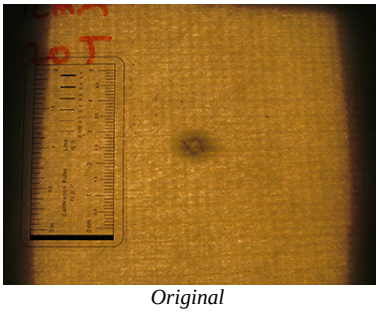

Original

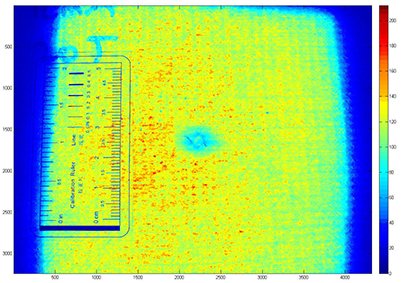

Image processing

(c)

Figure 6. Original and image processing view of 16 laminated sample subjected to (a) 10, (b) 20, and (c) 30 J impact energy levels. (12 mm in diameter hemispherical impactor)

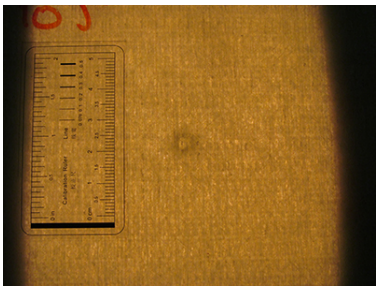

Original

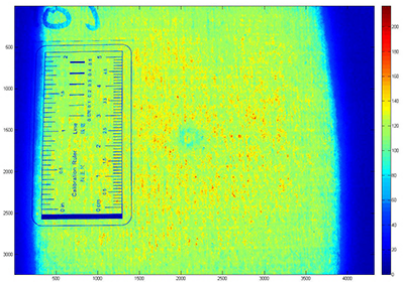

Image processing

(a)

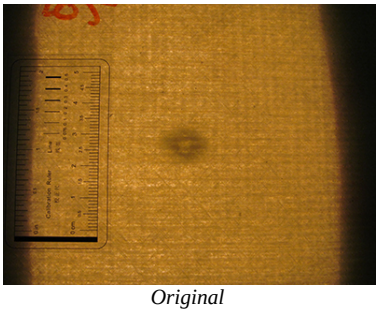

Original

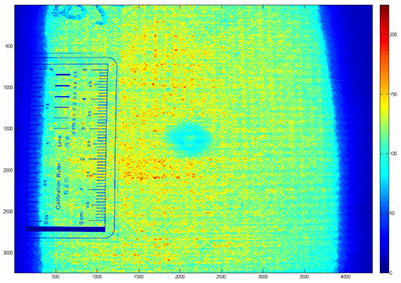

Image processing

(b)

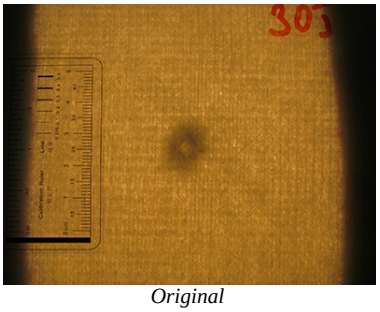

Original

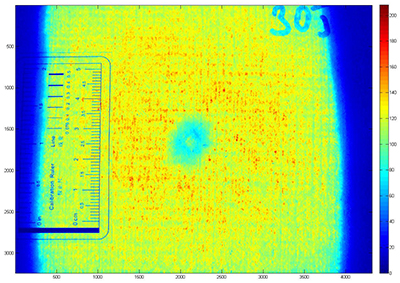

Image processing

(c)

Figure 7. Original and image processing view of 16 laminated sample subjected to (a) 10, (b) 20, and (c) 30 J impact energy levels. (24 mm in diameter hemispherical impactor)

5. CONCLUSIONS

The Image processing technique was used to detect and map damaged area. Practical results obtained from this study;

Using image processing techniques, it was possible to quantify the damage areas.

The result shows that for low velocity impact tests, as the impact energy increased the damage in the composite laminated increased.

Dimensions of sample, especially thickness of the specimen in this study, have significantly affected the damage area that increases as the thickness of the specimen increases.

In the tests conducted with various hemispherical taps, as the radius of the tap increases the damage area increases for the same energy level.

6. ACKNOWLEDGMENTS

This work was supported by Necmettin Erbakan University Scientific Research Projects (BAP) Coordinators hips.

REFERENCES

[1] M. Uyaner and M. Kara, “Dynamic response of laminated composites subjected to low-velocity impact.” *Journal of Composite Materials*, 2007, 41(24), p. 2877-2896.
[2] M. Uyaner, M. Kara and N. Ataberk, “Impact behavior of e-glass/epoxy laminated composite”, *7th. International Fracture Conference*, Kocaeli, Turkey, 2005, p:813-821.
[3] M. V. Hosur, C. R. L. Murthy, T. S. Ramamurthy and A. Shet, “Estimation of impact-induced damage in CFRR laminates through ultrasonic imaging”, *NDT & E International*, 1998, 31(5), p. 359-374.
[4] K. Srinivasan, W. C. Jackson, B. T. Smith and J. A. Hinkley, “Characterization of damage modes in impacted thermoset and thermoplastic composites”, *Journal of reinforced plastics and composites*, 1992, 11(10), p. 1111-1126.
[5] R. J. Chester and G. Clark, “Modelling of impact damage features in graphite/epoxy laminates”, *In Damage detection in composite materials*. ASTM International, 1992
[6] F. Aymerich, A. Bucchioni and P. Priolo, “Impact behaviour of quasi-isotropic graphite-peek laminates”, *In Key Engineering Materials*, Trans Tech Publications, 1997, vol. 144, p. 63-74
[7] F. Aymerich and S. Meili, “Ultrasonic evaluation of matrix damage in impacted composite laminates”, *Composites Part B: Engineering*, 2000, 31(1), p. 1-6
[8] J. Summerscales (Ed.), “Non-destructive testing of fibre-reinforced plastics composites”, *Springer Science & Business Media*, Vol. 2, 1990
[9] X. E. Gros, “Revıew of NDT technıques for detectıon of low-energy ımpacts ın carbon reınforcements”, *Sampe Journal*, 1995, 31(2), p. 29-34.
[10] S. L. Gao and J. K. Kim, “Three-dimensional characterization of impact damage in CFRPs”, *In Key Engineering Materials*, Trans Tech Publications, 1997, vol. 141, p. 35-54
[11] M. Uyaner and M. Kara, “Experimental study of the impact behavior of laminated composites stricken by sharp impactors”, *Science and Engineering of Composite Materials*, 2012, vol:3, p. 307-313
[12] D. Phillips, "*Image Processing in C*", 2000, Second Edition, ISBN 0-13-104548-2
[13] (2016) MathWorks web site. [Online.] Available: http://www.mathworks.com
[14] (2016) Wikipedia web site. [Online]. Available: https://en.wikipedia.org/wiki/Color_mapping
[15] S. Abrate, “*Impact on composite structures*” Cambridge university press, 2005

ICENS
INTERNATIONAL CONFERENCE ON ENGINEERING AND NATURAL SCIENCES
24-28 May 2016 /Sarajevo

A New Sigmoid Equation for Estimating the Point Load Index of Rocks

Zulfu Gurocak[1]

Abstract

In this study, relationships between corrected point load index ($Is_{(50)}$) with Schmidt hardness (N) and unit weight (□) of rocks were analyzed using simple linear, multiple regression analyses and feed forward-type ANN model. For this purpose, a total of 544 samples from different rock types were collected and laboratory tests carried out to create a data base. 80% of data sets from each rock type were selected randomly and were used for developing the models and remaining 20% were used as control data sets for validation of the models. Two regression models, namely, simple linear and multiple regressions, and one feed forward-type artificial neural network (ANN) model, namely, multi-layer perceptron network (MLPN) were developed. The $Is_{(50)}$ values were predicted using expressions obtained from the models, and then compared to the experimental $Is_{(50)}$ values. As a result of these analyses, the MLPN model was found to be the best model and a sigmoid equation was suggested based on ANN model to estimate the corrected point load index of rocks.

***Keywords**: Artificial neural network, Regression analysis, Point load index, Schmidt hardness, Unit weigh*

1. INTRODUCTION

Point load index (I_s) is an important parameter and used widely in rock mechanics applications to determine rock strength and strength anisotropy of rock materials, to estimate uniaxial compressive (σ_{ci}) and tensile strength (σ_t), as an input parameter for rock mass classifications. The I_s is determined by the point load test (PLT) which is an accepted rock mechanics testing procedure. The PLT has been used in geotechnical analysis for almost thirty years [1]. This test enables economical testing of core or lump rock samples in either a field or laboratory setting. The PLT involves the compressing of a shaped or irregular shaped rock sample between conical steel plates until failure occurs. The apparatus for this test consists of a rigid frame, two point load platens, a hydraulically activated ram with a pressure gauge and a device for measuring the distance between the loading points. The pressure gauge is designed to record the failure pressure. Then, the point load index (I_s) can be determined from an empirical equation.

Several researchers have used this test most widely to estimate uniaxial compressive strength and tensile strength of rock material [2], [3], [4], [5], [6], [7], [8], [9], [10], [11], [12], [13], [14], [15], [16], [17], [18], [19], [20], [21], [22], [23], [24], [25], [26], [27], [28], [29].

I_s was used as an input parameter in the Rock Mass Rating (RMR) classification system in case which the σ_{ci} cannot be determined [30], [31], [32]. Bieniawski [5] and Guidicini et al. [33] used to strength classification of rock material. Greminger [34] and Broch [35] used the I_s to investigate the strength anisotropy of rocks. The I_s was used as a parameter to estimate speed of tunnel boring machines [36] in tunneling and to classification of rocks excavatability [37], [38], [39], [40].

The focus of this paper is to investigate the possible correlation of Schmidt hardness (N) and unit weigh (γ) with the $I_{s(50)}$. For this purpose; sample collection, laboratory tests and statistical analyses were performed in the course of this study and different mathematical and artificial neural network (ANN) models were developed and evaluated. The outcomes of this study are expected to help rock mechanics engineers to estimate the I_s with other physical properties of rock namely, unit weight and Schmidt hardness given.

2. SAMPLING AND LABORATORY TESTS

To determine Point Load Index ($Is_{(50)}$), Schmidt hardness (N) and unit weigh (γ) of rocks, a total of 544 block samples from different rock types, igneous rocks (358 samples), metamorphic rocks (104 samples), and sedimentary rocks (82 samples), were collected from the study field (Eastern Turkey) and core samples were prepared from the block samples in laboratory with the ASTM standard [41].

The point load test (PLT) is carried out determination of the uncorrected I_s. It must be corrected to the standard equivalent diameter (D_e) of 50 mm. If the core being tested is nearly 50 mm in diameter, the correction is not necessary. Size correction can be performed graphically or mathematically, as outlined by the ISRM procedure [1]. The value for the uncorrected point load index (I_s) (MPa) is determined in accordance with ISRM [1] methods using following equation;

[1] Corresponding author: Firat University, Department of Geological Engineering, 23119, Elazig, Turkey. zgurocak@firat.edu.tr

$$I_s = \frac{P}{D_e^2} \quad (1)$$

In the Eq.1,

P = Failure load (MN), and

D_e = Equivalent core diameter (m).

Corrected point load index ($I_{s(50)}$) is calculated using equation 2.

$$I_{s(50)} = I_s . F \quad (2)$$

Where,

F = Size correction factor and it can be determined from equation 3.

$$F = \left(\frac{D_e}{50}\right)^{0.45} \quad (3)$$

Where,

D_e = Equivalent core diameter (mm) and

For diametric tests and axial tests De may be determined by Equations 4 and 5, respectively.

$$D_e^2 = D_e \quad (4)$$

$$D_e^2 = \frac{4.W.D}{\pi} \quad (5)$$

Where,

D = Diameter of sample; and

W = Width of sample.

In laboratory studies, the axial point load test was carried out on all cylindrical specimens. The size corrections were performed on samples with greater than 50 mm in diameter and calculated corrected point load index ($I_{s(50)}$) of rocks in accordance with the ISRM methods [1].

The results of the laboratory tests are presented in Table 1. It can be seen from Table 1 that the data are statistically significant with a standard deviation values ranging between 0.62 and 1.01.

The Schmidt hammer tests were conducted on rock samples in accordance ISRM [42] methods and L-type Schmidt hammer was used to determine Schmidt hardness of rocks in this study. A total of 10 impacts were performed to different points of the rock samples and the arithmetic average of the top five impacts was accepted as Schmidt rebound number of rock sample. The statistical results were given in Table 1. The Schmidt rebound number values of rocks are ranging between 44.00 and 58.00.

The unit weight (□) is defined as the per unit volume of the rock specimen. The unit weight of the core samples were determined according to ISRM [42] methods. The unit weight value is calculated by the equation 6.

$$\gamma = \frac{W}{V} \quad 5)$$

Where,

W = The weight of the rock sample, and

V = The volume of the rock sample.

The unit weights of the rock samples with statistical analyses results are presented in Table 1. The unit weight values of rock samples are ranging between 19.43 and 30.27 kN/m^3.

Table 16. A summary of statistical results of laboratory tests

Rock	**No.**	**Point Load Index, Is(50),**	**Schmidt Rebound Number,**	**Unit Weight,□□□(kN/m^3)**

Groups	Samples	MPa				N							
		Min	Max	Mean	St.dev	Min	Max	Mean	St.dev	Min	Max	Mean	St.dev
Igneous	358	3.71	9.70	6.02	1.01	49	58	51.22	2.86	19.43	30.27	27.22	2.08
Metamorphic	104	1.60	8.10	3.55	0.85	47	56	49.70	4.04	24.71	28.15	26.50	0.82
Sedimetary	82	1.14	6.25	3.49	0.62	44	53	48.84	1.56	21.76	27.07	26.01	0.99

3. DEVELOPMENT OF MODELS

In this study, simple linear and multiple regression models were developed. Furthermore, multi layer perceptron network (MLPN) of ANN models was developed.

80% of data points from each rock type were selected randomly and were used to generate the models and remaining 20% were used to control of prediction capacity of the models. The $I_{s(50)}$ values were predicted using expressions obtained from the models and then compared to the experimental $I_{s(50)}$ values. The coefficient of correlation (R^2) values were utilized as the basis of comparing the developed models as the goodness of fit.

3.1. Simple and Multiple Regression Models

Simple and multiple linear regression analyses were performed to investigate the relationships between $I_{s(50)}$ with □and N. The pairs of $I_{s(50)}$ □□□□and $I_{s(50)}$ – N were used in the simple regression analyses and the following equations obtained from the simple regression analyses are given in Table 2. Graphs of simple regression analyses were given in Figure 1.

Table 2. Expressions and determination coefficients (R^2) obtained from simple regression analyses

Equations	R^2	Equation Number
$Is_{(50)}$ = 0.516N-21.479	0.77	(7)
$Is_{(50)}$ = 0.819γ-17.188	0.61	(8)

As seen from Table 2, the simple linear model developed for the pairs of $I_{s(50)}$ - N had stronger correlations with R^2 = 0.77 value than the pairs of $Is_{(50)}$ - □(R^2 = 0.61).

Multiple regression analysis was evaluated to correlate the $I_{s(50)}$ with N and □ Following equation was found from the multiple regression analysis.

$$I_{s(50)} = 0.4N + 0.293\gamma - 23.43 \quad (R^2 = 0.81) \qquad (9)$$

It can be seen that the correlation obtained from multiple regression analysis was more significant than simple regression models with R^2 values of 0.77 and 0.61.The analysis of variance (ANOVA) results were given in Table 3. It can be seen from Table 3 that the R^2 value increased to 0.81.

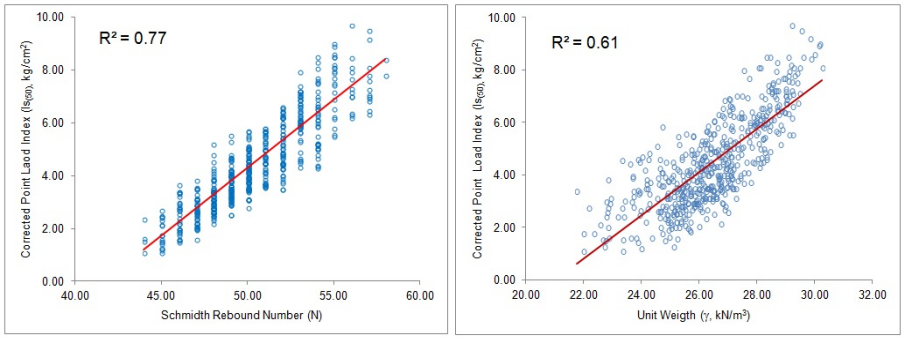

Figure 18. The relationships between $Is_{(50)}$ with N and γ

Table 3. Multiple regression model for the prediction of $Is_{(50)}$

Independent variable	Coefficient	St. error	t- value	Sig. level
Constant	-23.43	0.6108	-38.356	-24.632
N	0.400	0.0171	23.340	0.3664
γ	0.293	0.0311	9.404	0.2318

3.2. Artificial Neural Network Model

Multi-layer perceptron network (MLPN) is a feed forward-type ANN model was generated in this study using Statistica 8.0 [46] analyses computer programme. The MLPN is the most commonly used type of neural networks [43], [44], [45] and consists of multiple layers of nodes, a few hidden layers, and an output layer. Each layer of MLPN has one or more neurons which are linked with the neurons from the previous and the next layer.The values retrieved from the previous layer are summed up with certain weights, individual for each neuron, plus the bias term.

The weighted sums of input components are calculated using Equation 10.

$$S_j = \sum_{i=0}^{n} v_{ij} x_i - \theta_{ij} \tag{10}$$

Where;

S_j=The weighted sum of the j^{th} neuron for the input received from the previous layer with n neurons,

w_{ij}= The weight between the j^{th} neuron and the i^{th} neuron in the previous layer,

x_i=The output of the i^{th} neuron in the previous layer, and

θ_j= The intrinsic threshold that can be treated as an individual weight with a negative sign.

Once the weighted sum S_j is computed, the output of the j^{th} neuron y_j is calculated with a sigmoid function (Eq. 11).

$$y_i = f(S_j) = \frac{1}{1 + exp(-\eta S_j)} \tag{11}$$

Where,

η = a constant used to control the slope of the semi-linear region.

The sigmoid nonlinearity activates in every layer except the input layer.

In this study, Multi-Layer Perceptrons Network (MLPN) ANN model was generated in order to correlate relationships between parameters of I_s with □and N. A total of three nodes were used for each of the independent variables. To set the optimum model, the number of nodes in the hidden layers was found using a trial and error approach and all data was normalized using simple normalization method. Table 4 shows the values used in normalization.

Table 4. Input–output parameters and normalization values

Parameters	Range of Values		Normalization Values
	Min	Max	
$Is_{(50)}$, MPa	1.14	9.70	10
N	44	58	60
γ, kN/m^3	21.76	30.27	32

Afterwards, the MLPN model was developed with one hidden layer with six neurons. The R^2 value of the MLPN model was found to be as 0.84. The R^2 value is significantly better than the R^2 values of simple and the multiple regressions. A comparison between the experimental and predicted values of $I_{s(50)}$, obtained from the MLPN model was given Figure 2.

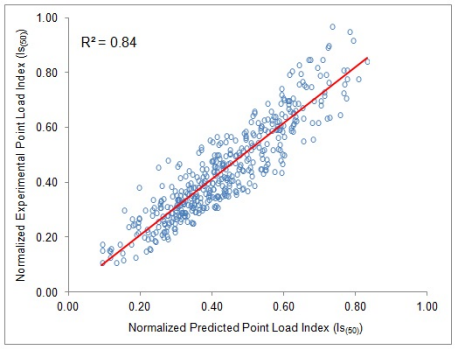

Figure 2. Comparison of experimental and predicted $Is_{(50)}$ for development dataset

To derive the formulation of the $I_{s(50)}$ was used the sigmoid function by utilizing the weight values obtained from the MLPN model [47]. The weights and bias values in the derivations of equations are given in Table 5.

The point load index ($I_{s(50)}$) can be calculated using following formulas:

$$I_{s(50)} = \frac{10}{1 + e^{\left(-\frac{32.46}{1+e^{-F_1}} - \frac{31.93}{1+e^{-F_2}} - \frac{14.78}{1+e^{-F_3}} - \frac{32.39}{1+e^{-F_4}} - \frac{31.59}{1+e^{-F_5}} + \frac{3.912}{1+e^{-F_6}}\right)}} \quad (12)$$

$$F_1 = -0.88\gamma - 3.677N \quad (13)$$

$$F_2 = -0.882\gamma - 3.658N \quad (14)$$

$$F_3 = -1.038\gamma - 2{,}704N \quad (15)$$

$$F_4 = -0.88\gamma - 3.675N \quad (16)$$

$$F_5 = -0.883\gamma - 3.645N \quad (17)$$

$$F_6 = 2.727\gamma - 0.561N \quad (18)$$

4. CONTROL OF PREDICTION CAPACITY OF THE MODELS

To evaluate the prediction capacity of the equations obtained from the multiple regression model and the MLPN model, the experimental $I_{s(50)}$ values were compared with the predicted $I_{s(50)}$ values using the control data set (Figure 3). It was found that the level of scatter in data points reduced and the MLPN model has better prediction capacity with $R^2 = 0.82$ than the multiple regression model with $R^2 = 0.79$. The results indicate that the MLPN model is satisfactorily capable of predicting the $I_{s(50)}$ values of the rocks in this study.

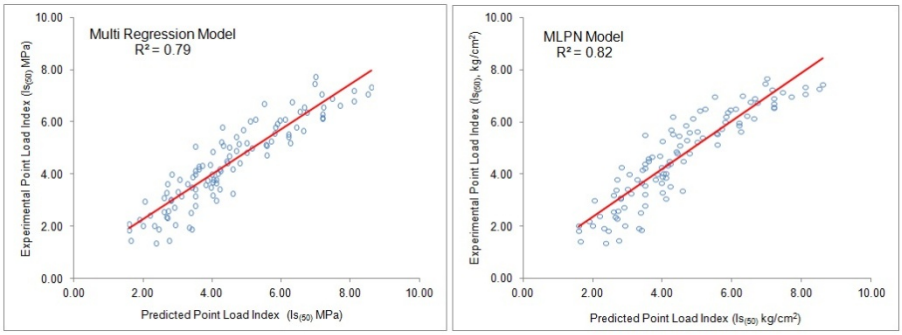

Figure 3. Comparisons of experimental and predicted $Is_{(50)}$ for control dataset.

5. CONCLUSIONS

In this paper, a total of two regression models, and a feed forward-type ANN model were developed to correlate relationships between point load index with Schmidt hardness and unit weight of rocks. The following results were obtained by the evaluation of models.

(1) The simple linear regression models developed between $I_{s(50)}$ with N and □ have the lowest R^2 value with 0.61 and 0.77. The R^2 value for the multiple regression model was found as 0.81. The value indicates that the multiple regression model has slight better than the simple linear regression model.

(2) The R^2 value of the MLPN model was found to be 0.84. Thus, this model appeared to be the best model developed and evaluated in this study. Moreover, MLPN was evaluated successfully using the control dataset and R^2 value was found as 0.82. This model has more prediction capacity then the other models.

(3) The sigmoid equation suggested using weight values obtained from the MLPN analyses can be used to predict corrected point load index of rocks. However, it should be specified that the sigmoid equation must be used to point load index of rocks which have same range of minimum, maximum and normalization values as used in this study.

ACKNOWLEDGMENT

The author would like to gratefully acknowledge the financial support provided by the Firat University Scientific Research Projects Unit of Turkey (Project No: FUBAP-2104).

REFERENCES

[1]. International Soil and Rock Mechanics (ISRM), "Suggested methods for determining point load strength," *Int J Rock Mech Min Sci Geomech Abstracts*, vol. 20(2), pp. 1985.
[2]. D. V. D'Andrea, R. L. Fischer and D. E. Fogelson, "US Department of the Interior Bureau of Mines," Report of Investigations 6702, 1-23, 1964.
[3]. D. U. Deere and R. P. Miller, "Engineering classification and index properties for intact rock," Air Force Weapons Lab. Technical report, Kirtland Base, New Mexico, AFWL-TR 65–116, 1966.
[4]. E. Broch and J. A. Franklin, "The point load strength test," *Int J Rock Mech Min Sci Geomech Abstract*, vol. 9, pp. 669-697, 1972.
[5]. Z. T. Bieniawski, "The point-load test in geotechnical practice" *Engineering Geology*, pp. 1-11, 1975.
[6]. J. R. L. Read, P. N. Thornten and W. M. Regan, "A rational approach to the point load test," *in: Proc of the 3rd Australian-New Zealand geomechanics conference*, 1980, pp. 35–39.
[7]. G. Wijk, "The point load test for the tensile strength of rock," *Geotechnical Testing Journal*, vol. 3, pp. 49-54, 1980.
[8]. D. P. Singh, "Determination of some engineering properties of weak rocks," *in: Akai K (ed) Proceedings of the international symposium on weakrock*, 1981, pp. 21–24.
[9]. K. L. Gunsallus and F. H. Kulhawy, "A comparative evaluation of rock strength measures," *Int J Rock Mech Min Sci*, vol. 21, pp. 233–248, 1984.
[10]. D. R. Norbury, *The point load test*, Site Investigation Practice Assessing BS 5930, Special Publication 2, pp. 325-329, 1986.
[11]. I. S. Cargill and A. Shakoor, "Evaluation of empirical methods for measuring the uniaxial compressive strength of rock," *Int J Rock Mech Mining Sci and Geomech Abstracts*, vol. 27, pp. 495-503, 1990.
[12]. D. K. Ghosh and M. Srivastava, "Point-load strength: an index for classification of rock material," *Bull Int Assoc Eng Geol*, vol. 44, pp. 27–33, 1991.
[13]. P. Grasso S. Xu and A. Mahtab, (1992) "Problems and promises of index testing of rocks," *in: Tillerson JR, Wawersik WR (eds) Proceedings of the 33rd US symposium on rock mechanics*, 1992, pp. 879–888.
[14]. K. T. Chau and R. H. C. Wong, "Uniaxial compressive strength and point load strength of rocks," *Int J Rock Mech Min Sci Geomech Abstracts*, vol. 33(2), pp. 183-188, 1996.
[15]. H. J. Smith, "The point load test for weak rock in dredging applications," *Int J Rock Mech Min Sci*, vol. 34 (3–4) p.702, 1997.
[16]. S. Kahraman, "Evaluation of simple methods for assessing the uniaxial compressive strength of rock," *Int J Rock Mech Min Sci*, vol. 38, pp. 981–994, 2001.
[17]. S. L. Quane and J. K. Russell, "Rock strength as a metric of welding intensity in pyroclastic deposits," *Eur J Min*, vol. 15, pp. 855–864, 2003.
[18]. G. Tsiambaos and N. Sabatakakis, "Considerations on strength of intact sedimentary rocks," *Eng Geol*, vol. 72, pp. 261–273, 2004.
[19]. V. Palchik and Y. H. Hatzor, "The influence of porosity on tensile and compressive strength of porous chalks rock," *Mech Rock Eng*, vol. 37(4), pp. 331-341, 2004.
[20]. I. Yilmaz and A. G. Yuksek, "An example of artificial neural network (ANN) application for indirect estimation of rock parameters," *Rock Mech. Rock Eng*, vol. 41(5), pp. 781-795, 2007.
[21]. I. Cobanoglu and S. B. Celik, "Estimation of uniaxial compressive strength from point load strength, Schmidt hardness and P-wave velocity," *Bull Eng Geol Environ*, vol. 67(4), pp. 491-498, 2008.
[22]. A. Kilic and A. Teymen, "Determination of mechanical properties of rocks using simple methods," *Bull Eng Geol Environ*, vol. 67(2), pp. 237-244, 2008.
[23]. R. Del Porto and M. Hurlimann, "A comparison of different indirect techniques to evaluate volcanic intact rock strength," *Rock Mechanics and Rock Engineering*, vol. 42(6), pp. 931-938, 2009.
[24]. K. Diamantis, E. Gartzos and G. Migiros, "Study on uniaxial compressive strength, point load strength index, dynamic and physical properties of serpentinites from Central Greece. Test results and empirical relations," *Engineering Geology*, vol. 108, pp. 199–207, 2009.
[25]. S. Kahraman and O. Gunaydin, "The effect of rock classes on the relation between uniaxial compressive strength and point load index," *Bull Eng Geol Environ*, vol. 68, pp. 345–353, 2009.
[26]. M. A. Jabbar, "Correlations of point load index and pulse velocity with the uniaxial compressive strength for rocks," *Journal of Engineering*, vol. 4(17), pp. 993-1006, 2011.

[27]. V. K. Singh, D. Singh and T. N. Singh, "Prediction of strength properties of some schistose rocks from petrographic properties using artificial neural networks," *Int J Rock Mec and Min Sci*, vol. 38, pp. 269–284, 2011.
[28]. Z. Gurocak, P. Solanki, S. Alemdag and M. Zaman, "New considerations for empirical estimation of tensile strength of rocks" *Engineering Geology*, vol. 145–146, pp. 1–8, 2012.
[29]. A. Kaya and K. Karaman, "Utilizing the strength conversion factor in estimation of the uniaxial compressive strength from the point load index. *Bull Eng Geol Environ*, vol. 75 (1), 341-357, 2016.
[30]. Z. T. Bieniawski, *Engineering rock mass classifications*, New York, USA: Wiley, 1989
[31]. E. Unal, *Modified rock mass classification: M-RMR System, Milestones in Rock Engineering: A Jubilee Collection*; *Z.T. Bieniawski*, Rotterdam the Netherlands: Balkema, 1996.
[32]. K. Karaman, A. Kaya, and A. Kesimal, "Use of the Point Load Index in Estimation of the Strength Rating for the RMR System," *Journal of African Earth Sciences*, vol. 106, pp. 40-49. 2015.
[33]. G. Guidicini, C. M. Nieble and A. X. Cornides, "Analysis of point load test as a method for preliminary geotechnical classification of rocks," *Bulletin of International Association of Engineering Geology*, vol. 7, pp. 37-52, 1973.
[34]. M. Greminger, "Experimental studies, of the influence of rock anisotropy on size and shape effects in point-load testing," *Int J Rock Mech Mining Sci and Geomech Abstracts*, vol. 19, pp. 241-246, 1982.
[35]. E. Broch, E "Estimation of strength anisotropy using the point load test," *Int J Rock Mech Mining Sci and Geomech Abstracts*, vol. 20, pp. 181-187, 1983.
[36]. S. McFeat and P. J. Tarkoy, "Assessment of tunnel boring, machine performance," *Tunnels and Tunnelling*, vol. 11(10), pp. 33-37, 1979.
[37]. J. A. Franklin, E. Broch and G. Walton, "Logging the mechanical character of rock," *Transactions of the Institution of Mining and Metallurgy*, vol. 80A, pp. 1–9, 1971.
[38]. R. N. Singh, B. Denby and I. Egretli, "Development of a new rippability index for coal measures excavations" in *proc. of the 28th U.S. Symposium on Rock Mechanics*, 1987, pp. 935–943.
[39]. J. Hadjigeorgiou and M. J. Scoble, "Ground characterization for assessment of ease of excavation," in: *Singhal, RK, Vavra M. (Eds.) proc. of the 4th International Symposium on Mine Planning and Equipment Selection*, 1990, pp. 323–331.
[40]. G. S. Pettifer and P. G. Fookes, "A revision of the graphical method for assessing the excavatability of rock," *Quarterly Journal of Engineering Geology*, vol. 27, pp. 145-164, 1994.
[41]. *Annual book of ASTM standards*, ASTM Std. 04:08-4543, 2000.
[42]. International Society of Rock Mechanics (ISRM), The complete *ISRM suggested methods for rock characterization, testing and monitoring: 1974-2006*, ISRM Turkish National Group, Ankara, Turkey, 2007.
[43]. D. Rumelhart and J. Mc Clelland, *Parallel distributed processing: explorations in the microstructure of cognition*, Cambridge United Kindom: Bradford books, MIT Press, 1986.
[44]. C. Bishop, *Neural networks for pattern recognition*, Oxford, Unite Kingdom: University Press, 1995.
[45]. S. Narayan, "Using genetic algorithms to adapt neuron functional forms," in: *Proc. Artificial Intelligence and Soft Computing*, 2002, p. 357.
[46]. StatSoft, Statistica (data analysis software system), version 8.0, 2008.
[47]. S. W. Liu, J. H. Huang, J. C. Sung and C. C. Lee, "Detection of cracks using neural networks and computational mechanics," *Computer Meth Applied Mechanics and Engineering*, vol. 191, pp. 2831-2845, 2002.

Using of SVM Sound Recognition Technique in Source Separation of Packaging Wastes: A New Approach for Reverse Vending Machines

Kemal Korucu[1], Ozgur Kaplan[2], Mehmet Kemal Gullu[3], Osman Buyuk[3]

Abstract

Reverse Vending Machines (RVMs) are used in recycling of packaging wastes. In this study, a sound recognition technique, which uses only cheap microphones, is used to identify the waste type.165 units of packaging wastes namely metal, plastic, glass and cardboard were used in this study. In order to generate sound, wastes were free fallen from a constant height. Generated sounds were recorded with dynamic and condenser microphones. For voice recognition studies, a model was developed by using Support Vector Machine (SVM) approach. Approximately 85% and 15% of the recordings were used in the trainings and tests, respectively. SVM model identified waste type with minimum classification accuracy of 85.7% (94.6% glass, 91.1% cardboard, 85.7% metal, 89.9% plastic) for dynamic microphone and 88.1% (94.6% glass, 90.5% cardboard, 88.1% metal, 92.3% plastic) for condenser microphone. According to results, it can be said that proposed new approach could provide a high separation performance for RVMs.

Keywords: *Packaging Waste, Solid Waste Management, Sound Recognition*

1. INTRODUCTION

Waste generation is decreased 4% in EU -27 countries and 12% in Turkey between 1995-2012 [1] but 2025 global waste generation levels are expected to double [2]. In Fig. 1, a general overview of Municipal Solid Waste (MSW) contents according to the income level of the countries are given. In low and lower-middle income countries, organic materials consists more than 50% of the total MSW generated. Sum of metals, glass, plastics and paper waste are 17%, 26%, 40% and 47% in low, lower-middle, upper-middle and high income countries, respectively. As the income level of the country increases, the proportion of metal, glass, plastic and paper wastes in total MSW also increase [3]. Low, lower-middle and upper middle income countries can be considered as developing countries [4, 5]. These developing countries try to reach developed country levels which could cause an increase in metals, glass, plastics and paper waste amounts. Improper handling of these wastes can create harmful environmental conditions. According to a World Economic Forum report [6], there would be more plastic wastes in the oceans then fish by 2050 which could adversely affect the sea life. These wastes are also valuable economic sources. The same report states that $80-120 billion valued plastic packaging waste is lost to the economy annually [6].

[1] *Kocaeli University, Umuttepe Campus, Engineering Faculty, Department of Environmental Engineering, Kocaeli, Turkey, kemal.korucu@kocaeli.edu.tr*

[1] *Corresponding author: Kocaeli University, Umuttepe Campus, Engineering Faculty, Department of Mechanical Engineering, Kocaeli, Turkey, ozgurkaplan1@gmail.com*

[3] *Kocaeli University, Umuttepe Campus, Engineering Faculty, Department of Electronics and Communications Engineering, Kocaeli, Turkey, kemalg@kocaeli.edu.tr,*

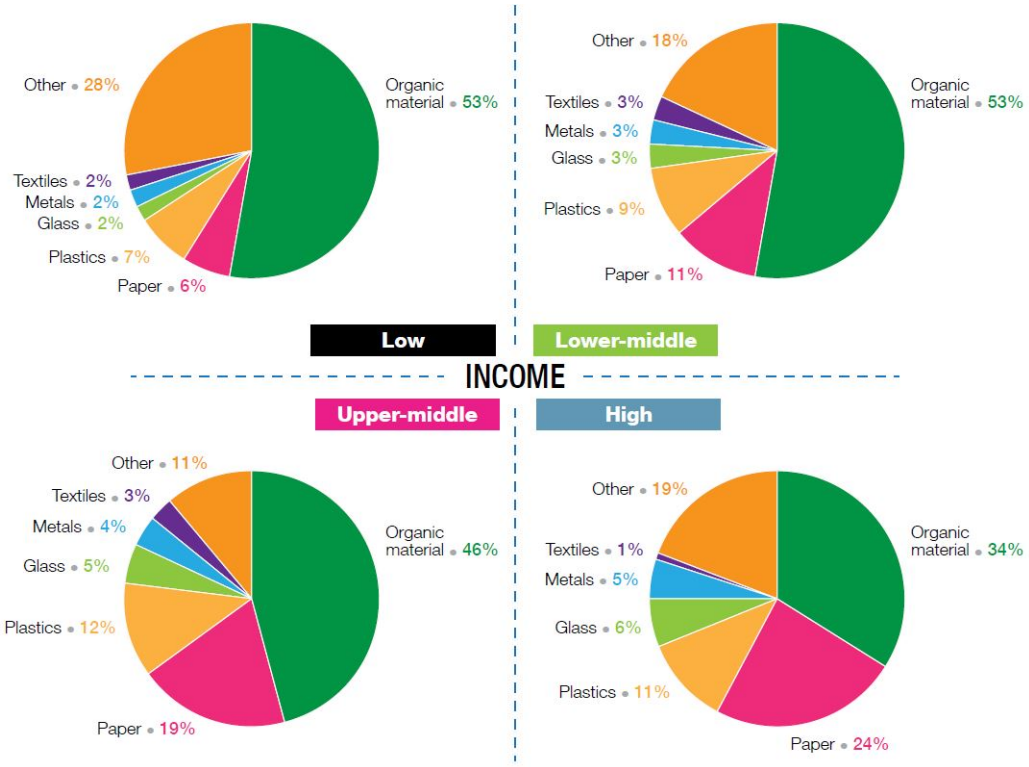

Figure 1. MSW content according to the income level of the countries [3]

The risk of contamination of recyclables is increased in mixed collection systems. This contamination reduces the marketing possibilities of the recyclables. Source separation of MSW can solve this problem as when recyclables collected separately, the risk of contamination from other sources decreases [7]. Reverse vending machines are used in the source separation of recyclables.

In this study, sound recognition technique is used as an identification tool for RVMs.

2. MATERIAL AND METHOD

Used metal, plastic, glass and cardboard wastes with different sizes such as big, medium and small were collected from student canteens in Kocaeli University Umuttepe Campus. In order to get accurate results, 5 various brand of every waste type were collected. Since wastes can be deformed when they are dumped, 3 different deformation conditions are created for every brand. Totally (11 waste type*5 brand*3 deformation condition) 165 unit of packaging wastes were collected. An experimental system which is available in Fig. 2 was built to generate sound from the wastes. In order to generate sound, the wastes were released from a 30 cm constant height. Generated sounds were recorded with dynamic and condenser microphones. Considering the experimental conditions, total number of recordings recorded during the study can be calculated as 330 (165 waste*2 microphones).

In the classification studies, 13 MFCCs and their first order derivatives were extracted from the signals for each 25 ms time window with 10 msec overlapping. Therefore, 26 features were obtained for each window. Cepstral mean subtraction was applied to obtain final feature vectors. Training and testing of the SVM classifier were performed in MATLAB software using LibSVM library [8]. Parameters were determined by 10-fold cross validation. Approximately 85% of the recordings (286 records) were used in the trainings and 15% of them (44 records) were used in the tests.

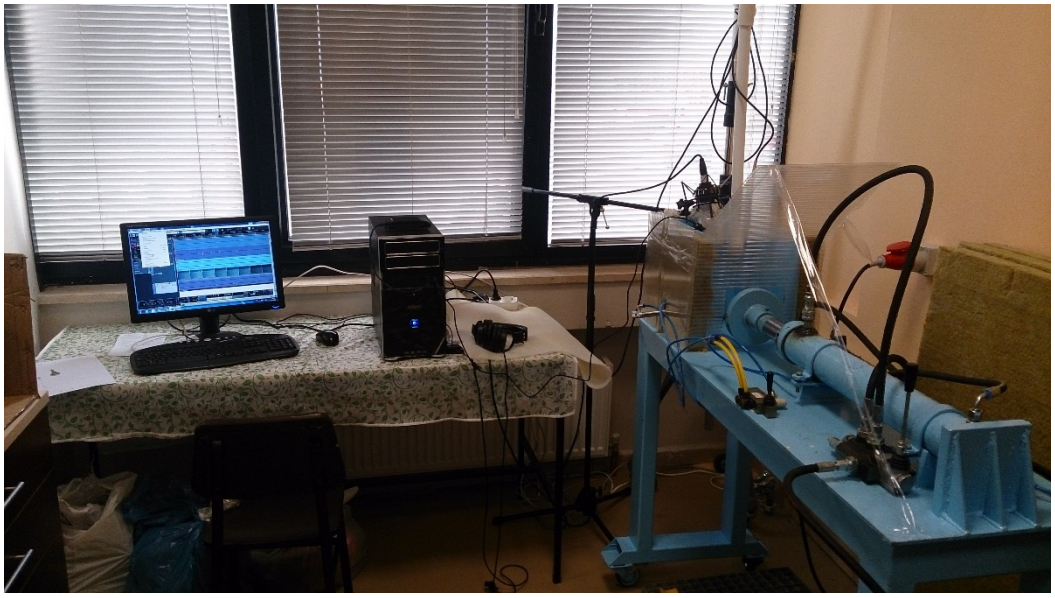

Figure 2. Experimental Setup

3. RESULTS AND DISCUSSION

SVM model identified the waste type with the minimum classification accuracy of 85.7% (94.6% for glasses, 91.1% for cardboards, 85.7% for metals and 89.9% for plastics) for dynamic microphone, and of 88.1% (94.6% for glasses, 90.5% for cardboards, 88.1% for metals and 92.3% for plastics) for condenser microphone which can also be observed in Table 1.

Table 17. Classification Efficiencies

Microphone Type	**Classification Efficiency (%)**				
	Minimum Classification Eff.	Glass	Cardboard	Metal	Plastic
Dynamic Microphone	85,7	94,6	91,1	85,7	89,9
Condenser Microphone	88,1	94,6	90,5	88,1	92,3

The results indicated that dynamic microphone could be used in the further studies since dynamic microphone is much cheaper than condenser microphone. But there are no ideal conditions available in real world waste management applications. In order to prevent that, different sound generation techniques should be investigated. According to the results, sound recognition technique can be used in waste type identification in reverse vending machines.

4. CONCLUSIONS

Recycling of recyclables is very important on both environmental and economic aspects. Reverse vending machines (RVMs) are used in the source separation of municipal solid wastes (MSW) and source separation of MSW is crucial for utilizing food waste and recycling. In this study, sound recognition technique is proposed as an identification tool for RVMs. Used metal, plastic, glass and cardboard wastes were collected. They were free fell from a constant height to a platform and the generated sounds were recorded. For sound recognition studies, a model was developed by using a Support Vector Machine (SVM) approach. It was found that the minimum classification accuracy for dynamic microphone and condenser microphone were 85.7% and of 88.1%, respectively. This results show that the proposed waste identification tool for reverse vending machines have high separation efficiency. More research is needed to commercialize this technique.

ACKNOWLEDGMENT

This study is financed by Kocaeli University Scientific Research Projects Unit. Authors of this article wish to express their gratitude to Mr. Berkan UZUN.

REFERENCES

[1]. Eurostat Pocketbooks, *Energy, Transport and Environment Indicators 2014 Edition*, Luxembourg, Eurostat, 2014.
[2]. D. Hoornweg, P. Bhada-Tata, What a Waste: A Global Review of Solid Waste Management. Urban development series; knowledge papers no. 15., Washington, DC., USA, World Bank, 2012.
[3]. D. C. Wilson, *Global Waste Management Outlook*, Vienna, Austria, International Solid Waste Association, 2015.
[4]. (2015) IAWP website. [Online]. Available http://www.iawp.org/joiniawp/countrylist.htm
[5]. (2015) Worldbank website. [Online]. Available http://data.worldbank.org/about/country-and-lending-groups#Low_income
[6]. Ellen MacArthur Foundation, *The New Plastics Economy Rethinking the Future of Plastics*, World Economic Forum, 2016.
[7]. T. Al Seadi, N. Owen, H. Hellström, H. Kang, *Source separation of MSW*, IEA Bioenergy, 2013.
[8]. Chang, C.C., Lin, C.J., 2011. LIBSVM: a library for support vector machines. ACM T. Intel. Syst. Tec. 2(3), 27

BIOGRAPHY

Özgür Kaplan is a research assistant in the mechanical engineering department of Kocaeli University, in Turkey. Özgür is studying for his Ph.D. in mechanical engineering, and his research interests are recycling of packaging materials, waste management and anaerobic digestion of municipal solid organic waste. He is collaborating with waste management professionals and academic researchers in his studies. Özgür received his M.Sc. in mechanical engineering from the department of mechanical engineering department in Kocaeli University, Turkey.

Evaluation of Commercial Type of Split Air Conditions by Using Condenser Waste Heat in a Boiler

Alper Ergun[1], Engin Gedik[1], Mehmet Ozkaymak[1], Bahtiyar Sansli[2]*

Abstract

Air conditioners are used for reducing the ambient temperature and they are manufactured in different versions. Especially, split type air conditioners are used widely. Because of increasing use of air conditioners, energy consumption has also increased, so researchers have attracted to search for production of more efficient air conditioners. The main objective of this study is to investigate thermal performance of the whole system. For this purpose, an experimental system was designed and manufactured by adding a boiler unit to the conventional split air conditioners condenser. At the end of the study, coefficient of performance (COP) of the system increased from 3.64 to 4.54. In addition, boiler which added to system increases degree of water from 10ºC to 40 ºC. When economical benefit is considered, electrical consumption is decreased 0.61 $ supposing that the device works 10 hours daily. Only 132.5 $ is paid for the device in addition to existing split air conditioners. Besides, domestic water at 40 ºC was produced.

Keywords: *Split air conditioner, boiler, energy efficiency, condenser.*

1. INTRODUCTION

Cooling is a technique that is decreasing the temperature of substance or local environment below the surrounding volume temperature [1]. Recently, local cooling has been popular in order to supply thermal comfort conditions. Besides, the devices that work according to the vapor compressing cooling cycle has used. Home type split air conditioners that work using vapor compressing cooling cycle phenomena has widely been used nowadays. According to the researches, energy in the world is consumed about 16% to 50% by cooling and heating systems in buildings [2]. Energy consumption of residential buildings is 30% of the total energy consumption in Turkey and 80% of this consumption is related to the heating and cooling systems [3-5]. Thus, it can be seen that energy which is used to perform home cooling and prepare domestic hot water is massive. Nowadays, there are many studies has been carried out to improve the performance of split type air conditioners Martinez et al. [6] covered the condenser unit of split type air conditioner with evaporative cooling pads that have various thicknesses and examined the energy performance of this system. Sumeru et al. [7] used an ejector as an expansion element in order to perform experiments and numerical analysis. Padalkar et al. [8] changed the HCFC-22 refrigerant to HC-290 of a split type air conditioner and determined the performance of this new refrigerant. Kumlutaş et. Al [9] performed heat and flow analysis in internal unit of split type air conditioner. Jie and Lee [10] placed a storage-enhanced heat recovery room into the split type air conditioner. They used a capillary tube and expansion valve in order to determine the system performance. Besides, [11] they used phase changed material in storage-enhanced heat recovery room and performed the analysis of modified system.

In this study, energy analysis were performed by adding boiler unite onset of the condenser unit in split type air conditioner that works with R-22 refrigerant.

2. MATERIAL AND METHODS

ın this study, split type air conditioner with boiler unit was designed and manufactured. The designed and produced system is shown in Figure 1. The system consists of compressor, evaporator, condenser, expansion valve and four way valve. The boiler unit was designed to prepare domestic hot water and placed in between condenser and four-way valve. Assembled boiler unit and built-in system can be seen in Figure 2.

* [1] *Corresponding author: Karabuk University, Faculty of Technology, Department of Energy Systems Engineering, 78050, Karabuk, Turkey.* alperergun@karabuk.edu.tr , egedik@karabuk.edu.tr, mozkaymak@karabuk.edu.tr
[2] *Karabuk University, Graduate School of Natural and Applied Sciences, 78050, Karabuk, Turkey,* bahtiyarsansli3535@gmail.com

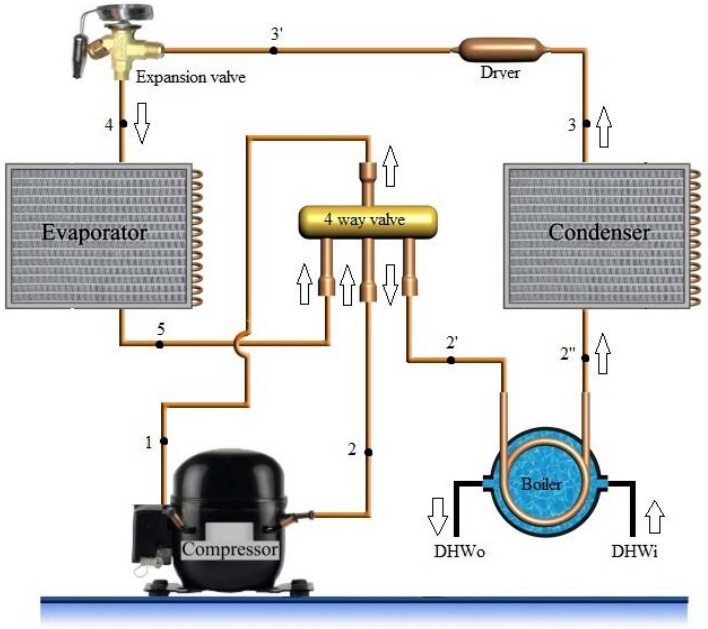

Figure 1. Design and manufactured system.

Figure 2. Designed boiler unit and assembled experimental setup

Designed boiler unit has 40 lt volume and 3/8" copper pipe with 18m length was placed in. boiler unit was covered with rubber isolation material that has 1cm thickness to prevent loosing of temperature. In the unit, 0.15 gr refrigerant was added for each 1 m pipe length

When high pressured refrigerant as superheated steam exited from outlet of the compressor, the heat of refrigerant is transferred to water in boiler unit instead of atmosphere air. The heat was sent to the boiler unit water when the condensation pressure was about 4.5-5 bar. At this stage, there was no need to work condenser fan. If this heat transfer is higher than boiler capacity, condenser fan started. This system works with a thermostat that opens at 55°C and closes at 35°C to regulate condenser unit properly. When the refrigerant transferred its heat, the refrigerant was accomplished its cycle by passing expansion valve and evaporator. The system can be by-passed using boiler valves. Thus, the analysis can be performed with and without boiler unit in terms of comparison between both designs.

3. THERMODYNAMIC ANALYSIS OF SYSTEM

The coefficient of performance was calculated for boiler and without boiler conditions. Energy balance of steady-flow condition can be determined as follow;

$$q_{net} - w_{net} = \Delta h + \Delta ke + \Delta pe \quad (1)$$

Here, q_{net} and w_{net} are described heat and work input, Δh, Δke and Δpe are impressed changing of enthalpy, kinetic energy and potential energy respectively. The changing of kinetic and potential energies can be neglected. Thus, steady-flow energy equation on a unit-mass basis reduces to;

$$(q_i - q_o) + (w_i - w_o) = h_0 - h_i \quad (2)$$

In equation 2, q, w and h are the heat, work and enthalpy respectively while i and o describe the subtitle of input and output.

Compressor work, condenser load and evaporator load were calculated related to energy equations. Energy transfer was not occurred because of the fact that there wasn't any enthalpy changes in expansion valve. When the loss of pressure in fittings equipment and loss of heat in pipes were ignored, the equation of conservation of energy principle can be expressed as follow;

$$W_{comp} + Q_{evap} = Q_{cond} \quad (3)$$

From this equation, compressor work, evaporator and condenser load can be calculated as follows;

Compressor work;

$$\dot{W}_{comp} = \dot{m}(h_2 - h_1) \quad (4)$$

Condenser load;

$$\dot{Q}_{cond} = \dot{m}(h_2 - h_3) \quad (5)$$

Evaporator load;

$$\dot{Q}_{evap} = \dot{m}(h_5 - h_4) \quad (6)$$

The most crucial parameter that determines the performance of vapor compressing cooling cycle is coefficient of performance (COP) and it can be calculated as follow;

$$COP = \frac{\dot{Q}_{evap.}}{\dot{W}_{comp.}} = \frac{h_5 - h_4}{h_2 - h_1} \quad (7)$$

The power of system (P) can be calculated as follow;

$$P = U \times I \quad (8)$$

In there, U is the voltage of the device (220V) and I is the current.

All the calculations were performed both boiler and without boiler unit conditions and analyzed.

4. RESULT AND DISCUSSION

The results were classified into two parts, both boiler and without boiler unit conditions. According to the inlet and outlet temperatures of each devices, the enthalpy values have been obtained from the thermodynamic tables of R-22 working fluid. Thermodynamic properties and energy values of both boiler and without boiler unit is given in Table 1 and Table 2 respectively.

Table 1. Thermodynamic properties and energy values for non-boiler unit condition

Point	Component	Temperature (°C)	Pressure (Bar)	Mass flow rate (kg/s)	Enthalpy (kj/kg)	Q (kW)
1	Compressor inlet	14	4.8	0.05151	415.777	21.4167
2	Compressor outlet	98	22	0.05151	459.992	23.6942
2'	Condenser inlet	95	22	0.05151	457.26	23.5535
3	Condenser outlet	43	21	0.05151	253.682	13.0672
3'	Expansion valve inlet	43	21	0.05151	253.682	13.0672
4	Expansion valve outlet	6	4.5	0.05151	253.682	13.0672
4'	Evaporator inlet	6	4.5	0.05151	253.682	13.0672
5	Evaporator outlet	12	4.5	0,05151	414.913	19.6572

Table 2. Thermodynamic properties and energy values for boiler unit condition

Point	Component	Temperature (°C)	Pressure (Bar)	Mass flow rate (kg/s)	Enthalpy (kj/kg)	Q (kW)
1	Compressor inlet	12	4.5	0.03878	414.913	16.089
2	Compressor outlet	90	22	0.03878	452.289	17.5383
2'	Boiler inlet	90	22	0.03878	452.289	17.5383
2"	Boiler outlet	43	21	0.03878	405.618	15.7286
2"	Condenser inlet	43	21	0.03878	405.618	15.7286
3	Condenser outlet	35	19	0.03878	243.101	9.42668
3’	Expansion valve inlet	35	19	0.03878	243.101	9.42668
4	Expansion valve outlet	4	6	0.03878	243.101	9.42668
4’	Evaporator inlet	4	6	0.03878	243.101	9.42668
5	Evaporator outlet	8	4	0.03878	413.048	16.0167

Compressor work, evaporator load and condenser load for boiler and non-boiler unit conditions are given in Table 3 by the helping of Table 1 and Table 2 data.

Table 3. Compressor work, evaporator load and condenser load for boiler and non-boiler unit conditions.

Device	W_{comp}	Q_{cond}	Q_{evap}
Boiler	1.449321	8.11164	6.59
Non-Boiler	1.807201	8.32085	6.59

The energy graphics of equipment of boiler and non-boiler unit conditions are shown in Figure 3.

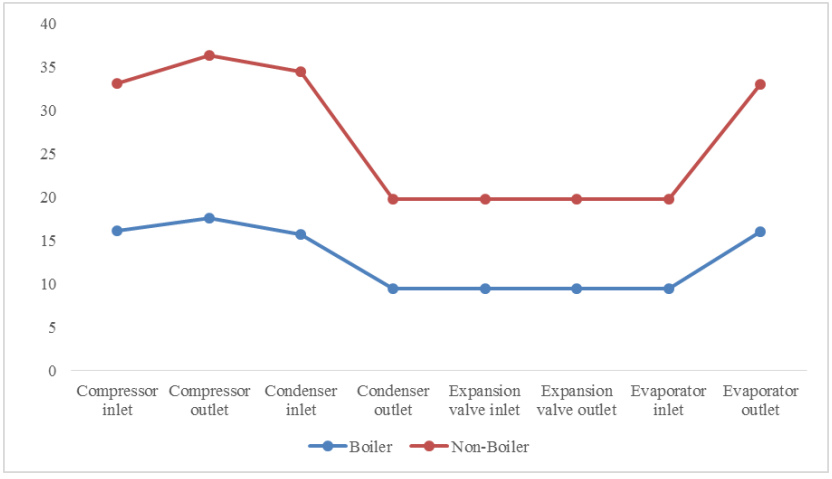

Figure 3. Energy graphics for Boiler and Non-Boiler unit conditions

COP values and operating currents for both conditions are given in Table 4.

Table 4. COP values and currents of systems

Device	COP Values	Current (A)
Boiler	4.54	8
Non-Boiler	3.64	10

It was determined that designed system with boiler unit operated 2A less current what it is compared with the system without boiler unit. From equation 8, it can be calculated that the power of system was decreased about 0.44kW. When the cost of electricity was taken into account, the electricity kW per an hour is 0.139 $ and it can be seen that if the designed system works during 10 hours per a day, the cost of electricity will decrease about 222.04$ per a year.

Moreover, designed system with boiler produce 40°C domestic hot water. When the boiler with 50LT consumes 1.5kW electricity per a day, it can be calculated that designed system with boiler has profits about 75.34$ per a year.

5. CONCLUSIONS

In this study, the boiler unit system was added to split type air conditioner with R22 refrigerant and the experimental results were analyzed thermodynamically. The results can be listed as follows;

Using the boiler unit, the COP of the system was increased from 3.64 to 4.54.

Compressor work and condenser load were decreased using boiler unit. Thus, the more efficient working condition was obtained.

The operating current was decreased about 2A by means of boiler system.

City water entered the boiler system about 10°C and exited from boiler about 40°C. Thus, domestic hot water at 40°C was produced without another energy sources.

The consumed electricity of the system was decreased and the cost of electricity about 296.48$ as well.

ACKNOWLEDGMENT

The authors would like to thank the Karabük University Scientific Research Projects Unit, Karabük/TURKEY for providing the financial supports for this study under the KBÜ-BAP- 16/1-YD-021 project

REFERENCES

[1]. T. Menlik, A. Demircioğlu, and M.G. Özkaya, "Energy and Exergy Analyses of R22 and its Alternatives R407c and R410a in a Vapor Compression Refrigeration System", *Journal of Exergy*, vol. 12 (1), pp. 11-30, 2013.
[2]. R. Saidur, H.H. Masjuki and M.Y. Jamaluddin, "An application of energy and exergy analysis in residential sector of Malaysia", *Energy Policy*, vol. 35, pp. 1050–1063, 2007.
[3]. A. Ergün, T. Menlik, T. and M.G. Özkaya, "Energy and Exergy Analyses of the Heating System in a Multipurpose Building", *Gazi Journal of Engineering Science*, vol. 1, pp. 195-218, 2015.
[4]. A. Ergün, T. Menlik, T. and M.G. Özkaya, "First and Second Law Analysis of Central Cooling System of a Multipurpose Buildings", *International Symposium on Innovative Technologies in Engineering and Science*, vol. 12(A) pp. 1974-1983, Karabuk Turkey. 2014.
[5]. A. Ergün, "Energy and Exergy Analyses of a Shopping Center Which Needs 80.000 M^2 Heating and Cooling", Master Thesis, Gazi University Graduate School of Natural and Applied Sciences, Ankara, 2010.
[6]. P. Martínez, J. Ruiz, C.G. Cutillas, P.J. Martínez, A.S. Kaiser and M. Lucas, "Experimental study on energy performance of a split air-conditioner by using variable thickness evaporative cooling pads coupled to the condenser", *Applied Thermal Engineering*, In press (doi: 10.1016/j.applthermaleng.2016.01.06.) 2016.
[7]. K. Sumeru, S. Sulaimon, H. Nasution and F. N. Ani, "Numerical and experimental study of an ejector as an expansion device in split-type air conditioner for energy savings", *Energy and Buildings*, vol. 79, pp. 98–105. 2014.
[8]. A. S. Padalkar, K.V. Mali and S. Devotta, "Simulated and experimental performance of split packaged air conditioner using refrigerant HC-290 as a substitute for HCFC-22", *Applied Thermal Engineering*, vol. 62, pp. 277-284, 2014.
[9]. D. Kumlutaş¸ Z. H. Karadeniz and F. Kuru, "Investigation of flow and heat transfer for a split air conditioner indoor unit", *Applied Thermal Engineering*, vol. 51 pp. 262-272, 2013.
[10]. J. Jia and W.L. Lee, "Experimental investigations on the use of capillary tube and thermostatic expansion valve in storage-enhanced heat recovery room air-conditioner", *Energy and Buildings*, vol. 101, pp. 76–83, 2013.
[11]. J. Jia and W.L. Lee, "Experimental investigations on using phase change material for performance improvement of storage-enhanced heat recovery room air-conditioner", *Energy*, vol. 93 pp. 1394-1403, 2015.

ICENS
INTERNATIONAL CONFERENCE ON ENGINEERING AND NATURAL SCIENCES
24-28 May 2016 /Sarajevo

Analysis of Seasonal Solar Energy: A Case Study for Osmaniye, Turkey

B. Yaniktepe[1], O. Kara[1], C. Ozalp[1], I. Aladag[1]

Abstract

Nowadays, solar energy has taken a significant place in many industries and application areas in terms of photovoltaic cell and supplying energy to natural processes like photosynthesis. As one of the most important renewable energies, solar energy has certain accessibility in many parts of the world such as building thermal systems and photovoltaic across the world. This study focuses on the variability (changeability) of the seasonal global solar radiation over the area of Osmaniye (37.05 N, 36.14 E, and 120 m.) is located in the Eastern Mediterranean region in Turkey. Solar radiation data were measured during June 2012–June 2015 period from the five-minute recorded by using the meteorological measurement device (vantage PRO2) installed at the University of Osmaniye Korkut Ata. The seasonal solar energy potential (assumed winter period (November-January) and summer period (June-August)) in Osmaniye is evaluated by using the actual measurements data according to the averaged values of hourly, daily, monthly and yearly. As a result of this measurement, on an annual scale the maximum global seasonal solar radiation changes from 7.33 kWh/m^2-day by June in 2013 (for summer) to 2.47 kWh/m^2-day by November in 2014 (for winter). Minimum global seasonal solar radiation changes from 6.03 kWh/m^2-day by August in 2014 (for summer) to 2,00 kWh/m^2-day by January in 2013. Yearly average energy potential during the measurement period was 1.63 kWh/m^2-day by December in 2012 (for winter).

Keywords: *Seasonal Solar Radiation, Solar Energy, Photovoltaic, Osmaniye*

1. INTRODUCTION

Energy is essential to economic and social development and improved quality of life in Turkey, like other countries. Much of the world's energy, however, is currently produced and consumed in ways that could not be sustained if technology were to remain constant and if overall quantities were to increase substantially. The need to control atmospheric emissions of greenhouse and other gases and substances will increasingly need to be focused on efficiency in energy production, transmission, distribution and consumption in the country. On the other hand, electricity supply infrastructures in Turkey, as in many developing countries, are being rapidly expanded, as policymakers and investors around the world increasingly recognize electricity's pivotal role in improving living standards and sustaining economic growth. But, in the coming decades, global environmental issues could significantly affect patterns of energy use around the world, as in Turkey. Any future efforts to limit carbon emissions are likely to alter the composition of total energy related carbon emissions by energy source in the country [1].

Solar energy is the portion of the sun's energy available at the earth's surface for useful applications, such as exciting electrons in a photovoltaic cell and supplying energy to natural processes like photosynthesis. It is vital, free, clean and abundant in most places throughout the year and is important especially at the time of high fossil fuel costs and degradation of the atmosphere by the use of these fossil fuels. Solar energy includes two main parts; extraterrestrial solar energy which is above the atmosphere and global solar energy which is under the atmosphere. The global solar energy incident on a horizontal surface may have direct beam and diffuse solar energy. Pyranometers generally measures diffuse solar radiation whereas pyrheliometer measures a direct beam solar radiation [2].

Although modeling is an economical and essential tool for the estimation of solar radiation, the accuracy of such models depends on long-term measurements of the data used. Though less accurate, modeling is a better tool for the predicting of solar radiation at locations where measurements are unavailable but have similar climatic conditions to the measured location [3].

The renewable energy market has grown rapidly in the last decade. In particular, electricity production by solar energy is promoted in many countries and is considered to be a strategic objective for governments. Increasing interest in solar energy has made photovoltaic (PV) systems a promising alternative as a conventional energy sources. For this reason, the demand for appropriate equipment to test PV systems has been on the rise. The output power of PV systems is directly affected by solar radiance and temperature. The testing of early solar equipment, such as inverters and maximum power point trackers (MPPTs), was possible under real weather conditions because of the low power of these old systems [4].

The literature search showed that energy applications and predicting radiations of solar were studied by several researchers [5, 7]. The present study is to evaluate the seasonal solar energy potential (assumed winter period (November-January) and summer period (June-August)) in Osmaniye.

*[1] Corresponding author: Osmaniye Korkut Ata University, Department of Energy Systems Engineering, 80000, Osmaniye, Turkey. byaniktepe@osmaniye.edu.tr

2. PLACE AND MEASUREMENT

Osmaniye is located in the eastern Mediterranean region of Turkey. Its coordinates are 37.05 north latitude and 36.14 east longitude. The altitude is 120 m above the sea level. And as can be seen from the figure 1, distance from the Mediterranean Sea is 20 km. Solar radiation values were experimentally measured with meteorological measuring device which is called Vantage Pro2 Weather Stations and experimental set-up is located at the building of Department of Energy Systems Engineering (Figure 2) of Osmaniye Korkut Ata University. Measuring device was set up 20 m from the ground level and measured actual global solar radiation data on horizontal surface in five-minute time interval for three seasonal years. The temperature, humidity, pressure, wind direction and speed, solar radiation, rains were measured. Its resolution and range are 1 W/m^2, 0 to 1800 W/m^2 respectively and nominal accuracy is 5% of full scale [5].

Figure 1. Location of Osmaniye

Figure 2. Location of measuring device at Osmaniye Korkut Ata University

From five minutes time period solar radiation data set, hourly, daily, monthly and yearly radiation data were calculated in order to obtain how much solar energy with photovoltaic (PV) will be produced in Osmaniye.The monthly averages of daily global solar radiation for about 3 year's seasonal period (assumed winter period (November-January) and summer period (June-August)) between June 2012 and June 2015 are shown graphically in Table 1. Moreover, Fig. 3 indicate also that the daily mean and maximum solar radiation are generally higher values in summer (June-July-August), whereas comparatively lower values in winter months (November-December-January). The monthly averaged values of global solar radiation were ranged from higher values of 7,10 kWh/m^2-day to lower values of 1,63 kWh/m^2-day in 2012, 7,33 kWh/m^2-day to lower values of 2,00 kWh/m^2-day in 2013, and 7,08 kWh/m^2-day to lower values of 2,02 kWh/m^2-day in 2014 and 6,74 kWh/m^2-day to lower values of 2,09 kWh/m^2-day in 2015.

Table 1. Measured Data for seasonal period

	Years			
	2012	**2013**	**2014**	**2015**
June	7,10	7,33	7,08	6,74
July	7,03	7,08	6,44	-
August	6,68	6,49	6,03	-
November	2,53	2,04	2,47	-
December	1,63	2,16	2,02	-
January	-	2,00	2,18	2,09

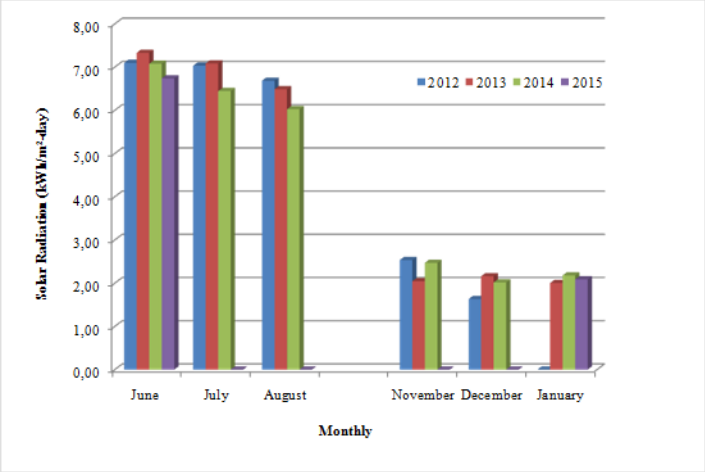

Figure 3. Monthly averages of daily solar radiation on horizontal surface for seasonal period

Table 2 shows the comparison between our measured data from the year of 2012 to the year of 2015 and solar energy potential map (GEPA-Ministry of Energy). The results also concluded that the four year average data seems to be nearly the same of GEPA.

Table 2. Compared between Measured Data and GEPA for seasonal period

		2012-2015	***GEPA[8]***
Summer	June	7,06	6,67
	July	6,85	6,41
	August	6,40	5,88
Winter	November	2,35	2,34
	December	1,94	1,81
	January	2,09	1,96

3. CONCLUSIONS

This study aimed to identify the seasonal energy potential of Osmaniye in Turkey. Average solar energy potential in summer is 6,77 kWh/m2-day while the average solar energy in winter is 2,12 kWh/m2-day. Likewise, the average value of GEPA in summer and in winter are 6,32 kWh/m2-day and 2,03 kWh/m2-day respectively. As a result, Osmaniye province has a considerable solar energy potential to produce electricity from photovoltaic such as irrigation, lightening and thermal process such as absorption cooling, heating water etc.

REFERENCES

[1]. K. Kaygusuz, Energy situation, future developments, energy savin ʒ, and energy efficiency in Turkey. Energy Sources vol.21, pp. 405–16, 1999.
[2]. J. Kreider, F. Kreith, Solar energy handbook. New York: McGraw-Hill; 1981.
[3]. L.E. Akpabio, S.O. Udo, S.E. Etuk, Modeling Global Solar Radiation for a Tropical Location: Onne, Nigeria. Turk J.Phys vol.29, pp. 63-68, 2005
[4]. H. Can, Model of a photovoltaic panel emulator in MATLAB-Simulink. Turkish Journal of Electrical Engineering & Computer Sciences, vol.21, pp.301-308,2013.
[5]. B. Yanıktepe & A. Genç, Establishing new model for predicting the global solar radiation on horizontal surface, International Journal of Hydrogen Energy vol. 40, pp. 15278-15283, 2015.
[6]. S. AlYahya, M. A. Irfan, Analysis from the new solar radiation Atlas for Saudi Arabia. Solar Energy, vol.130, pp.116-127, 2016.

[7]. Y. El Mghouchi, A. El Bouardi, Z. Choulli, T. Ajzoul, Models for obtaining the daily direct, diffuse and global solar radiations. Renewable and Sustainable Energy Reviews, vol.56, pp. 87-99, 2016.
[8]. GEPA, 2016, Güneş Enerjisi Potansiyel Atlası,http://www.eie.gov.tr/MyCalculator/Default.aspx (E.T: 27.04.2016)

ICENS
INTERNATIONAL CONFERENCE ON ENGINEERING AND NATURAL SCIENCES
24-28 May 2016 /Sarajevo

Determination of P (MMA-comb-AN) Comb-Type Copolymer Monomer Reactivity Ratios

Guzin Pihtili[1], Kadir Demirelli[2]

Abstract

Poly(MMA-comb-AN) comb-type copolymers was synthesed by Free Radical Polymerization. The comb-type copolymers include acrylonitrile unit (AN) were analyzed by FT-IR, 1H-NMR and 13C NMR spectroscopies. The conversion of the synthesized comb type copolymer were calculated from 1H-NMR spectrum. The monomer reactivity ratios of Methylmethacrylate macromonomer (MMA macromonomer) and acrylonitrile (AN) were computed using Kelen-Tudos (K-T) and Fineman-Ross (F-R) methods. Kelen-Tudos and Finemann Ross parameters (K-T and F-R) was calculated from the initial monomer ratio and utilizing the polymer monomer ratios. And its monomer reactivity ratios were found to be r1 = 0.58, r2 = 0.20; r1=0.61, r2 =0.32, respectively (r1 is monomer reactivity ratio of MMA macromonomer)

Keywords: *Comb-type copolymer, monomer reactivity ratio, Kelen-Tüdös and Finemann Ross*

1. INTRODUCTION

During the past decade, comb-type copolymers have attracted about their unique properties in polymer chemistry. This polymers is special copolymers with many branches grafted to a polymer backbone [1]. It can be named as “Brush-type copolymer. Comb-type copolymer consist of a linear backbone with a high grafting density of side chains and main polymer chain [2,3,4,5-10]. Total molar mass of com-type polymers, are determined with backbone length, grafting density, and side chain lengths.

A copolymer’s composition is an important factor in the estimation of its advantage [11] Reactivity ratios are in the most significant parameters for the composition of copolymers. Because they can offer information about copolymer composition and monomers units dispersion [11,12,13]. The monomer reactivity ratios must be known to calculate the polymerization rate and copolymer composition [14,15]. So, for the calculation of the monomer-reactivity ratios, the mathematical procedure of experimental information on the composition of copolymers and monomer in polymerization [16].The molar basis of copolymer composition must be known for the determination monomer reactivity ratios(r1 and r2). The most fundamental quantities characterizing a copolymer is its on a, which eventually is using preferably 1H-NMR spectroscopy [16,17,18]. Reactivity ratio can be calculated by linear procedures, nonlinear procedures, [19,20]. The method for determined of reactivity ratio are classified as Alfrey, san Roman and Madruga, Mayo &Lewis, Fineman and Ross (F-R) , Kelen-Tudos (K-T). This method is the widely used for copolymers [19,21].

In this work, a series of copolymer systems were prepared include acrylonitrile (AN) monomer and methylmethacrylate macromonomer units. Thus, this paper describes synthesis of polymers prepared by free radical copolymerization of MMA macromonomer and AN copolymer series, to determine monomer reactivity ratios of MMA-AN copolymer series, and characterization of the copolymers with FTIR, 1H,13C-NMR. 1H-NMR spectroscopic analysis has been established as a powerful tool for the estimation of copolymer composition [22]. So, the determination of monomer reactivity ratios of the monomers by 1H-NMR spectroscopy. Determined for the copolymerization monomer reactivitiy using the Finemann–Ross (F-R) and Kelen-Tudos (K-T) methods.

2. MATERIALS AND METHODS

2.1. Materials

Methylmethacrylate monomer, acrylonitrile (AN) (Aldrich) were distilled under vacuum before use. 2,2Azobisisobutyronitrile (AIBN), CuBr, methacryloyl chloride, tetrahydrofuran (THF), and ethanol (Fluka) were used without further purification.

2.2. Measurements

Infrared spectra (IR) of comb-type copolymer were recorded on a Perkin-Elmer Spectrum One FTIR spectrometer.^{1}H NMR spectra were obtained on a AVANCE III 400MHz Bruker, using $CDCl_3$ as the solvent and tetramethylsilane as an internal standard.

[1] *Corresponding author: Tunceli University, Pertek Sakine Genç Vocational School Department of Food Processing, 62500, Tunceli, Turkey.* gpihtilil@tunceli.edu.tr

[2]*Department of Chemistry, Science Faculty, 23100, Elazig, Turkey.* kdemirelli@firat.edu.tr

2.3. Free Radical Copolymerization of P(MMA-comb-AN)

Methylmethacrylate macromonomer (MMA macromonomer) was prepared according to method described in [23]. MMA macromonomer and AN were solved in 1,4-dioxane (4 mL) in the asset of AIBN. MMA macromonomer and acrylonitrile monomer, AIBN and the solvent were mixed in a polymerization tube. The mixture was passed for about 10 min. with argon and kept in a thermostated oil bath at 60°C. The copolymers were precipitated into excess ethanol and purified by reprecipitation, and then the copolymers were dried at 40°C for 24h. Polymerization was shown in *Figure 2*. The conditions of copolymerization was as in *Table 1*.

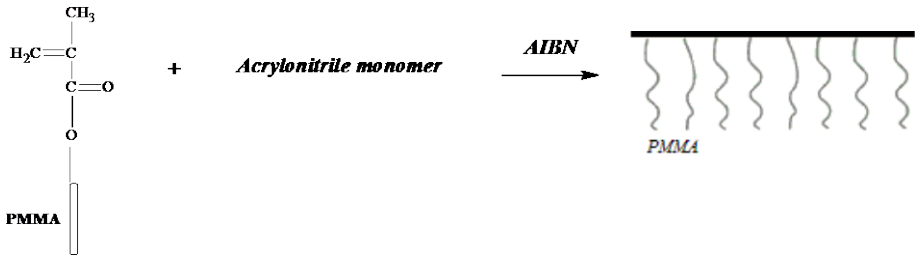

Figure1. Synthesis of comb-type copolymer

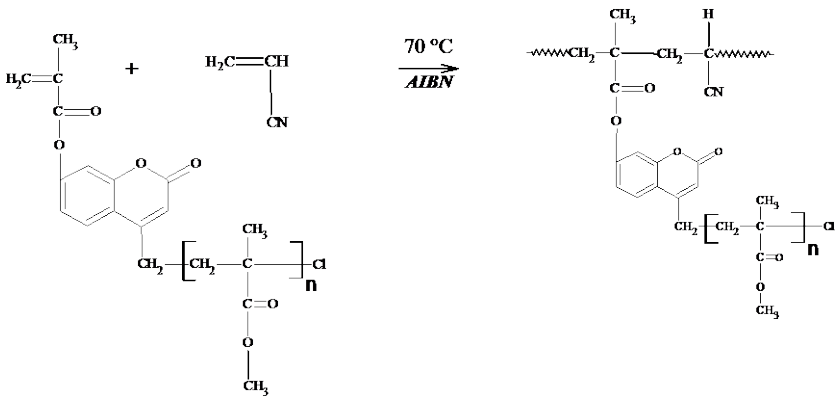

Figure 2. Synthesis of P(MMA-comb-AN

Table 1. Conditions of polymerization

MMA : AN (mol)	Macromonomer (g)	Acrylonitrile (g)	AIBN (g)	Time (hour)	Temperature (°C)
1:5	0,5	0,02	0,0005	96	70
1:20	0,5	0,09	0,0006	96	70
1:50	0,5	0,2	0,007	96	70
1:70	0,5	0,3	0,0085	96	70
1:100	0,5	0,4	0,009	96	70

3. RESULTS AND DISCUSSION

3.1. Analyses

FT-IR analysis is a dynamic technique for chemical compounds. This technique gives knowledge about the strength of the bonds of the compound. We get more information by ^{1}H-NMR and ^{13}C-NMR. The structure of copolymer synthesized was characterized by FT-IR, ^{1}H-NMR and ^{13}C-NMR spectroscopy.

The FT-IR and ^{1}H-NMR spectra of P(MMA-comb-AN) were shown in Figures 3 and 4, respectively. According to IR spectrum; the bands at 2995 - 2940 cm^{-1} are aliphatic C-H stretching vibration, the peak at 2243-2242 cm^{-1} are C≡N stretching vibration, and the strong band at 1730 cm^{-1} is assigned to the vibration of ester carbonyl (–C(=O)–O–C) in MMA group. The other peaks, 1497 and 1367 cm^{-1} are due to the aliphatic C-H bending vibration. ^{1}H NMR spectra of polyP(MMA-comb-AN) showed important signals at 6.91–6.25 ppm aromatic protons, signals at 3.66 ppm –OCH_3 in MMA unit, the signals, 1.1–2.2 ppm, are due to the C≡N linked CH protons (with aliphatic protons) and the signals at 2,2 - 0,6 ppm are CH_2 and CH_3 protons in the main chain and side groups. The ^{13}C NMR spectrum illustrated in Figure 5 of the comb-type copolymer. The most characteristic peaks of the monomeric units at 177.5 ppm ester carbonyl (C=O) in MMA units, 54.41 ppm –OCH_3 in MMA units, between 45.08 and 44.54 ppm about CH_2 carbon in the main chain, the signals at 18.94-16.4 are assigned to CH_3 carbon in side chain.

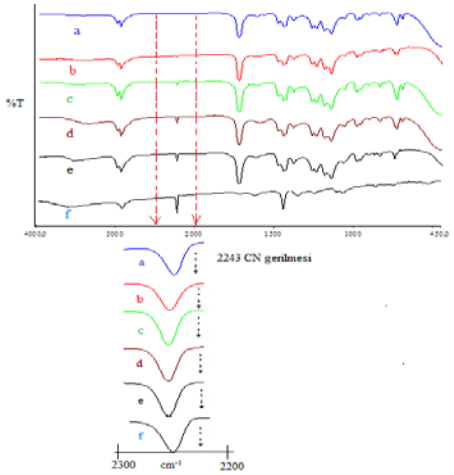

Figure 3. IR spectrum ofa) P(MMA-comb-AN%10), b) P(MMA-comb-AN%15), c) P(MMA-comb-AN%26), d) P(MMA-comb-AN%31), e) P(MMA-comb-AN%63), f) PAN

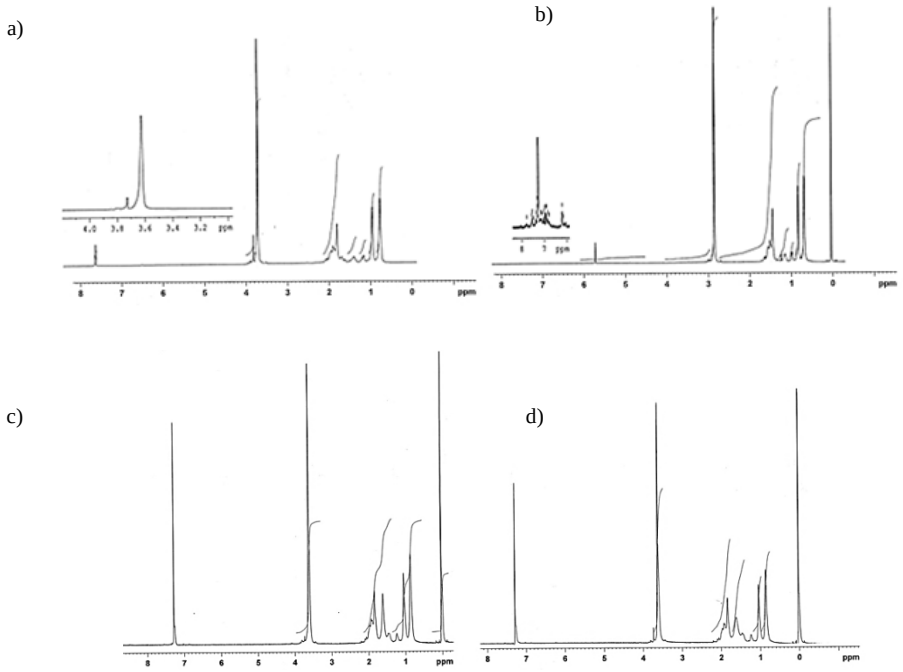

e)

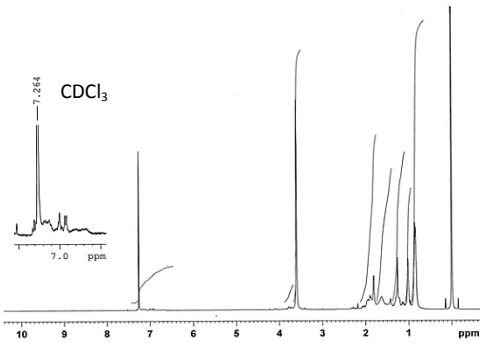

Figure 4. ^{1}H-NMR of a) P(MMA-comb-AN%10), b) P(MMA-ko-AN%15), c) P(MMA-comb-AN%26), d) P(MMA-comb-AN%31), e) P(MMA-comb-AN%63) ($CDCl_3$)

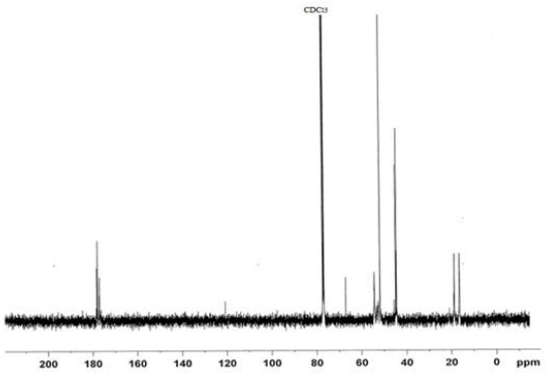

Figure 5. ^{13}C-NMR spectrum of P(MMA-comb-AN%31) ($CDCl_3$)

3.2. Determination of Copolymer Composition by ^{1}H NMR

The 1H NMR technique is well established as a simple rapid, and accurate method for the determination of copolymer composition [16,17,18]. The appointment of the resonance peaks in the ^{1}H-NMR spectrum allows the correct assessment of the content of each kind of monomer incorporated into the copolymer chain.Thus, the mole fraction of MMA in the copolymer chains was calculated from integrated intensities of OCH_3 protons of MMA macromonomer and aliphatic protons of AN. The comb-type copolymer compositions can be obtained using Equation (1):

$$C = \frac{Integral\ heights\ of\ the\ -OCH3\ protons}{Integral\ height\ of\ aliphatic\ protons} = \frac{3m1}{5m1+3m2} \quad (1)$$

$$m_1 + m_2 = 1$$

Where; m_1 is the mole fraction of the MMA macromonomers and m_2 is the mole fraction of AN. Table 2 gives the value ofmole fraction of MMA macromonmer on the comb-type copolymers.

Table 2. Initial and experimental data of MMA macromonomer in copolymer compositions

Comb-type copolymers [a]	M_1 [b]	*Intensity of OCH_3 protons*	*Intensity of aliphatic protons*	m_1 [c]
1	0,9	11.44	20,28	0,9
2	0,74	3	5,52	0,85
3	0,57	2	4,03	0,74
4	0,5	1	2,1	0,69
5	0,4	3	10,8	0,37

a: Conditions of polymerization; FRP at 70˚C. b: mole fraction of MMA macromonomer in feed; c: mole fraction of MMA macromonomer in copolymer

3.3. Monomer Reactivity Ratio

The free radical copolymerization of MMA macromonomer and acrylonitrile monomer (AN) initiated AIBN for various ratios of AN has been synthesized 70°C. Table 2 shows initial and experimental data of MMA macromonomer in comb-type copolymer compositions for free radical copolymerization [24, 16].

The copolymer composition is an important step for its estimation. The copolymer composition based on monomer reactivity ratios- r6. This property can offer the information of the relative reactivity of comonomers. [24, 25-27]. Determine of the comb-type copolymer compositions monomer reactivity ratios were by ^{1}H-NMR spectra. Monomer reactivity ratios of the comb-type copolymer series were evaluated by the methods of Fineman-Ross [22, 28] (F-R), Kelen-Tudos [22, 29] (K-T). The K–T and F–R parameters were calculated, using data in Table 2, and the results were summarized in Tables 3.

Kelen Tudos [24, 30, 31] equation was used, which is "$\eta = (r_1 + r_2/\alpha)\xi - r2/\alpha$." And for the Fineman–Ross [24, 30, 32,] was used "$G = r_1H - r_2$. ". We can see the notation descriptions and the calculation results in Table 3. In Figure 6 " ξ " it was plotted against the Kelen-Tudose parameters " η". To determine the reactivity ratios via Finemann-Ross method, F-R parameters passed to the graph "*G versus*" to "*H versus*" in Figure. 7.

Table 3.Kelen-Tudos (K-T) and Fineman-Ross (F-R) parameter for the comb-type copolymer

Comb-type copolymer	*$F=M_1/M_2$*	*$f=m_1/m_2$*	*$G=F(f-1)/f$*	*$H=F^2/f$*	*$\eta= G/(\alpha+H)$*	*$\xi=H/(\alpha+H)$*
1	12,8	9	11,3	18	0,54	0,86
2	3,08	5,6	2,53	1,7	0,5	0,37
3	1,42	2,8	0,91	0,62	0,26	0,18
4	1	2,22	0,54	0,45	0,16	0,13
5	0,66	0,58	-0,44	0,75	-0,12	0,1

M_1 = Mole fraction of MMA macromonomer in feed; M_2 = mole fraction of AN in feed, m_1 = mole fraction of MMA macromonomer in copolymer, m_2 =mole fraction of AN in copolymer. $(H_{min}\ H_{max})^{1/2}$ =2.84, H_{min}: lowest value of H, H_{max}: highest value of H.

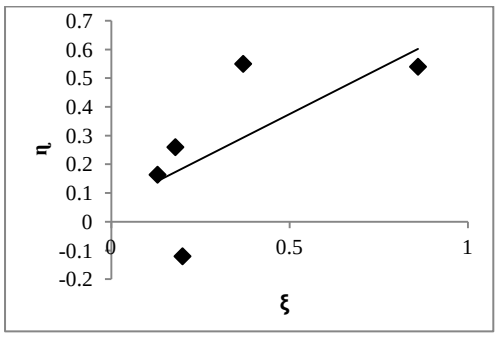

Figure 6. Kelen–Tüdös plots for the free radical polymerization of MMA macromonomer and Acrylonitrile monomer

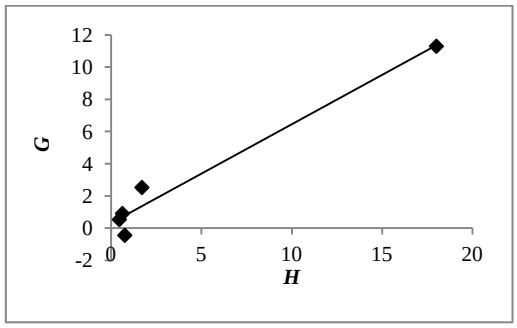

Figure 7. Finemann-Ross plots for the free radical polymerization of MMA macromonomer and Acrylonitrile monomer

Using this equation of graphics (Fig.6 and 7); from the slope and intercept, the monomer reactivity ratios of MMA macromonomer (r_1) and AN (r_2) were calculated. According to K-T and F-R metod; the monomer reactivity ratios of MMA macromonomer and AN found to be r_1 = 0.58, r_2 = 0.20; r_1=0.61, r_2 =0.32, respectively. We can see this value in Table 4. The

monomer reactivity ratio of MMA macromonomer is higher than that of AN. These results suggest that MMA macromonomer is more reactive than AN. Distributions of the monomeric units along the copolymer chains are sequential.If $r_1.r_2 < 1$ and $r_1.r_2$ are close to zero, this implies that monomers tend to form alternating copolymers [11, 33]. At this results $r_1.r_2$ is very much less than 1 suggesting that the system shows strong alternating tendency.

Table 4. Monomer reactivity ratios obtained by Kelen- Tudos and Fineman–Ross methods

System	*Metod*	r_1	r_2	$r_1.r_2$	
MMA Macromonomer-AN	*K-T*	*0,58*	*0,20*	*0,12*	
F-R	*0,61*	*0,32*	*0,19*		

4. CONCLUSIONS

P(MMA-comb-AN) comb-type copolymers were prepared by free radical polymerization. Characterization was made by ^{1}H, ^{13}C-NMR, and FT-IR. Determination of comb-type copolymer composition was made by ^{1}H-NMR. When acrylonitrile ratio increases, the spectrum has also increased the intensity of the peak. To be found copolymers composition by ^{1}H-NMR as; P(MMA-*comb*-AN 0,10), P(MMA-*comb*-AN 0,15), P(MMA-*comb*-AN 0,26), P(MMA-*comb*-AN 0,31), P(MMA-*comb*-AN 0,63). The monomer reactivity ratios for MMA macromonomer-AN system were calculated from the feed composition and copolymer composition. The monomer reactivity ratios were calgulated using Kelen-Tudos (K-T) and Fineman-Ross (FR) methods and were found to be $r_1 = 0.58$, $r_2 = 0.20$; $r_1 = 0.61$; $r_2 = 0.32$, respectively (r_1 is monomer reactivity ratio of MMA macromonomer). The distribution of the units along the copolymer chain in the AN series are considered to be consecutive.Prefer not to participate in other types of monomers from your own types.

ACKNOWLEDGMENT

The authors thank the Firat University Research Fund for financial support of this Project (FUBAP-1135).

REFERENCES

[1] L. Zhang, H. Zeng, and Q. Liu, "Probing Molecular and Surface Interactions of Comb-Type Polymer Polystyrene-graft-poly(ethylene oxide) (PS-g-PEO) with an SFA", *The Journal of Physical Chemistry C*
vol. 116, pp. 17554–17552, July, 2012.
[2] M. Balcı, A. Allı, B. Hazer, O. Güven, K. Cavicchi, M. Cakmak, "Synthesis and characterization of novel comb-type amphiphilic graft copolymers containing polypropylene and polyethylene glycol" , *Polym. Bull.*, vol. 64, pp. 691-705, April, 2010.
[3] M-Q. Chen, T. Serizawa, M. Akashi, "Graft copolymers having hydrophobic backbone and hydrophilic branches. xvi. Polystyrene microspheres with poly(N-isopropylacrylamide) branches on their surfaces: size control factors and thermosensitive behavior", *Polym. Adv. Technol.* Vol. 10, pp. 120–126, 1999.
[4] S. Hiraoka, K. Harano, M. Shiro, M. Shionoya," A self-assembled organic capsule formed from the union of six hexagram-shaped amphiphile molecules", *J. Am. Chem. Soc.*,vol. 130, pp.14368–14369, 2008.
[5] N. Hadjichristidis, H. Iatrou, M. Pitsikalis, J. Mays, "Macromolecular architectures by living and controlled/living polymerizations", *Prog. Polym. Sci.*,vol. 3, pp.1068–1132, 2006.
[6] B. Wesslen, KB. Wesslen, "Preparation and properties of some water-soluble, comb-shaped, amphiphilic polymers", *J. Polym. Sci. A Polym. Chem.*, vol. 27, pp. 3915–3926, 1989.
[7] M. Zhang, A.H.E. Mueller, "Cylindrical polymer brushes", *J. Polym. Sci. A Polym. Chem.* vol. 43, pp. 3461– 3481, 2005.
[8] T. Pakula, Y. Zhang, K. Matyjaszewski, H-I. Lee, H. Boerner, S. Qin, GC. Berry,"Molecular brushes as super-soft elastomers", *Polymer*, vol. 47,pp. 7198–7206, 2006.
[9] JS. Katz, J. Doh, DJ. Irvine, "Composition-tunable properties of amphiphilic comb copolymers containing protected methacrylic acid groups for multicomponent protein patterning", *Langmuir*, vol.22, pp. 353–359, 2006.
[10] B. Lessard, M. Maric, " Nitroxide-mediated synthesis of poly(poly(ethylene glycol) acrylate) (PPEGA) comb-like homopolymers and block copolymers", *Macromolecules*, vol. 41, pp. 7870–7880, 2008.
[11] S. S. Al-Deyab, H. Mohamed El-Newehy, A. M. Al-Hazmi," Synthesis, Characterization and Reactivity RatioStudy of Poly(di(tri-n-butyltin) citraconate-co-N-vinylimidazole)", Molecules, vol. 15, pp. 4750-4756, 2010.
[12] S.S. Al-Deyab, A.M. Al-Hazmi,; M.H. El-Newehy , "Synthesis and characterization of organotin containing copolymers: reactivity ratio studies", Molecules, vol. 15, pp.1784–1797, 2010.
[13] I. Erol, O. Sen, A. Dedelioglu, C. Cifci, "Synthesis and characterization of novel fluorinecontaining methacrylate copolymers: Reactivity ratios, thermal properties, and antimicrobial activity", J. Appl. Polym. Sci., vol. 114, pp. 3351–3359, 2009.
[14] H. Mohamed El-Newehy, S. Salem Al-Deyab, A. M. Ali Al-Hazmi, "Reactivity Ratios for Organotin Copolymer Systems", Molecules, vol. 15, pp. 2749-2758, 2010.
[15] A. Habibi, E. Vasheghani-Farahani, M.A. Semsarzadeh, K. Sadaghiani, "Monomer reactivity ratios for lauryl methacrylate–isobutyl m thacrylate in bulk free radical copolymerization", Polym. Int., vol. 52, pp. 1434–1443. 2003.
[16] N. Ayaz, F. Bezgin, K. Demırellı," Polymers Based on Methacrylate Bearing Coumarin Side Group: Synthesis via Free Radical Polymerization, Monomer Reactivity Ratios, Dielectric Behavior and Thermal Stabilities", ISRN Polymer Science, vol. 2012, pp. 13, 2011.
[17] K.Rajendrakumar, R. Dhamodharan, "Ambient temperature atom transfer radical copolymerization of tetrahydrofurfuryl methacrylate and methyl methacrylate: reactivity ratio determination," European Polymer Journal, vol. 45, pp. 2685–2694, 2009.
[18] M. L. Houchin, E. M. Topp, "Physical properties of PLGA films during polymerdegradation," Journal of Applied Polymer Science, vol. 114, pp. 2848–2854, 2009.

[19] T. Abdul-Jaleel, W. Younis, "Reactivity Ratios of the Copolymerization Styrene/ Methyl Methacrylate Using FT-IR Spectroscopy with Comparing to Mathematically Method ", Baghdad Science Journal, vol. 9, pp. 695-702, 2012.
[20] C. Hou, C. Ji, L. Ying," Synthesis and Characterization of Maleimide –Co - Polymers with Pendant Benzoxazine Groups by Photo induced Radical Polymerization", J. Appl. Polym. Sci, vol. 103, pp. 3920–3923., 2007.
[21] S.R. Liu, B.X. Li, J.Y. Liu, Y.S. Li," Determination of Reactivity Ratios in the Copolymerizationof Phosphaalkene and Styrene", Polymer, vol. 51, pp. 1921- 1925, 2010.
[22] P.Pazhanisamy, B.S.R. Reddy, "Copolymers of N-cyclohexylacrylamide and n-butyl acrylate: synthesis, characterization, monomer reactivity ratios and mean sequence length", Express Polymer letters, vol. 1, pp. 391-396, 2007.
[23] G. Pıhtılı, G. Torğut, K. Demirelli, Gaziosmanpaşa University, 5th National Polymer Science and Technology Convention and Exhibition Event, Semp.Tokat, 2014.
[24] E. Kaya," Copolymers of 4 -Methoxybenzyl Methacrylate and Isobornyl Methacrylate: Synthesis, Characterization and Determination of Monomer Reactivity Ratios", J.Chem.Soc.Pak. vol 33, 555-561, 2011.
[25] V. Percec, B. Barboiu, H. J. Kim, Journal of theAmerican Chemical Society, vol. 120, pp. 305, 1998.
[26] H. Shinoda, P. J. Miller, K. Matyjaszewski, Macromolecules, vol.34, pp.3186, 2001.
[27] L. H. Yee, J. P. A. Heuts, T. P. Davis, Macromolecules, vol. 34, pp. 3581, 2001.
[28] M. Finemann, S.P. Ross, Journal of Polymer Science,vol. 5, pp. 259-262,1950.
[29] T. Kelen, F. Tüdös, Journal of Macromoleculer Science,vol. 15 pp. 3047-3074, 1975.
[30] F. Tüdös, T. Kelen, Journal of Macromolecular Science Chemical A, vol. 9, pp. 1, 1975.
[31] L. H. Yee, J. P. A. Heuts, and T. P. Davis, "Copolymerization propagation kinetics of dimethyl itaconate and styrene: strong entropic contributions to the penultimate unit effect,", Macromolecules, vol. 34, pp. 3581–3586, 2001.
[32] M. Fineman, S. Ross, Journal of Polymer Science - Polymer Chemistry Edition, 9, 1 (1975).
[33] Odian, G. "Principles of Polymerization", 3rd ed.; John Willy & Sons Inc.: New York, NY, USA, 1995.

Biography:I was born in Elazığ in 1983.In 2002, I started Firat University Faculty of Arts department of Chemistry. I graduated in 2006. I started master in 2007, and the doctora program in 2009. I finished this programme in 2013. I have been working in Tunceli University since 2014.

ICENS
INTERNATIONAL CONFERENCE ON ENGINEERING AND NATURAL SCIENCES
24-28 May 2016 /Sarajevo

Efficiency Evaluation of Crow Search Algorithm in Benchmark Functions for Optimization

Sinem Akyol[1*], Bilal Alatas[2]

Abstract

Metaheuristics algorithms are the algorithms that utilize a simple approach as a solution technique of search and optimization problems and are recently getting strong and becoming more popular due to their advantages. They are population based techniques and begin to search the solution with multiple points. They have good reputation and wide acceptability as being powerful tools for many different fields such as management science, engineering, computer, etc. and new versions of these algorithms have been proposed. Due to the philosophy of continually searching the best and absence of the most efficient metaheuristic algorithm for all types of problems, novel algorithms or new variants of current algorithms are being proposed. Crow Search Algorithm (CSA) is the most current nature inspired metaheuristic algorithm proposed in 2016 and based on intelligent behavior of the crows in obtaining better food sources. This paper explains the operators of CSA used in optimization and search problems and represents the comparative results obtained from current metaheuristic algorithms for different benchmark functions. CSA is one of the newest metaheuristic algorithm and there is only one work in the related literature. Although no optimization has been implemented for its parameters and no variants have been proposed, obtained results from the experiments are promising. CSA seems a simple and efficient global optimization algorithm that may efficiently be used in many complex search and optimization problems. Its variants with optimized parameters may be proposed for more efficient solutions in future works.

Keywords: *Crow Search Optimization, Global Optimization, Metaheuristic Algorithms.*

1. INTRODUCTION

Metaheuristic algorithms are the methods that utilize a simple approach as a solution technique of search and optimization problems and are recently getting strong and becoming more popular. They provide general solution strategies that can be applied to the problem in case of concurrent different decision variables, objective functions, and constraints and they do not depend on the solution space type, the number of decision variables, and the number of constraints. Furthermore, they do not require very well defined mathematical models that are hard to organize for system modeling and objective function. Their computation power is also good and they do not require excessive computation time. Their transformations and adaptations are easy. They give efficacious solutions to the high-scale combinatorial and non-linear problems.

These algorithms do not require the assumptions that are hard to be approved to adapt a solution algorithm to a given problem as done in classical algorithm. They do not require the alteration on the interested problem as done in the classical algorithms. They are adaptable in order to solve different types of search and optimization problems. Due to these advantages, these algorithms are densely being used in many different fields such as management science, engineering, computer, etc. Due to the philosophy of continually searching the best and absence of the most efficient metaheuristic algorithm for all types of problems, novel algorithms or new variants of current algorithms are being proposed [1, 2].

General purposed metaheuristic methods are generally classified in different groups like biological based, social based, music based, sports based, chemistry based, and physics based. There are also hybrid methods formed with these methods. Genetic Algorithm, Differential Evolution Algorithm, and Ant Colony Algorithm are biological based; Tabu Search is social based; Artificial Chemical Reaction Optimization Algorithm is chemistry based; Harmony Search Algorithm is musical based algorithms and models. Although there are many effective and successful methods that have been introduced to the literature, it is an important task for the science that there should be always effort to improve and search for the best. Also, there have not been any algorithm that can solve all types of problems effectively, often new algorithms are introduced and also improved versions of the introduced ones are proposed in order to improve their effectiveness. Especially in recent years, researchers have introduced such new metaheuristic methods to the literature and performed successful applications [3].

Crow Search Algorithm (CSA) is one of the newest population based metaheuristic algorithm and aims to simulate the intelligent behavior of the crows to find the solution of search and optimization problems [4]. CSA has been recently proposed and there is only one article introducing the CSA.

In this paper, the operators of CSA has been introduced and the comparative results obtained from other novel metaheuristic algorithms for different benchmark functions have been presented. In Section 2, CSA has been explained. Section 3 defines the benchmark functions used for comparisons. Section 4 presents the experimental results and finally Section 5 concludes the paper along with future research directions.

[1] *Corresponding author: Tunceli University, Department of Computer Engineering, 62000, Tunceli, Turkey.* sakyol@tunceli.edu.tr
[2] Firat University, Department of Software Engineering, 23119, Elazıg, Turkey. balatas@firat.edu.tr

2. CROW SEARCH ALGORITHM

Crows are considered to be among the world's most intelligent animals by showing remarkable examples of intelligence and scoring very highly on intelligence tests [4-6]. They can memorize faces, use tools, communicate in sophisticated ways, and hide and retrieve food across seasons [6]. Crows are greedy birds since they follow each other to obtain better food sources. CSA considers crows' living in a form of swarm, their capability of memorizing the position of their hiding places, their following each other to do thievery, and their protecting caches from being pilfered by a probability. Based on these explanations, the analogy between crows' behaviors and a population based metaheuristic algorithm can be summarized as shown in Table 1. The flow chart of CSA is demonstrated in Figure 1 [4].

Table 1. Analogy between crows and metaheuristic optimization

Crows	Metaheuristic Optimization
Crows	Search agents
Environment	Search space
Each position of the environment	Feasible solution
Quality of food source	Objective function
Best food source of the environment	Global solution

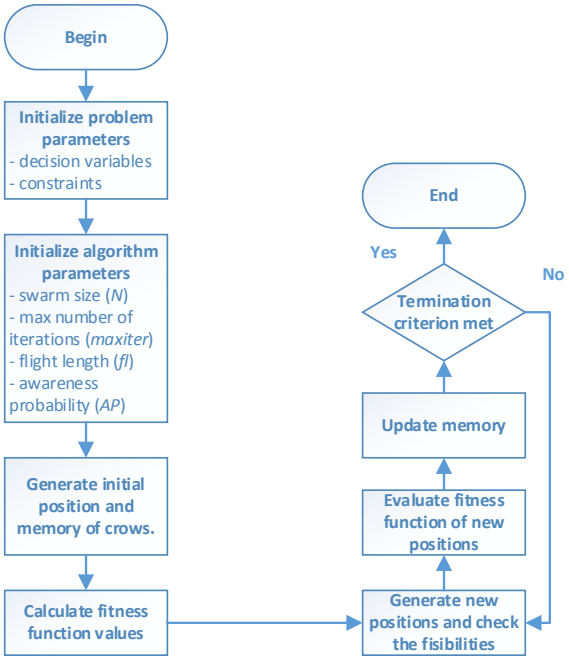

Figure 1. Flow chart of CSA

3. BENCHMARK FUNCTIONS

Benchmark test functions are used to evaluate and compare the characteristics of optimization algorithms in terms of convergence, precision, robustness, and general performance as a rule. The nature, complexity and other properties of these benchmark functions can be easily obtained from their definitions. The difficulty levels of most benchmark functions are adjustable by setting their parameters [7]. The selected benchmark functions and its properties have been demonstrated in Table 2. The dimensions for all functions have been determined as 30. Sphere function is unimodal with less complexity and it can be used to evaluate the converging behaviors of algorithms [8]. Rastrigin function is multi-modal function with many local optima and it can be used to test the global search ability of the algorithms in avoiding premature convergence [9].

Their graphs with two dimensions have been shown in Figure 2 and Figure 3.

Table 2. Benchmark functions

Function No	Function Name	Definition	Interval
1	Sphere	$f_1(x) = \sum_{i=1}^{n} x_i^2$	-5.12≤x_i≤5.12
2	Rastrigin	$f_2(x) = \sum_{i=1}^{n} (x_i^2 - 10cos(2\pi x_i) + 10)$	-5.12≤x_i≤5.12

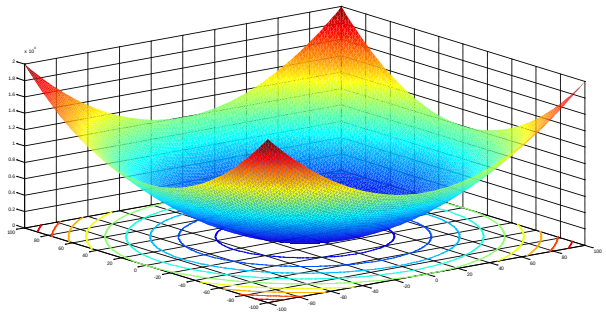

Figure 2. Sphere function with two variables

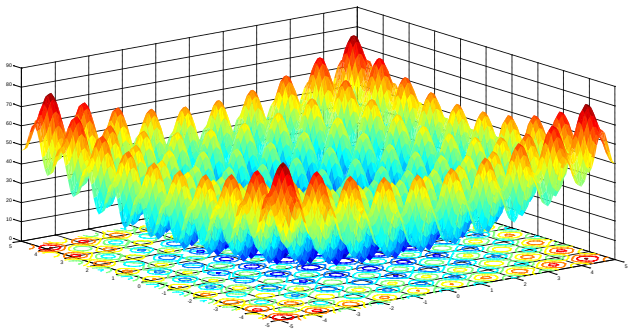

Figure 3. Rastrigin function with two variables

4. EXPERIMENTAL RESULTS

The obtained results from CSA for Sphere function has been compared with those obtained from other swarm based algorithms named, Artificial Bee Colony (ABC) algorithm and Firefly Algorithm (FA). The population size is 20 and the maximum iteration number is 100 for all of the algorithms. The dimension of Sphere function has been selected as 10. The results have been shown in Table 3. From these reported results, CSA has better performance than ABC and worse performance than FA in average.

Table 3. Obtained results for Sphere function

Ex. #	CSA	ABC	FA
1	7.0415E-11	2.1648E-05	2.9838E-20
2	1.6546E-09	8.1556E-05	4.4044E-20
3	1.7442E-09	1.3730E-04	1.8559E-20
4	9.2679E-10	3.5413E-05	3.5473E-20
5	2.5182E-10	1.6395E-05	2.0127E-20
6	3.1762E-10	1.1738E-05	2.4187E-20
7	6.4772E-10	2.5686E-05	2.8672E-20
8	3.5581E-09	2.0350E-05	3.1599E-20
9	5.5607E-10	7.1572E-05	3.8230E-20
10	3.4238E-10	4.1840E-05	3.3916E-20
11	5.3568E-10	5.4121E-05	2.6177E-20
12	1.7065E-09	5.1888E-05	3.5126E-20

13	1.8914E-10	5.8253E-05	4.9251E-20
14	4.7940E-10	4.6977E-05	3.5501E-20
15	5.0392E-10	4.7526E-05	2.9081E-20
16	2.8276E-10	3.1649E-05	1.6694E-20
17	1.0444E-09	4.3167E-05	2.2371E-20
18	1.7543E-09	5.7215E-05	3.1555E-20
19	6.1233E-10	8.2616E-05	2.7970E-20
20	4.2983E-10	3.6246E-05	2.3090E-20
21	1.3733E-09	2.2778E-05	1.4210E-20
22	9.3621E-10	1.6274E-04	2.4114E-20
23	1.3038E-09	4.0086E-05	2.1891E-20
24	1.5196E-09	7.9326E-05	1.9927E-20
25	2.7984E-10	4.0023E-05	2.9608E-20
26	3.6455E-09	4.0845E-05	3.8187E-20
27	1.0548E-09	2.6900E-05	4.3384E-20
28	1.0401E-10	3.9796E-05	2.5276E-20
29	2.3977E-10	6.8282E-05	1.5396E-20
30	2.7492E-09	3.2722E-05	2.4930E-20
Best	7.0415E-11	0.000011738	1.421E-20
Average	1.02713E-09	5.08885E-05	2.86128E-20

The obtained results from CSA for multi-modal Rastrigin function has also been compared with those obtained from ABC and FA. The population size is 20 and the maximum iteration number is 100 for all of the algorithms. The dimension of Rastrigin function has been selected as 10. The results have been shown in Table 4. The performance of CSA is worse than other used swarm based algorithms.

Table 4. Obtained results for Rastrigin function

Ex. #	CSA	ABC	FA
1	1.29E+01	21.0705	1.5919E+01
2	6.77E+01	29.8808	1.4924E+01
3	7.86E+01	23.8904	1.6914E+01
4	5.27E+01	18.2482	2.2884E+01
5	7.76E+01	22.6007	1.2935E+01
6	7.56E+01	23.2418	1.7909E+01
7	4.48E+01	27.8793	1.2935E+01
8	3.08E+01	34.4016	1.2935E+01
9	5.07E+01	28.1810	1.1940E+01
10	3.08E+01	26.6447	1.4924E+01
11	6.57E+01	30.5570	5.9698E+00
12	2.19E+01	23.8983	9.9496E+00
13	2.39E+01	33.3502	1.0945E+01
14	4.97E+01	34.0638	1.9899E+00
15	7.66E+01	26.9575	4.9748E+00
16	6.07E+01	32.9025	1.0945E+01
17	9.25E+01	18.2772	9.9496E+00
18	3.88E+01	27.6977	1.8904E+01
19	2.29E+01	32.5641	8.9546E+00
20	4.08E+01	27.7296	5.9697E+00
21	3.28E+01	22.3006	1.3929E+01
22	3.68E+01	25.1764	7.9597E+00
23	4.28E+01	32.7083	1.0945E+01
24	3.08E+01	25.9530	2.0894E+01
25	7.36E+01	30.3455	5.9698E+00
26	4.48E+01	29.6141	2.1889E+01
27	8.06E+01	33.0932	1.2935E+01
28	4.28E+01	29.8907	8.9546E+00
29	5.47E+01	37.9465	1.5919E+01
30	3.18E+01	35.2776	9.9496E+00

Best	12.93491495	18.2482	1.9899
Average	49.58221951	28.21142667	12.40381333

5. CONCLUSIONS

Metaheuristic optimization algorithms are efficient and robust in solving of high-dimensional and hard problems. Especially nowadays, swarm intelligence based algorithms become more popular. Due to the philosophy of continually searching the best and absence of the most efficient metaheuristic method for all types of problems, novel algorithms or new variants of current algorithms are being proposed. Crow Search Algorithm (CSA) is one of the newest population based metaheuristic algorithm and aims to simulate the intelligent behavior of the crows to find the solution of search and optimization problems. In this paper, CSA has been briefly described and its performance has been tested with another swarm based metaheuristics method, namely Artificial Bee Colony (ABC) and Firefly Algorithm (FA) for different types of benchmark functions. CSA is one of the newest metaheuristic algorithm and no optimization has been done for its parameters. Obtained results from unimodal function seem promising, however results from multi-modal function is worse. After proposal of new and efficient versions for CSA for global optimization algorithm it may be alternatively used in many complex search and optimization problems. Its variants containing multi objectivity, dynamic parameter selection, different initial population methods, different termination criterion, and its hybrids with other heuristic or metaheuristic methods may be proposed for efficient solutions as future works.

REFERENCES

[1]. S. Akyol and B. Alatas, "The Current Swarm Intelligence Optimization Algorithms", *Nevsehir Universitesi Fen Bilimleri Enstitusu Dergisi*, vol. 1, pp. 36-50, 2012.
[2]. S. Akyol and B. Alatas, "A New Field in Social based Computational Intelligence: Social Impact Theory based Optimization", in *1st International Conference on Engineering Technology and Applied Sciences ICETAS*, 2016.
[3]. S. Akyol and B. Alatas, "Fizik Tabanlı En Güncel Yapay Zekâ Algoritması "Elektromanyetik Alan Optimizasyonu"'nun Performansının İncelenmesi" (in Turkish), *1st International Conference on Engineering Technology and Applied Sciences ICETAS*, 2016.
[4]. A. Askarzadeh, "A Novel Metaheuristic Method for Solving Constrained Engineering Optimization Problems: Crow Search Algorithm", *Computers & Structures*, vol. 169, pp. 1-12, 2016.
[5]. P. Rincon, "Crows and Jays Top Bird IQ Scale", *Science/Nature*, BBC News, 2005.
[6]. Corvus (Genus). Available: https://en.wikipedia.org/wiki/Corvus_%28genus%29
[7]. B. Alatas, E. Akin and A. B. Ozer, "Chaos Embedded Particle Swarm Optimization Algorithms", *Chaos, Solitons & Fractals*, vol. 40, pp. 1715-1734, 2009.
[8]. (February 2016) GEATbx: Examples of Objective Functions. Available: http://www.pg.gda.pl/~mkwies/dyd/geadocu/fcnfun1.html
[9]. (February 2016) GEATbx: Examples of Objective Functions. Available: http://www.pg.gda.pl/~mkwies/dyd/geadocu/fcnfun6.html

BIOGRAPHY

Sinem Akyol: She received her BSc in Computer Engineering from Ege University, Turkey in 2009. She completed her MSc in Electrical and Electronics Engineering at Tunceli University. At present she is pursuing Ph. D. in Computer Engineering, Firat University, Turkey. She is a Research Assistant in the Department of Computer Engineering at the Tunceli University. Her research interests include social network analysis, data mining, and metaheuristic optimization.

Bilal Alatas: He received his B.S., M.S., and Ph.D. degrees from Firat University. He has been working as Head of Software Engineering Department at Firat University in Elazig, Turkey. His research interests include artificial intelligence, data mining, and metaheuristic computation. Dr. Alatas has published over 50 papers in many well-known international journals and proceedings of refereed conference since 2001. He has been editor of nine international journals and reviewer of twenty international journals.

Investigation of Wear Strength of Fly Ash Blended Polymer Materials

Ibrahim Gunes[1], Nezihi Sam[1], Tayfun Uygunoglu[2]*

Abstract

Polymermatrix composites are gaining in popularity because of theyhavesymmetricaland balancedmaterial properties, production and usedue tothe ease ofconstruction, aerospace and automotivestructures forbuildings. In addition, they do not conductelectricity and heat. Today,one ofthe newpolymeric materialsareepoxy based floorcoating or adhesive materialsfield.both is reducing the cost ofthe surfaceand increasesthestrength. One of the fillers is fly ash. In the study, mechanical, hardness, surface roughness, physical andchemical properties of polymer-based surface coating or adhesive materials that were producedusing fly ash was characterized. Wear tests were performed with pin-on-disc under conditions of dry friction, 5, 10, 15 and 30 N load, 0.3 m/s slip velocity and 500 m distance. According to the results, it was observed that fly ash powders can be used in the polymer based covering or adhesive material. In this way, both environmental pollution would be decreased by evaluation of fly ash which is an environmental problem in our region, and competitiveness of the country and region basis would be increased by improving of the quality of existing products.

Keywords: *Epoxy, fly ash, hardness, surface roughness, wear resistance.*

1. INTRODUCTION

The polymer composite material is usually composed of two components, i.e. matrix and filler called also reinforcement or more broadly dispersed phase; sometimes also additional compounds are used, mostly compatibilisers. The matrix, known also as continuous phase, integrates filler particles and allows also to shape products appropriately and determines most of physical and chemical properties of material. The dispersed phase is responsible for additional enhancement of selected material properties. While, the compatibiliser is added to increase interactions between matrix and filler what has significant impact on material cohesion and homogeneity, and as a result on its processing properties and strength [1].

Epoxy resins (EP) are a thermoset resin with good thermal and environmental stability, high strength and wear resistance. This combination of properties permits the application of EP in polymer-based heavy duty sliding bearings. For these purposes, EP usually is compounded with reinforcements like glass or carbon fibers, ceramic, mineral oxides and inorganic fillers. The use of fillers in polymeric composites helps to improve tensile and compressive strengths, tribological characteristics, toughness (including abrasion), dimensional stability, thermal stability, and other properties. In addition to the higher mechanical strength obtained due to the addition of fillers in polymeric composites, there is cost reduction in terms of consumption of resin material [2-4] .

The wear behavior of polymeric materials has drawn a considerable interest in recent years. Polymers and their composites are being increasingly used in a various applications where resistance to abrasive wear is important [5]. These range from its use as a material (in applications such as machinery parts and biomedical joint replacements) to its use as a glazing material where damage results in loss of optical properties. Polymers are ideal materials for bearing applications due to their general resistance to corrosion, galling and seizure, their tolerance to small misalignments and shock loading and their low coefficients of friction; as glazing materials, their low density and high toughness along with high transparency are desirable properties [6,7]. The acceptability of polymeric materials for abrasive wear conditions largely depends upon its mechanical load carrying capacity and the wear rate. The practical choice of polymeric materials is however not only determined by the mechanical and tribological properties, but also by the price, simplicity of production, processing and the practical limitations in the real application [8,9]. The performance of polymers sliding against hard and smooth counterface is determined by the transfer ability and buildup of a polymer film. Efficiency of materials in reducing friction and wear depends on the molecular polymer structure and counterface type. However, only few publications are available on the comparison of the tribological properties of composites under dry sliding and abrasive wear conditions [10-14].

In general, studiestake into account to enhance thewear resistanceof polymer materials [15-18]. Epoxy resins are the most commonly used thermoset plastic in polymer matrix composites which do not give off reaction products when they cure and so have low cure shrinkage. They also have good adhesion to other materials, good chemical and environmental resistance, good chemical properties and good insulating properties. In this study, particularly, it was investigated that the influence of fly ash containing waste addition as filler on wear and friction characteristics of epoxy composite.

[1] *Corresponding author: Afyon Kocatepe University, Department of Metallurgical and Materials Engineering, 03200, Afyonkarahisar, Turkey*
2 Afyon Kocatepe University, Engineering Faculty, Civil Engineering Department, 03200, Afyonkarahisar, Turkey, uygunoglu@aku.edu.tr

2. EXPERIMENTAL STUDIES

2.1. Materials and sample preparation

The fly ash used in the study was provided by the Tunçbilek Thermal Power Plant in Tavşanlı/Kütahya. It's maximum particle size was 113.78 µ. Chemical component of waste is presented in Table 1.

Table 1. Chemical content of fly ash

Oxide	CaO_2	SiO_2	AI_2O_3	Fe_2O_3	K_2O	Na_2O	MgO	LOI
Content, %	6.66	47.4	19.8	11.8	2.62	0.57	4.76	6.39

Commercially available Teknobond 300 epoxy resin along with hardener was used as matrix material in fabrication of different specimens. Epoxy resin has modulus of 3.42 GPa, and possess density of 1100 kg/m^3. For processing the mix ratio (by weight) of epoxy resin (2 parts) and hardener (1 part) were used as specified. The required mixture of resin and hardener (Table 2) were made by mixing them in (2:1) parts in a beaker by stirring the mixture in a beaker by a rod taking into care that no air should be entrapped inside the solution. Production of the polymer matrix composite was done at room temperature. The required ingredients of resin, hardener and fly ash were mixed thoroughly and the mixture so made was transferred to mould cavity of the mould which is coated with separator. Steel moulds in size Ø50 mm were used for casting of polymer matrix composite specimens. Curing was done at room temperature for approximately 24 h. After curing, the specimens were de-molded.

Table 2. Composition of epoxy based polymer composites

Mixture code	**Epoxy resin*, kg/m^3**	**Fly Ash, kg/m^3**	**Hardness (H_D)**
FA0	100	-	84
FA10	90	10	86
FA20	80	20	88
FA30	70	30	91

*Epoxy resin was used with hardener (2:1)

2.2. Wear Tests on polymer composites

To perform friction and wear of epoxy based samples, scratch tests were performed by using a ball-on-disc test device. In the wear tests, WC-Co balls of 6 mm in diameter supplied by H.C. Starck Ceramics GmbH were used. Errors caused by the distortion of the surface were eliminated by using a separate abrasion element (WC-Co ball) for each test. The wear experiments were carried out in a ball-disc arrangement under a dry friction condition at room temperature with applied loads of 5, 10, 15 and 30N and with sliding speed of 0.3 m/s at a sliding distance of 500 m. Before and after each wear test, each sample and abrasion element was cleaned with alcohol. After the test, the wear volumes of the samples were quantified by multiplying cross-sectional areas of wear by the width of the wear track obtained from the device Tribotechnic Rugosimeter. The wear rate was calculated with the following formula (1).

Wear rate = Worn volume / (Applied load x Sliding distance), mm^3/Nm (1)

Friction coefficients depending on sliding distance were obtained through a friction coefficient program. Surface profiles of the wear tracks on the samples and surface roughness were measured by a Tribotechnic Rugosimeter.

3. RESULTS AND DISCUSSIONS

3.1. Surface roughness

Figure 1 shows the surface roughness values of no added the waste material and added polymer composites. The surface roughness values were obtained close to each other in samples that control and with low waste material content. However, in samples with high volume waste content, the surface roughness is lower than control specimens.

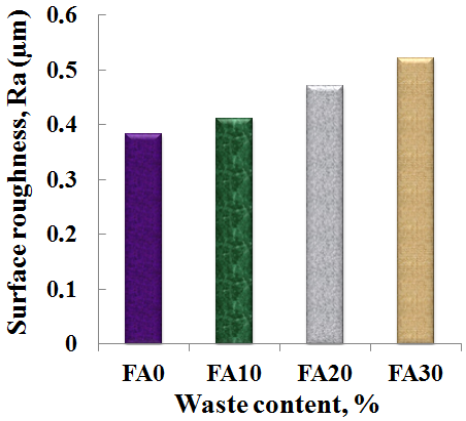

Figure 1.Surface roughness values of epoxy composites with fly ash waste.

Friction coefficients at different load are presented in Figure 2 for control and waste material containing samples. While the lowest friction coefficient is obtained in FA0 samples as 0.039, it was increased to 0.053 in 30% of waste material containing series. Use of fly ash containing waste in polymer composites provides higher friction coefficient when compared to control series. The friction coefficient of all the series are increased by increasing of load.

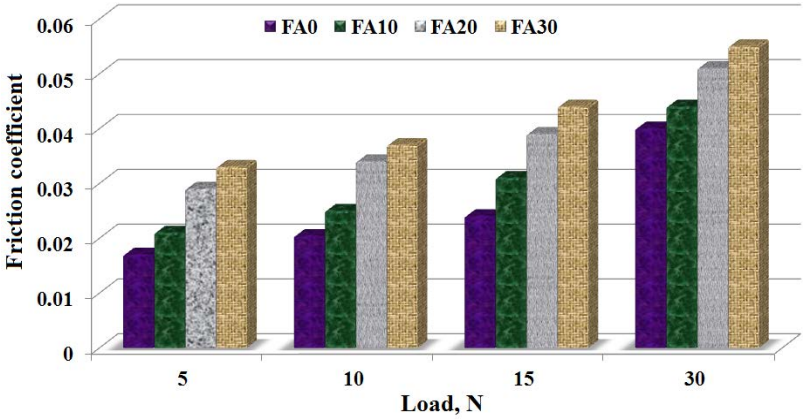

Figure 2. Friction coefficient values of epoxy composites with fly ash waste.

3.2. Wear rate

Wear rate of polymer composites are given in Fig. 3 for 5, 10, 15 and 30N depending on fly ash content. As seen from the Fig. 3, wears of composites decreased by increasing the content of on fly ash waste material. The highest wears were obtained for control series at each loading conditions. The range of wear varied from $62x10^{-4}$ to $19x10^{-4}$ mm^3/Nm at 5N, from $84x10^{-4}$ to $36x10^{-4}mm^3/Nm$ at 10N, from $121x10^{-4}$ to $47x10^{-4}mm^3/Nm$ at 15N, from $172x10^{-4}$ to $64x10^{-4}$ mm^3/Nm depending on waste content. In other words, there was about 2.68 times enhancement in wear resistance of polymer composites at 30 N by increasing of waste content. Increase of fly ash containing waste addition ratio resulted with decrease of wear rate. This means that addition of waste material makes the polymer material harder and also changes the character of the surface. Wear strength is higher in high waste ratio than in low waste ratio due to more homogeny distribution of particles with high resist to abrasion. On the other hand, when the wear loading value was considered, the wear rate for all specimens increased with load regardless of waste material ratio. The wear rate increased with an increase of load from 5 to 30N due to increase of abrasion and friction on surface of polymer composite.

One of the important findings of this study was relationship between hardness and wear rate for epoxy based and boron containing waste blended polymer composites. The relationship between abrasion resistance is obtained from this test, and shown in Figures 1 and 3. It can be seen from Fig. 3 that the abrasion resistance of epoxy based polymers increased with an increase of the hardness.

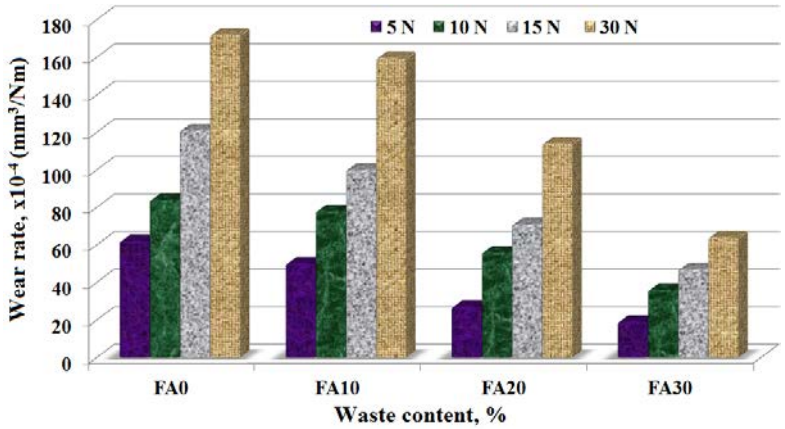

Figure 3.Wear rates of epoxies for various fly ash waste concentrations.

3.3. Wear Microstructure

In Figure 4a, the cracks and deformations can be clearly seen on the surface of control (pure epoxy) specimen. In addition, the highest track width is also observed on this specimen. This is probably due to small air bubbles in the mixtures during the hardening. It was considered that a region centered around the middle of the concentration range. The ball moves over large areas of control specimens. Each of these phenomenons makes its own significant contributions to the overall friction [19].

The hardness values of the samples are increased by increase of waste material content. So, the wear resistance is increased when compared to control specimens due to high degree of hardness values of waste material blended polymer composites (Fig. 4a-d). The border makes the movement of the ball more difficult at high loading condition (see Fig. 3) [20]; now the indenter moves across the entire surface of each region. The indenter is not just jumping from bump to bump as it was doing before-then with little contact with the surface between the bumps. A high friction results, in fact even higher than friction values for pure components [21,22]. In addition, trace widths are decreased by increasing the waste material content. While the deformations such as tears, breaks and cracks are observed on control specimens, there is only trace on the waste material added samples after the wear tests (Fig. 7a-d). Moreover, trace width is homogeneous on the surface of samples with fly ash containing waste.

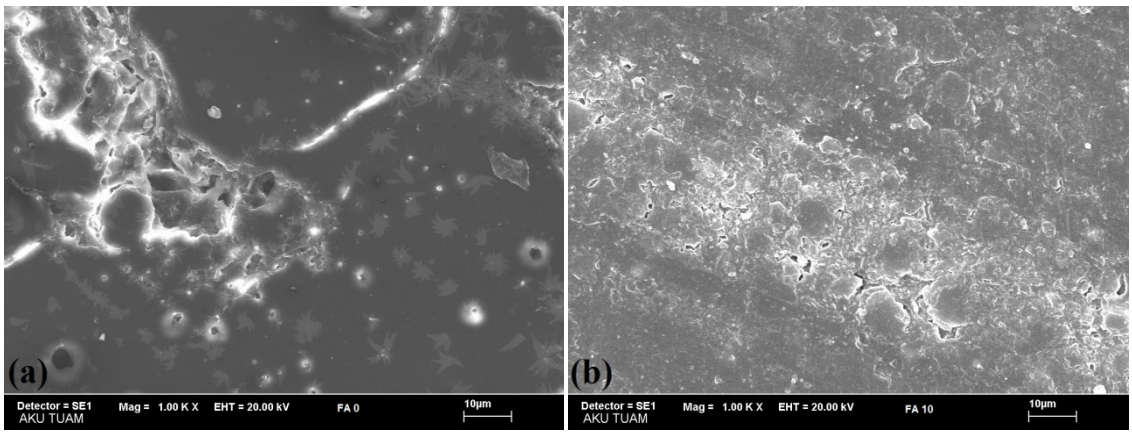

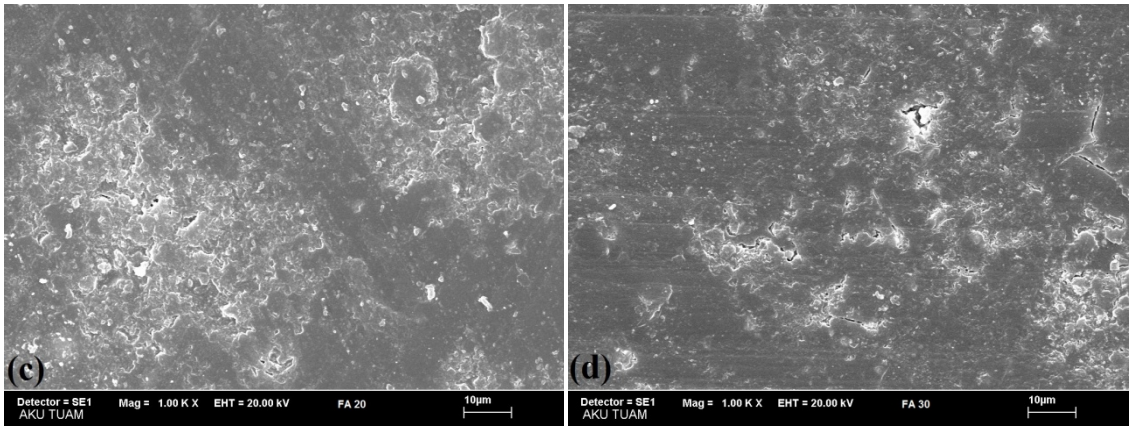

Figure 4. The wear SEM micrographs of epoxy composites after tribometry for various fly ash waste concentrations: (a) for pure epoxy, (b) for 10% waste, (c) for 20% waste, (d) for 30% waste,

4. CONCLUSIONS

The objective of this report has been to describe the wear and friction characteristics of epoxy based polymer composites as well as the role of how fly ash containing waste additives can enhance the polymer composites properties. The following conclusions may be derived from the present study:

The hardness values of samples are increased three times by using fly ash containing waste material when compared to control series. The surface roughness values were obtained close to each other in samples that control and with low waste material content. Use of fly as containing waste material in polymer composites provides higher friction coefficient when compared to control series. The friction coefficient of all the series are increased by increasing of load. Wear strength is higher in high waste material ratio than in low waste material ratio due to more homogeny distribution of particles with high resist to abrasion. There is about 2.68 times increase in wear resistance of polymer composites at 30 N by increasing of fly ash content. Increase of load provides the 'border effect' on the surface. The border effect leads to increase of friction coefficient at higher loading conditions.In microstructure investigations, it has been found that waste material particles are uniformly distributed in the epoxy matrix. While the deformations such as tears, breaks and cracks are observed on pure epoxy specimens, there is only trace on the waste material added samples after the wear tests.

ACKNOWLEDGEMENT

The authors are grateful to the Scientific Research Project (15.FEN.BİL.10) Council of Afyon Kocatepe University. This article was written based on Nezihi ŞAM's master thesis.

REFERENCES

[1] J. Barton, A. Niemczyk, K. Czaja, Ł. Korach, and B. Sachermajewska, "Polymer composites, biocomposites and nanocomposites. Production, composition, properties and application fields," *Chemik*, vol.68, pp. 280-287, 2014.
[2] I. Abdalrazaq, W. A. Soud, and O. S. Abdullah, "Effects of different types of ceramic fillers on wear characteristics of glass fibres-epoxy composite," *Journal of Engineering and Development*, vol. 17, pp. 1813-1822, Dec. 2013
[3] B. Suresha, G. Chandramohan, and Prakash J. N., "The role of fillers on friction and slide wear characteristics in Glass," *Journal of Minerals and Materials Characterization and Eng.*, vol. 5, pp. 87-101, 2006.
[4] B. Suresha, G. Chandramohan, J.N. Prakash, V. Balusamy and K. Sankarayanasamy, "The Role of Fillers on Friction and Slide Wear Characteristics in Glass-Epoxy Composite Systems", *Journal of Minerals and Materials Characterization and Engineering*, Vol.5, No.1, (2006).
[5] A. P. Harsha, "An investigation on low stress abrasive wear characteristics of high performance engineering thermoplastic polymers", *Wear*, vol. 271, pp. 942-951, 2011.
[6] P. H. Shipway, and N. K. Ngao, "Microscale abrasive wear of polymeric materials", *Wear*, 255, pp.742-750, 2003.
[7] J. Cayer-Barrioz, D. Mazuyer, Ph. Kapsa, A. Chateauminois, and G. Robert, "Abrasive wear micromechanismsof oriented polymers,"*Polymer*, vol.45, pp. 2729-2736, 2004.
[8] .B. M. Ginzburg, D.G. Tochil'nikov, V.E. Bakhareva, A.V. Anisimov, and O.F. Kireenko," Polymeric materials for water-lubricated plain bearings,"R*ussian J. Appl. Chemistry*, vol.79, p.695-70, 2006.
[9] A. Golchin, G.F. Simmons, S. Glavatskih, and B. Prakash, "Tribological behaviour of polymeric materials in water lubricated contacts" in: 15th Nordic Symposium on Tribology - NordTrib 2012, p.12 , Trondheim, Norway- (2012).
[10] P. Samyn, G. Schoukens, J. Quintelier, and P. De Baets, "Friction, wear and material transfer of sintered polyimides sliding against various steel and diamond-like carbon coated surfaces," *Tribology International*, vol.39, pp.575-589, 2006.
[11] M. Cirino, K. Friedrich, and R.B. Pipes, "Evaluation of polymer composites for sliding and abrasive wear applications,"*Composites*, vol.19, pp.383-392, 1988.
[12] M. Cirino, and R.B. Pipes, "The abrasive wear behaviour of continuous fibre polymer composites," *Journal of Materials Science*, vol.22, pp.2481-2492, 1987.

[13] M. Cirino, K. Friedrich, and R.B. Pipes, "The effect of fiber orientation on the abrasive wear behavior of polymer composite materials," *Wear*, vol.121, pp. 127-141, 1988.
[14]. G. Zhao, I. Hussainova, M. Antonov, Q. Wang, and T. Wang, "Friction and wear of fiber reinforced polyimide composites," *Wear*, vol.301, pp.122-129, 2013.
[15] M. Rao, C. J. Hooke, S. N. Kukureka, P. Liao, and Y.K. Chen, "The effect of PTFE on the friction and wear behavior of polymers in rolling-sliding contact,"*Polymer Engineering Science*, vol.38, pp. 1946-1958, 1998.
[16] H. Pihtili, "An experimental investigation of wear of glass fibre–epoxy resin and glass fibre–polyester resin composite materials," *European Polymer Journal*, vol. 45, pp. 149-154, 2009.
[17] P. Svancarek, S. Lendvayova, D. Galusek, M. Hnatko, I. Vavra, and X. Wang, "Abrasive wear resistance of
SiO2-doped polycrystalline alumina." *Wear*, vol. 271, pp. 760-769, 2011.
[18] W. Brostow, V. Kovacevic, D. Vrsaljko, and J. Whitworth, "Tribology of polymer and polymer-based composites," *Journal of Materials Education*, vol. 32, pp. 273-290, 2010.
[19] W. Brostow, W. Chonkaew, K. P. Menard, and T. Scharf, "Modification of an epoxy resin with a fluoroepoxy oligomer for improved mechanical and tribological properties," Materials Science and Engineering A., vol.507, pp. 241-251, 2009.
[20] I. Gunes, T. Uygunoglu, A. Ergen, T. Kısıkcılar, E. Aksoy, "Investigation of wear behavior of borided DIN 20MoCr4 steel," *El-Cezerî Journal of Science and Engineering*, vol. *2*, pp. 53-58.
[21] W.Brostow, P. Kumar, D. Vrsaljko, and J. Whitworth, "Optimization of tribological and mechanical properties of nanocomposites of polyurethane/poly(vinyl acetate)/$CaCO_3$," *Journal of Nanoscience and Nanotechnology*, vol 11, pp. 3922-3928, 2011.
[22] O. Olea-Mejla, W. Brostow, and E. Buchman, "Wear Resistance and wear mechanisms in Polymer + Metal Composites," *Journal of Nanoscience and Nanotechnology*, 10, p.8524-8530, 2010.

BIOGRAPHY

Ibrahim Gunes received his PdD from institute of natural and applied science, Afyon Kocatepe University, Turkey in 2010. He is a Associate Professor at Afyon Kocatepe University, Afyonkarahisar, Turkey, since 2014. His area of interest is Materials characterization, surface engineering for tribological applications such as oxidative and high temperature at unlubricated conditions. He has published around 33 papers in international peer reviewed journals.

Investigation of Using Biofuels in Mobile Power Plants in Terms of Performance, Emission and Cost

***Hikmet Esen*[1]**

Abstract

In this study, biodiesel (Canola oil) is produced from oils that have different characteristics applying the trans-esterification of acid and base catalyzed. It is seen that to be appropriate for the TS-EN 14214 standards these values obtained from fuels. Produced Canola oil have mixed with fuel (5%, 10% and 20%) and tested in three-cylinder direct injection diesel engine. The engine performance characteristics and exhaust emission changes were examined in comparison with diesel fuel. In addition, electricity production costs in the long-term use of biodiesel in diesel generators is calculated. Experimental results are indicated that biodiesel and mixed fuels show similar characteristics. With increasing biodiesel percentage in the fuel specific, the fuel consumption and exhaust temperature has increased. Compared to diesel fuel in the use of biodiesel, while CO, HC and smoke emissions decrease, NO_x, CO_2 and O_2 have increased.

***Keywords**: Biofuel, Canola oil, mobile power plants, emission, cost*

1. INTRODUCTION

There is numerous usage area of diesel generators. Petroleum-based fuels are used in these diesel generators, having a wide usage area. Depending on increase in world population and development of technology, oil sector cannot meet demands and as a result there is an excessive increase in oil prices. Thus factors meeting the energy requirements from the diesel generators will be affected negatively. Alternative fuel research sees important support across the world. The alternative fuel that can be used in diesel engines need to have some qualities like; being economic, renewable, environmentally friendly and easy to obtain. Biodiesel is considered as an alternative fuel type having features that can meet these requirements for diesel engines [1]. Despite the fact that availability of diesel is studied in agriculture, transportation and shipping sectors, it has not been investigated enough in energy production sector. Although in some studies diesel generators are used when the details of the study are investigated, it is seen that diesel generators are used for electromagnetic load in the internal combustion engine. Various studies have been made related to usage of biodiesel in vehicle engines. Roy et al. [2] produced biodiesel from canola oil and mixed it with diesel by 5%, 10%, 20% and 50% to investigate performance and emissions of a diesel engine working with this fuel. How et al. [3] carried out production of biodiesel from coconut oil and classified in four different fuel samples as B10, B20, B30 and B50. In this way performance, emissions, combustion and vibration parameters were studied experimentally at different inner pressure of cylinder. Abedin et al. [4] emphasized that biodiesel work in Malaysia contributed substantially to public transportation and shipping sector. Palash et al. [5] produced biodiesel with oil obtained from the Aphanamixis polystachya plant growing in Bangladesh and mixed it with diesel in different volumetric ratios and stressed that the best mixture percentages are 5% and 10%.

The main objective of this study is to produce biodiesel from canola oil with different properties and mix these with diesel fuel by different ratios (% 5 (B5), % 10 (B10) and % 20 (B20)). In this way performance and exhaust emissions values of diesel generator are compared with diesel fuel and each other. Also, cost of electricity production is calculated for long-term usage of biodiesel fuel diesel generator.

2. PREPARATION OF BIODIESEL FUELS

Diesel fuel is a third main product obtained during distillation of crude oil between 200 to 300 ° C boiling point. It incorporates various hydrocarbon variants having carbon atoms of 8 to 16. Diesel fuel has a major importance for the economy because in the absence of high-efficiency diesel fuel, land and sea freight will invest in inefficient fuels. Diesel fuel has more energy density than gasoline. Its smell is different from gasoline, it is quite greasy and heavier.

2.1. Biodiesel Production Methods

Different vegetable oils must be subjected to some pre-treatment to be used smoothly as fuel in diesel engines. These operations can be classified as transesterification, dilution, micro-emulsions and pyrolysis in order of preference.

Biodiesel is a green fuel and it contributes to the national economy and this can only realize in expected level with a production in accordance with international standards. As well as causing the loss of raw materials and products, deficiencies in production process decrease the productivity by causing interruptions in production and deteriorate quality of the product. Low quality product causes usage challenges and direct damage to engine using it. Although there are various methods of

[1] *Corresponding author: Fırat University, Faculty of Technology Department of Energy Systems Engineering, 23119, Elazığ, Turkey.* esenhikmet@gmail.com

biodiesel production, most commonly used method is transesterification. The following process steps are followed in the production of biodiesel. Also; biodiesel production process is shown schematically in Figure 1.

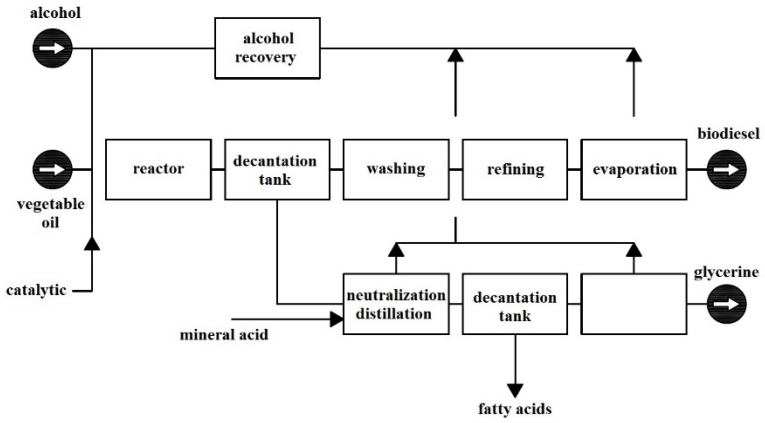

Fig.1. Process steps of biodiesel [6].

2.2. Cautions in Biodiesel Production

Methyl alcohol should be used with caution because it is very harmful to health.
Sodium hydroxide should be stored under exclusion of moisture because it is a very alkaline and has moisture retention property. It can cause permanent damage if not used carefully.
When using waste oils in biodiesel production, must be heated before adding the chemicals if these oils are in the form of concentrates and clot.
Chemical materials used in production must be heat and corrosion resistant.

Sodium methoxide (methanol + sodium hydroxide) solution is very toxic and very corrosive against paint. Sodium hydroxide reacts with zinc and aluminum tin cans. Therefore, such containers should never be used. Steel containers should be used if possible [7].

In this study, the production of biodiesel from rapeseed oil was performed. In this section vegetable oil (canola oil) used for biodiesel production and biodiesel production steps of this oil is indicated with specific images (Figures 2-4). Rates of biodiesel and diesel fuel mixture are also offered.

Fig. 2. The evaporation of removed moisture in the oil

Fig. 3. Transesterification

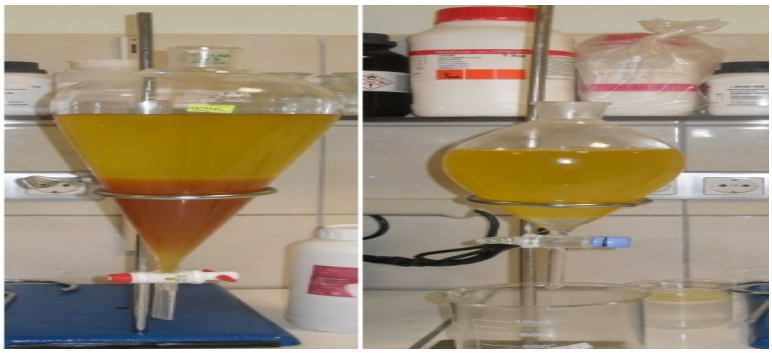

Fig. 4. Canola oil; phase separation, the washing process

3. ENGINE TESTING MATERIALS

The experiment set consists of diesel engine, generator, precision scale, AC load group, exhaust gas analyzer and smoke meter. Experimental studies were performed on a diesel generator Genpower brand. During operation any modification was not made in the motor, generator or any component. fuel samples were tested in same standard conditions. Schematic representation of the experimental setup is given in Figure 4.1.

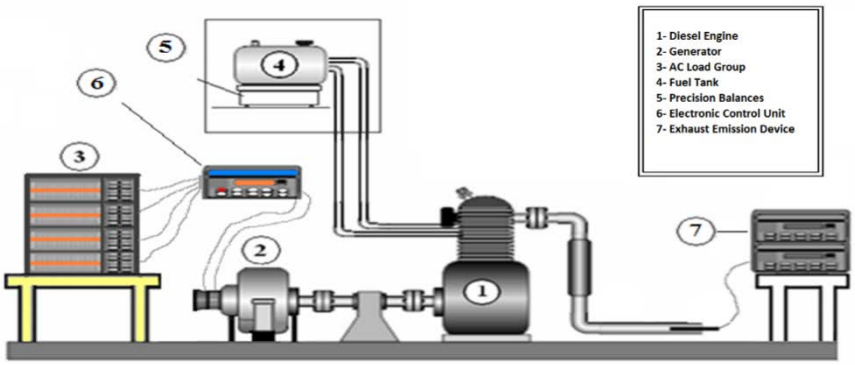

Fig. 5. Schematic representation of the experimental setup

Before starting the experiment, routine engine maintenance such as cleaning the air filter, exchange of lubricant oil is made. The controls are made by removing the engine fuel injectors. All fuel engine tests were carried out without any modification. Engine was run unloaded with standard diesel fuel and after engine arrive optimum operating temperature, load was applied to engine in 4 different value; (25%) - 5 kW (50%) - 7.5 kW (75%) - 10 kW (100%). This operation was repeated three times and average of measured values was calculated. After completion of measurement for a fuel type, engine was stopped and after waiting a while it started to work with other types of fuel. Specific fuel consumption (g / kWh), HC (ppm), CO (%) CO_2 (%), O_2 (%), NO_x (ppm), exhaust temperature (° C) and smoke (is) values were measured in above-mentioned variable load experimental study.

4. EXPERIMENTAL RESULTS AND DISCUSSION

Three different samples are obtained by biodiesels derived from canola oils and diesel fuels mixture with certain proportions. Specific fuel consumption and exhaust emissions of obtained new fuel samples are tested.

Specific fuel consumption values of a diesel generator, prepared taking into account the standard of mobile power plants and running at a constant rate of 1500 rev / min, were measured at variable load conditions; 25%, 50%, 75% and 100%. specific fuel consumption NOx, CO, HC, soot emission and exhaust gas temperature values are given in Table 1-6 respectively for canola oil fuel sample at variable load.

Table 1. Specific fuel consumption (g/kWh) of the variable load values

	% 25	**% 50**	**% 75**	**% 100**
Diesel	368	326	299	281
B5	375	338	303	285

B10	372	341	312	290
B20	380	344	320	308

Table 2. NOx emissions (ppm) in variable load values

	% 25	**% 50**	**% 75**	**% 100**
Diesel	292	491	635	734
B5	300	502	651	760
B10	305	536	689	806
B20	319	579	740	850

Table 3. CO emissions in variable load

	% 25	**% 50**	**% 75**	**% 100**
Diesel	0.04	0.08	0.17	0.29
B5	0.03	0.055	0.14	0.22
B10	0.035	0.04	0.1	0.2
B20	0.03	0.045	0.08	0.15

Table 4. Hydrocarbon (HC) emissions in variable load

	% 25	**% 50**	**% 75**	**% 100**
Diesel	27	44	54	59
B5	25	39	40	45
B10	20	35	35	41
B20	15	30	29	30

Table 5. Smoke (soot) emission in variable load

	% 25	**% 50**	**% 75**	**% 100**
Diesel	13	20	25	34
B5	12	18	22	29
B10	11	14	20	24
B20	8	11	17	20

Table 6. Exhaust temperature in variable load

	% 25	% 50	% 75	% 100
DY	161	174	209	258
B5	163	180	215	268
B10	170	190	228	284
B20	178	196	233	292

Increase in SFC values ratio of biodiesel fuels is found 2.11% at B5 fuel, 3.21% at B10 fuel and 12.6% at B20 of fuel compared to diesel fuel. When NOx emissions of biodiesel fuels and diesel fuels are compared increase ratios of 15.60%, 8.55% and 2.80% are determined respectively at B5, B10 and B20 fuels. Reduction in CO emissions are identified as 23.27% at B5, 35.34% at B10 and 47.58% at B20 compared to diesel fuel. Also reduction in HC emissions are identified as 19.02% at B5, 28.80% at B10 and 43.47 % at B20 compared to diesel fuel. The other reduction in smoke emissions are identified as 11.95% at B5, 25% at B10 and 39.13 % at B20 compared to diesel fuel. Finally increase in exhaust temperature values of biodiesel fuels is found 3% at B5 fuel, 8.72% at B10 fuel and 12.09% at B20 of fuel compared to diesel fuel.

With increasing the load on the engine, increases in fuel exhaust temperatures are observed for all samples. The main reason for the difference in exhaust emissions of diesel fuels and biodiesel, is having high cetane number and containing oxygen in biodiesel. Good combustion characteristics, always leads to achieve high exhaust temperature values.

With the lower heating value of biodiesel compared to diesel fuel, it results in reducing engine performance and increasing the specific fuel consumption. It is showed that Biodiesel fuels produced in experimental studies and mixtures obtained from these can be used direct injection diesel engine without any modification instead of diesel fuel.

Amount of consumables used in the production stage and their unit prices (1 euro = $ 3) are analyzed separately for each of the oil and are given in Table 7.

Table 7. Quantity and price of reactive materials

The materials used in the reaction	The amount of product used	Unit price (Euro)	Total amount (EUR)
Canola Oil	1 liter	0.56	0.56
Methyl alcohol	0.2 liter	1.42	0.284
NaOH	4 gr	3.06	0.012
Total			0.856

According to Table 7 cost of biodiesel derived from canola oil is determined to be 0.856 Euro. 9.78 lt of biodiesel is produced from 10 lt of canola oil with a production yield of 97.8%. 0.856 Euro is divided by production yield (0.856 / 0.978 = 0.875) to determine actual cost. Electric costs are 0.72 euros. process cost is calculated as 0.72 / 30 = 0.024 Euros for 30 lt capacity production. When cost of the electrical appliances is added to the cost of material cost of the electrical appliance (0.875 + 0.024 = 0.899) total cost of biodiesel derived from canola oil is found. In other words, 1 liter of canola biodiesel costs approximately 0.9 euros.

Values of the fuel cost of power generation for B5, B10 and B20 prepared with canola oil are compared with diesel fuel value. When power generation cost of fuel containing canola oil, is compared with diesel fuel there is a decrease in 0.7% at B5 fuel and 1% at B10 fuel while an increase in 8% at B20 fuel.

When values related to canola are examined, in B5 there is a portion of increase, in B10 there is a reduction and in B20 there is a significant increase. Based on this observation addition amount of canola biodiesel to standard diesel is very important in terms of costs. due to the thermal energy value of biodiesel is lower than diesel fuel, a rise is expected in all B5, B10 and B20 fuel unlike in B5 and B10 there is a reduction. The main reason for this decrease detected is believed that due to biodiesel has high cetane number and contains oxygen it has a catalyst effect which provides high quality combustion performance. Although B20 also acts as a catalyst in the combustion reaction, it is known that the high proportion of biodiesel in the mixture decreases heat energy by 20%. This decline in the value of heat energy is believed to cause a cost increase of 8%. As a result of this analysis, 10% of canola biodiesel and diesel fuel mixture (B10) is found to be the most appropriate mixing ratio.

REFERENCES

[1]. E. Alptekin and M. Çanakçı, "Optimization of pretreatment reaction for methyl ester production from chicken fat", *Fuel*, 89, 4035-4039, 2010.
[2]. M.M. Roy, W. Wang, and M. Alawi, "Performance and emissions of a diesel engine fueled by biodiesel–diesel, biodiesel–diesel-additive and kerosene–biodiesel blends", *Energy Conversion and Management*, 84, 164-173, 2015.
[3]. H.G. How, H. H. Masjuki, M.A. Kalam, and Y. H. Teoh, "An investigation of the engine performance, emissions and combustion characteristics of coconut biodiesel in a high-pressure common-rail diesel engine", *Energy*, 69, 749–759, 2014.
[4]. M.J. Abedin, H.H. Masjuki, M.A. Kalam, A. Sanjid, S.M. Ashrafur Rahman, and I.M. Rizwanul Fattah, "Performance, emissions, and heat losses of palm and jatropha biodiesel blends in a diesel engine", *Industrial Crops and Products*, 59, 96-104, 2014.
[5]. S.M. Palash, H.H. Masjuki, M.A. Kalam, A.E. Atabani, I.M. Rizwanul Fattah, and A. Sanjid, "Biodiesel production, characterization, diesel engine performance, and emission characteristics of methyl esters from Aphanamixis polystachya oil of Bangladesh", *Energy Conversion and Management*, 91, 149–157, 2015.
[6]. K. Güler, "Biyodizel Teknolojisi, Sistem Tasarımı ve Deneysel Olarak Biyodizel Üretimi", *Yüksek Lisans Tezi* S.D.Ü. Fen Bilimler Enstitüsü, Isparta, 2008.
[7]. http://www.cevreorman.gov.tr/belgeler/yaglar.pdf 19 Aralık 2014.